

1991

The SYNOP Experiment: Thermocline Depth Maps for the Inlet Array October 1987 to August 1990

Karen L. Tracey

University of Rhode Island, krltracey@uri.edu

D. Randolph Watts

University of Rhode Island, randywatts@uri.edu

Creative Commons License



This work is licensed under a [Creative Commons Attribution-Noncommercial-Share Alike 3.0 License](#).

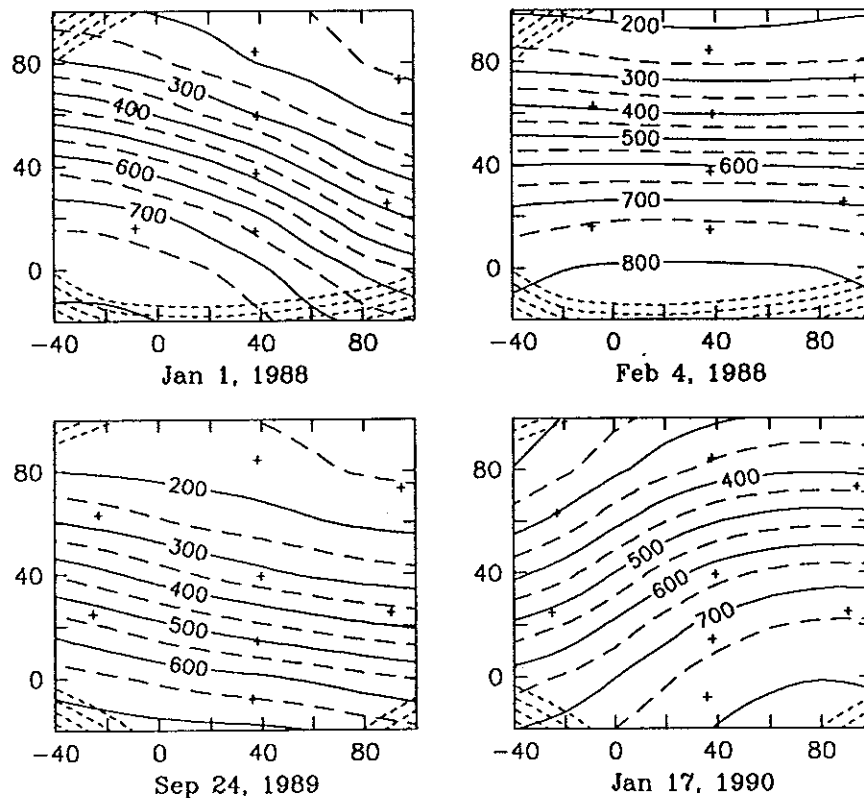
Follow this and additional works at: http://digitalcommons.uri.edu/physical_oceanography_techrpts

Recommended Citation

Tracey, Karen L. and Watts, D. Randolph, "The SYNOP Experiment: Thermocline Depth Maps for the Inlet Array October 1987 to August 1990" (1991). *Physical Oceanography Technical Reports*. Paper 22.
http://digitalcommons.uri.edu/physical_oceanography_techrpts/22
http://digitalcommons.uri.edu/physical_oceanography_techrpts/22

GRADUATE SCHOOL OF OCEANOGRAPHY
UNIVERSITY OF RHODE ISLAND
NARRAGANSETT, RHODE ISLAND

THE SYNOP EXPERIMENT:
Thermocline Depth Maps for the Inlet Array
October 1987 to August 1990



by

Karen L. Tracey and D. Randolph Watts

GSO Technical Report No. 91-6
August 1991

This research program has been sponsored by the National Science Foundation under grant number OCE87-17144 and by the Office of Naval Research under contracts N00014-87K-0235, N00014-90J-1568 and N00014-90J-1548.

Abstract

Between October 1987 and August 1990, two arrays of inverted echo sounders were deployed in the Gulf Stream northeast of Cape Hatteras as part of the SYNoptic Ocean Prediction Experiment. The "Inlet Array" consisted of 9 inverted echo sounders (IES). Centered at 74°W, the Inlet Array was designed to measure key parameters that describe the Gulf Stream path variability near Cape Hatteras. The large "Central Array" of 24 IESs was centered on the current near 68°W, about 400 km downstream of the Inlet Array. Spanning nearly 300 km in both the cross-stream and downstream directions, the Central Array was designed to monitor the thermocline structure of the Gulf Stream in the region of large meanders and frequent ring interactions.

Using objective analysis, we have mapped the Gulf Stream thermal field measured by the IESs in the Inlet Array. In this report, the objective analysis technique is described and the mapping parameters are documented. Daily maps of the thermocline depth field are presented for the period 14 October 1987 through 31 August 1990.

Contents

Abstract	i
List of Tables	iv
List of Figures	iv
1 Introduction	1
2 Inlet Array IES Data	3
3 Objective Mapping of the Thermocline Depth Field	6
3.1 The Space-Time Correlation Function	7
3.2 Mean Z_{12} and STD Fields	11
3.3 Construction of the Z_{12} Maps	12
4 Estimated Error Fields	14
5 Average Z_{12} Maps	16
6 Daily Z_{12} Maps for the Inlet Array	18
References	136

List of Tables

1	IES88 Inlet Array - Locations and Duration	5
2	IES89 Inlet Array - Locations and Duration	5
3	IES90 Inlet Array - Locations and Duration	5
4	OA Mapping Control Parameters	12
5	Corner Positions of Mapping Regions	18

List of Figures

1	Array Map for October 1987 to August 1990	3
2	Observed and Analytic Correlation Functions	8
3	Spatial Correlation Function	10
4	Temporal Correlation Function	10
5	Mean Z_{12} and Standard Deviation Fields	12
6	IES Standard Deviations	13
7	Estimated Error Maps	14
8	Deployment-Long Average Z_{12} Fields	16
9	Seasonally-Averaged Z_{12} Fields	17

1 Introduction

Although the Gulf Stream has been studied more than any other current system, many fundamental questions concerning the dynamics and energy balances governing its meandering still remain. To address these questions, a multi-investigator, multi-institutional research effort, entitled the SYNoptic Ocean Prediction (SYNOP) experiment, was undertaken. To accomplish the objectives, the observational phase of SYNOP was designed such that the results could eventually be integrated with numerical models of the Gulf Stream.

As one part of the SYNOP initiative, Randy Watts of the University of Rhode Island and John Bane of University of North Carolina conducted a joint field experiment in the region northeast of Cape Hatteras, NC, where the instantaneous path of the Gulf Stream is convoluted by large time-varying meanders. The study area extended from Cape Hatteras on the west to 67°W on the east. In this region, the Gulf Stream can shift laterally through an envelope which exceeds the instantaneous width of the current itself. The Gulf Stream is closely associated with the surrounding flow fields to the north and south where rings frequently form and interact with the current.

Between October 1987 and August 1990, our field program consisted of two moored arrays. The "Inlet Array" was composed of 9 inverted echo sounders (IES) and 5 deep current meters. Centered at 74°W, the Inlet Array was designed to measure key parameters that describe the path variability near Cape Hatteras as the Gulf Stream leaves the continental margin and flows into deeper water. The large "Central Array" of 24 IESs was centered on the current near 68°W, about 400 km downstream of the Inlet Array. The Central Array also consisted of thirteen tall current meter moorings, that reached from the bottom into the high-velocity Gulf Stream core. In addition, twelve IESs in the interior of the array were outfitted with bottom pressure gauges. Spanning nearly 300 km in both the cross-stream and downstream directions, the Central Array was designed to monitor the Gulf Stream thermocline structure in this region of large-amplitude meanders and ring interactions. The field phase of the program ended in August 1990.

The subsequent data processing tasks were divided among the groups at URI and UNC. The basic steps for both the current meters and IESs included transcription, editing and conversion into scientific units. The IES and bottom pressure data from both the Inlet and Central Arrays were processed at URI. These data have been documented in three technical reports [Qian *et al.*, 1990; Fields and Watts, 1991a; Fields and Watts, 1990b]. The current meter records from the Inlet Array will be documented in Pickart *et al.* [1991]. The current meter records for the Central Array,

processed at UNC, will be documented separately [Shay *et al.*, 1991].

After the individual IES records were scaled into thermocline depths, we combined the data for each array to produce maps of the Gulf Stream and adjacent thermal fields. This report documents the mapping procedures for the Inlet Array for October 1987 to August 1990. Maps of the Central Array for this same time period are documented separately [Tracey and Watts, 1991].

2 Inlet Array IES Data

From October 1987 to August 1990, the Inlet Array consisted of 9 IESs located on three cross-stream lines (Figure 1). During the summers of 1988 and 1989, all instruments were recovered,

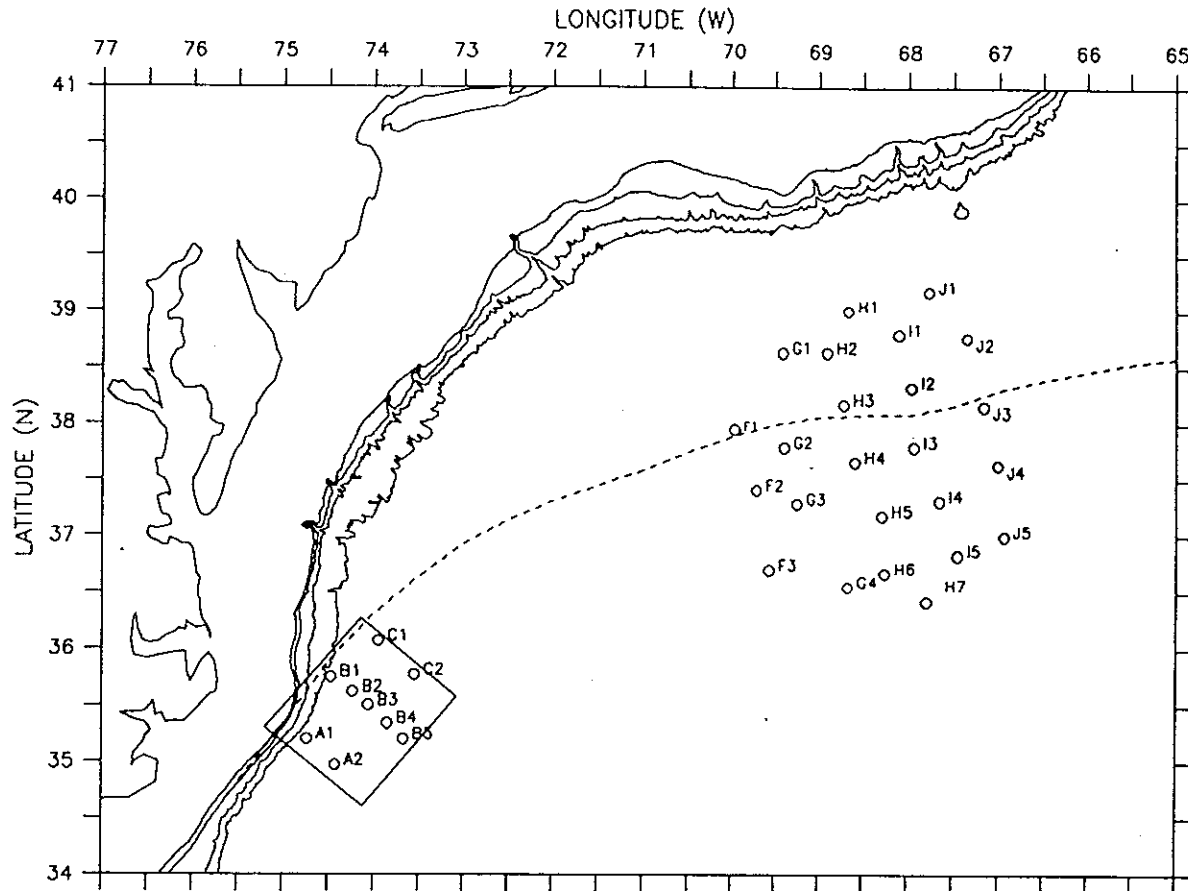


Figure 1: Inlet and Central Arrays: October 1987 to August 1990. IES sites are denoted by the open circles. The box outlines the 140 km by 120 km region of the Inlet Array which has been mapped by objective analysis. The dashed curve indicates the mean path of the Gulf Stream for 1975 to 1986 from Gilman and Cornillon [1990]. Bottom depths of 100, 200, 1000, 2000 m are shown.

refurbished, and redeployed. The IES positions and durations for the three deployment periods are given in Tables 1–3. Unfortunately during the second deployment period, both IESs along the A line failed; thus the array was limited to only two cross-stream lines from June 1988 to August 1989.

The mean downstream distance between lines A, B, and C was 55 km. Along the A and C lines, the cross-stream separation distance between IES sites was approximately 40 km, whereas

on the central **B** line, the spacing was only about 25 km. The array was designed so that key path parameters, displacement, angle, and curvature, could be measured. Additionally, the IES locations were selected so that the objectively estimated error fields would indicate accurate mapping of the thermocline topography even if isolated instruments in the array either malfunctioned or were lost. Furthermore, a couple of IES sites were chosen in order to locate them along the suborbital ground tracks of GEOSAT.

After recovery, the IES data were edited and calibrated using a suite of processing steps [Fields *et al.*, 1991]. Using the techniques described in Watts and Johns [1982], Tracey and Watts [1986] and Howden *et al.* [1991], the travel times measured by the IESs were scaled to thermocline depths and subsequently smoothed using a 40-hour low-pass filter to remove the inertial and tidal signals. For convenience, the thermocline depth is expressed as the depth, in meters, of the 12°C isotherm (Z_{12}). The data were subsampled at daily intervals prior to performing the objective analysis.

Table 1: IES88 Inlet Array - Locations and Duration

IES Site	Latitude (N)	Longitude (W)	Start Date	End Date
IES88A1	35° 18.56	74° 36.94	18 Oct 1987	28 May 1988
IES88A2	35° 02.05	74° 12.29	14 Oct 1987	12 Jun 1988
IES88B1	35° 45.06	74° 27.97	12 Oct 1987	26 May 1988
IES88B2	35° 36.71	74° 14.30	14 Oct 1987	28 May 1988
PIES88B3	35° 28.81	74° 02.84	13 Oct 1987	28 May 1988
PIES88B4	35° 20.74	73° 50.97	13 Oct 1987	28 May 1988
IES88B5a	35° 11.98	73° 40.01	13 Oct 1987	18 Oct 1987
IES88B5b	35° 12.07	73° 40.09	21 Oct 1987	14 Nov 1987
IES88C1	36° 04.54	73° 56.98	14 Oct 1987	29 May 1988
IES88C2	35° 45.93	73° 33.55	14 Oct 1987	30 May 1988

Table 2: IES89 Inlet Array - Locations and Duration

IES Site	Latitude (N)	Longitude (W)	Start Date	End Date
IES89A1	35° 18.61	74° 36.85		Instrument lost
IES89A2	34° 58.06	74° 24.96		No data
IES89B1	35° 45.10	74° 28.00	29 May 1988	9 Jun 1989
IES89B2	35° 36.92	74° 14.20	31 May 1988	9 Aug 1989
IES89B3	35° 28.96	74° 02.63	30 May 1988	9 Aug 1989
IES89B4	35° 20.70	73° 51.00	30 May 1988	10 Jun 1989
IES89B4	35° 20.80	73° 50.50	12 Jun 1989	10 Aug 1989
IES89B5	35° 12.06	73° 40.01	30 May 1988	10 Jun 1989
IES89B5	35° 12.04	73° 39.95	12 Jun 1989	10 Aug 1989
IES89C1	36° 04.67	73° 56.90	1 Jun 1988	11 Jun 1989
IES89C2	35° 46.20	73° 32.90	1 Jun 1988	10 Aug 1989

Table 3: IES90 Inlet Array - Locations and Duration

IES Site	Latitude (N)	Longitude (W)	Start Date	End Date
IES90A1	35° 12.32	74° 43.91	14 Aug 1989	1 Sep 1990
IES90A2	34° 58.18	74° 24.53	12 Aug 1989	1 Sep 1990
IES90B1	35° 45.13	74° 27.90	11 Jun 1990	31 Aug 1990
TIES90B2	35° 37.01	74° 13.82		Instrument lost
TIES90B3	35° 30.07	74° 03.40	11 Aug 1990	1 Sep 1990
TIES90B4	35° 20.75	73° 50.60	12 Aug 1990	1 Sep 1990
TIES90B5	35° 12.13	73° 39.66	12 Aug 1990	1 Sep 1990
IES90C1	36° 04.57	73° 56.84	13 Jun 1990	2 Sep 1990
TIES89C2	35° 46.15	73° 33.00	13 Aug 1989	16 Oct 1989
TIES90C2	35° 46.22	73° 32.75	18 Oct 1989	2 Sep 1990

3 Objective Mapping of the Thermocline Depth Field

In order to produce gridded maps of the Gulf Stream Z_{12} field, we used objective analysis (OA) to interpolate between the irregularly-spaced observations. The interpolation is made at each output grid point as a weighted average of input values at the neighboring measurement sites. The optimal weighting was determined according to the Gauss-Markov theorem using knowledge of the space-time correlation function (see below). For our application, the correlation function was dependent on radial distance and time, $\rho(r, t')$.

The basic OA equations are clearly formulated in Bretherton *et al.* [1976] and extensions to anisotropic fields are given in Carter [1983] and Carter and Robinson [1987]. The method was further modified by Watts and Tracey [1985] and Watts *et al.* [1989] to apply the technique to the Gulf Stream frontal region. To summarize briefly, their adaptations include preconditioning the observations by removing a spatially-dependent mean thermal field and subsequently normalizing the residual perturbations by the standard deviation (STD) field. These techniques combine to produce perturbation fields which have homogeneous statistics, a requirement of objective analysis. After running the OA, both the mean and STD fields are restored to the output fields, producing maps of the Gulf Stream Z_{12} field. We used the procedures of Watts *et al.* [1989] to generate the OA maps shown in this report.

Since we have a large set of observations, we adapted programs generously provided by E. Carter (documented in Carter and Robinson [1987]) that make the computing much more efficient. We took advantage of the fact that data values which are distant (both spatially and temporally) from the output point have little influence on the estimate when compared with the nearby observations. We increased the efficiency by restricting the available data to a smaller subset prior to running the OA at each output point. First, we specified a maximum time lag (t'_{\max}) and maximum radial separation distance (r_{\max}) and eliminated observations which exceeded these restrictions. For the Inlet Array OA maps, we specified $t'_{\max} = \pm 1$ day and $r_{\max} = 120$ km. When determining the radial distance for each data point, we took into account downstream phase propagation of Gulf Stream meanders (discussed below) such that

$$r = \left[(x' - ct')^2 + (y')^2 \right]^{\frac{1}{2}} \quad (1)$$

where the phase speed $c = 24$ km d⁻¹.

To further reduce the data around a given output grid point to use only the most influential input data, we selected a smaller subset of these restricted observations. We chose only the N points

with the highest correlations to be used for the estimation at the output grid point. The choice for N is a trade off between wanting enough observations to reduce random noise and wanting fewer points to increase computational efficiency. The Gauss-Markov procedure involves inversion of an $N \times N$ matrix, repeated for each output grid point of every map. If N is too large (such that the input data are themselves not sufficiently independent) then the matrix inversions are computationally unstable and the errors actually increase. We used $N = 6$ points to produce the Inlet Array Z_{12} maps.

While the choices for t'_{\max} , r_{\max} , c , and N place restrictions on the data to be used for interpolation, they do not directly appear in the OA equations. Aside from the correlation function, the only user-specified parameter that is explicitly a factor in the equations is the noise level of the data (ϵ). By specifying a non-zero noise level, the interpolation scheme is not required to fit the data values exactly, and some smoothing is permitted. We specified $\epsilon = 0.05$ (in terms of percentage of the data variance), since it is our best estimate of the true error associated with the IES measurements.

3.1 The Space-Time Correlation Function

To produce the OA maps of the Inlet Array thermal field, it was necessary to determine a correlation function appropriate for that region of the Gulf Stream. We followed the procedures described in Watts *et al.* [1989] to calculate the spatial and temporal correlations from our observations. In all, we used Z_{12} records from 28 IESs obtained during three separate deployment periods between 1987 and 1990. We calculated the spatial separations (x', y') between pairs of IESs within each deployment period and determined their cross-correlations for several time lags t' . Subsequently, the correlations were smoothed by a 60-km Gaussian-weighted low-pass filter to remove some of the small scale noise. Figure 2 shows the observed correlations in the full (x', y') plane for lag times of 0, 1, and 2 days.

Next, to examine the observed correlations for spatial anisotropy, we sorted the pairs into downstream, cross-stream and diagonal categories and recomputed the correlations for $t' = 0$ days. Figure 3 reveals the similarity between the three groups, indicating no significant directional dependence. Thus, we expressed the spatial decay of the correlations as a function of radial distance, rather than of both x' and y' . The best fit to the observed correlations, shown in Figure 3, was an exponential-cosine function of the form

$$\rho(r) = F_0 \exp\left(\frac{-r}{A}\right) \cos\left(\frac{\pi r}{2B}\right) \quad (2)$$

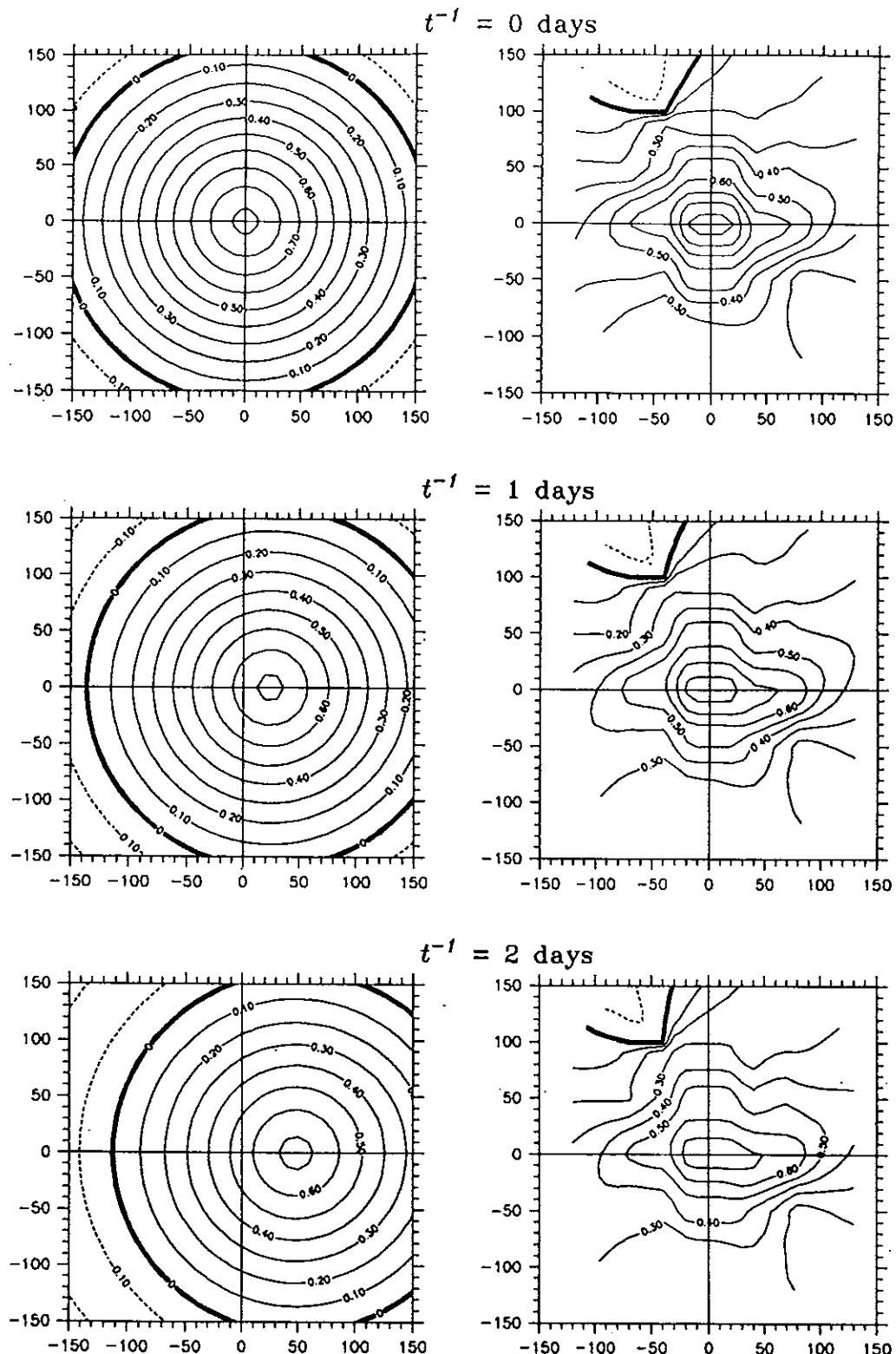


Figure 2: Two correlation functions, (left) analytic function ρ_{Inlet} and (right) observed, are contoured in plan view for time lags of 0, 1, and 2 days. The contour interval is 0.1, and negative contours are dashed. Axes tick marks indicate spatial separation distances of 20 km.

where $r^2 = (x')^2 + (y')^2$, $A = 254$ km, and $B = 160$ km. The scale factor is defined as $F_0 = 1 - \epsilon$, where $\epsilon = 0.05$ is the error associated with the observations.

To determine the temporal decay of the correlation function, we calculated the auto-correlations of 19 IESs using positive time lags of 0 to 24 days. For this analysis, we were careful to select only IESs with long deployment periods, requiring the record length to exceed 180 days. The auto-correlations, averaged for each time lag, are shown in Figure 4. To determine an analytic expression for the temporal decay rate, we fitted an exponential-cosine of the form

$$\rho(t') = \exp(-a_1 t') \cos\left(\frac{a_2 t' \pi}{180}\right) \quad (3)$$

to the correlations. From symmetry requirements, the correlations for negative time lags are $\rho(-x', -y', -t') = \rho(x', y', t')$. For the full set of correlations (time lags out to 24 days), the best fit is shown by the dashed curve in Figure 4 and is obtained by specifying $a_1 = 0.0527 \text{ d}^{-1}$ and $a_2 = -2.3056 \text{ d}^{-1}$. However, this curve does not adequately describe the rapid decay rate of the shorter time lags. Since we only use lags out to 2 days when performing the objective mapping, we wanted to use a temporal decay rate which is more appropriate for these shorter time scales. By specifying $a_1 = 0.1182 \text{ d}^{-1}$ and $a_2 = 0.0831 \text{ d}^{-1}$, we obtained the solid curve shown in Figure 4. This is the temporal decay rate used to define the correlation function for the Inlet Array.

Subsequently, we examined the propagation of the correlation peak with time. We expected the peak to move downstream at a rate comparable to that of Gulf Stream meanders. We selected 21 pairs of IESs which were located downstream of one another and calculated their cross-correlations for $t' = 0$ to 20 days. For each pair, we found the time associated with the maximum correlation and determined the speed based on the spatial separation between the instruments. The rates ranged from $10-55 \text{ km d}^{-1}$, averaging $43 \text{ km d}^{-1} \pm 14 \text{ km d}^{-1}$. However, in Figure 2, the observed correlation peak at $t' = 2$ days occurs at $x' = 40-60$ km, indicating phase speeds of only $20-30 \text{ km d}^{-1}$. To examine the effect of phase speed (c) on the output Z_{12} maps, we produced three sets of maps using $c = 12, 24$, and 42 km d^{-1} . Then we determined the mean and standard deviation of the differences between the mapped Z_{12} fields. For the 18 Z_{12} maps examined, there were only small differences between the maps generated with $c = 12 \text{ km d}^{-1}$ and $c = 24 \text{ km d}^{-1}$. The mean difference was less than one meter and the standard deviation was under 3 m. Not surprisingly, the largest differences occurred between the maps produced with $c = 12 \text{ km d}^{-1}$ and $c = 42 \text{ km d}^{-1}$. But even then, the mean difference between the 18 OA maps was less than 4 m and the standard deviation was about 7 m. In all cases, the largest differences (about 30 m) occurred in

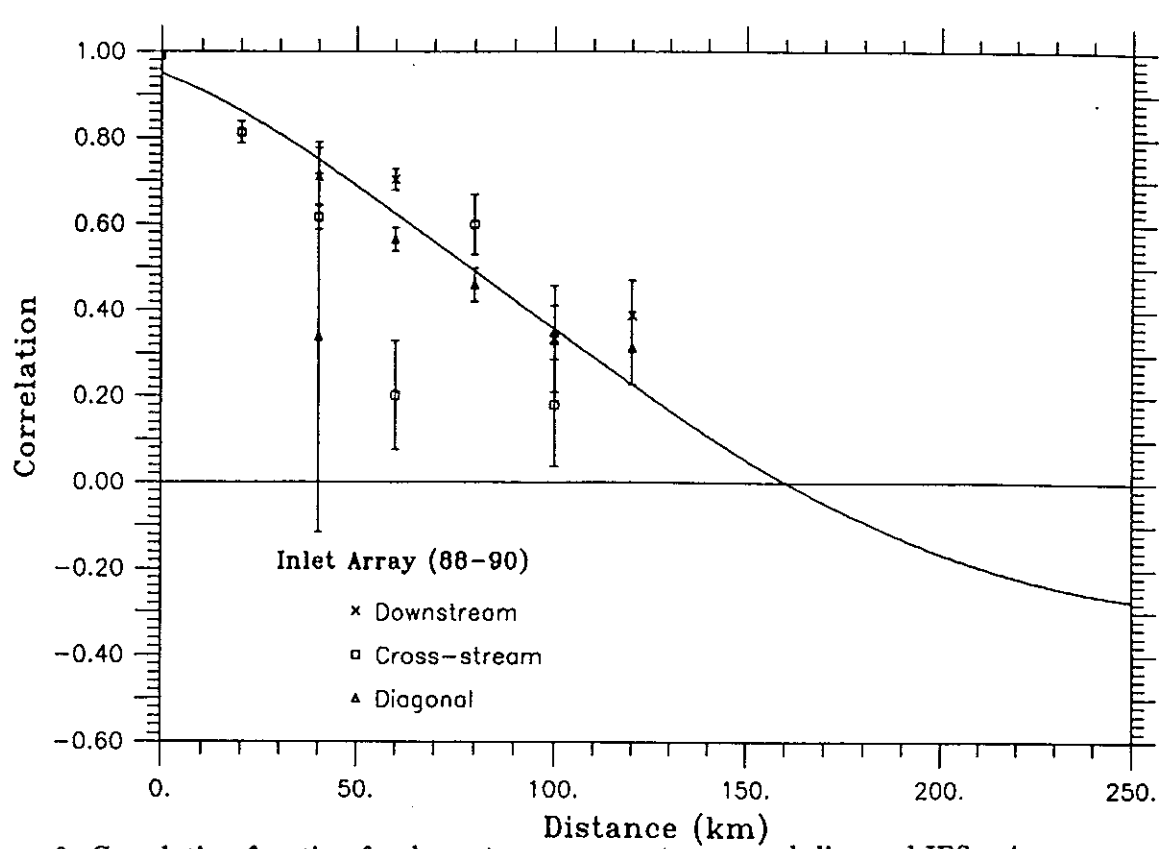


Figure 3: Correlation function for downstream, cross-stream, and diagonal IES pairs versus radial distance. The solid curve is the analytic function $\rho(r)$.

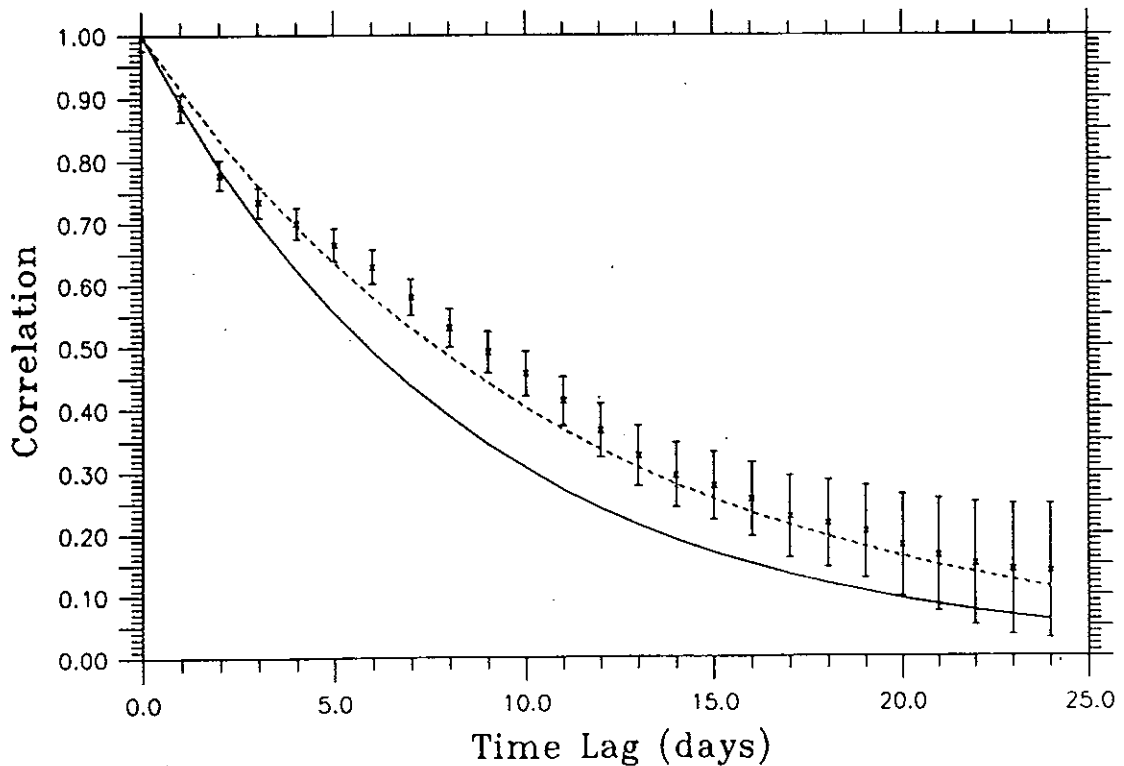


Figure 4: Average auto-correlations for 19 IESs versus lag time. The solid and dashed curves are the best fits of the analytic function $\rho(t')$ to the correlations at shorter and longer time lags, respectively.

the extrapolated portions of the mapping region. Since the average differences between the maps are quite small compared with the mapping accuracy of 47 m, the choice for phase speed is not crucial to the quality of the output maps. We chose a mid-range phase speed of $c = 24 \text{ km d}^{-1}$ (cf. Equation [1]) to produce the Inlet Array OA maps.

Finally we combined Equations [2] and [3] to obtain the full analytic expression for the correlation function of the thermocline depth in the Inlet Array:

$$\rho_{\text{Inlet}}(x', y', t') = F_0 \exp(-a_1 t') \cos\left(\frac{a_2 t' \pi}{180}\right) \exp\left(\frac{-r}{A}\right) \cos\left(\frac{\pi r}{2B}\right) \quad (4)$$

where r is defined in Equation [1]. Figure 2 shows ρ_{Inlet} in plan view for the same time lags as the observed correlations.

3.2 Mean Z_{12} and STD Fields

Watts *et al.* [1989] showed that the quality of the OA maps is influenced most strongly by the choice of mean Z_{12} field that is removed from the observations prior to performing the objective analysis (and restored later). They found that the best accuracy was obtained with a time-averaged mean field. In the past we determined the temporal mean field by fitting a third-order polynomial to the deployment-long average Z_{12} values obtained at the IES sites. Unfortunately, this method tended to give unrealistic values along the edges of the mapping region and we were required to tweak the inputs to obtain a smooth field. Thus for the Inlet Array, we elected to determine the mean Z_{12} field manually. First, we combined the Z_{12} averages for all IES sites from the three deployment periods onto a single map. Next, we picked, by eye, the relative cross-stream positions of several thermocline depths along the upstream and downstream edges of the mapping region. Then we used a cubic spline to interpolate between these positions to obtain Z_{12} values at 20 km intervals along the edges. Finally, we linearly interpolated between the two edges to fill in the remainder of the grid. The mean Z_{12} field chosen is shown in Figure 5.

The standard deviations of the 28 Inlet Array IESs varied systematically with the mean Z_{12} value, related to the proximity of the IES sites to the mean location of the steeply sloping thermocline. This relationship is shown in Figure 6. We approximated the STD field by a Gaussian function of the form

$$\sigma_{\text{Inlet}} = D + C e^{-\Upsilon}$$

where $D = 16 \text{ m}$ and $C = 80 \text{ m}$. The exponent is defined as $\Upsilon = \left[\frac{\overline{Z}_{12}(x, y) - A}{B} \right]^2$, where $A = 470 \text{ m}$ and $B = 270 \text{ m}$. The STD field for the Inlet Array is shown in Figure 5 along with the associated

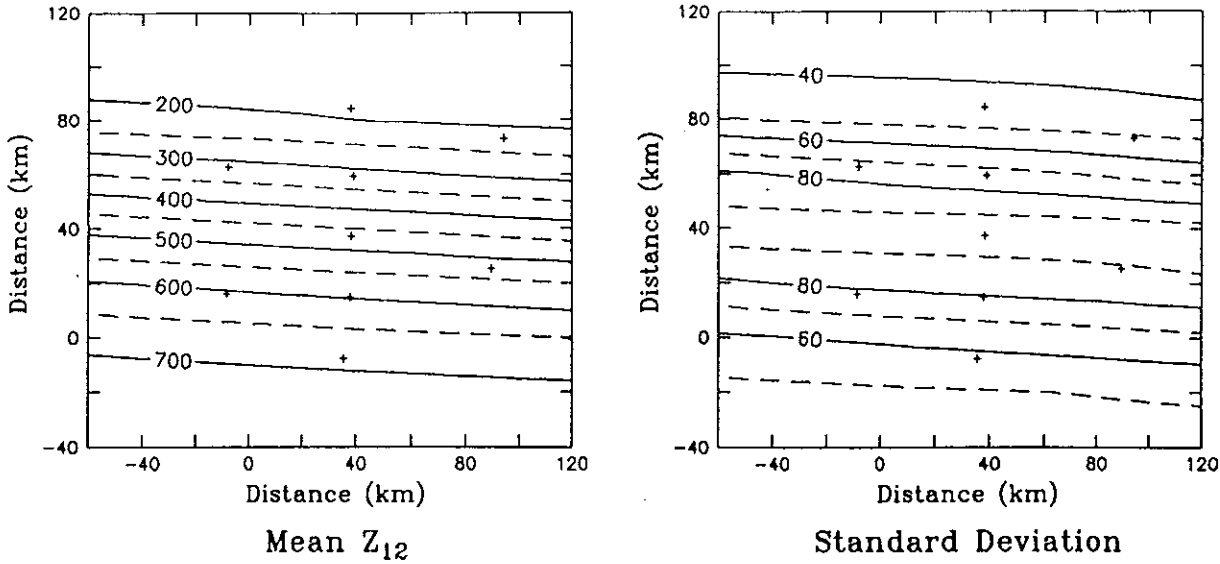


Figure 5: Mean Z_{12} (left) and standard deviation (right) fields are contoured in plan view. Contour intervals are 50 m for the mean field and 10 m for the standard deviation field. IES sites are indicated by the + marks. Axis tick marks are at 20 km intervals.

mean Z_{12} field.

3.3 Construction of the Z_{12} Maps

The objective analysis was performed on the “perturbation” IES Z_{12} records (i.e., the means were removed and the standard deviations normalized). The correlation function ρ_{Inlet} was computed using Equation [4] each time a (x', y', t') triplet was specified. This resulted in a smooth, continuously changing function which produced better quality output maps than the lookup table method that we had used previously. Data restrictions were controlled by several user-specified parameters, summarized in Table 4.

Table 4: User-specified control parameters for OA mapping.

Parameter	Specification
N	6 points
r_{max}	120 km
t'_{max}	± 1 day
ϵ	0.05
c	24 km d^{-1}

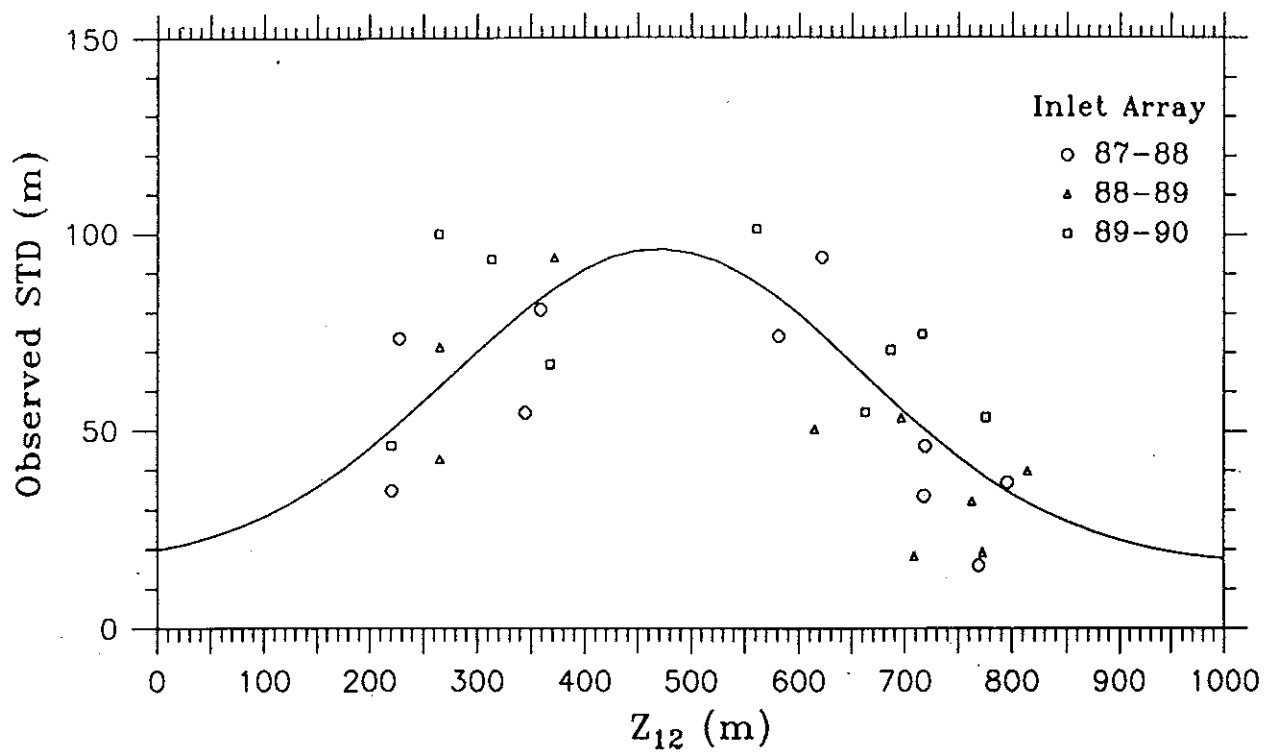


Figure 6: Observed standard deviations for 28 IESs during three deployment periods from 1987–1990 versus mean Z_{12} depth. The solid curve is the analytic function σ_{Inlet} .

The output of the objective mapping is the perturbation field on a full grid of points, with 20 km spacing. The perturbations were converted to thermocline depths by renormalizing by the STD field and restoring the mean Z_{12} field. Subsequently the Z_{12} fields were smoothed using a second-order Shapiro filter to remove small-scale ($\sim 2\Delta x$ waves) features and the outermost grid points were dropped. The final size of the Z_{12} grid for the Inlet Array was 140 km by 120 km (8 by 7 grid points). From June 1988 to August 1989, when no data were obtained along the A line, the mapping region was shortened to 80 km by 120 km (5 by 7 points).

4 Estimated Error Fields

Statistical estimates (percent standard deviation) of the accuracy of the output Z_{12} fields were produced during the objective analysis. The error associated with each output grid point depends only on the locations, in space and time, of the observations and the correlation function. The error is independent of the measurements themselves. Thus, the same error field applies for all daily OA maps produced from a given array of instruments.

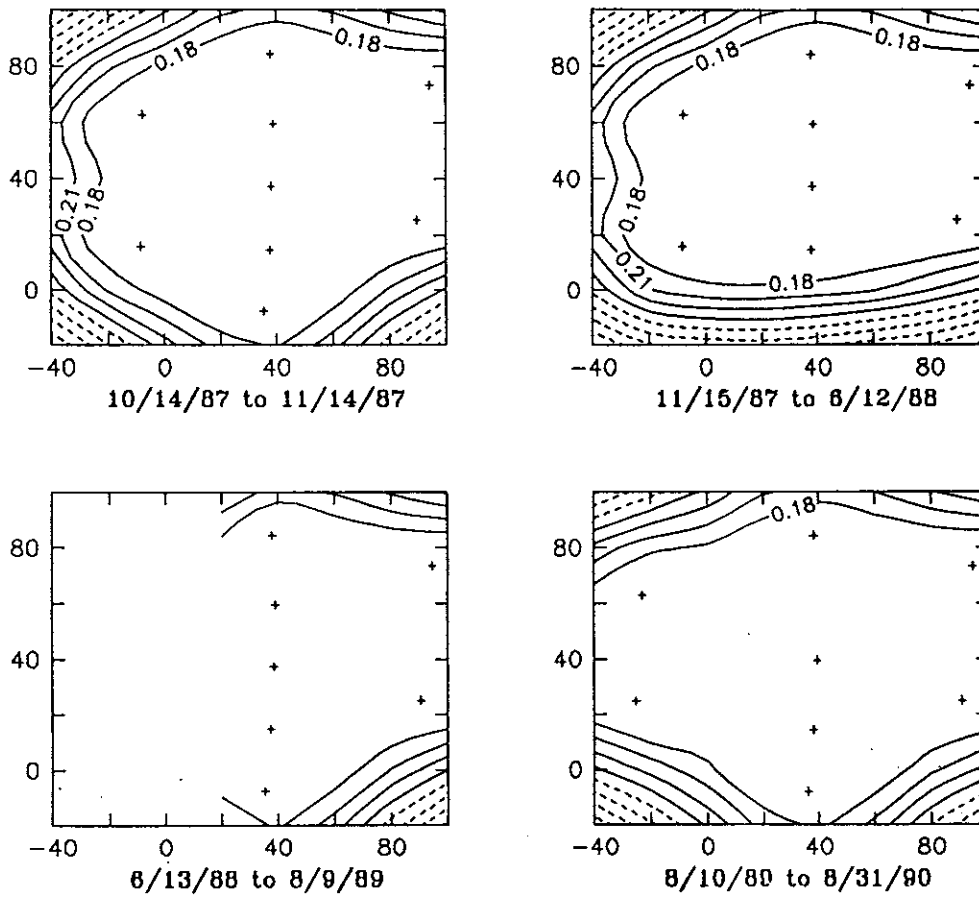


Figure 7: Estimated error (percent STD) fields for four different array configurations apply to the Z_{12} fields for the dates shown. Errors greater than 0.18 are contoured at intervals of 0.03. For clarity, errors between 0.30 and 0.48 are indicated by dashed contours. IES sites are shown by the '+' marks. The common plotting grid was chosen for the four arrays out of convenience.

During the 34-month-long deployment period, there were four different array configurations due to the loss or repositioning of several IESs. The corresponding error fields, along with the IES sites, are shown in Figure 7. The four error fields are basically the same because the close spacing of the IESs gave rise to low errors throughout the mapping region even when isolated instruments were

lost. The errors are low near the IES sites and increase with distance from those sites. During the cruises to cycle the array (May-June 1989, May-June 1990, August 1989, and August 1990), the array configurations changed frequently while the IESs were being recovered and redeployed. During these periods, the actual error fields associated with the Z_{12} maps changed daily. These 'transitional' error fields are not shown in Figure 7, but areas of higher error are indicated on the individual objective maps.

We use the estimated error fields to mask out portions of the OA maps where the map quality is predicted to be poor. On the Z_{12} maps, regions with predicted error 30–48% are shaded by dashed contours, and larger errors are indicated by solid contours. Based upon analogies drawn from Watts *et al.* [1989], our preliminary estimate is that the dimensional uncertainty of the Z_{12} field is less than 50 m within the mapping region for which the predicted error is less than 30%. We have used 50 m as the contouring interval for the subsequent maps of the Z_{12} field.

5 Average Z_{12} Maps

To produce average maps of the Z_{12} field in the Inlet Array, we summed the maps (presented in the following section) by grid point and then divided by the number of maps. We averaged two ways, by deployment period and by season. The deployment-long average Z_{12} fields for the three periods are shown in Figure 8 with the averaging dates indicated below each map. Next, we divided the maps into twelve groups of approximately 90 days, corresponding to the four seasons. Two of the groups were for shorter time periods due to the timing of the start and end dates; the group for October-December 1987 consisted of 81 days and the July-September 1990 group of only 63 days. Average Z_{12} maps were produced for each group and these are shown in Figure 9.

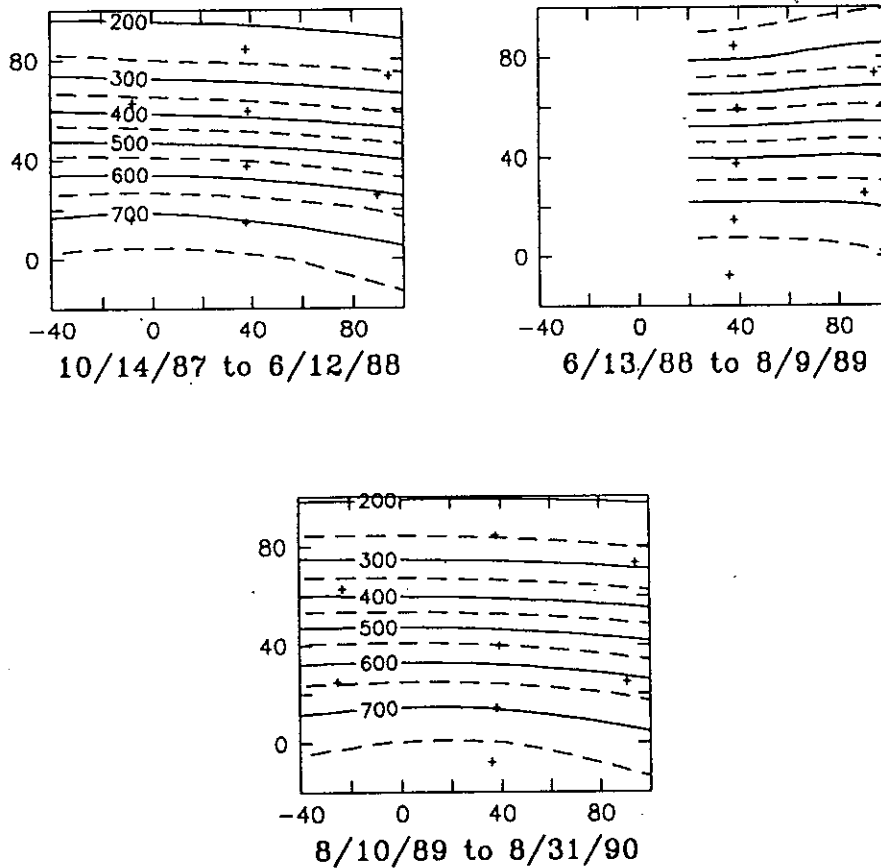


Figure 8: Z_{12} fields averaged, by grid points, for the three deployment periods. Averaging periods are indicated below each map. Depth contours are in meters. Distances on the axes are in kilometers.

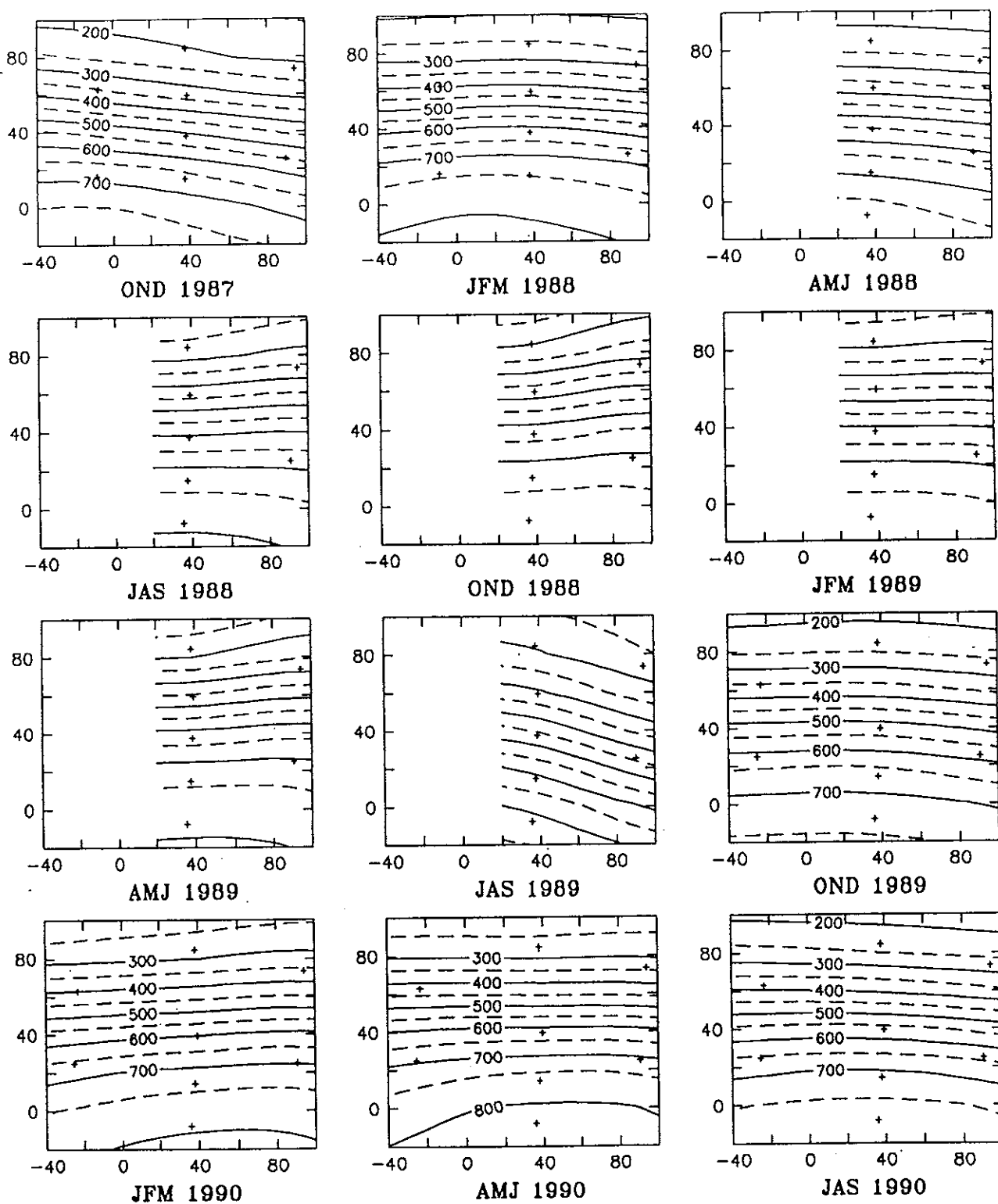


Figure 9: Seasonally-averaged Z_{12} fields. The months and year are indicated below each frame. Depth contours are in meters. Distances on the axes are in kilometers.

6 Daily Z_{12} Maps for the Inlet Array

Objective maps of the Gulf Stream thermal field were produced at daily intervals for October 14, 1987 through August 31, 1990. The maps are shown for 1200 UT on the dates indicated below each frame.

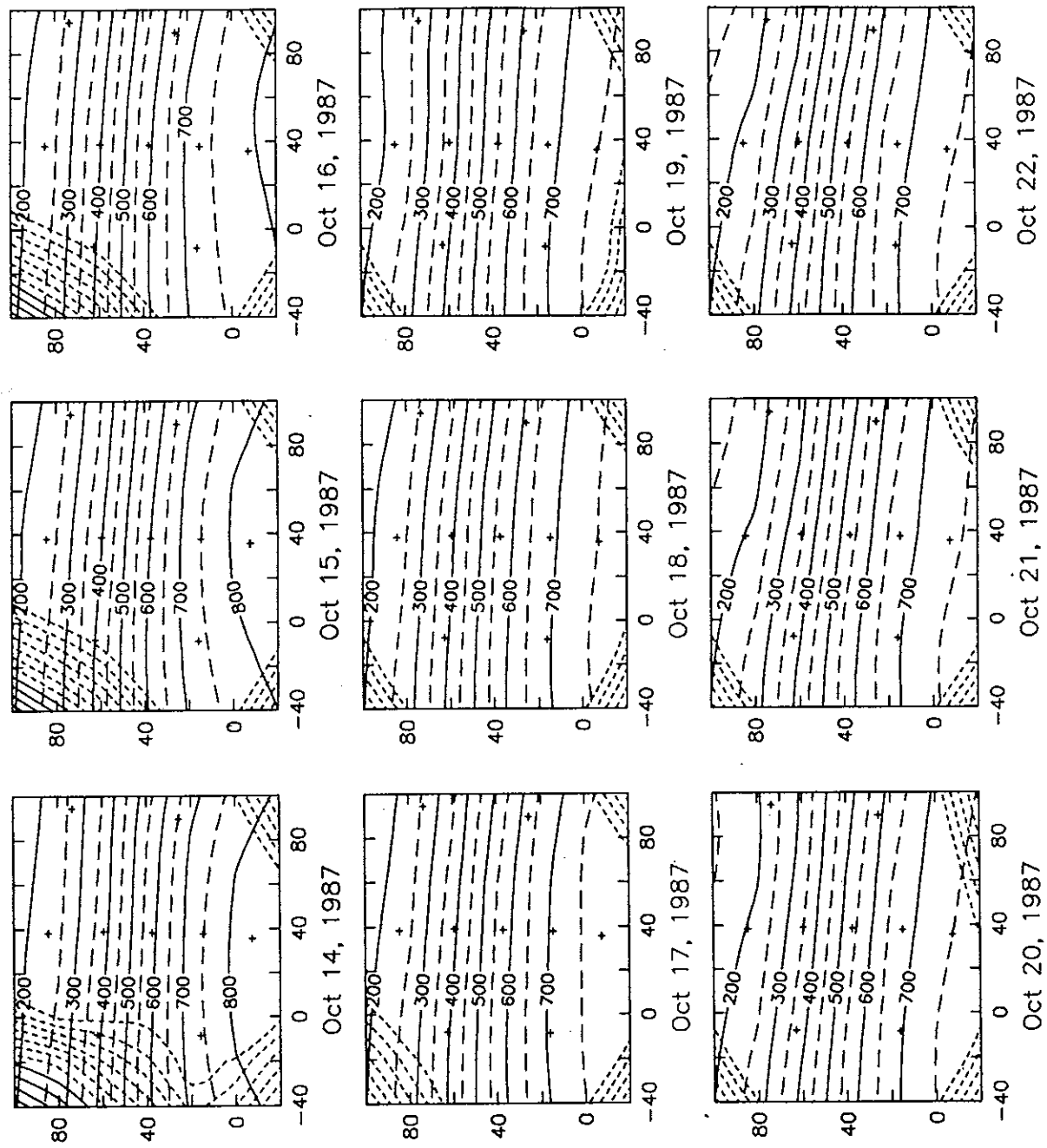
The frames correspond to the boxed region shown in Figure 1. The actual IES sites are indicated by the '+' marks and the positions are listed in Tables 1-3. Each IES position was converted to grid coordinates using scale factors of 111 km per degree latitude and 86.263 km per degree longitude; distances were referenced to the grid origin at 35°N, 74°W. Subsequently the grid was rotated 50° so that the base was oriented 040°T. This rotation was done prior to running the objective analysis for plotting convenience, not as a requirement of the OA technique. The latitude-longitude positions of the grid corners are listed in Table 5.

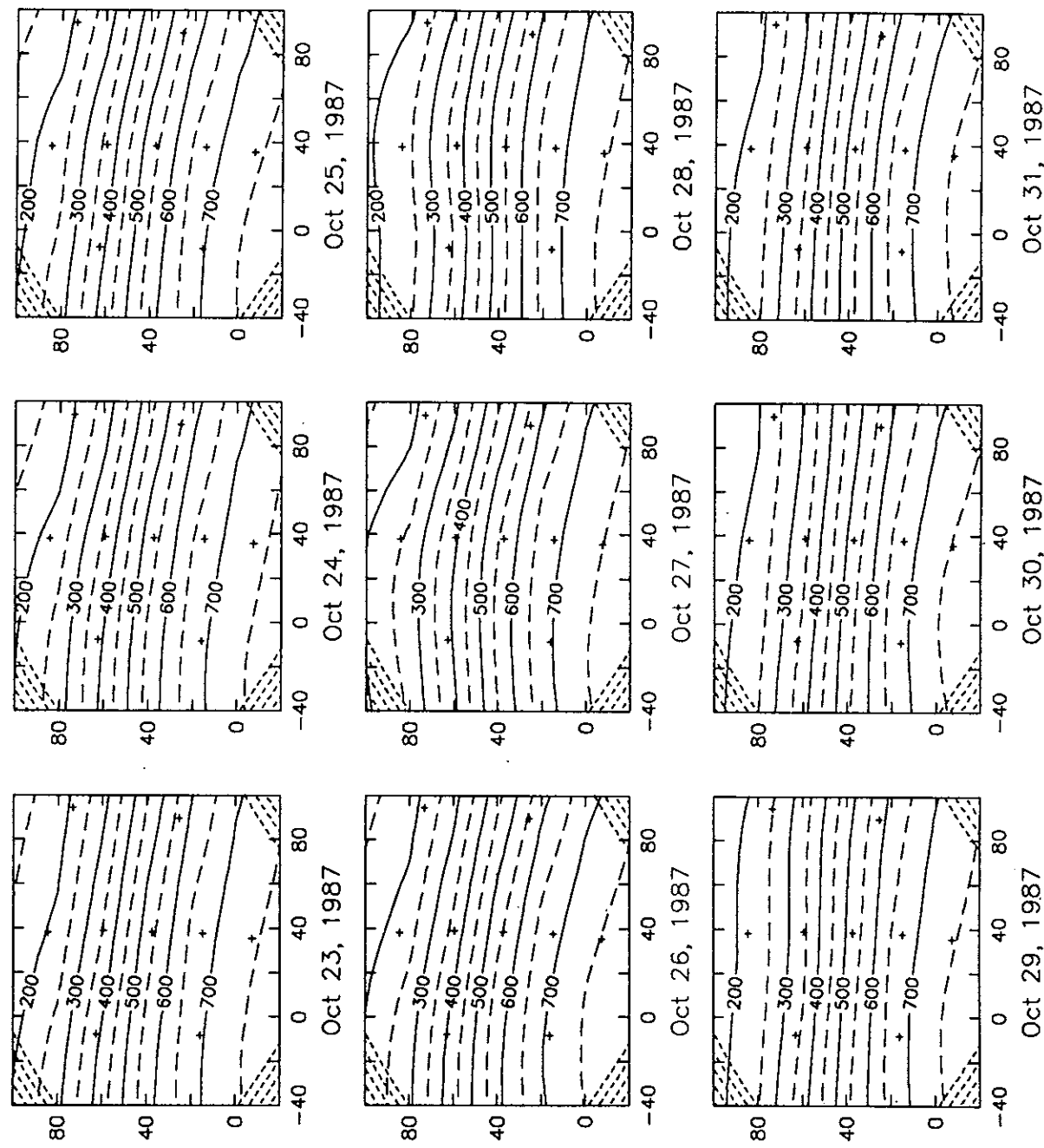
The Z_{12} field is contoured at 50 m intervals. Extrapolated regions of the OA maps have been masked out where the estimated errors are high; errors of 30-48% are indicated by dashed contours and higher errors by solid contours. The contour interval of the estimated errors is 3%.

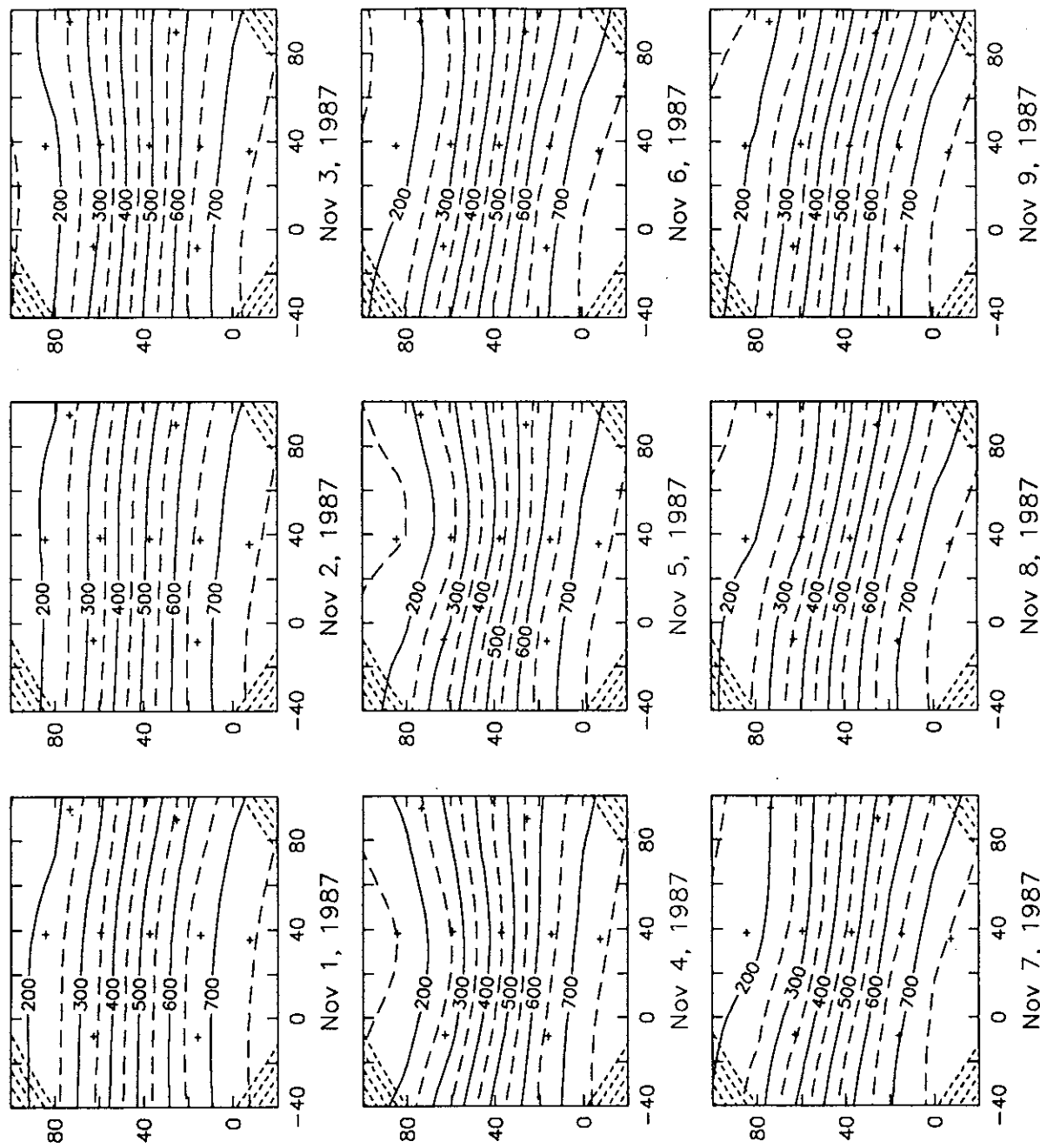
Table 5: Corner Positions of Mapping Regions

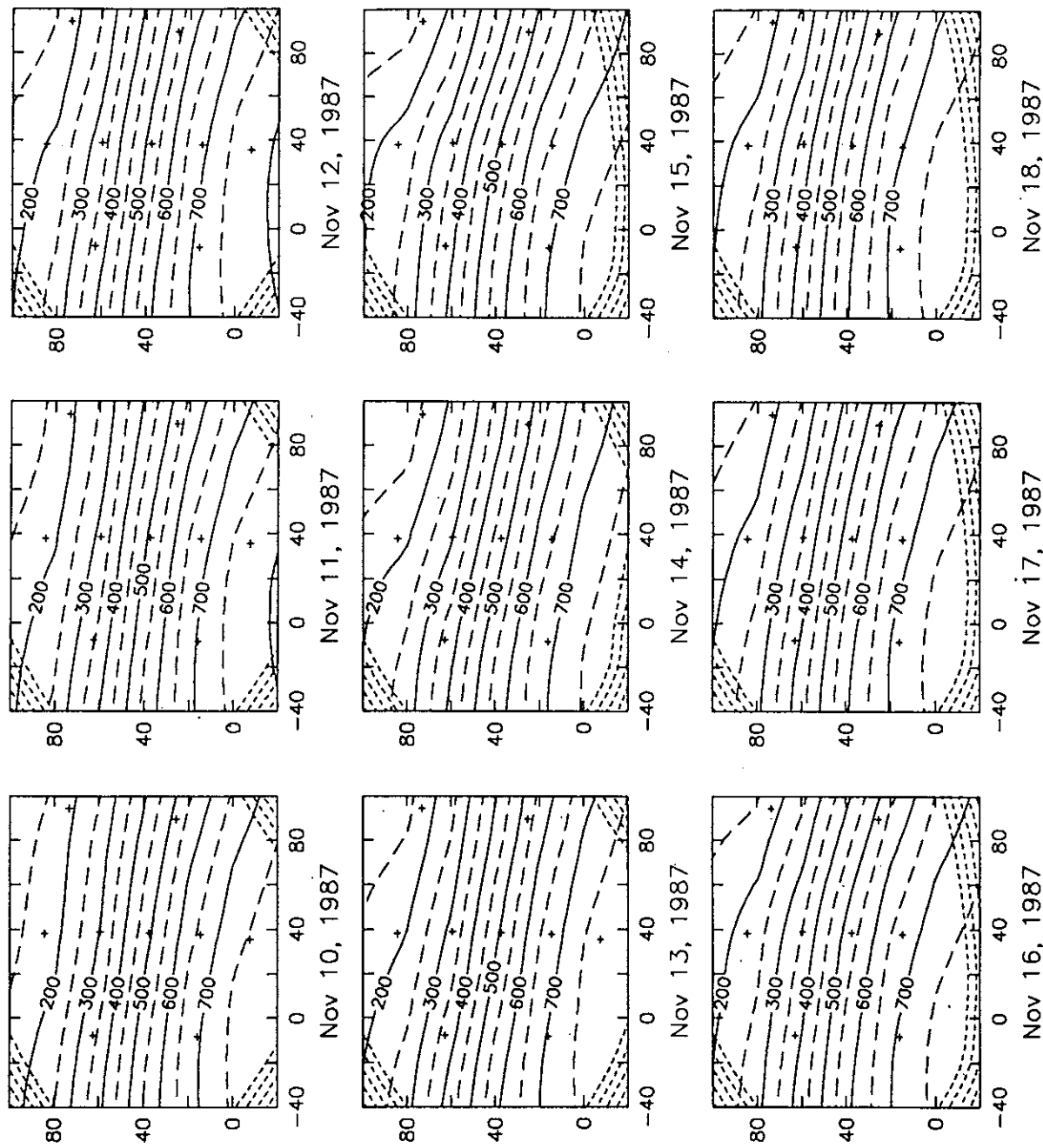
Map Dates: 14 October 1987 to 12 June 1988 and 10 August 1989 to 31 August 1990				
Corner	x (km)	y (km)	Latitude (N)	Longitude (W)
Upper Left	-40	+100	35° 18.18	75° 11.17
Lower Left	-40	-20	34° 36.49	74° 07.23
Upper Right	+100	+100	36° 16.15	74° 08.57
Lower Right	+100	-20	35° 34.46	73° 04.63

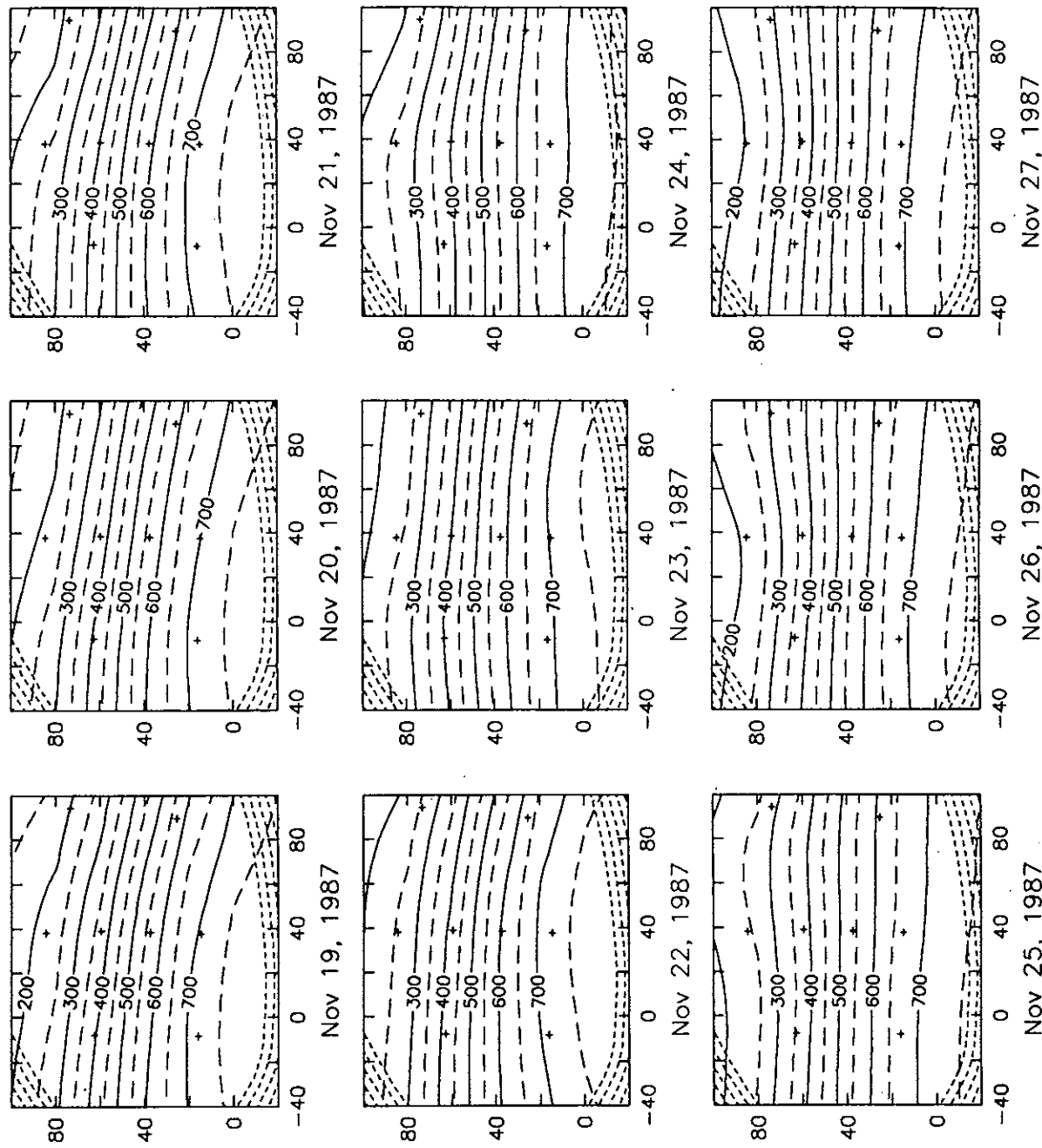
Map Dates: 13 June 1988 to 9 August 1989				
Corner	x (km)	y (km)	Latitude (N)	Longitude (W)
Upper Left	+20	100	35° 43.03	74° 44.34
Lower Left	+20	-20	35° 01.33	73° 40.40
Upper Right	+100	+100	36° 16.15	74° 08.57
Lower Right	+100	-20	35° 34.46	73° 04.63

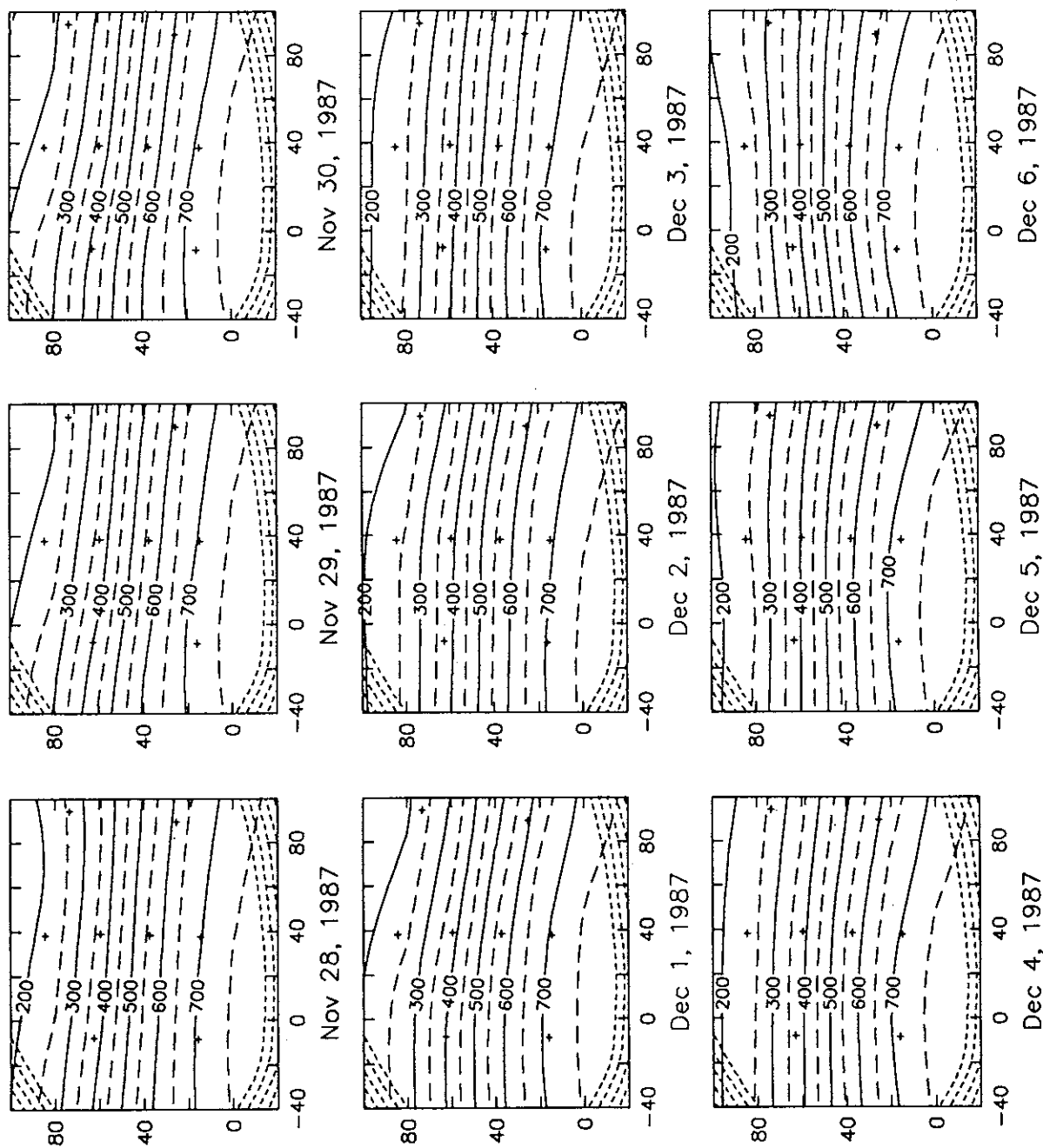


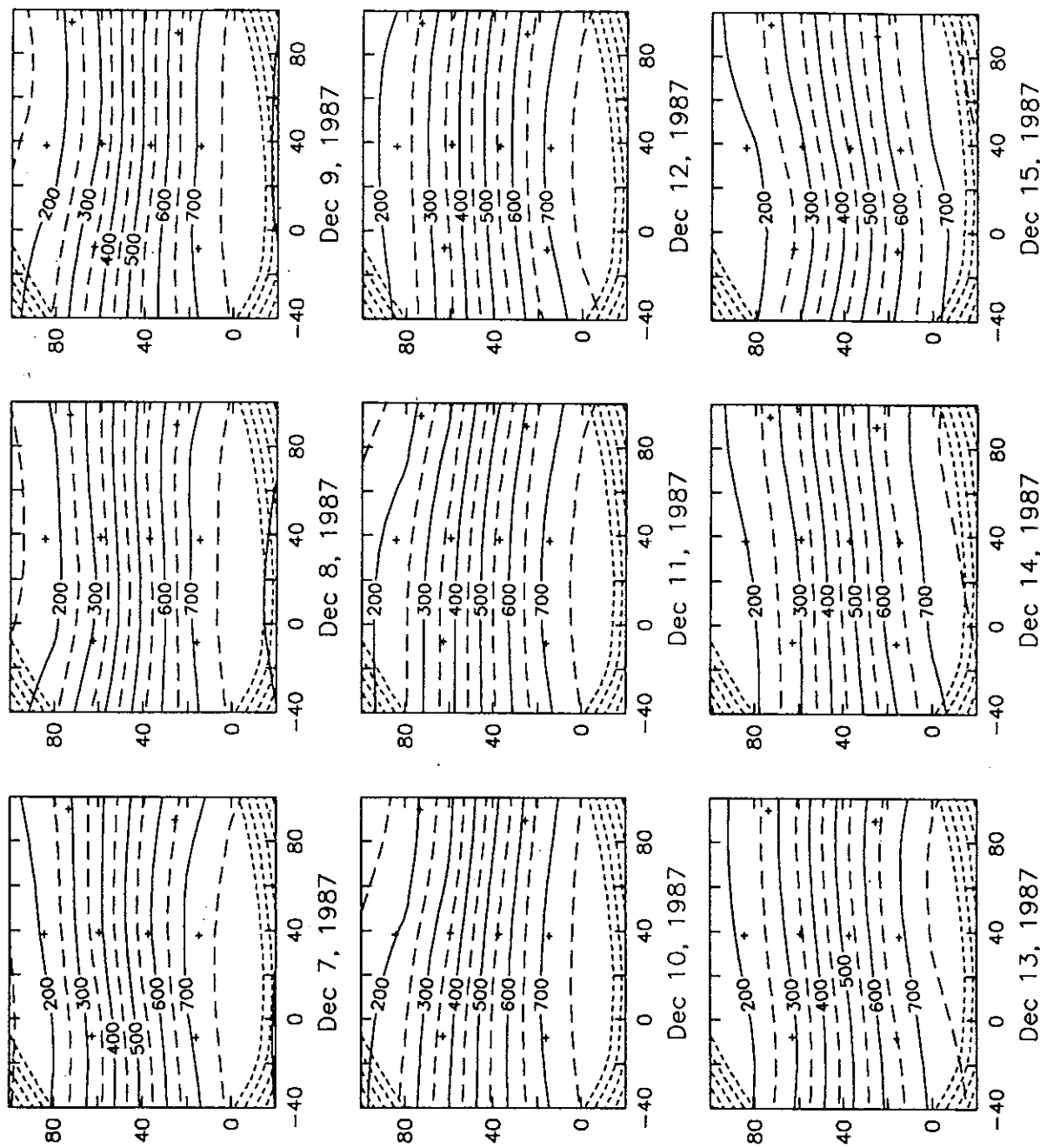


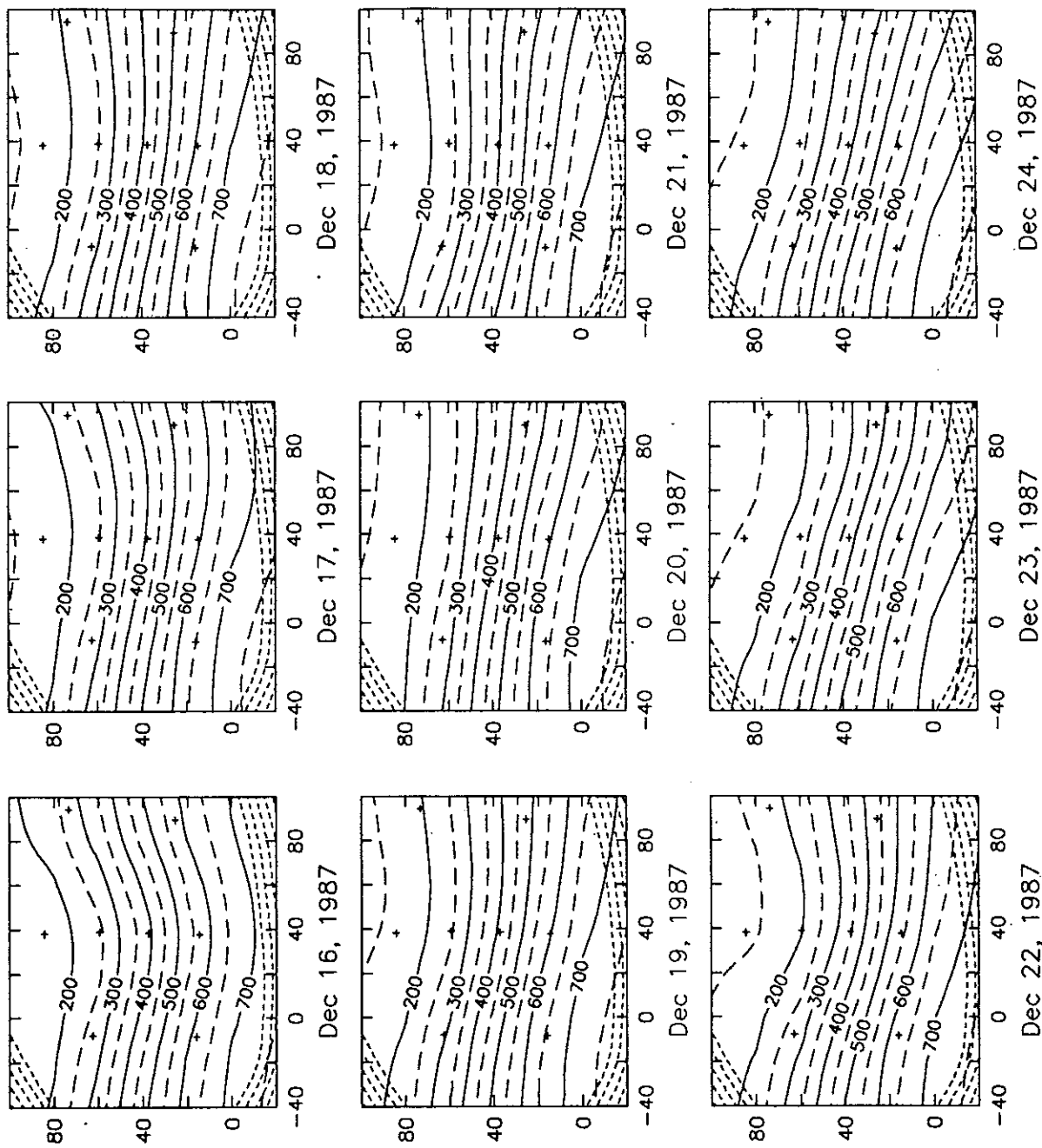


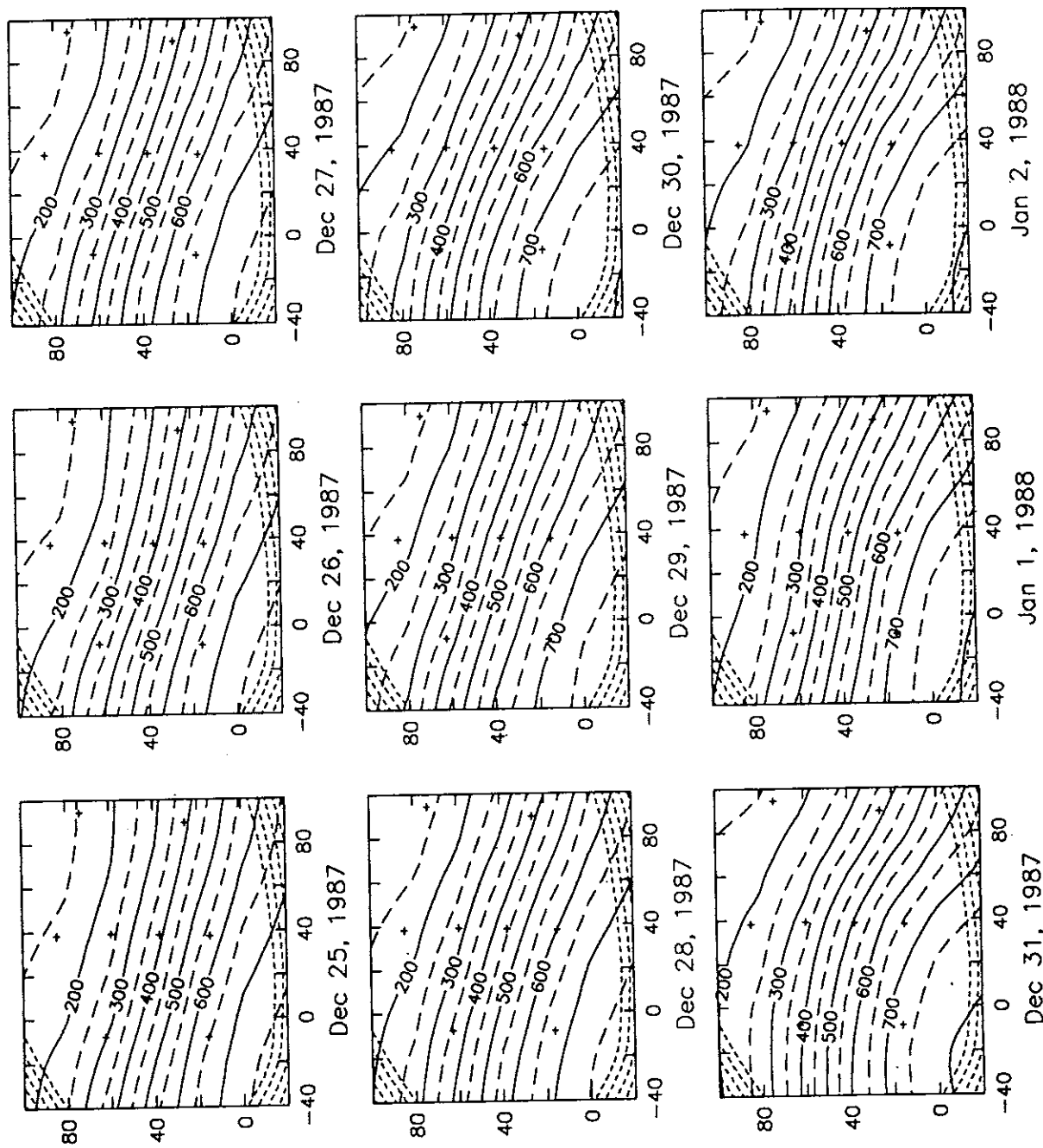


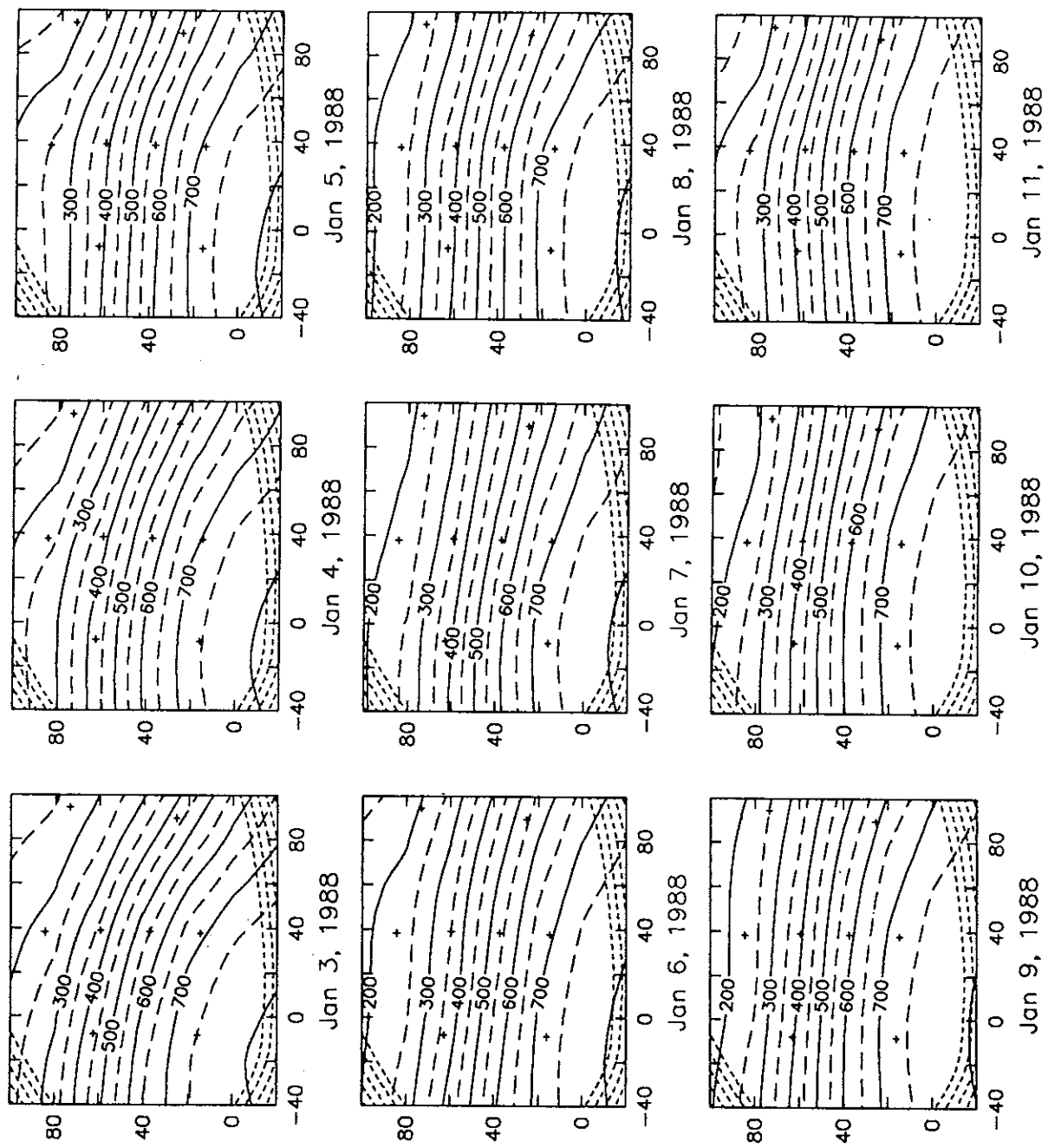


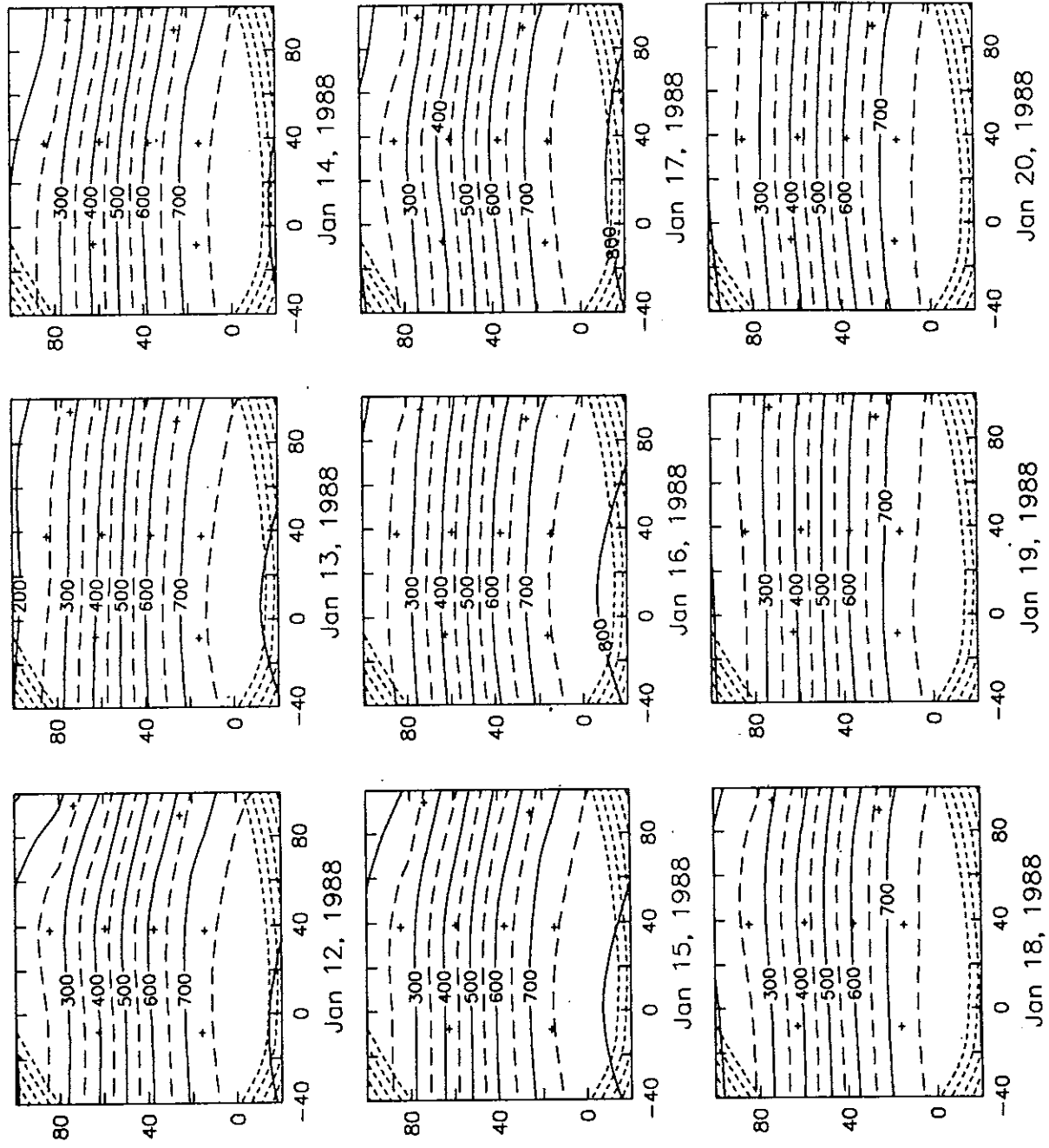


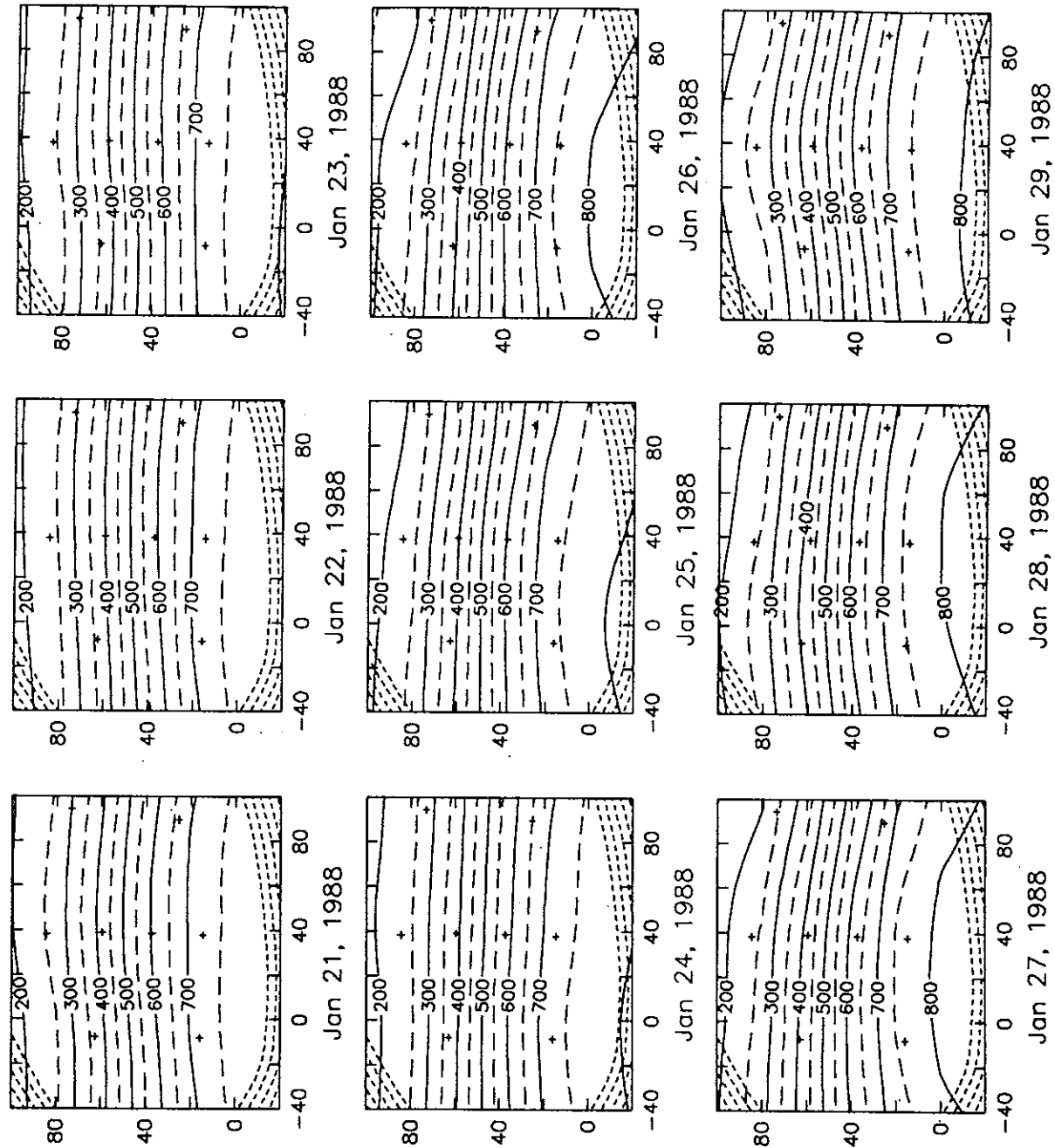


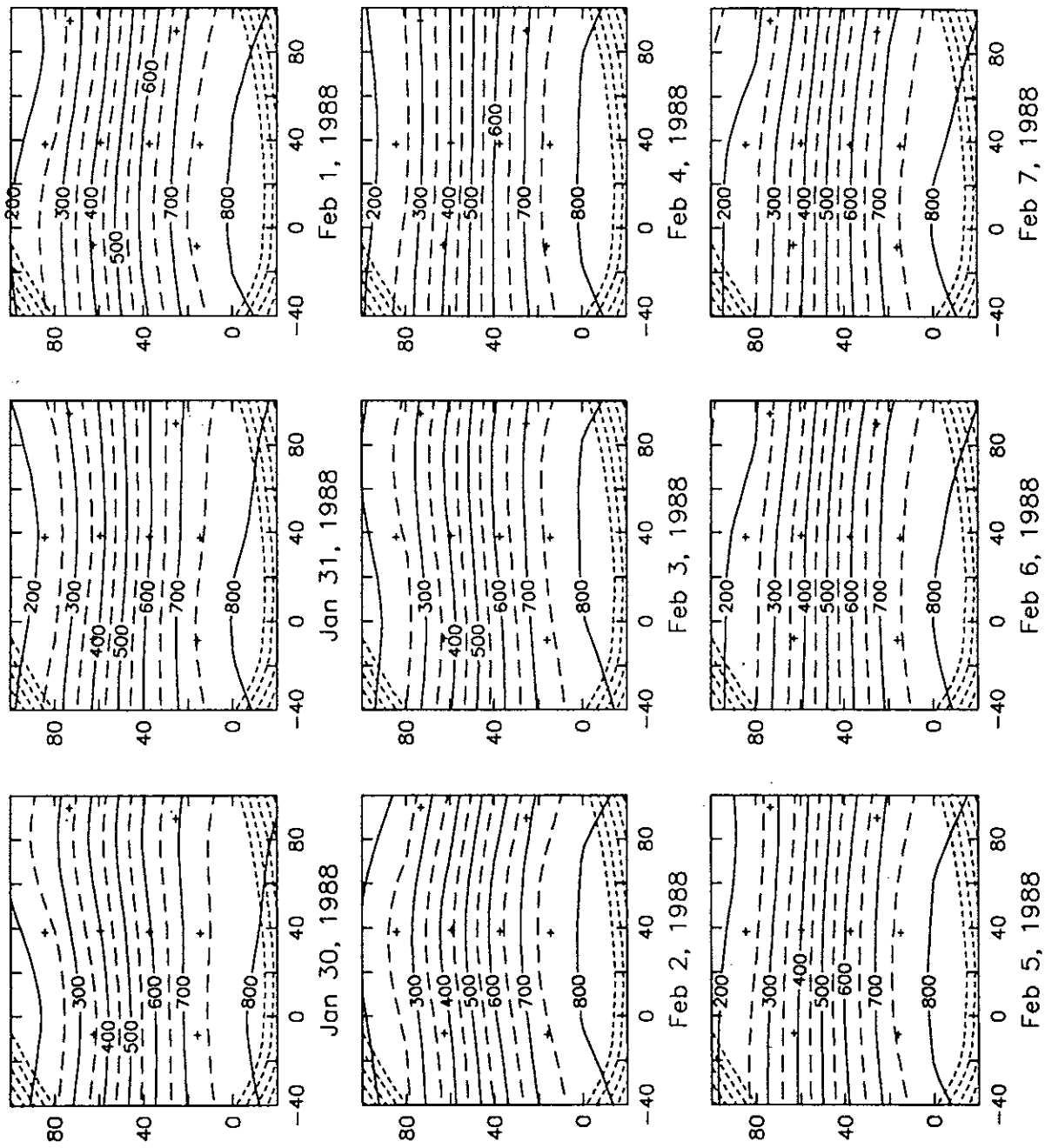


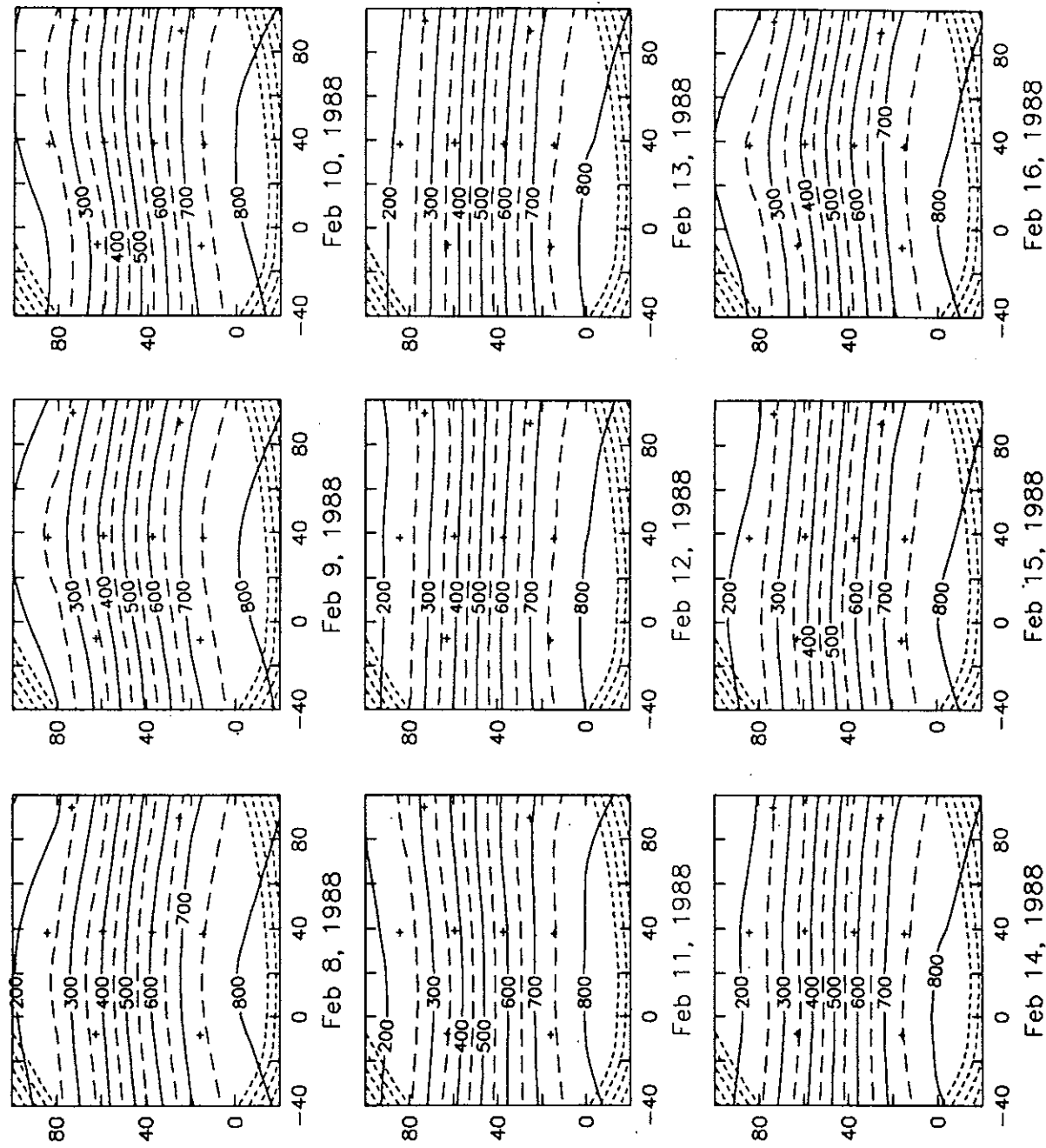


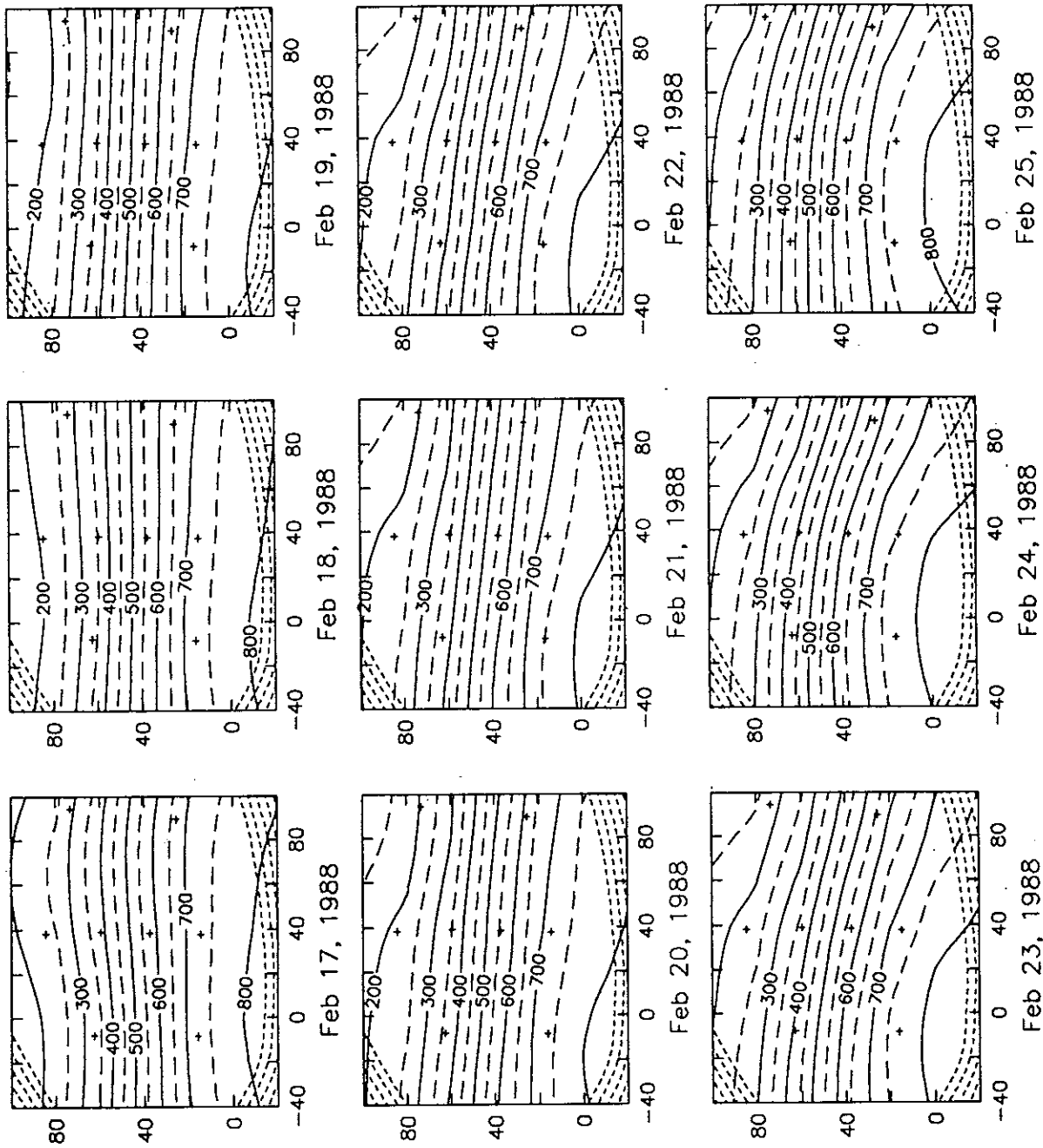


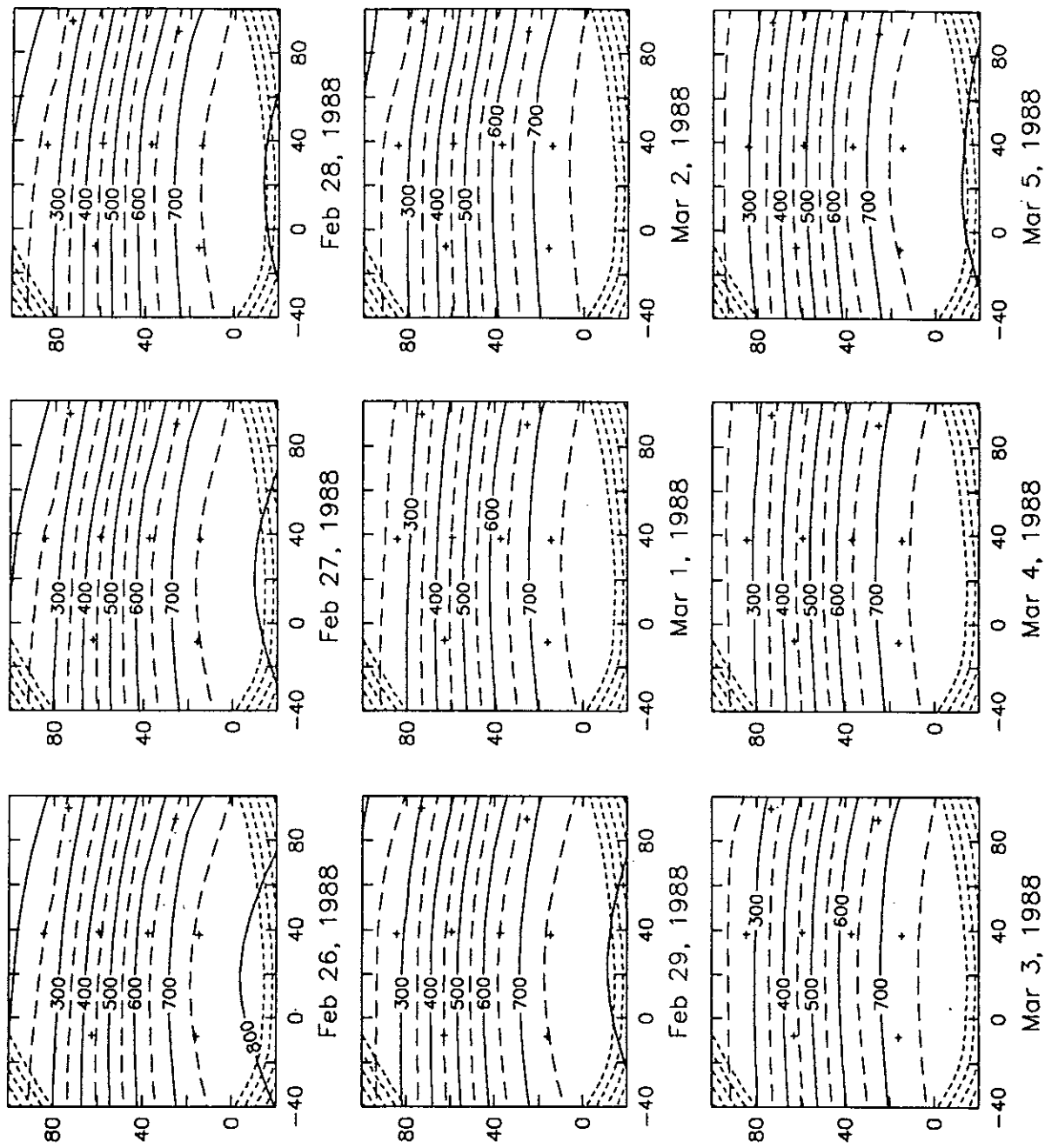


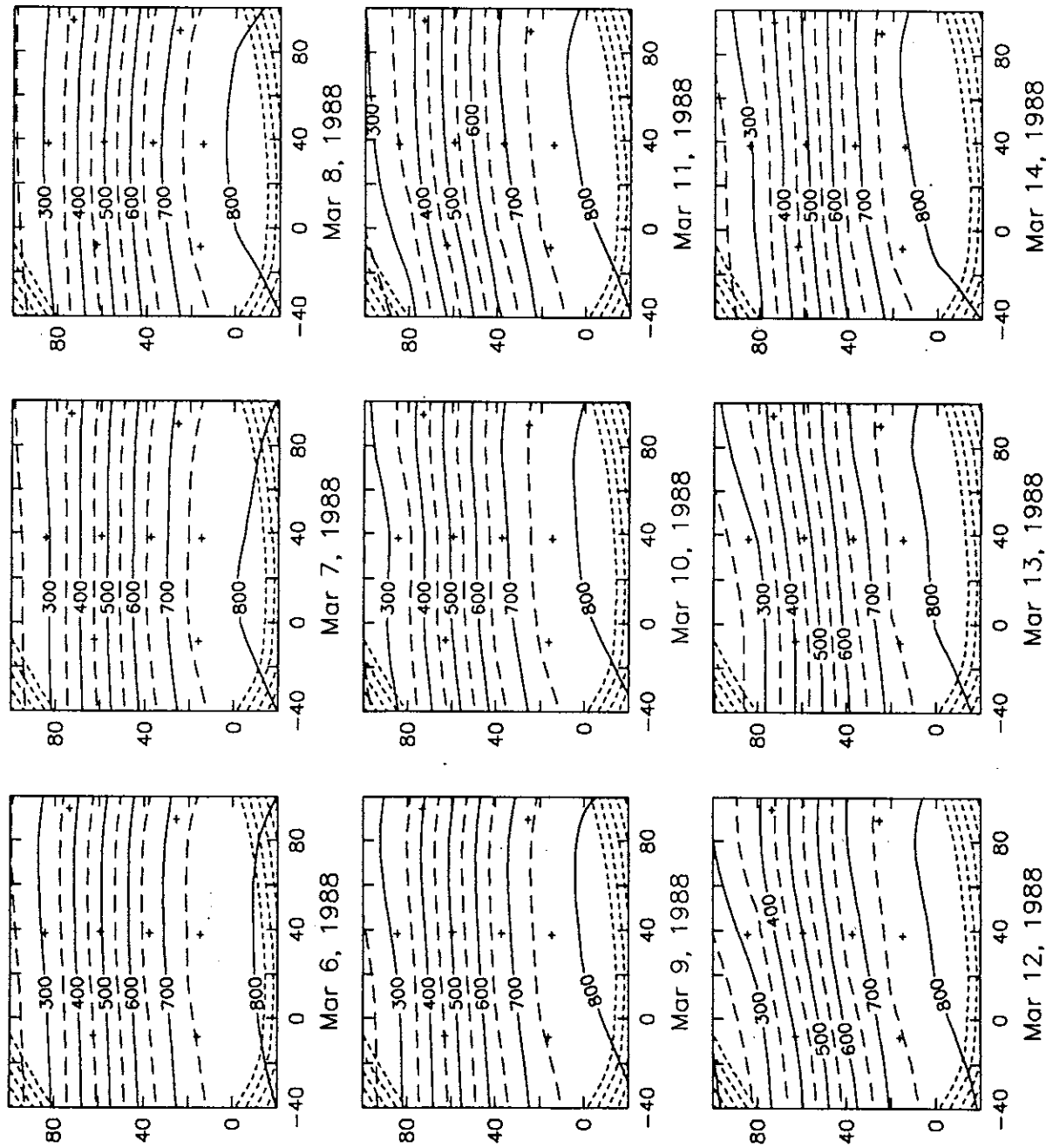


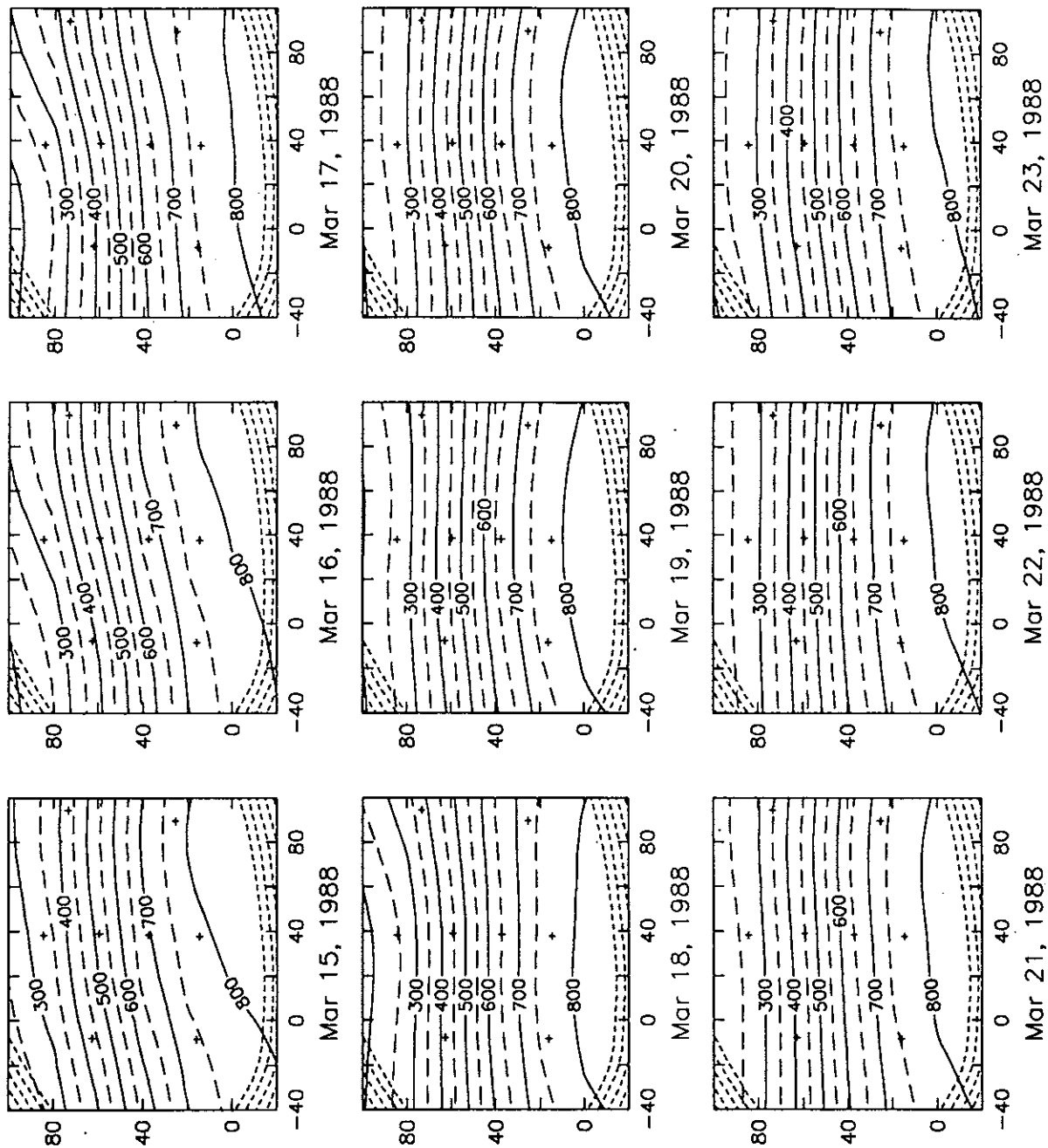


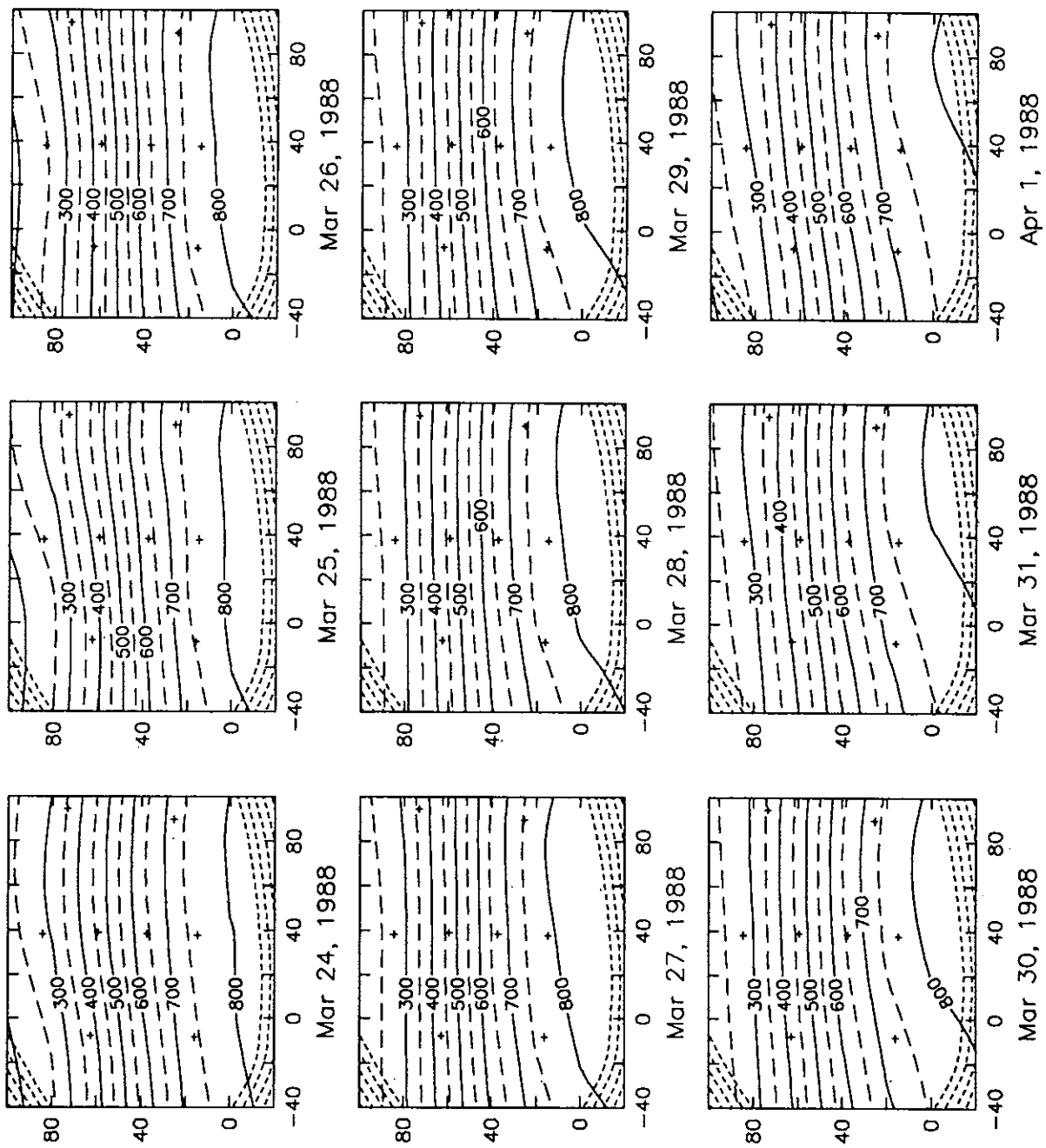


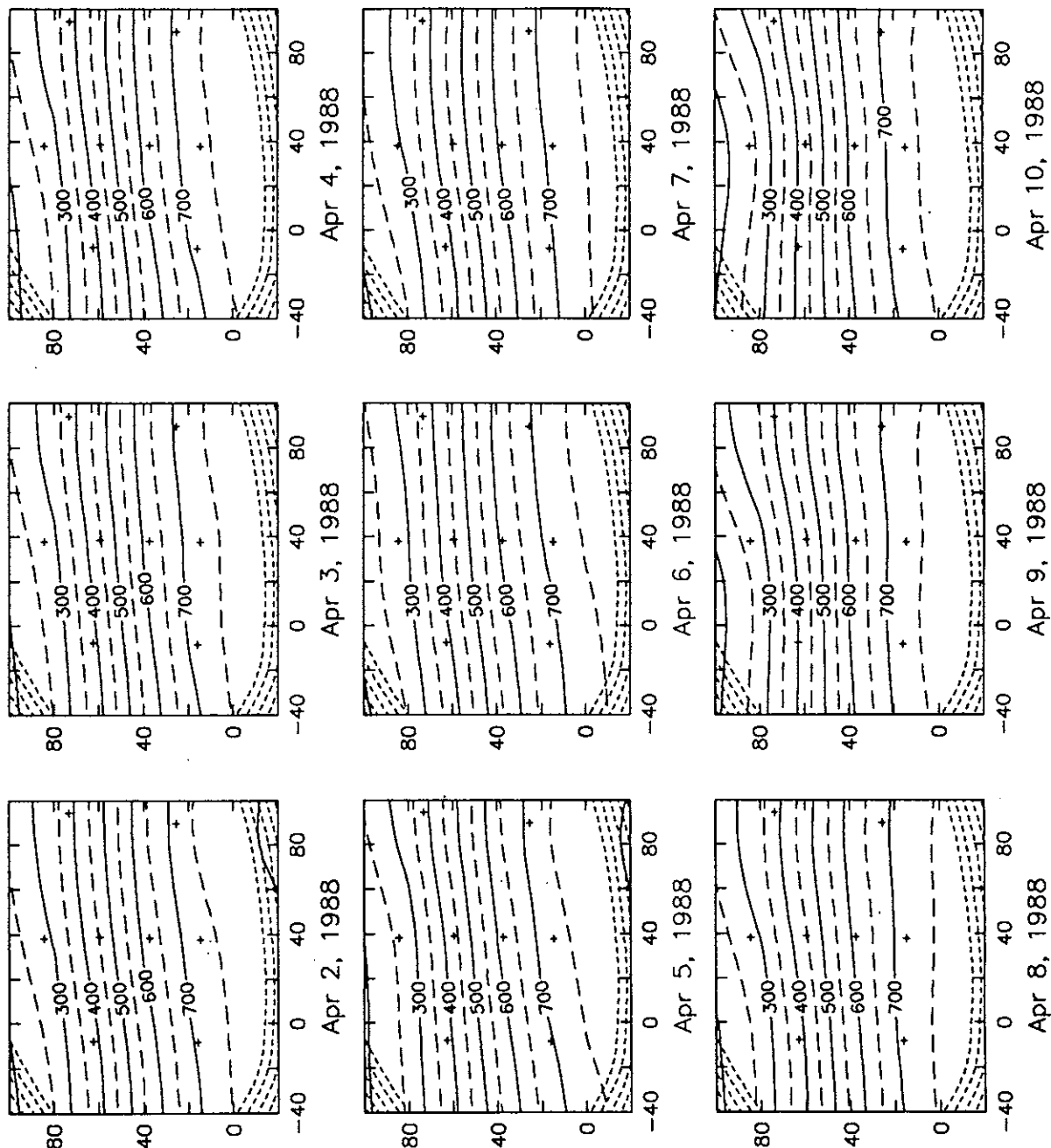


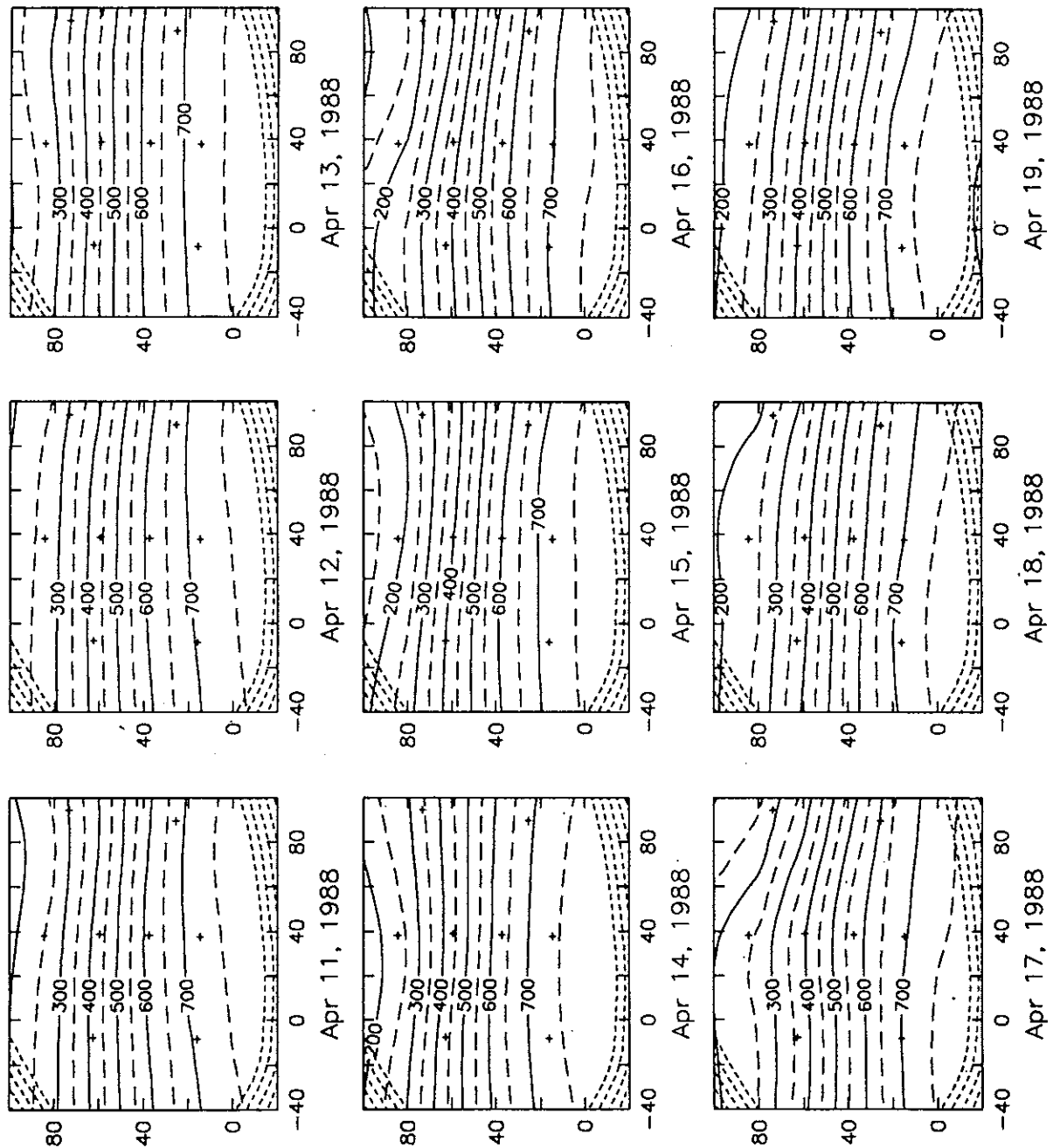


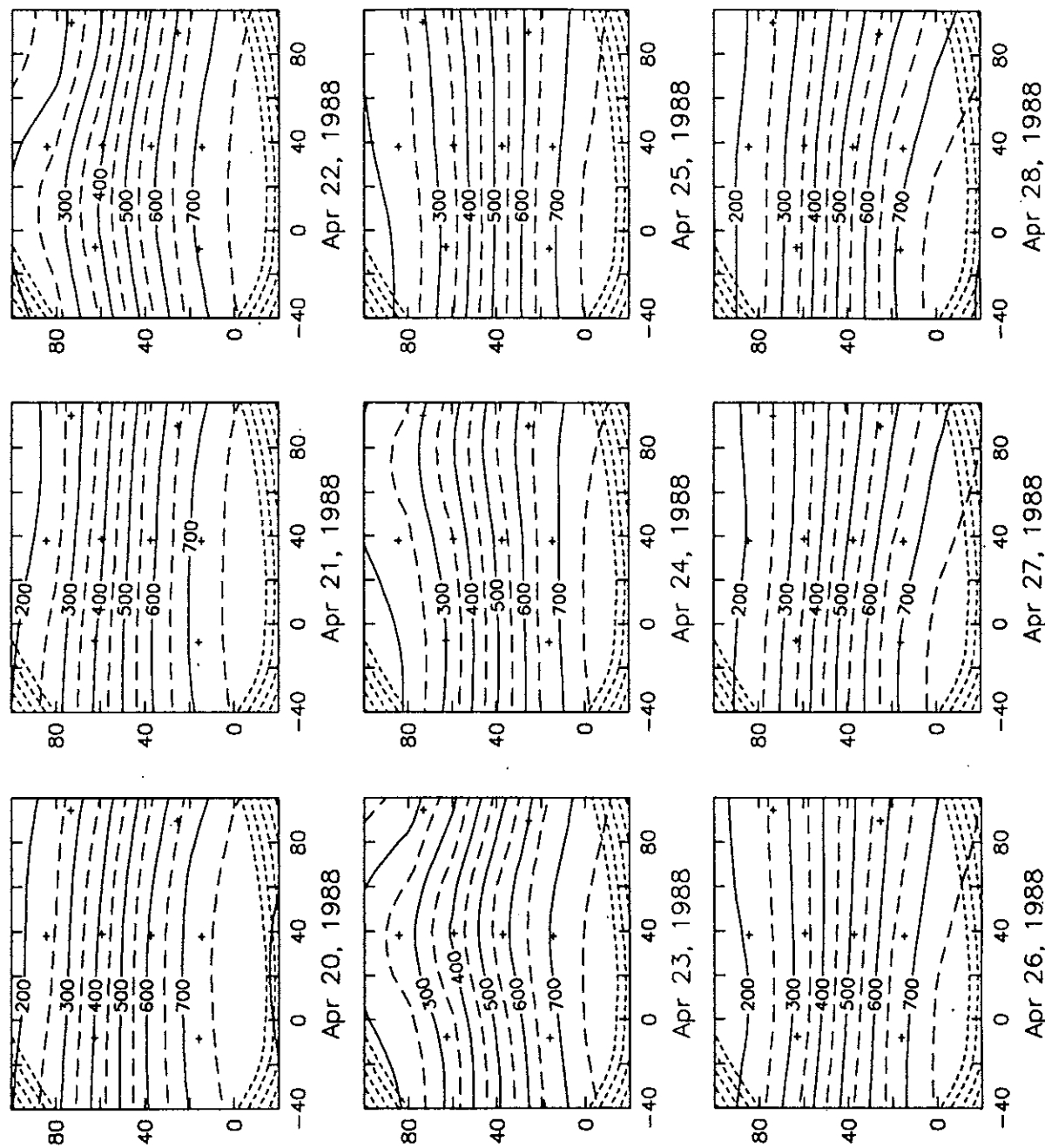


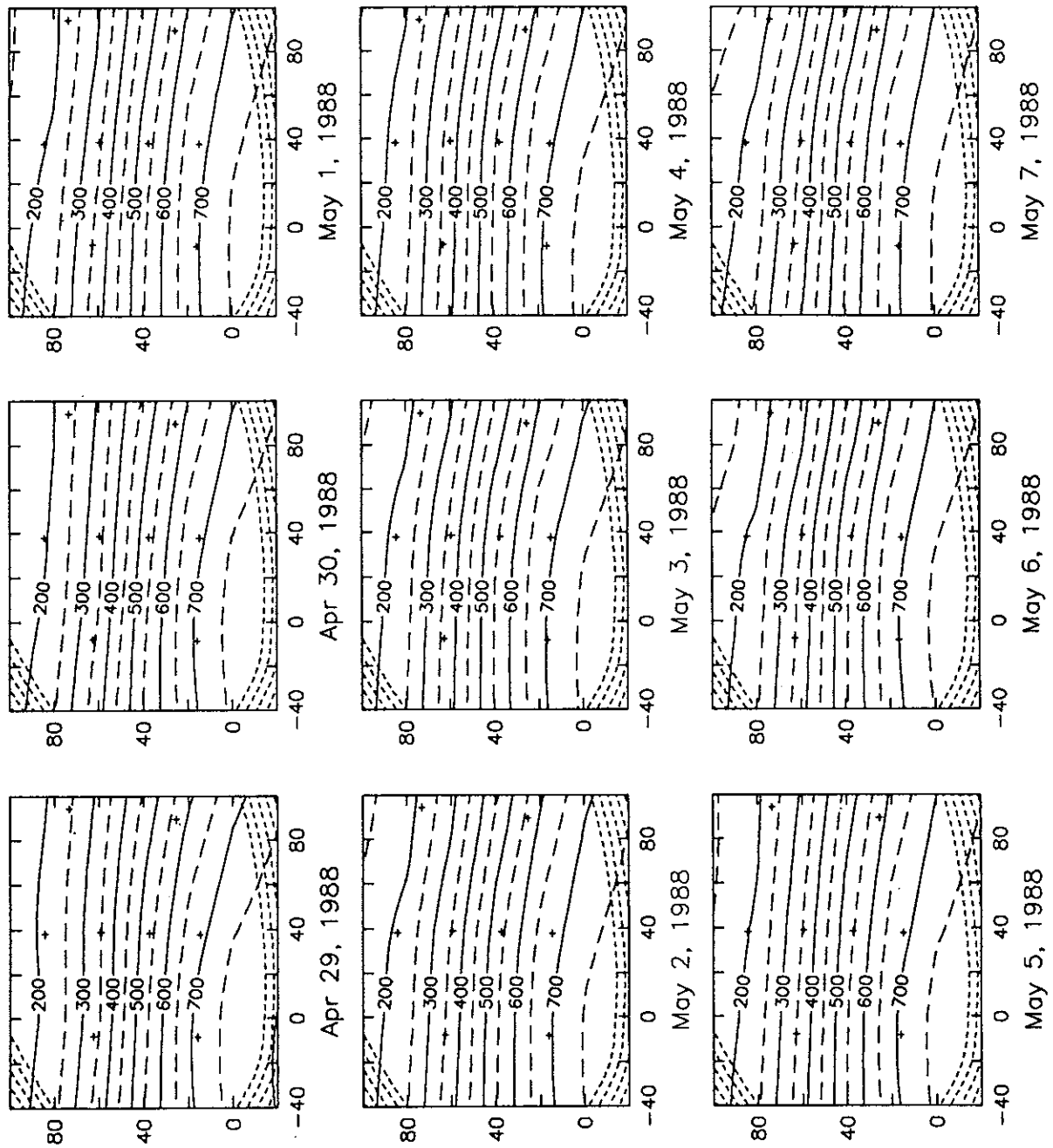


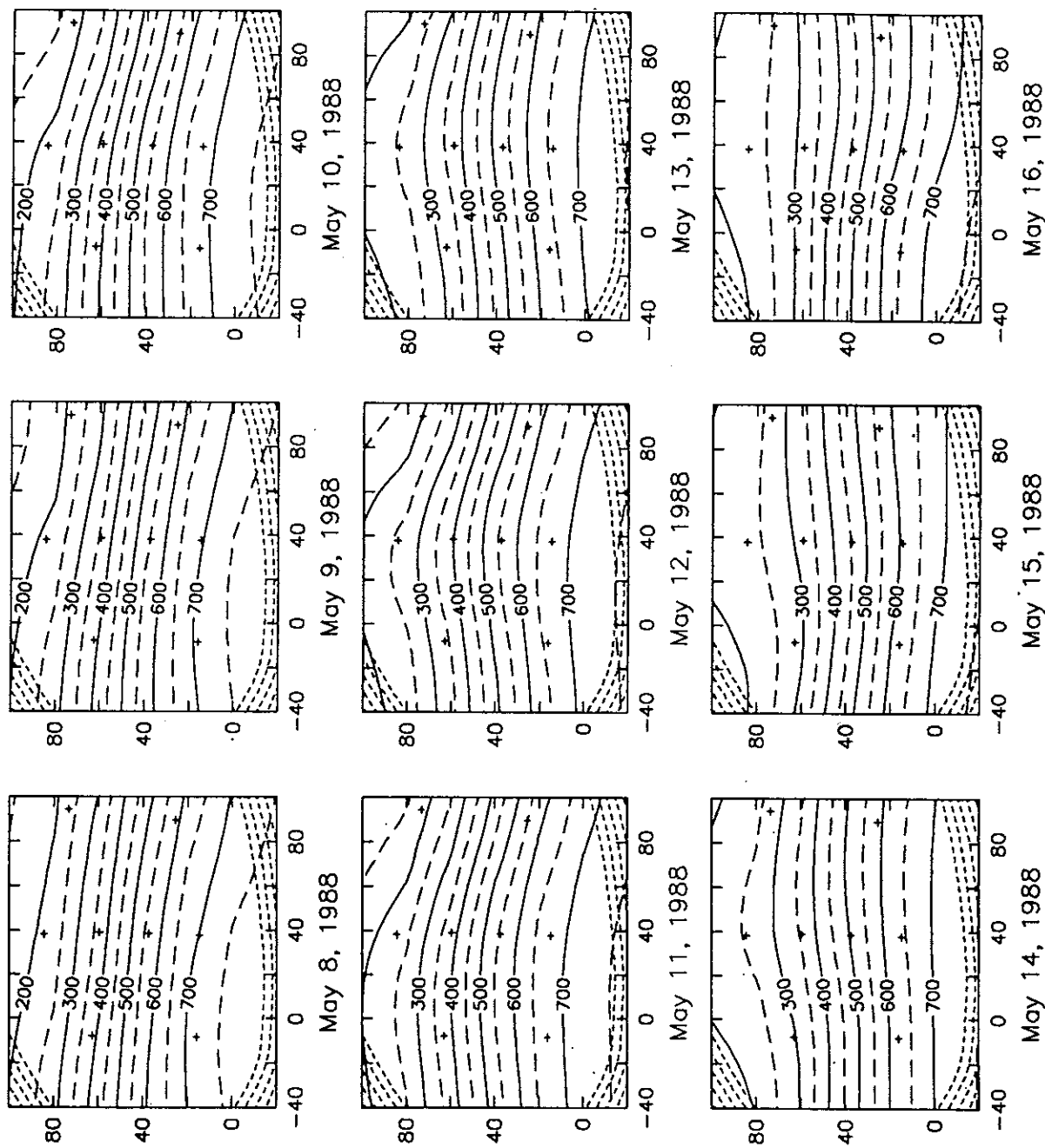


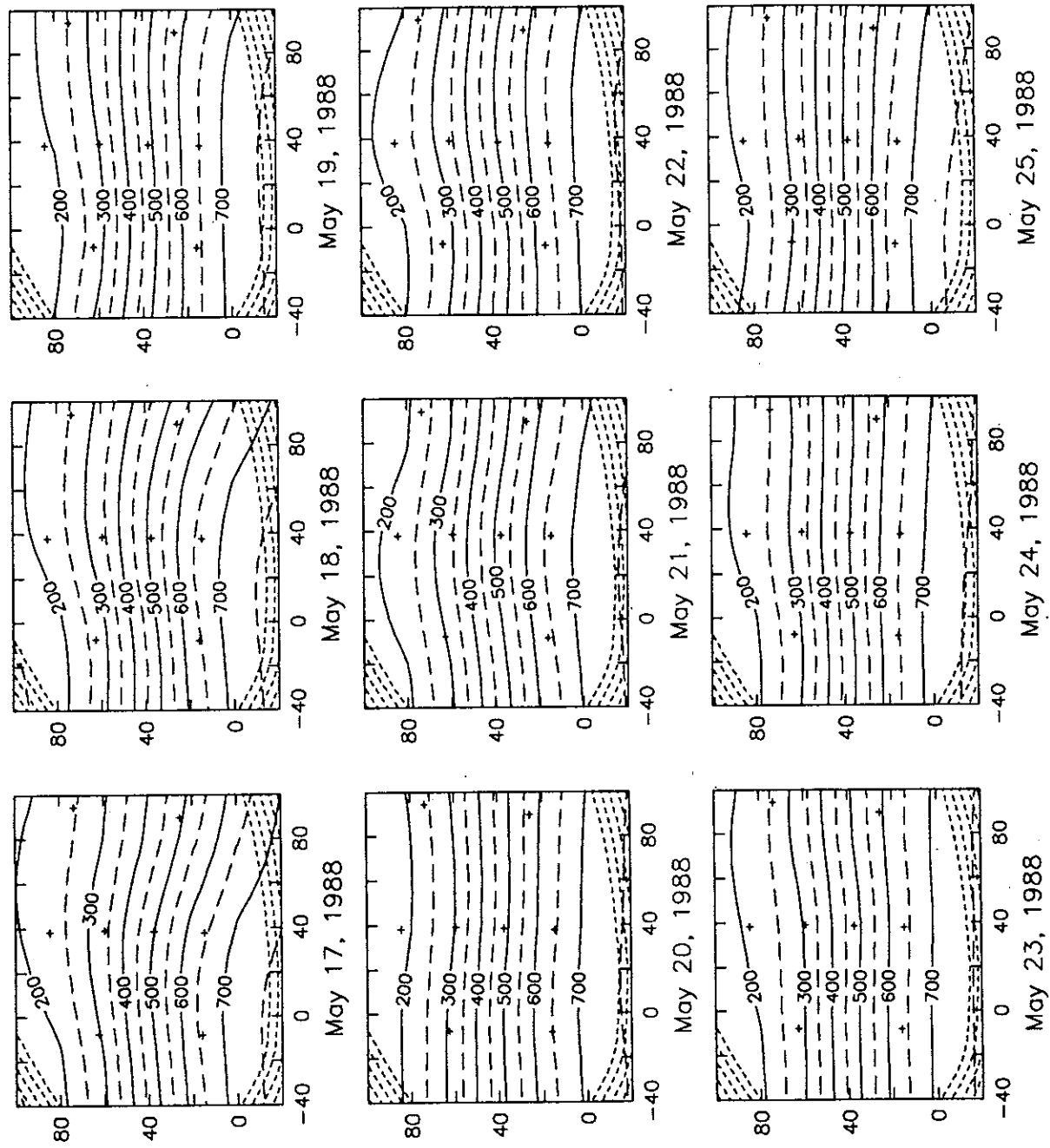


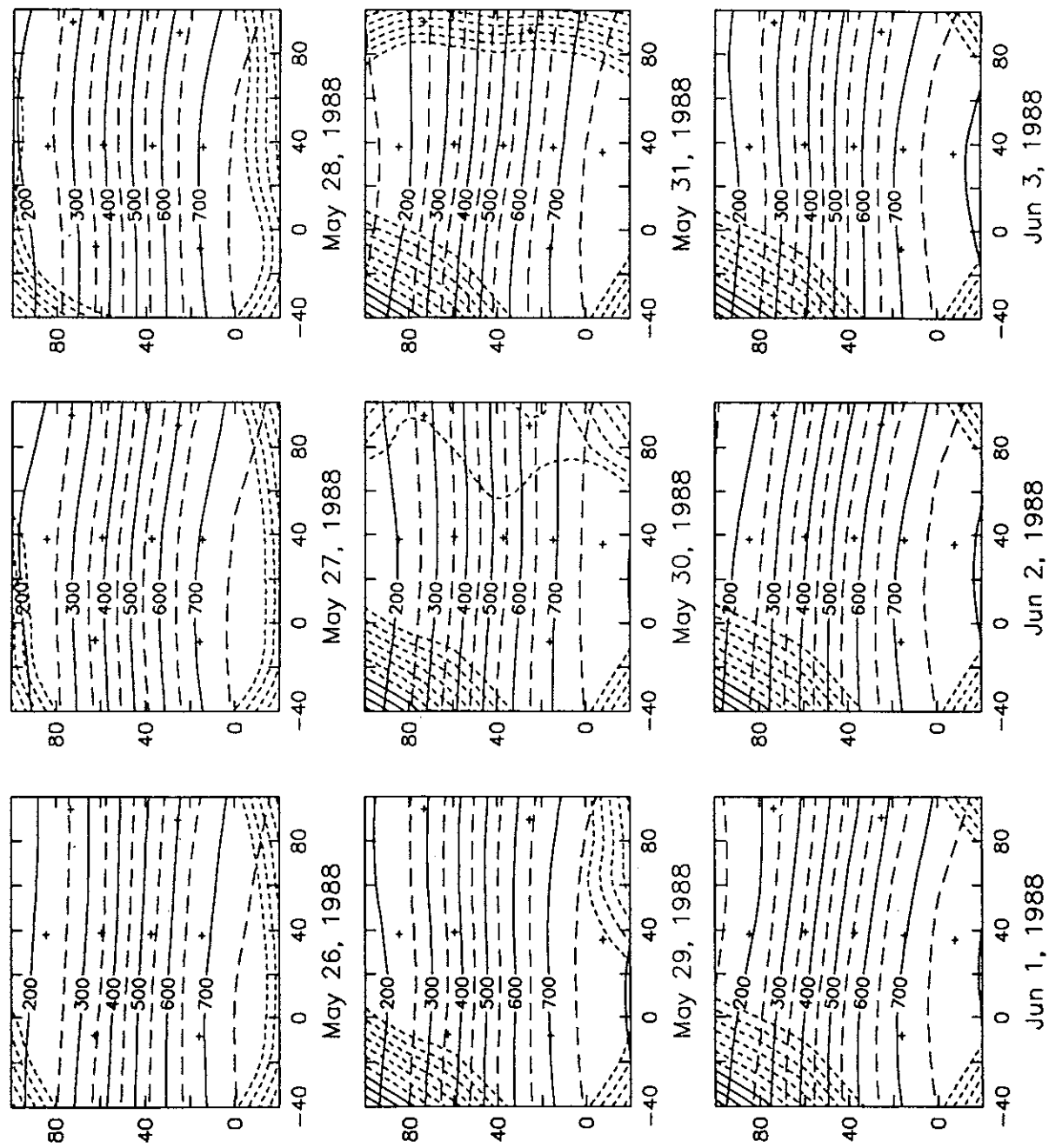


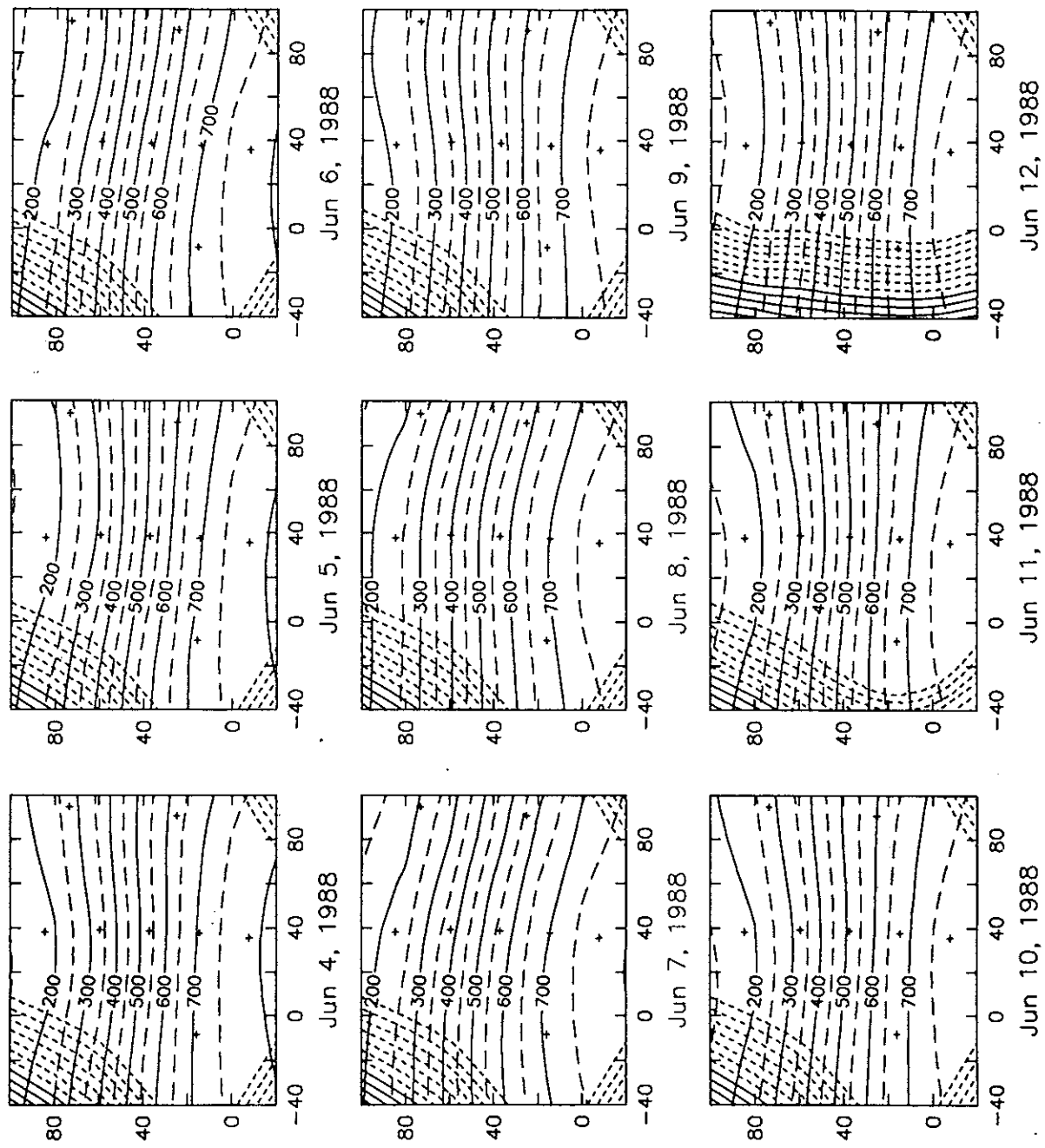


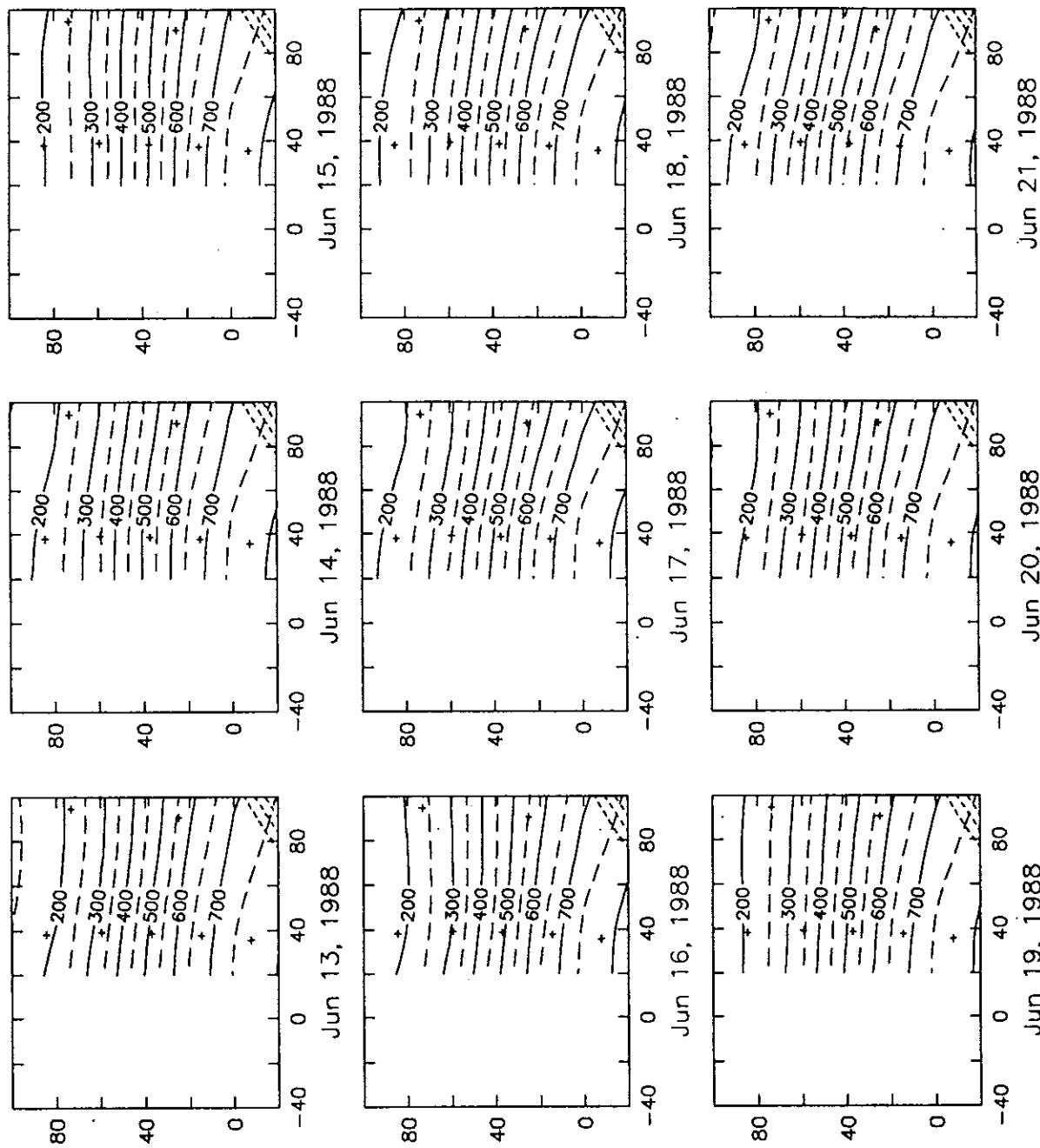


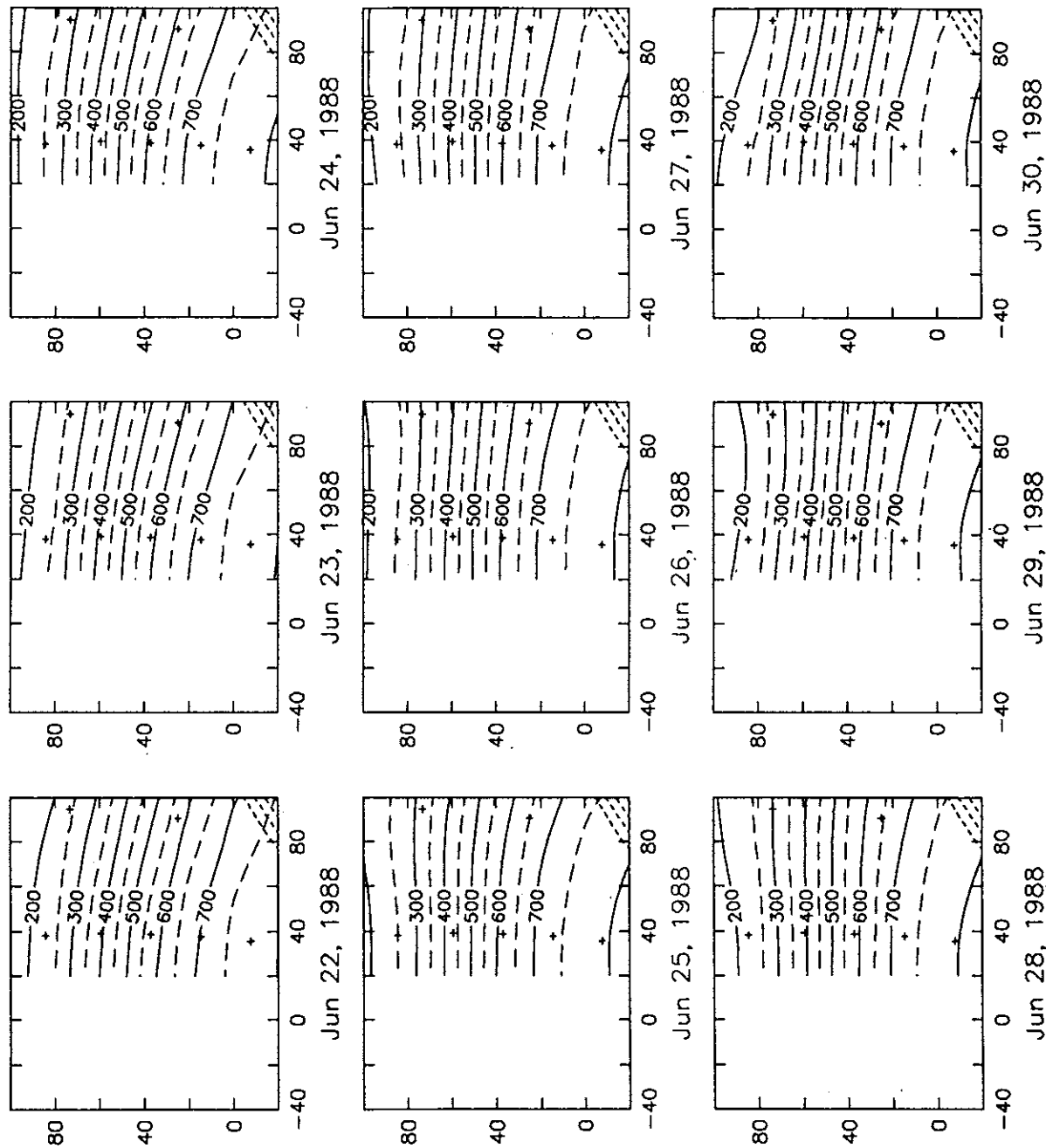


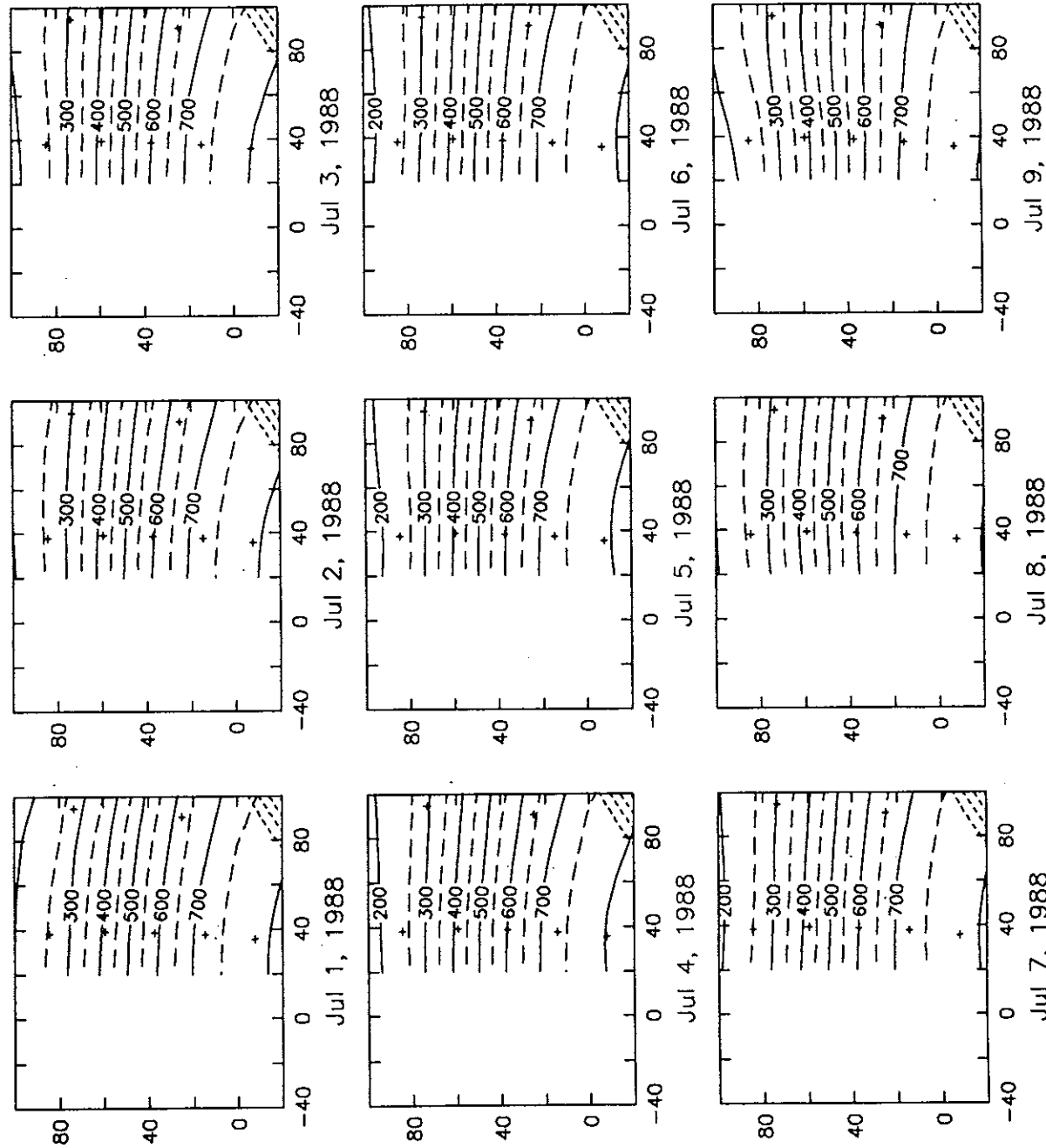


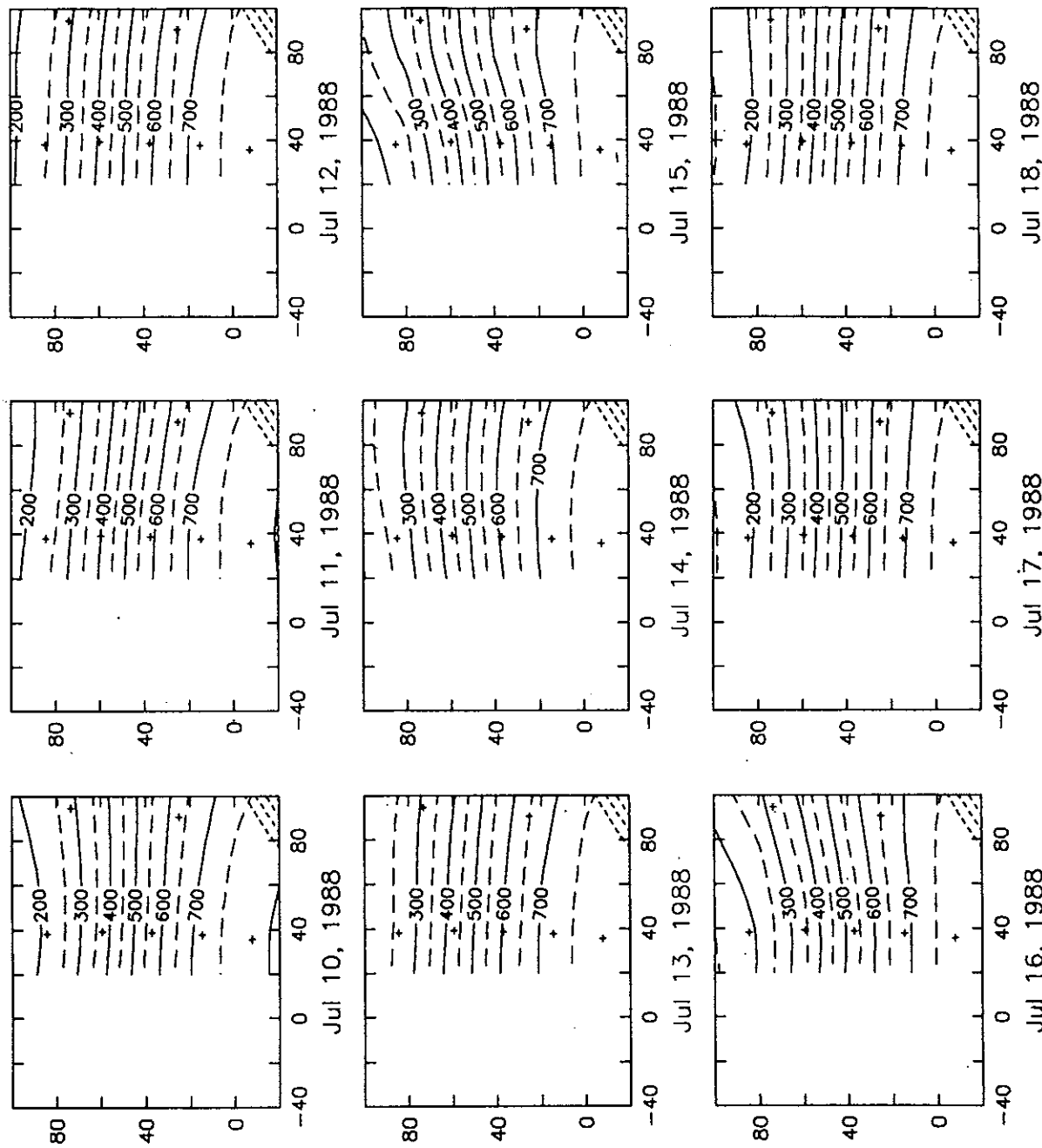


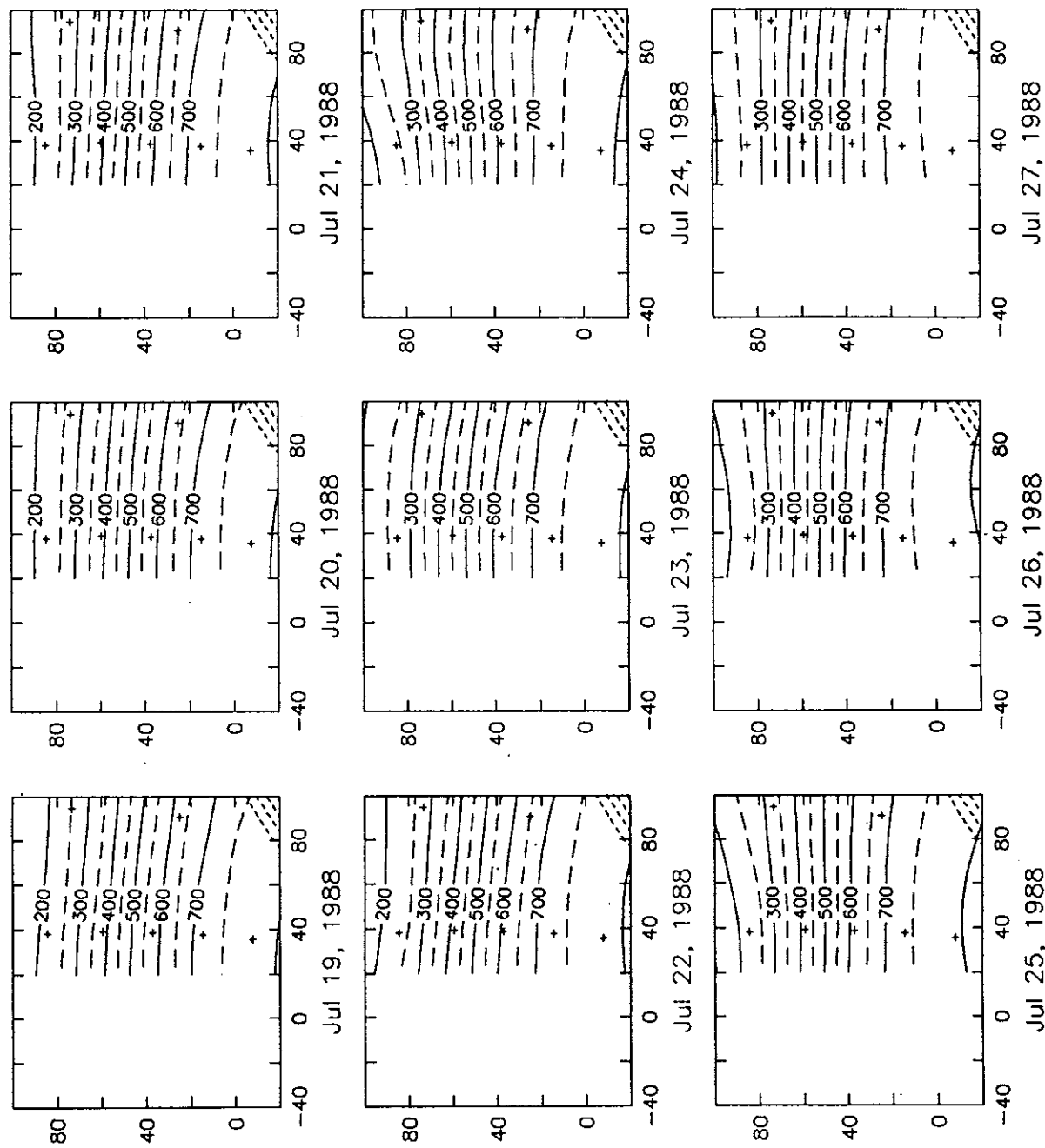


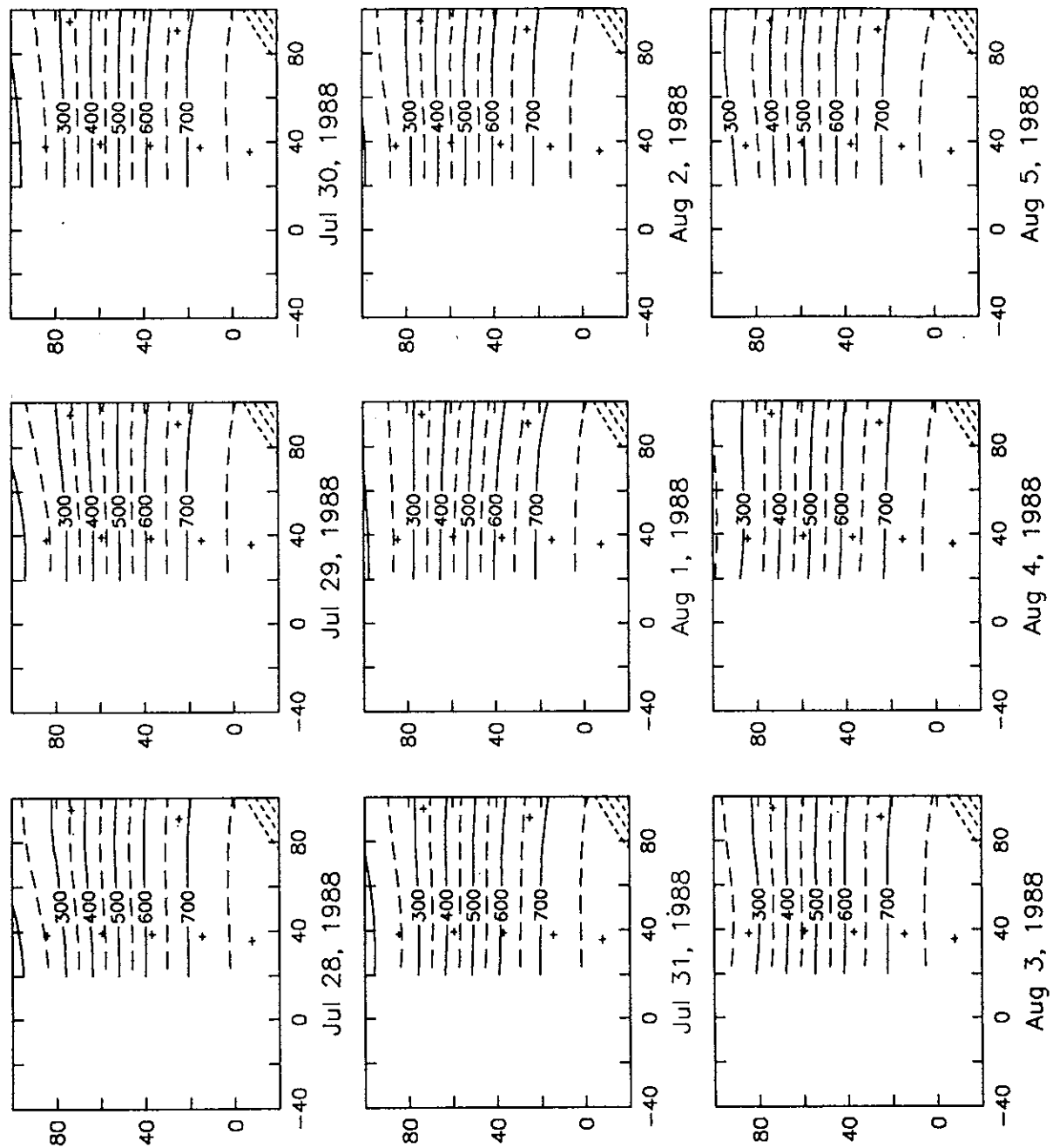


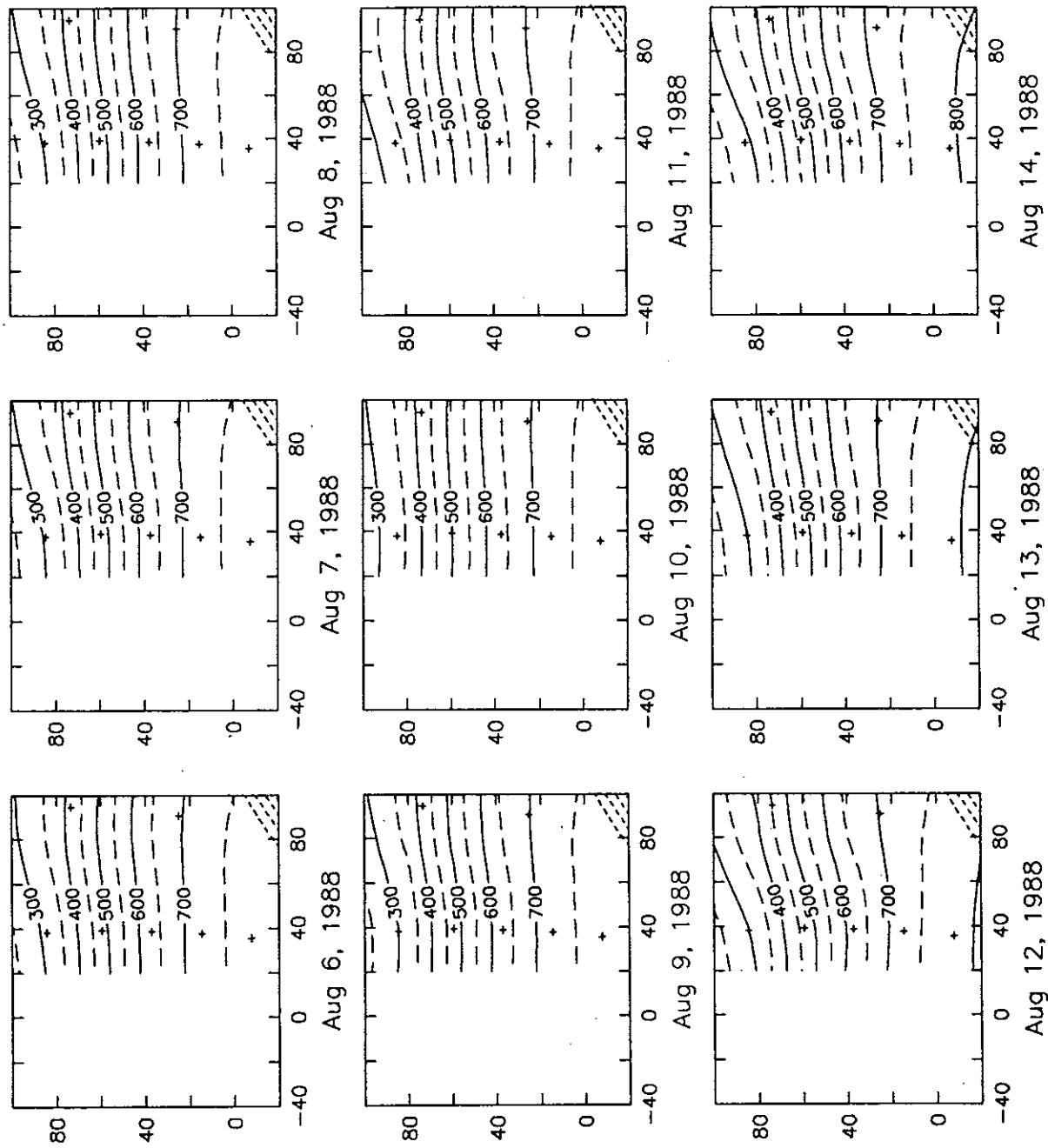


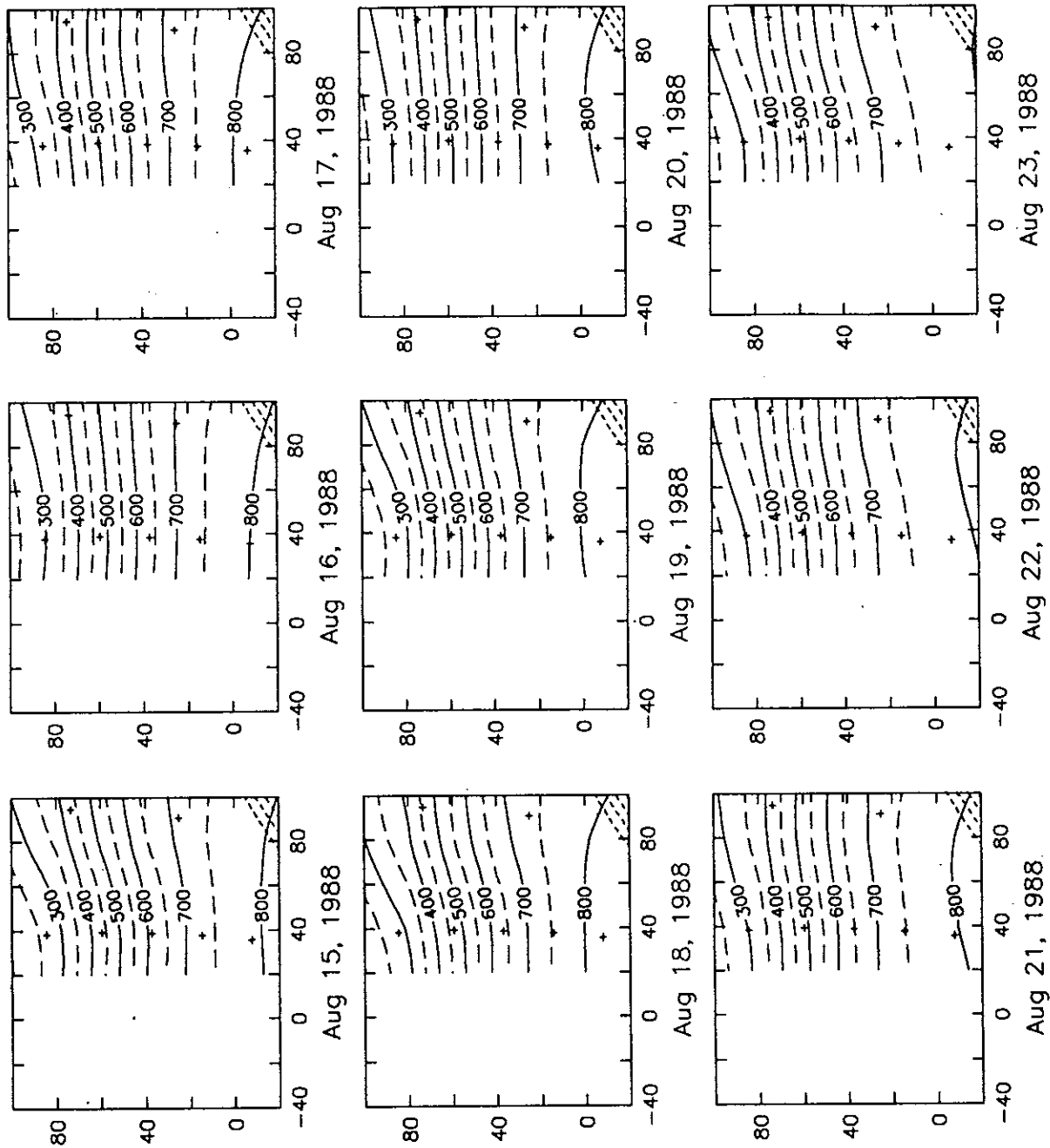


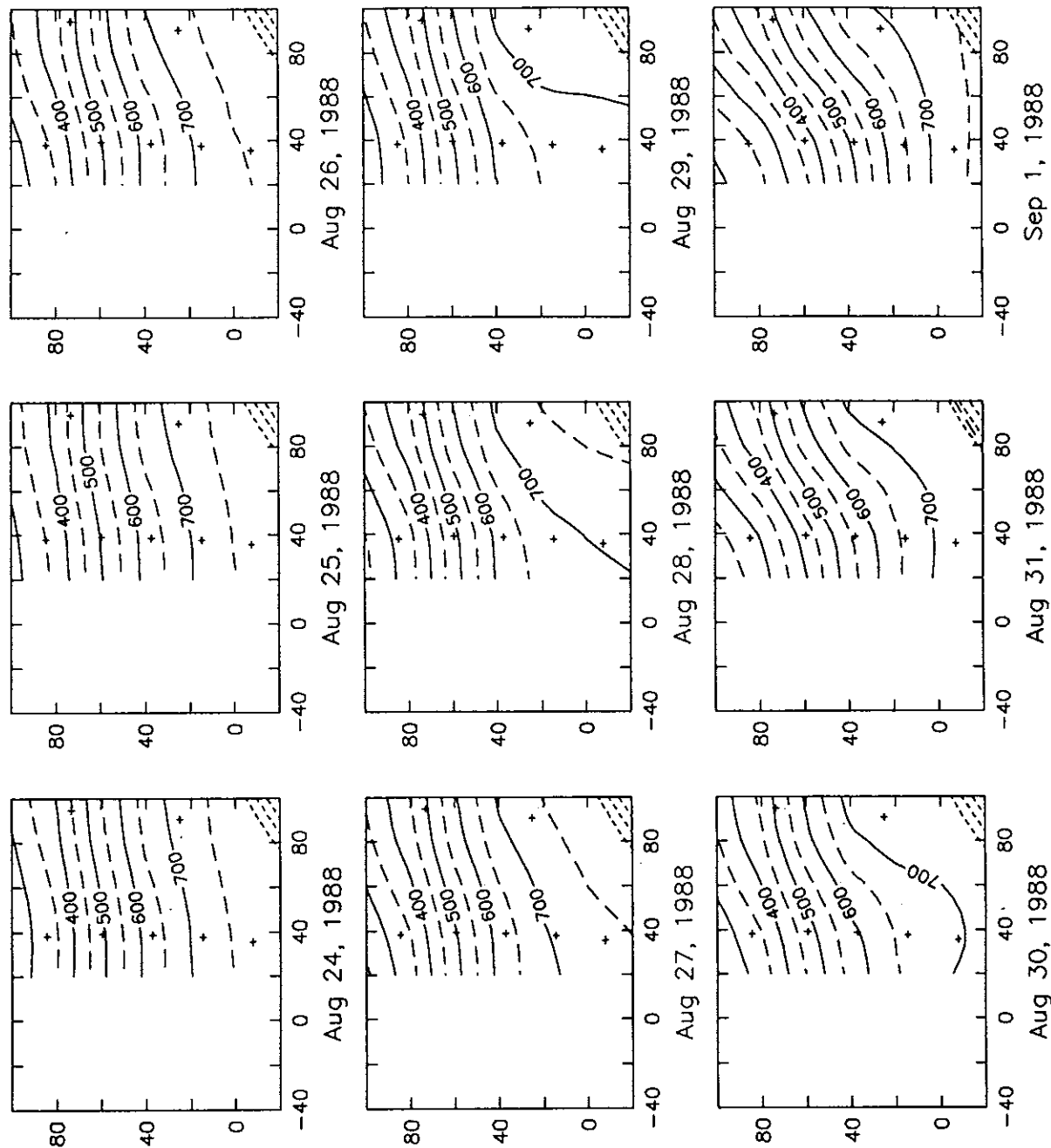


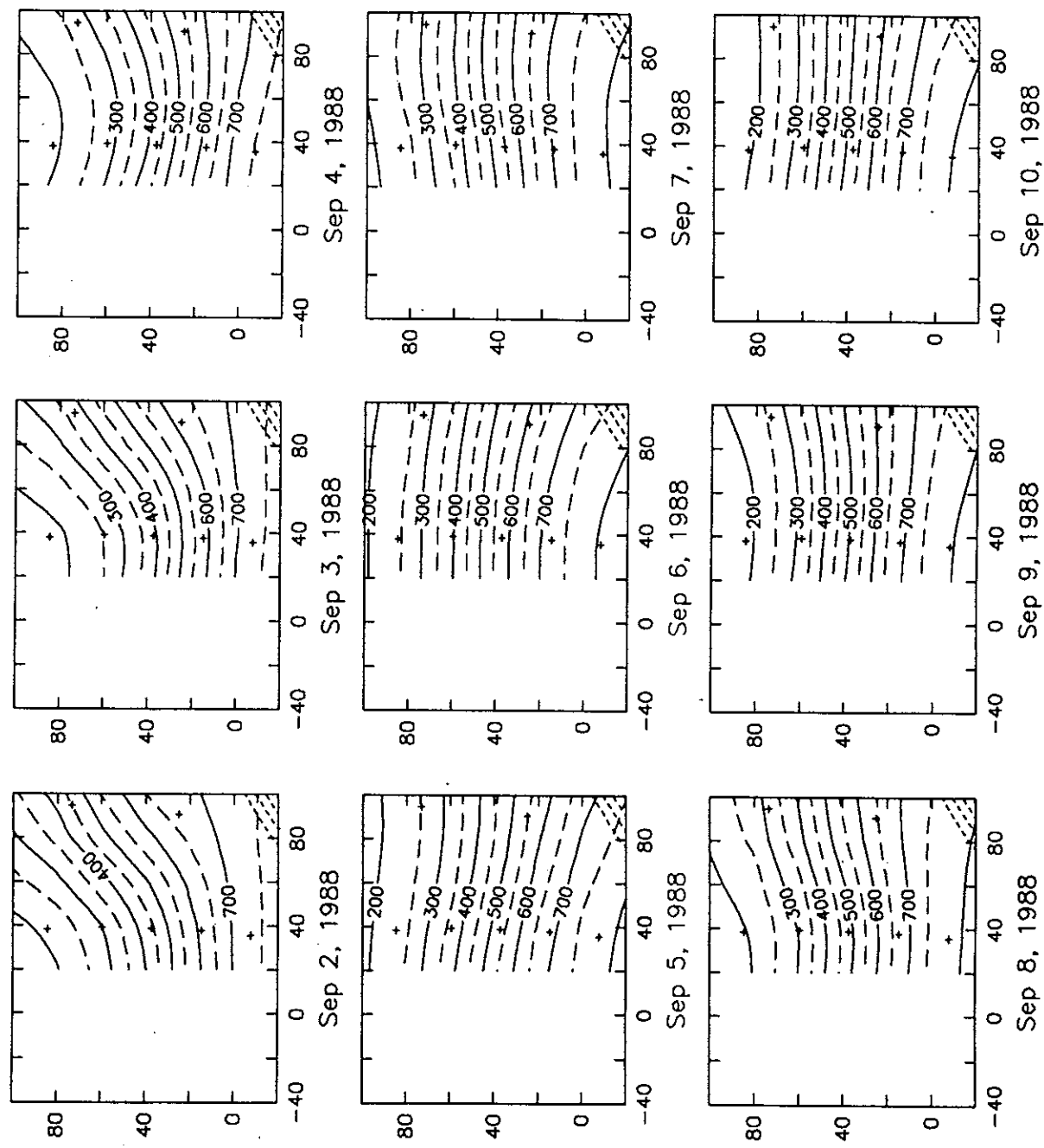


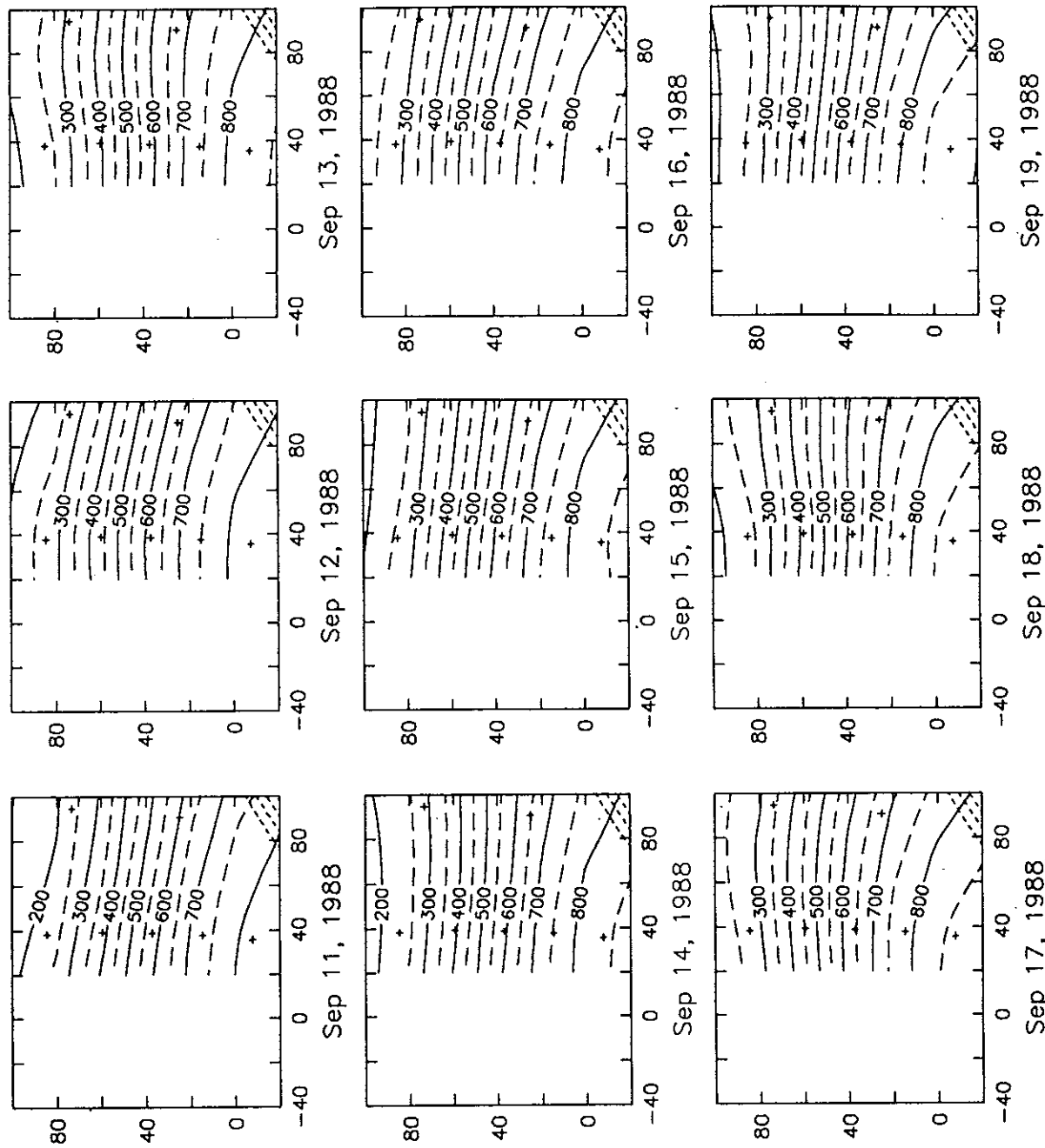


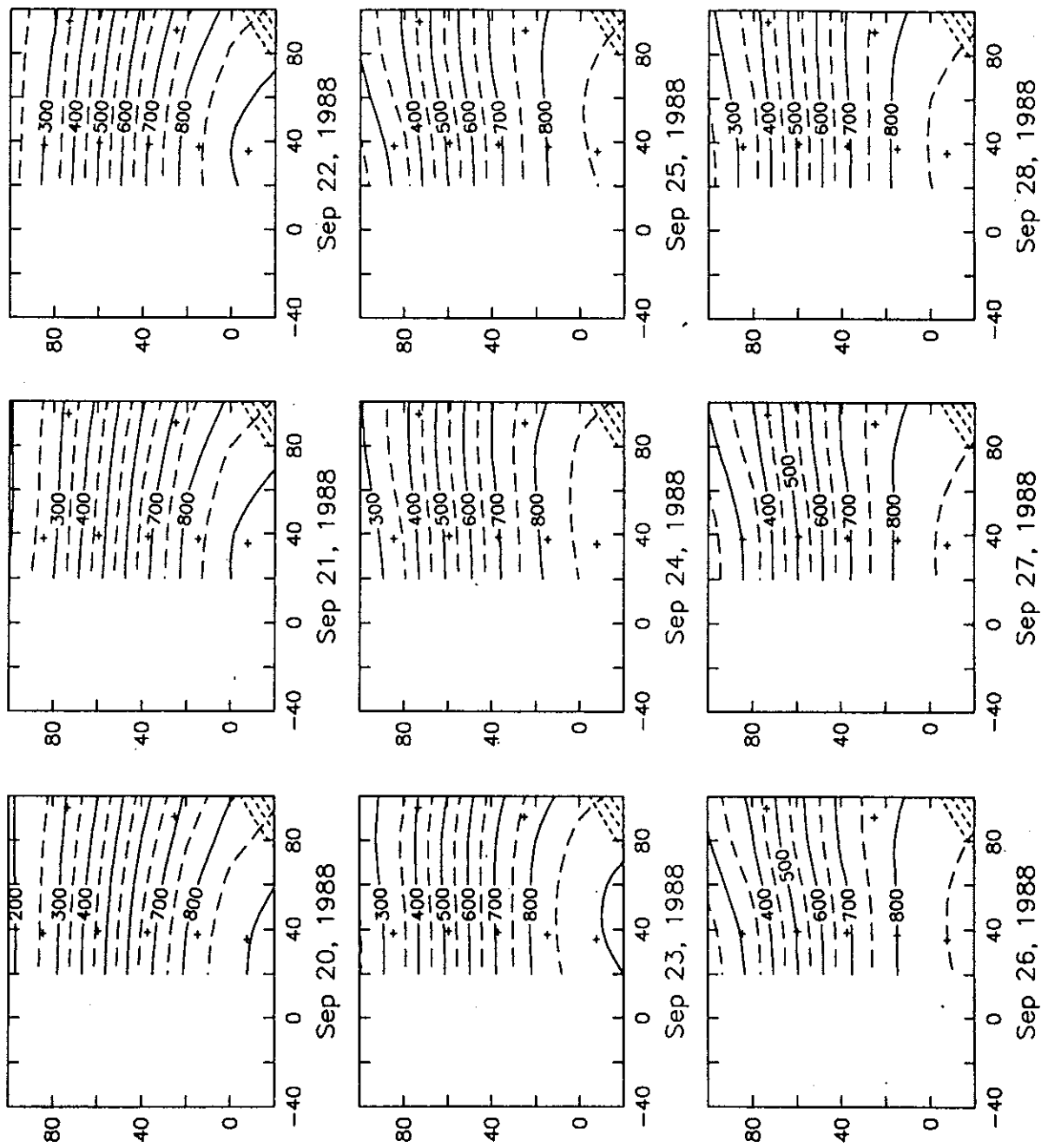


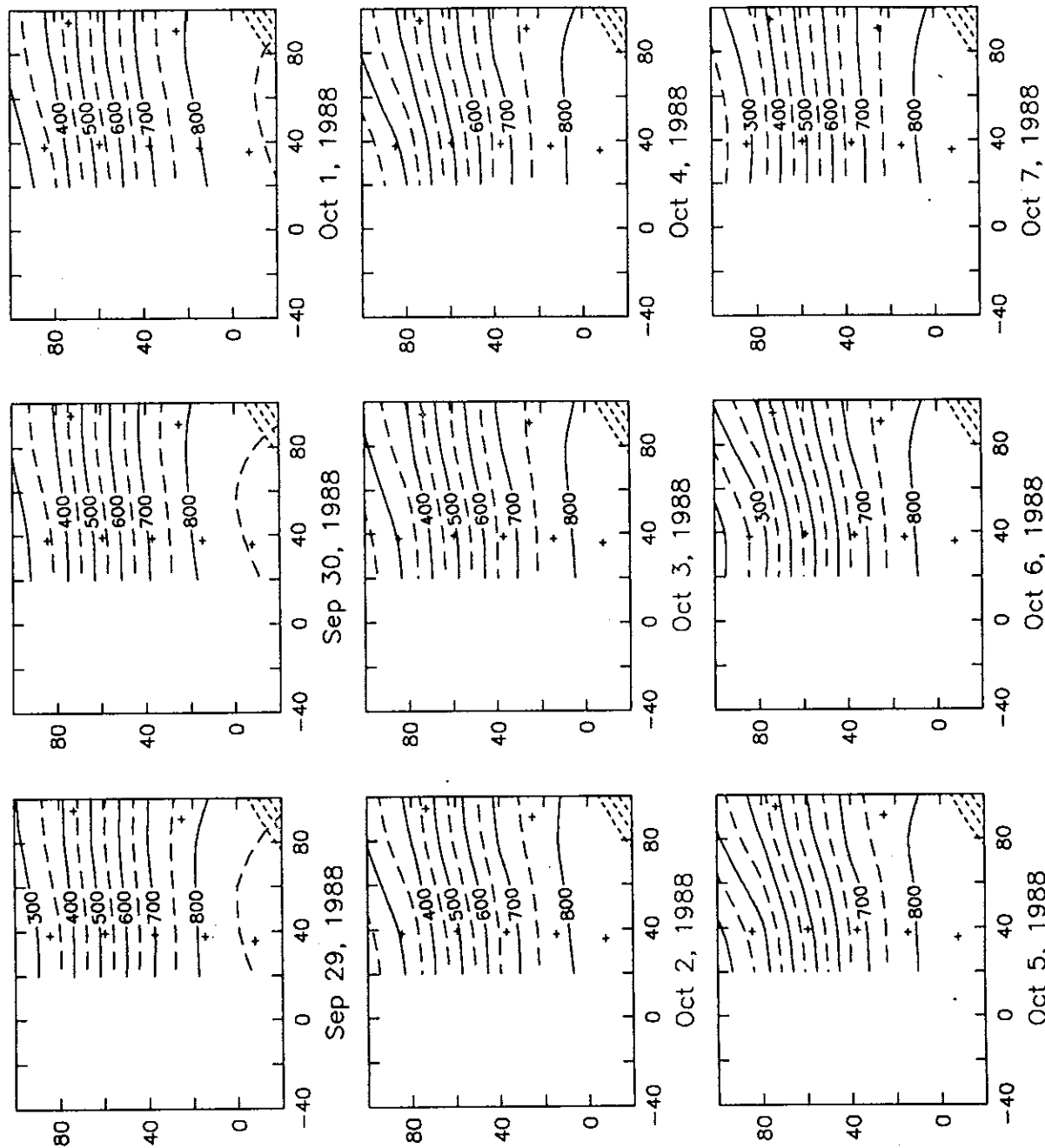


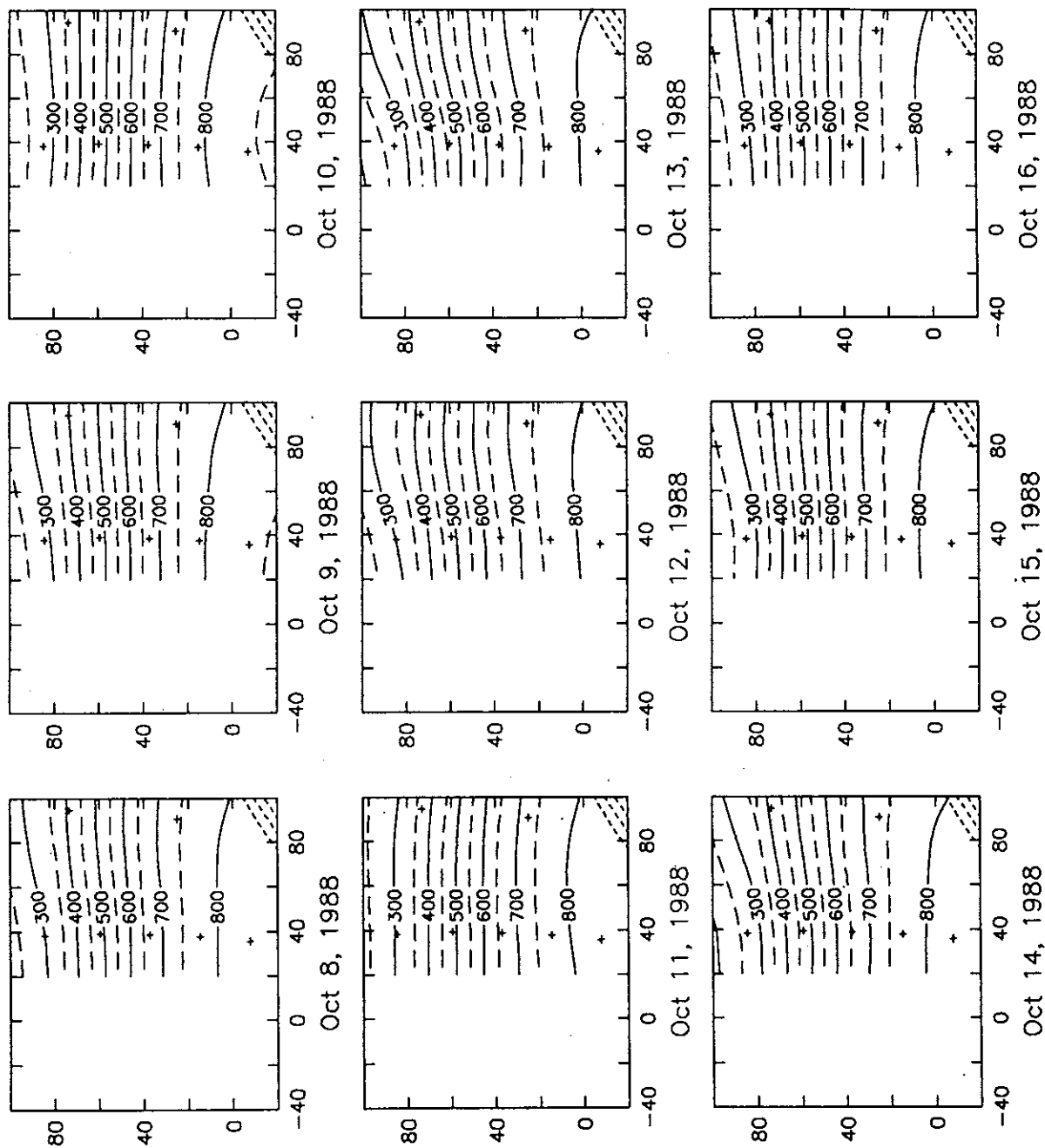


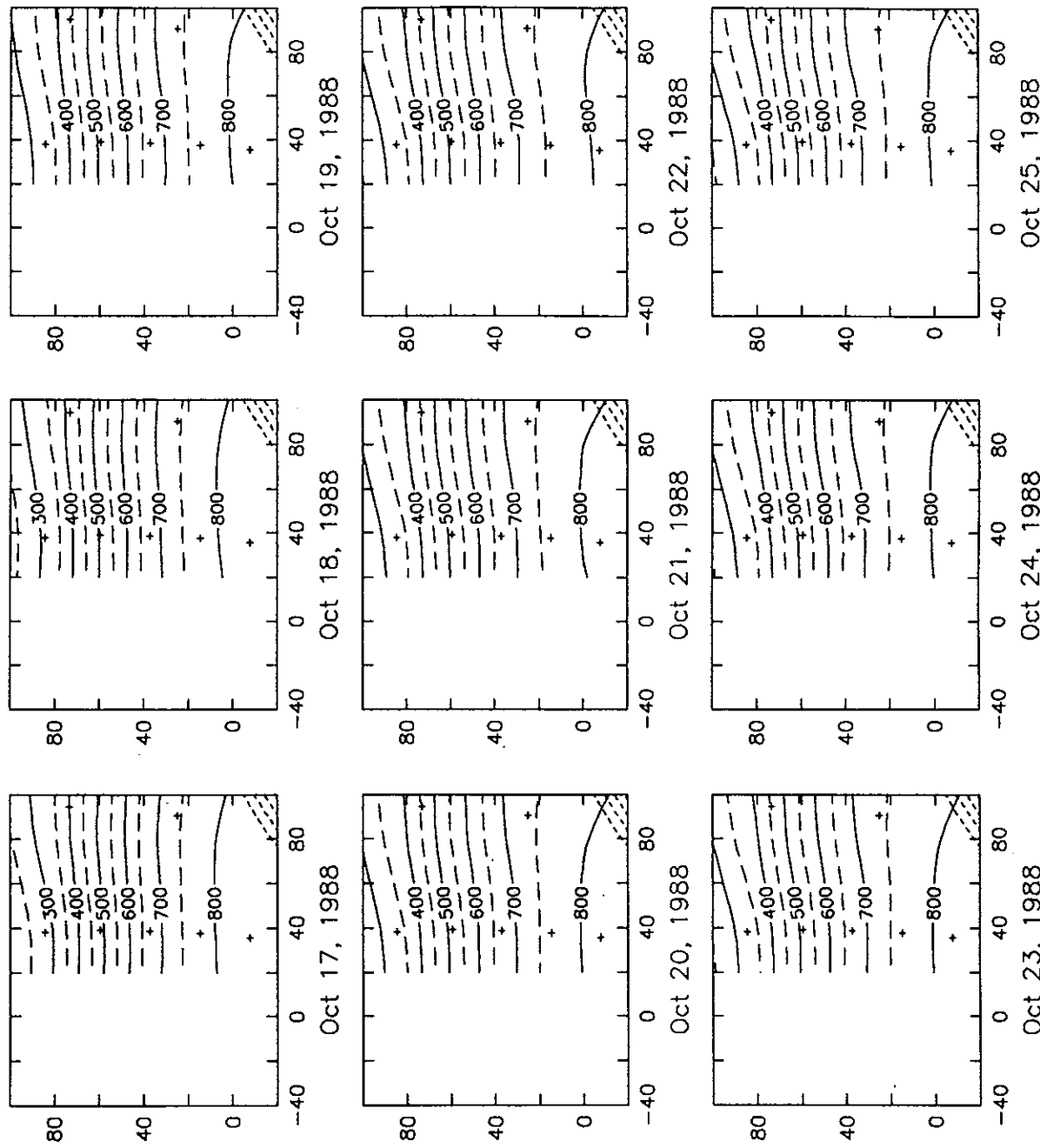


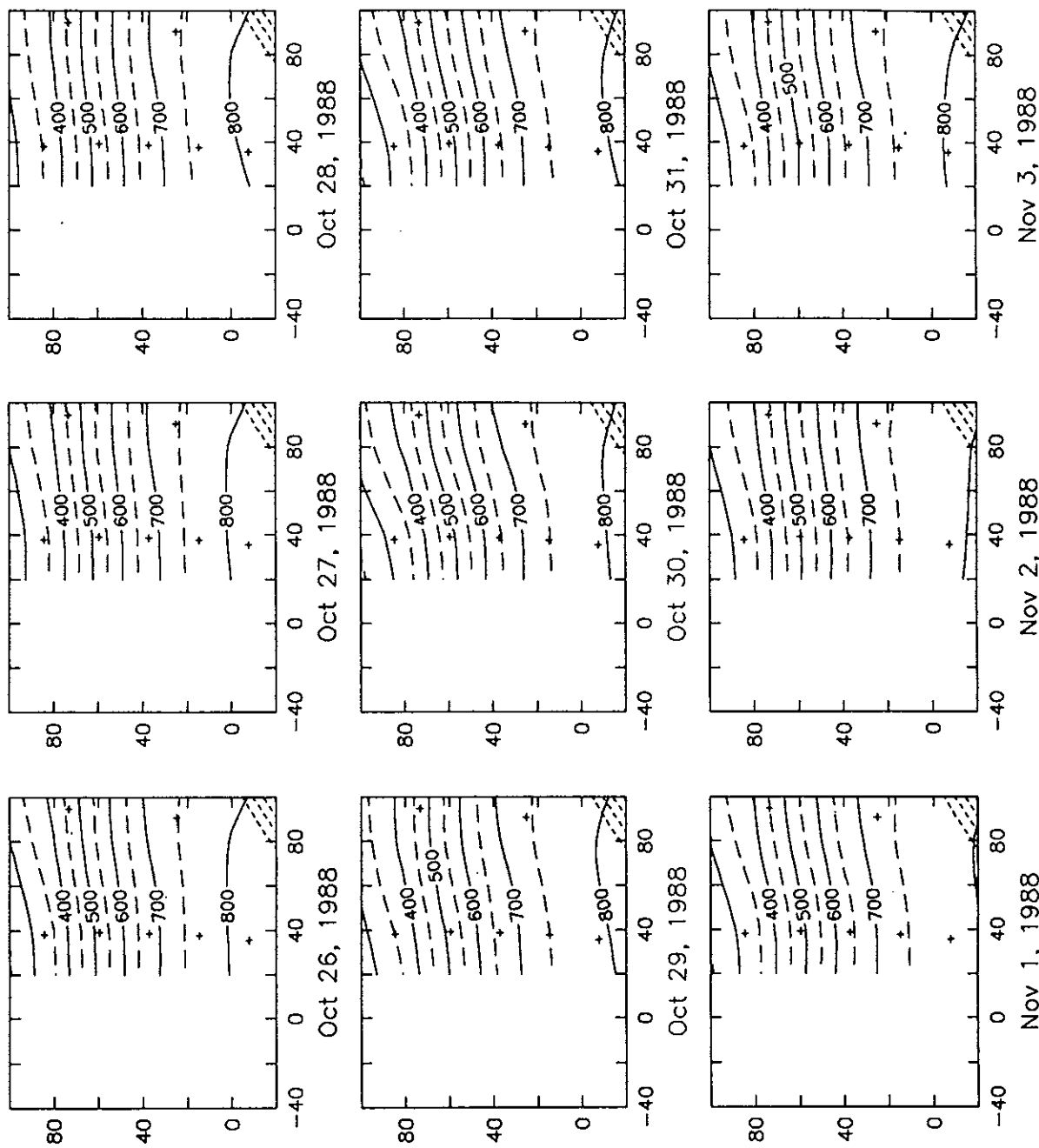


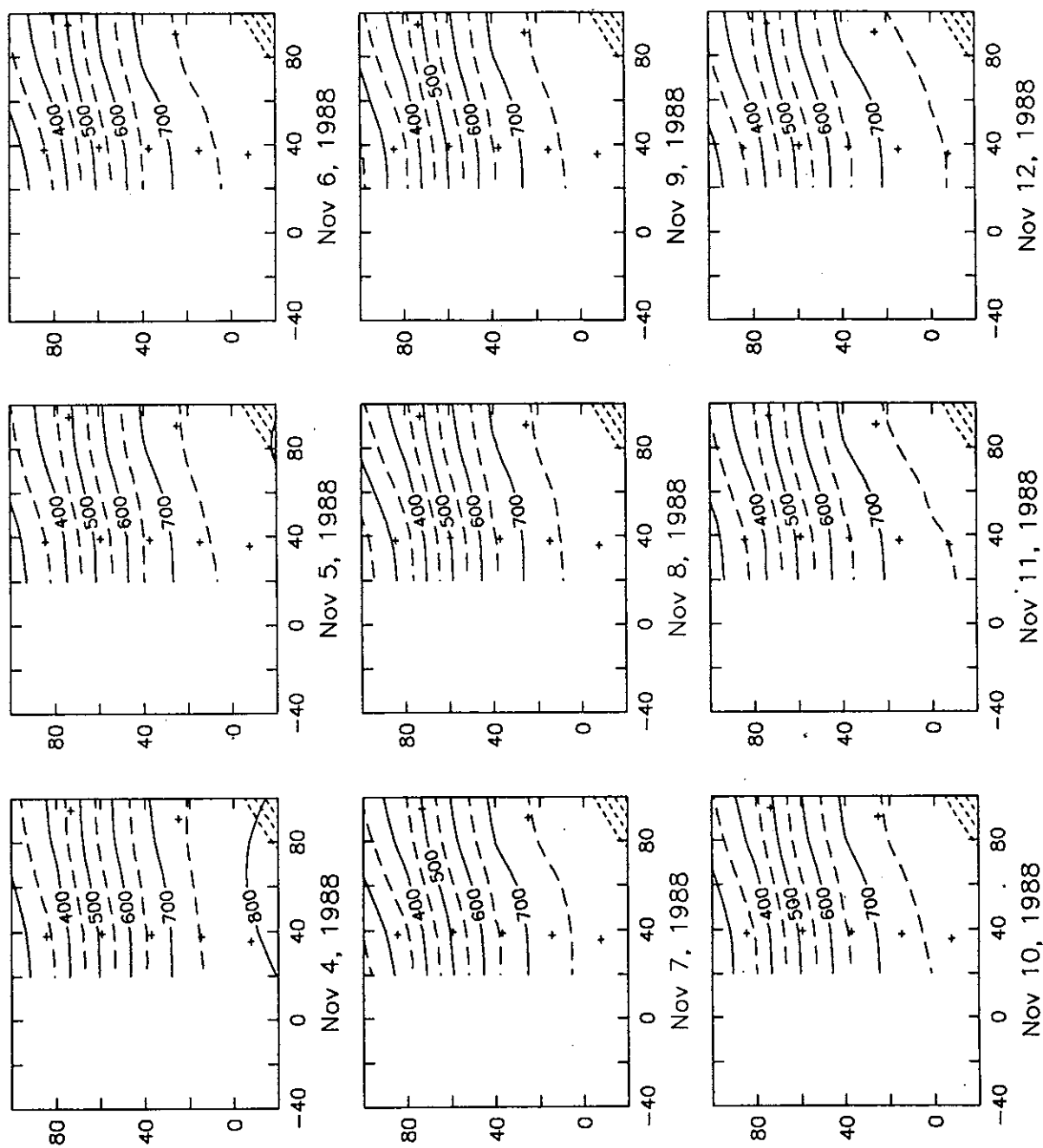


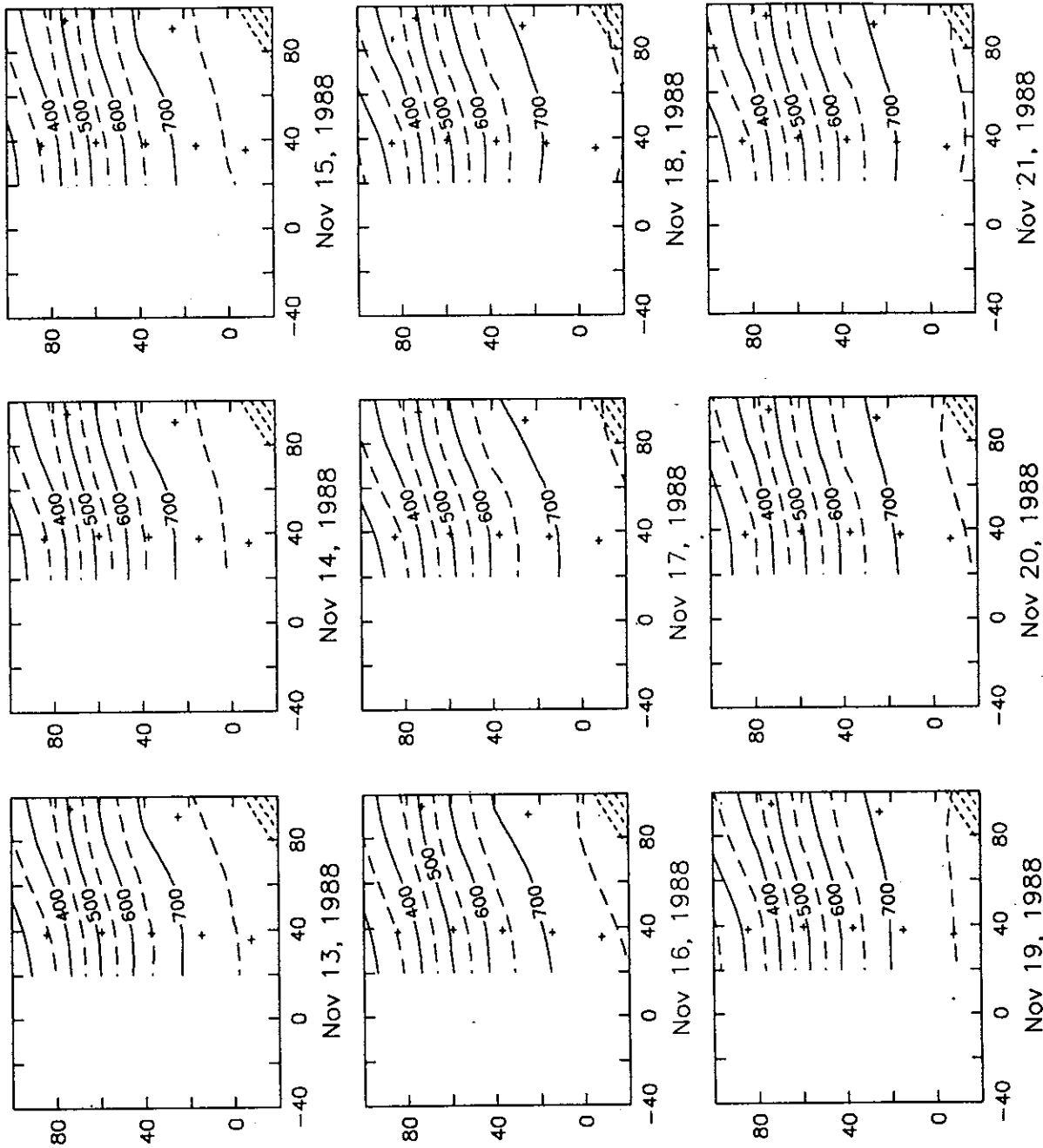


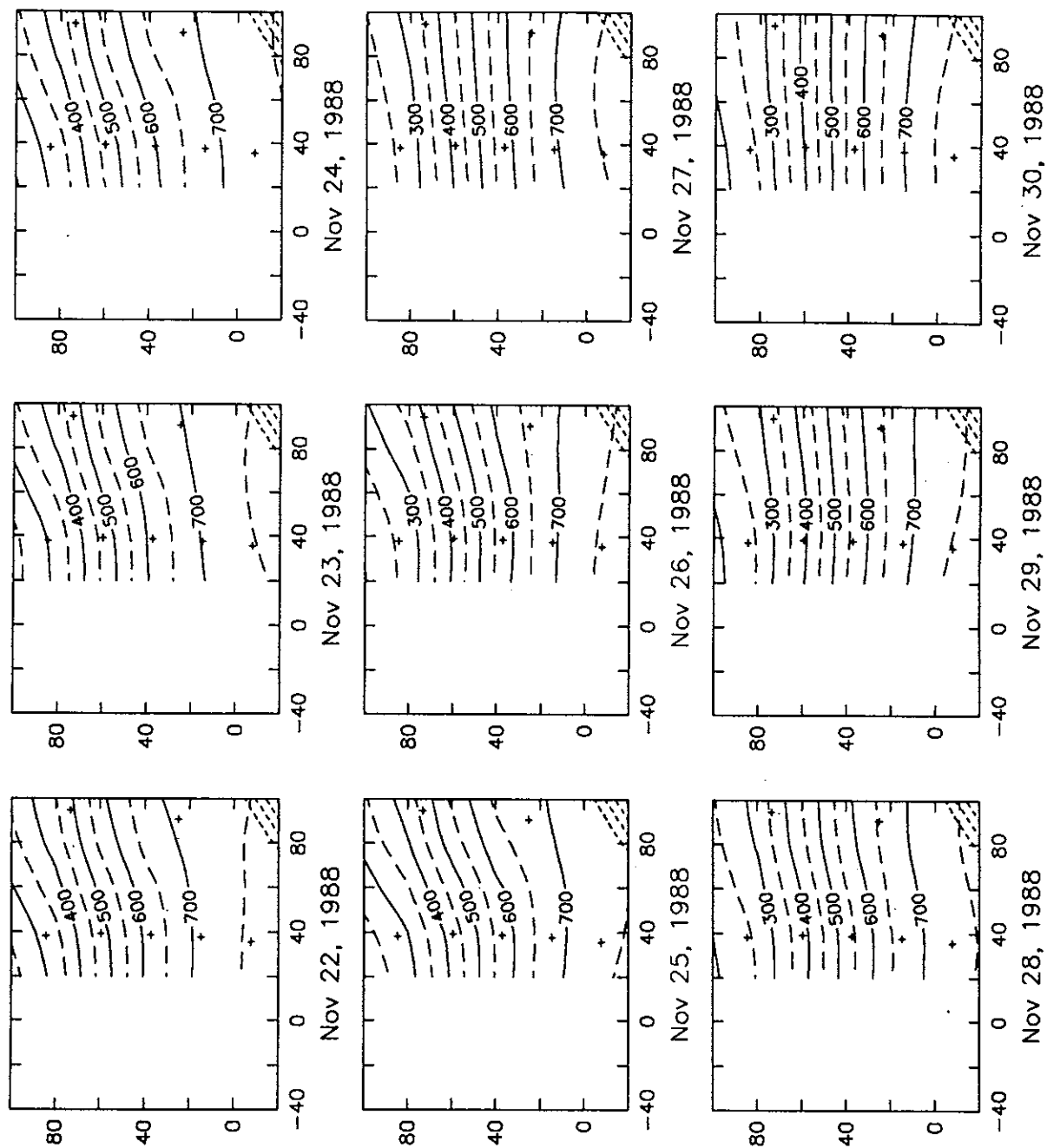


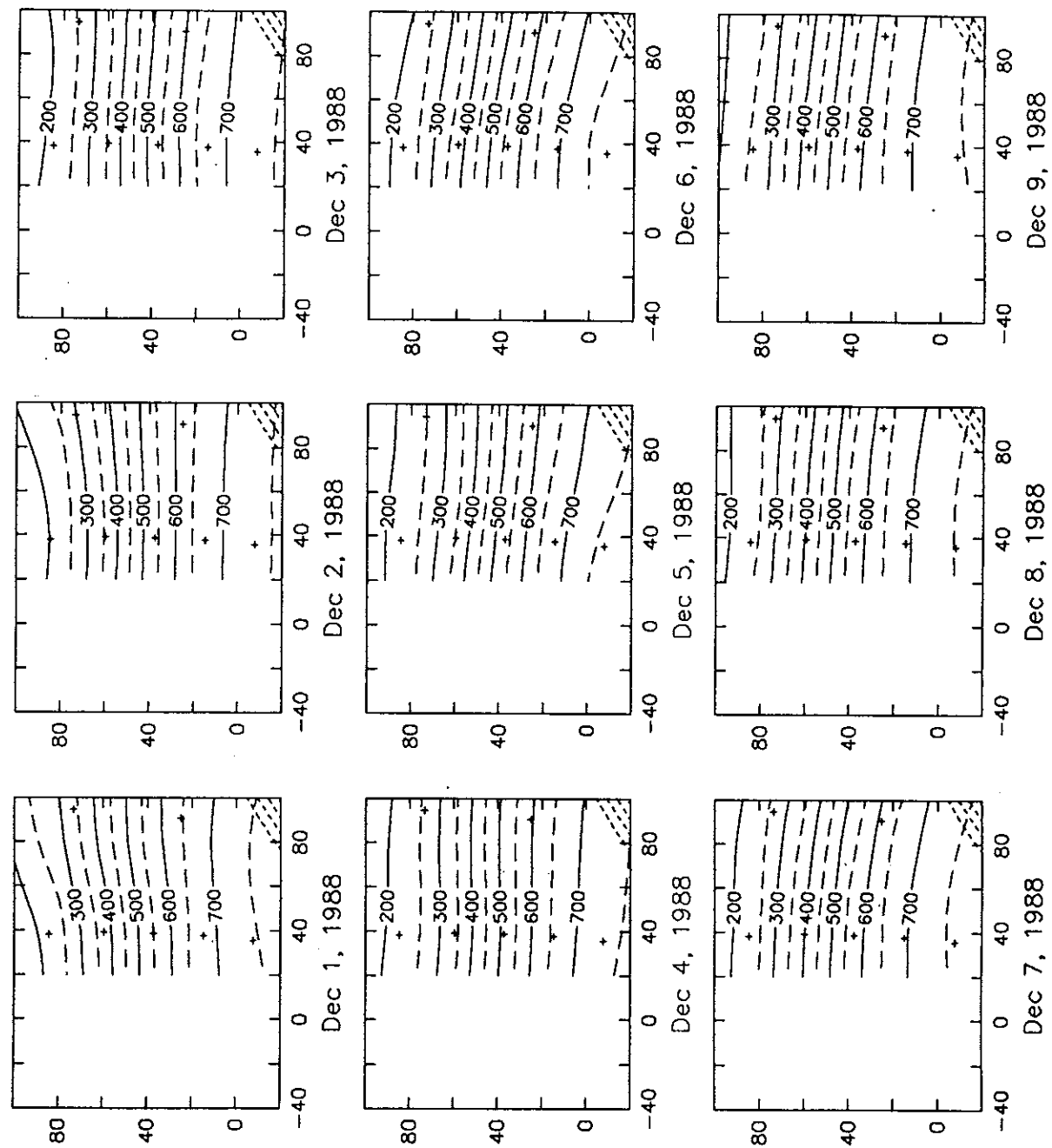


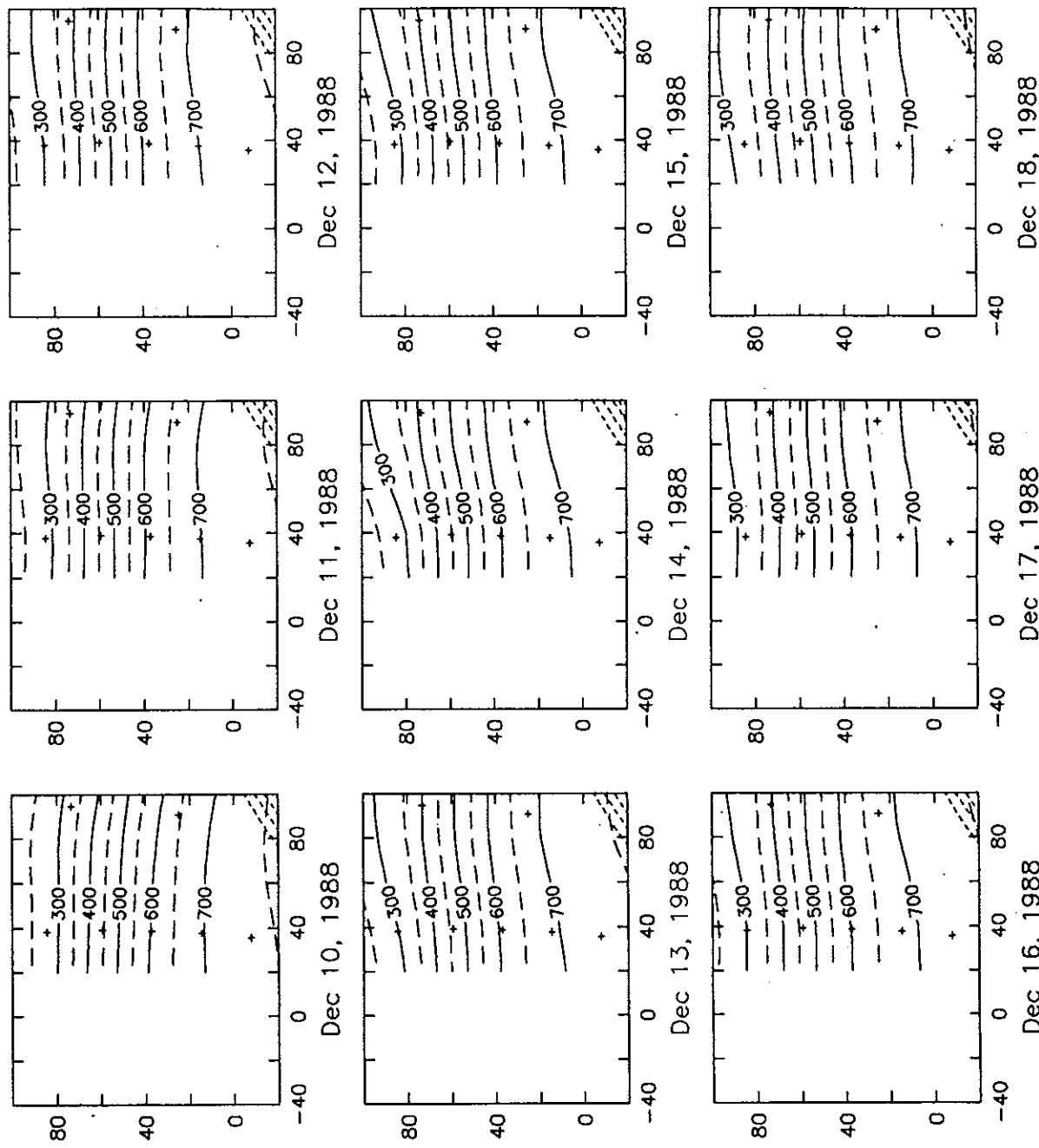


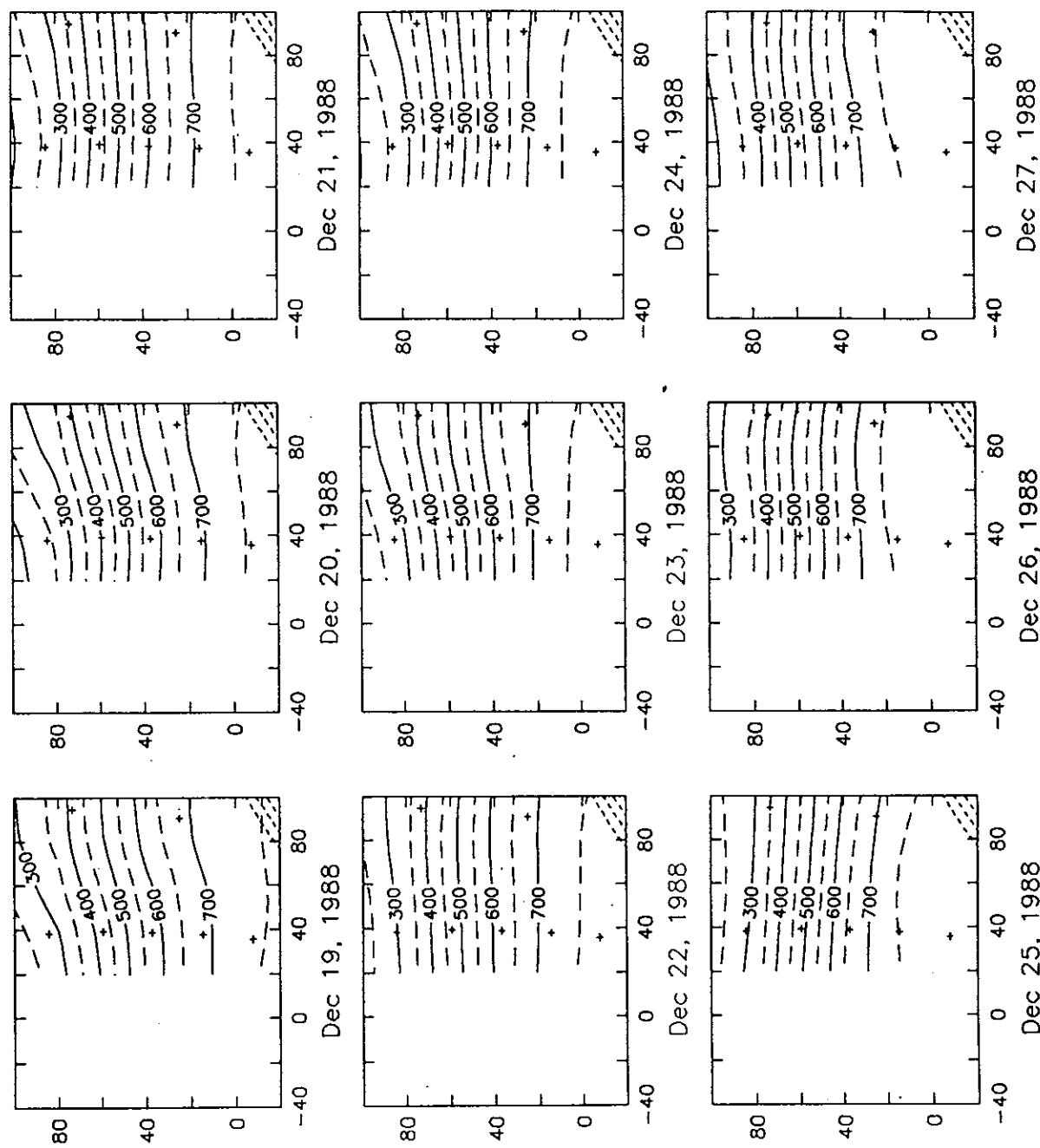


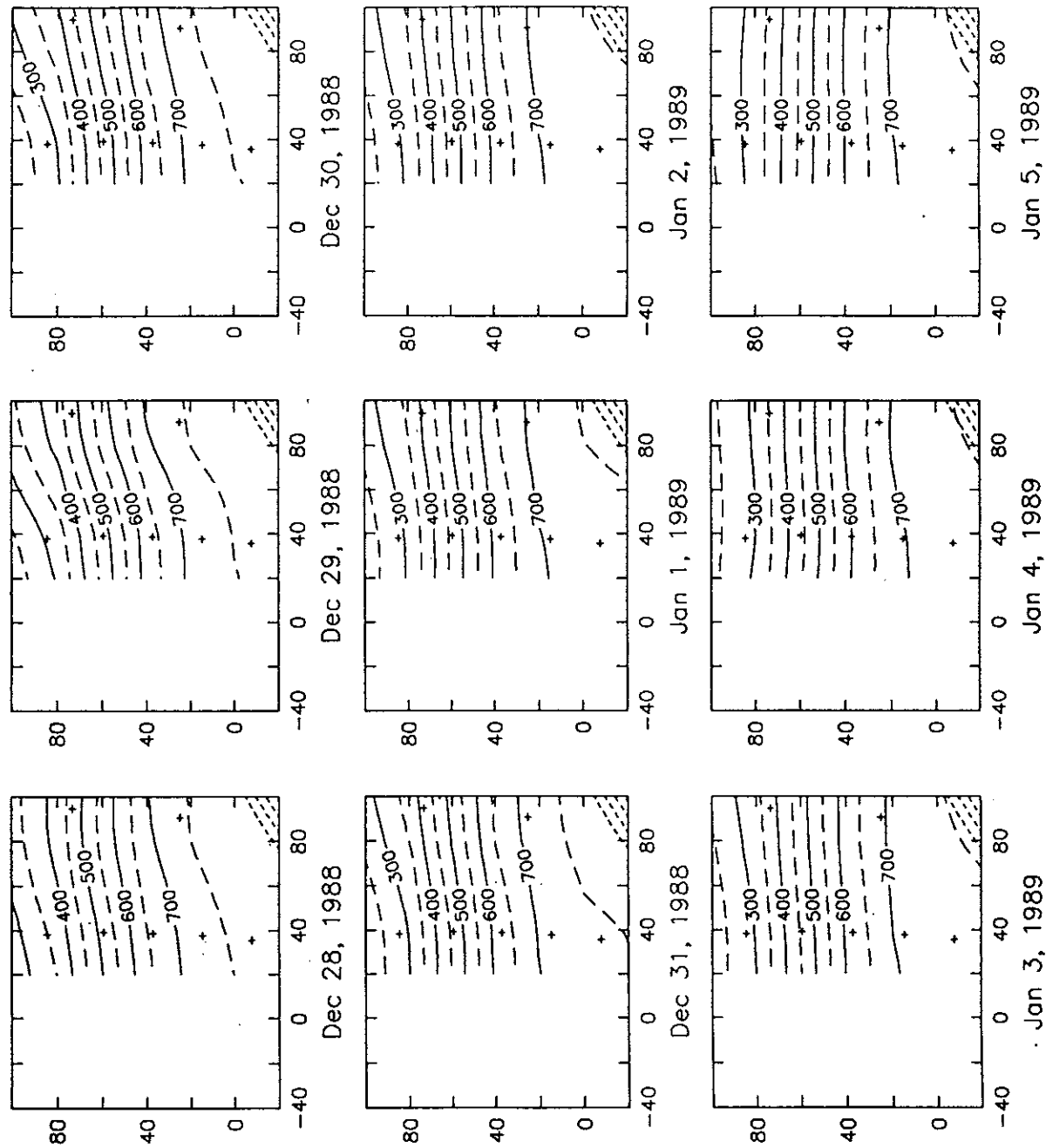


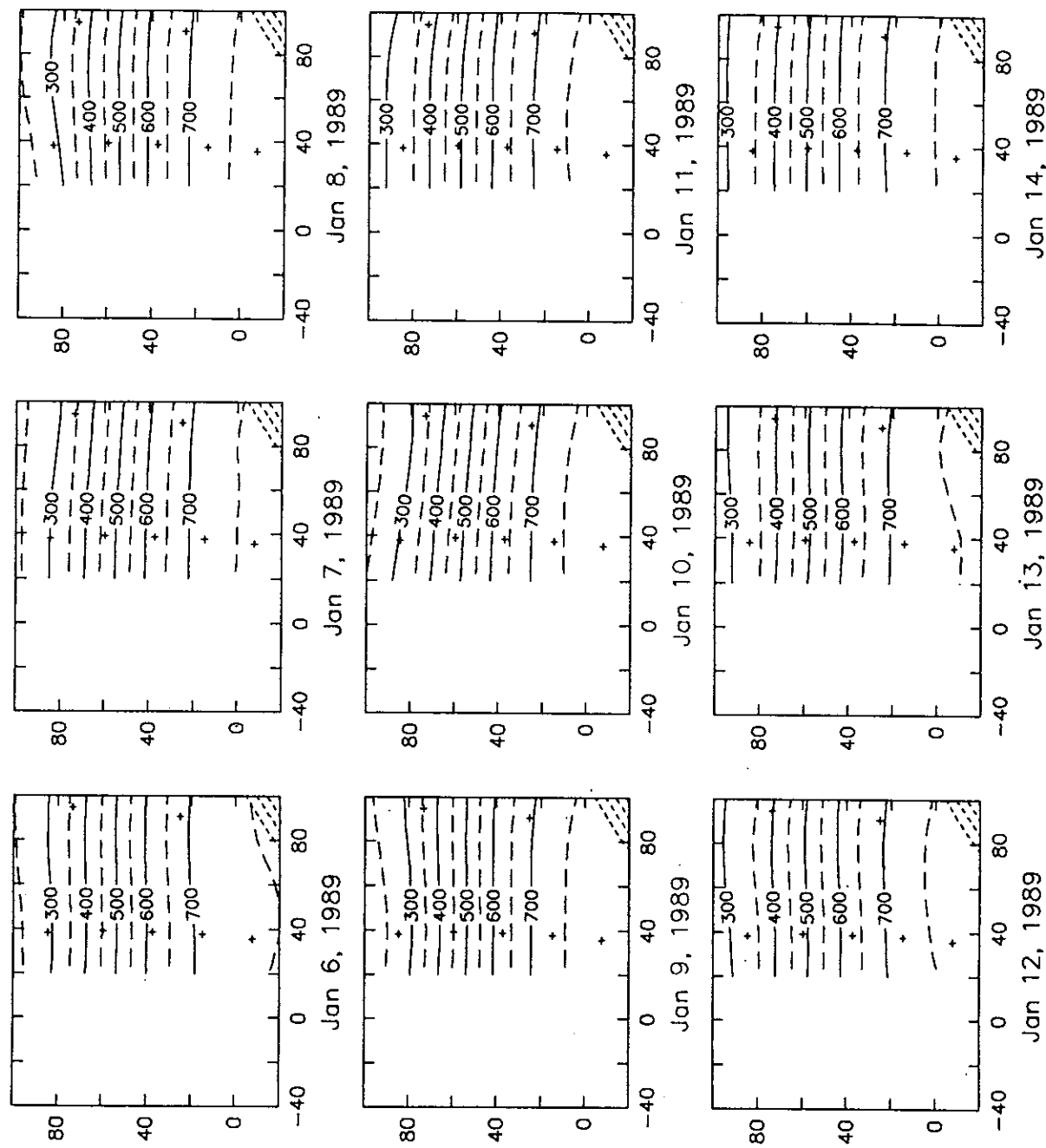


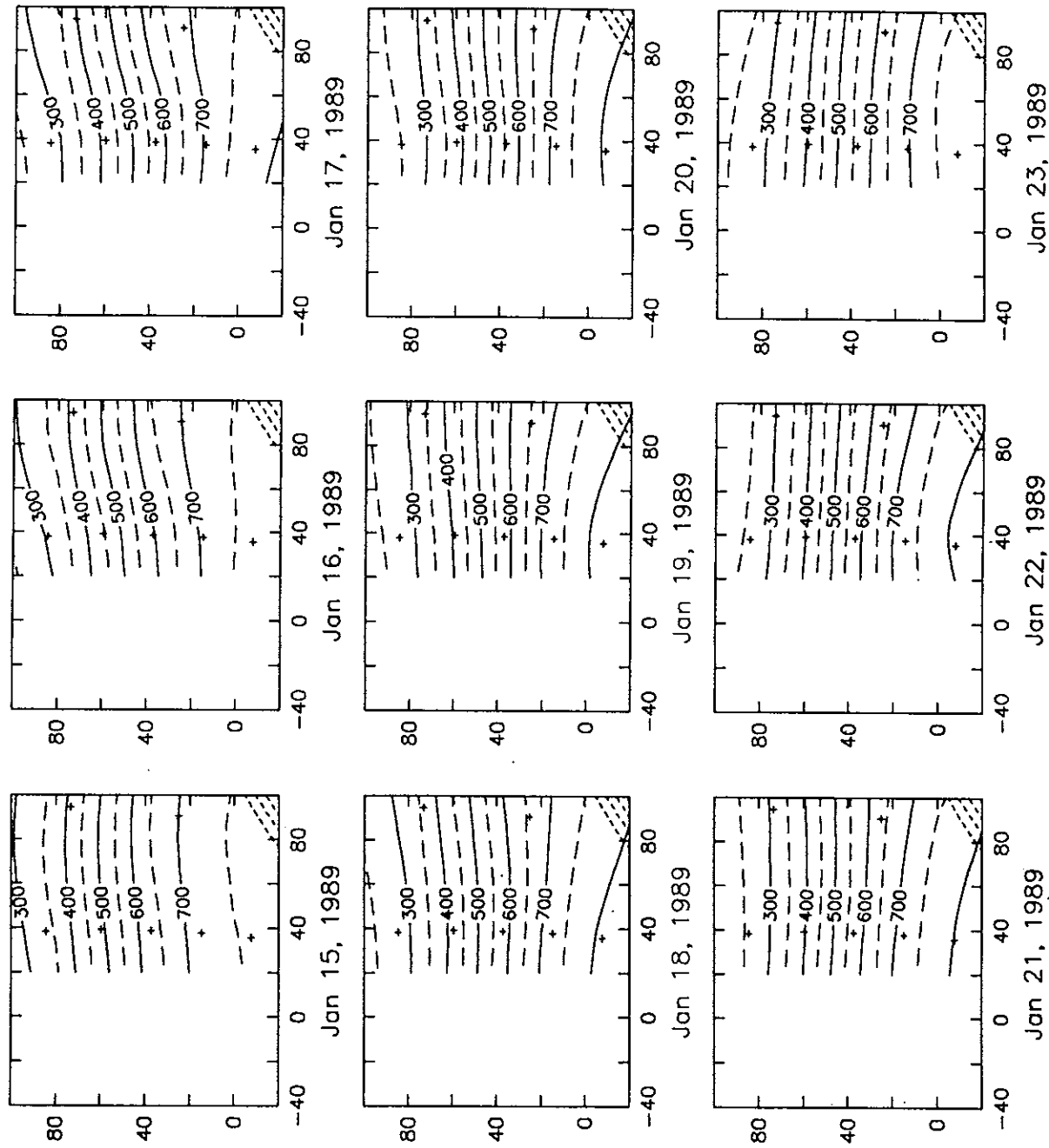


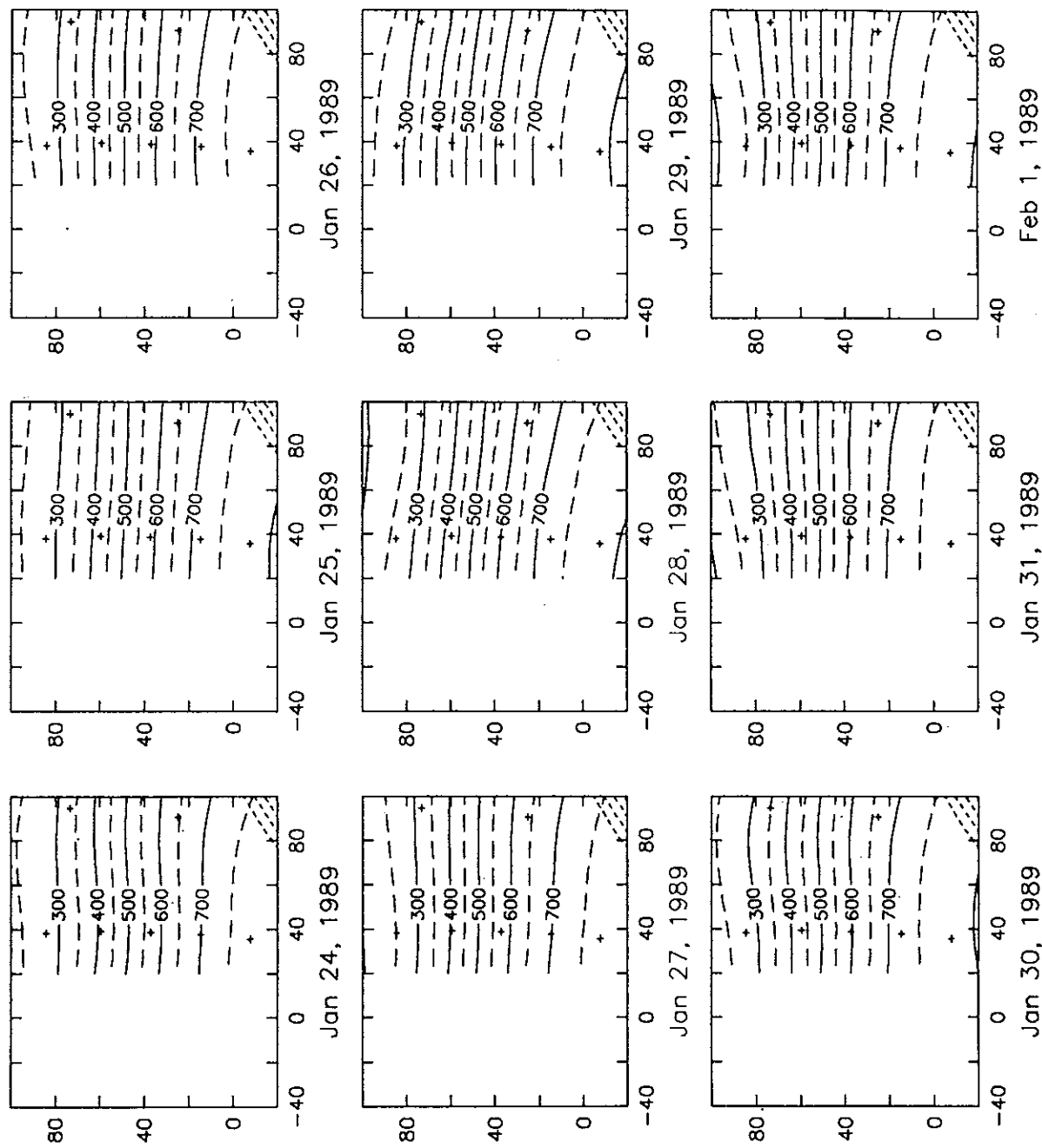


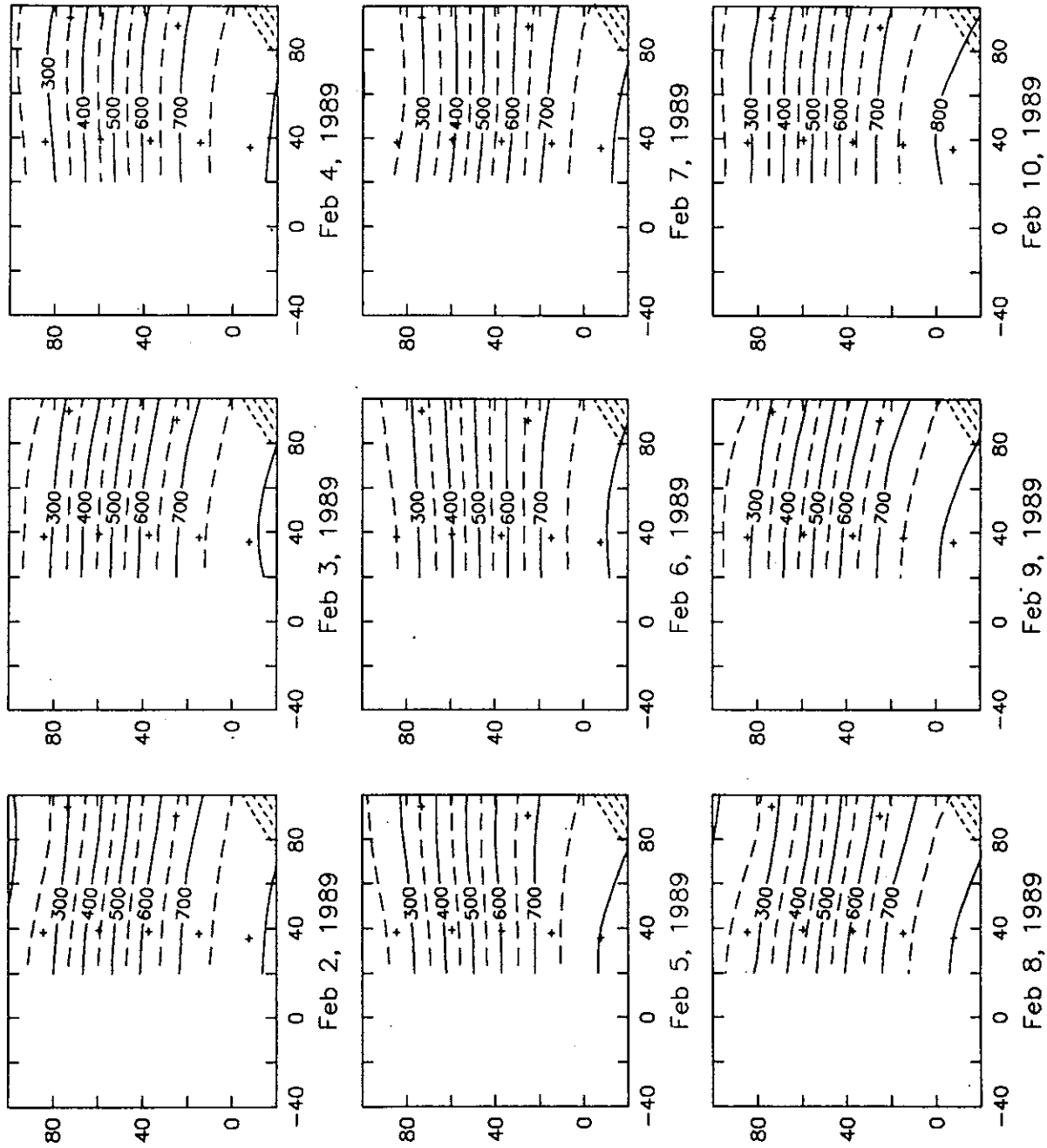


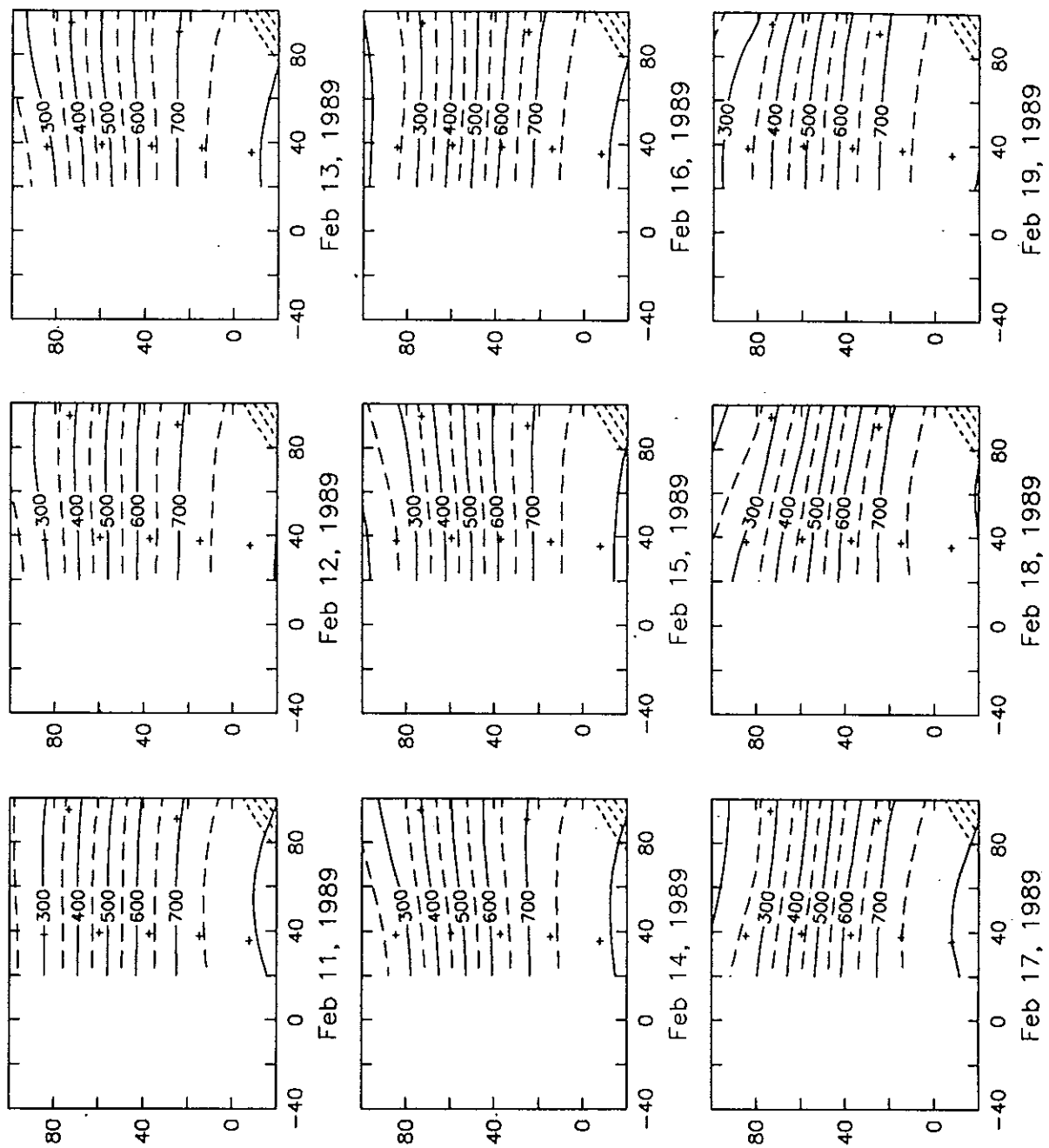


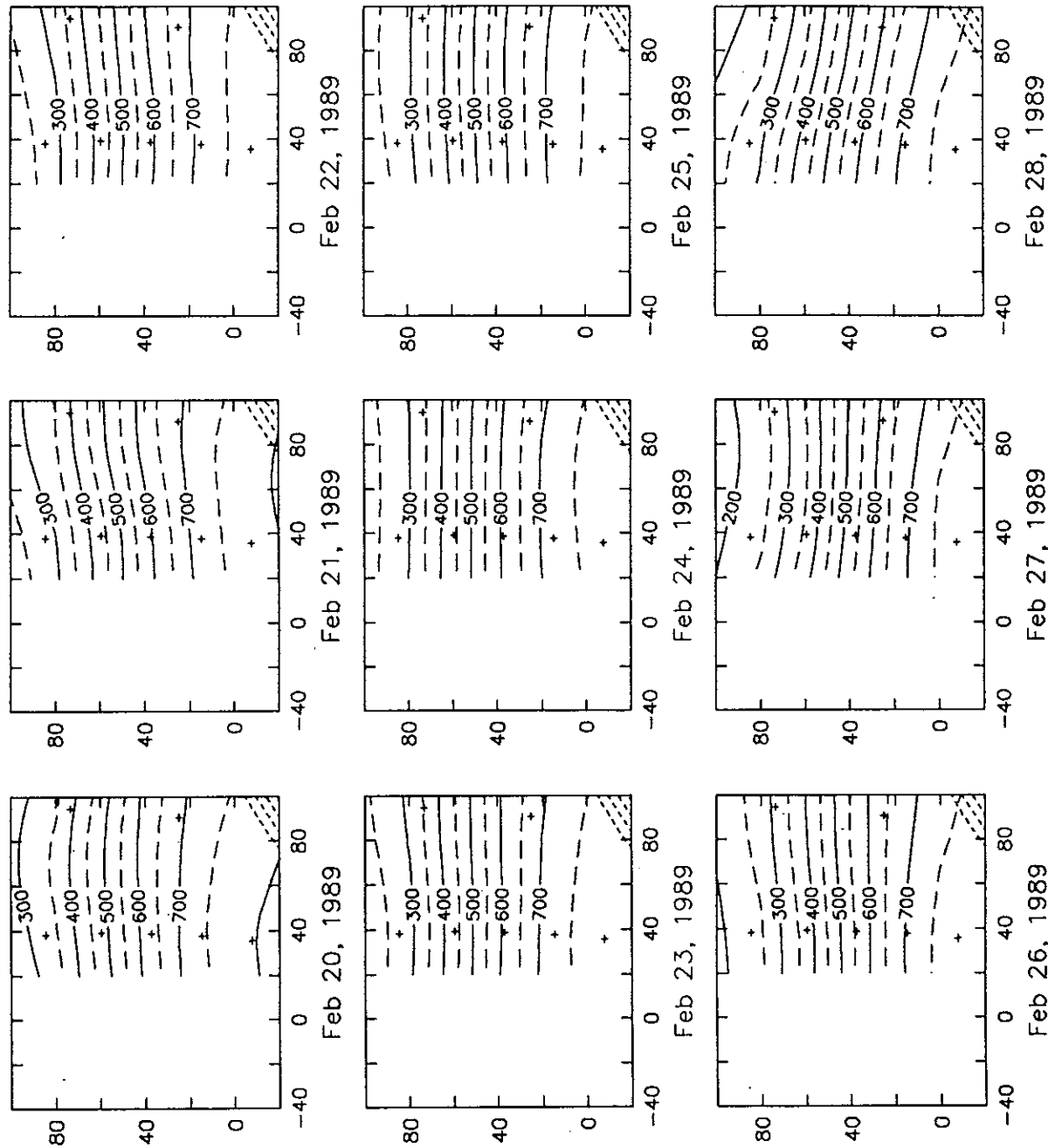


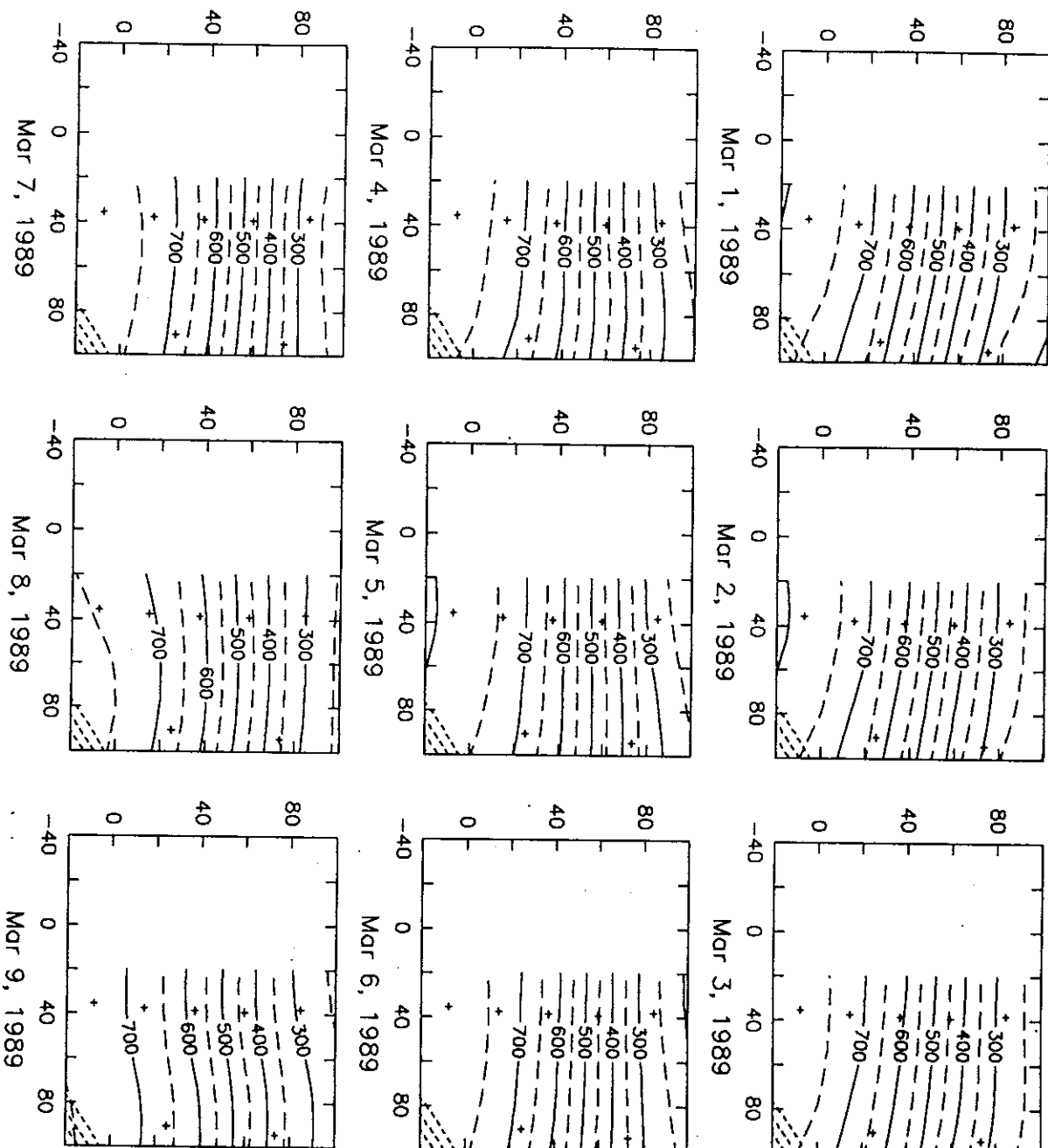


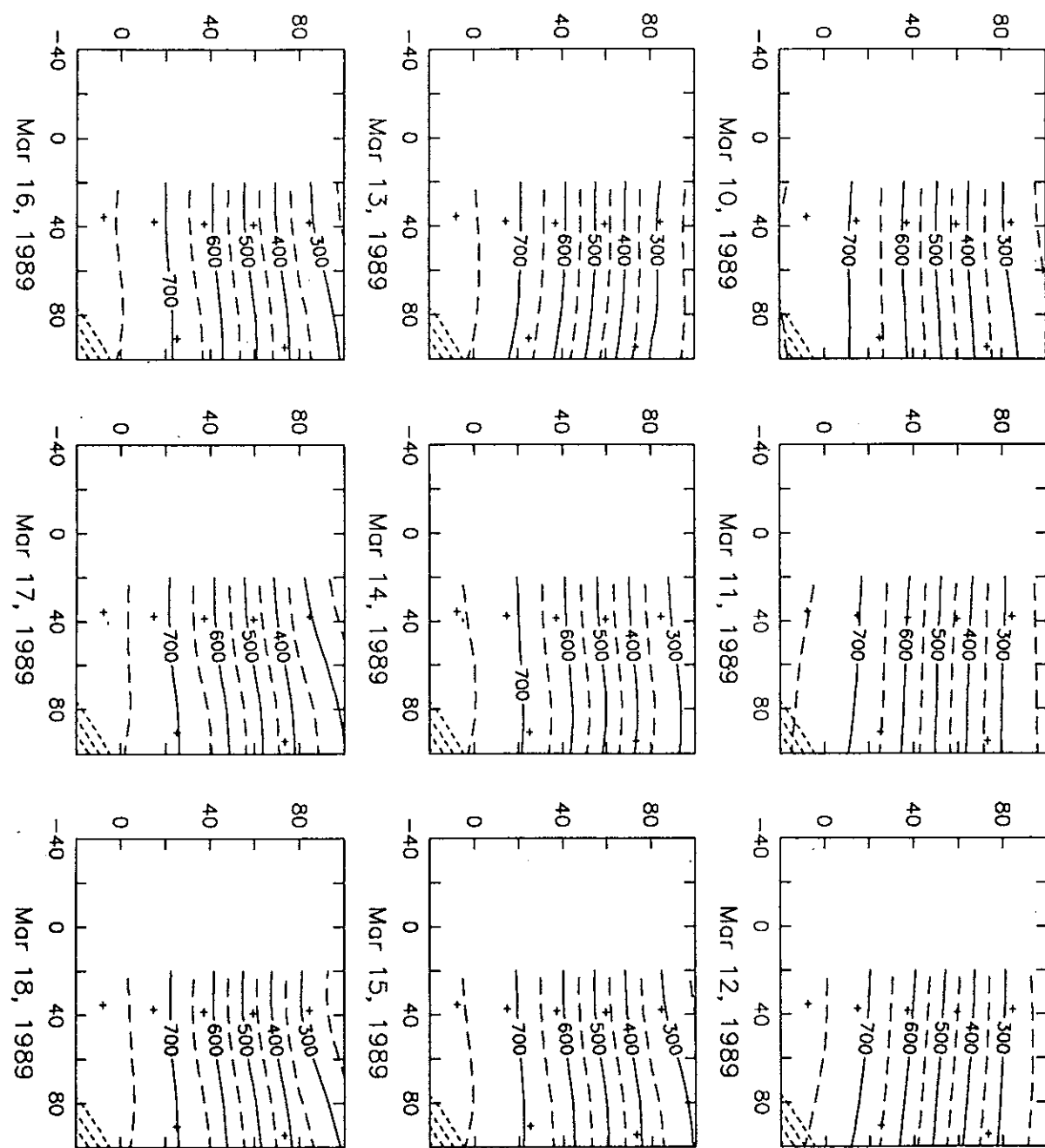


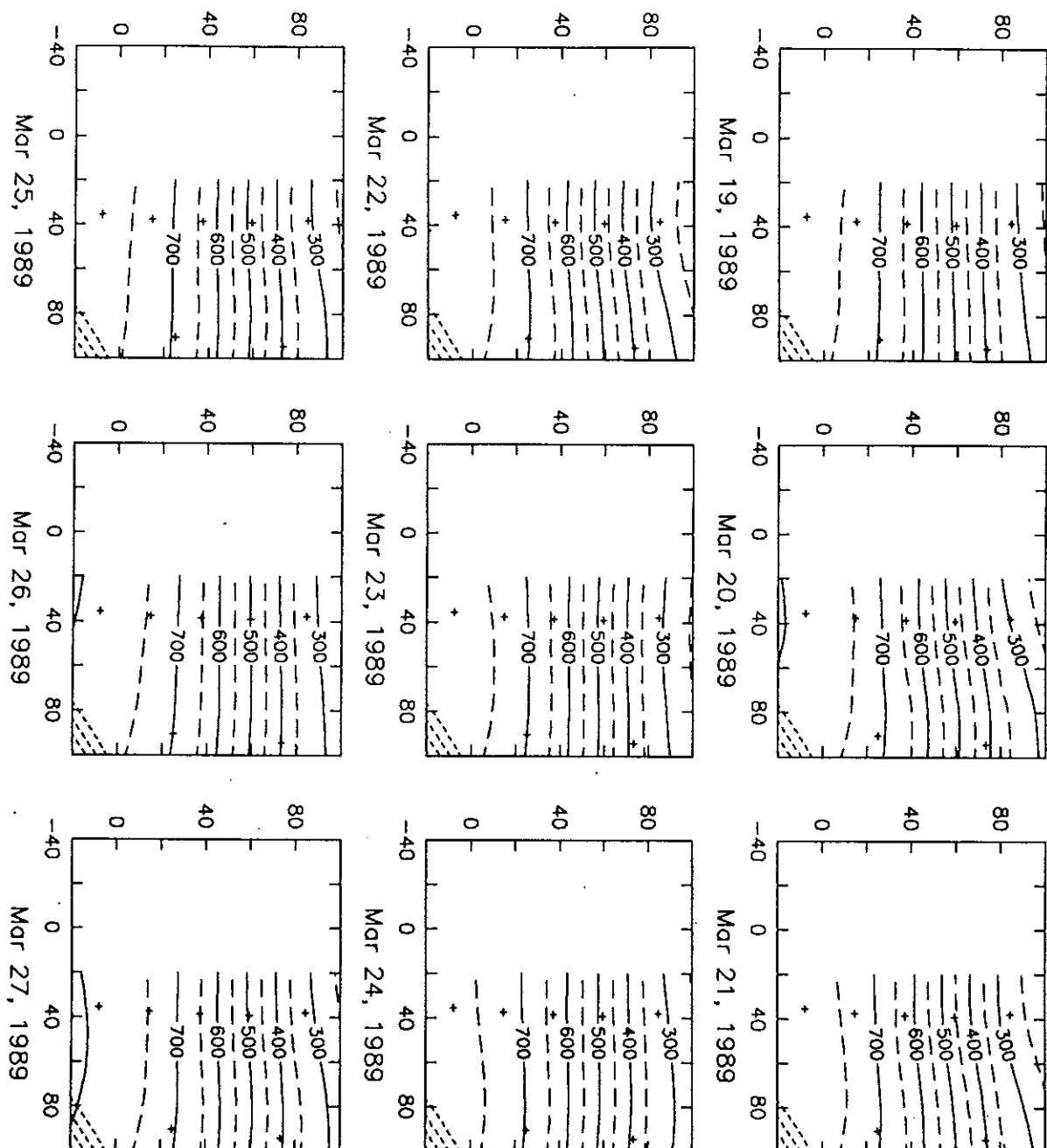


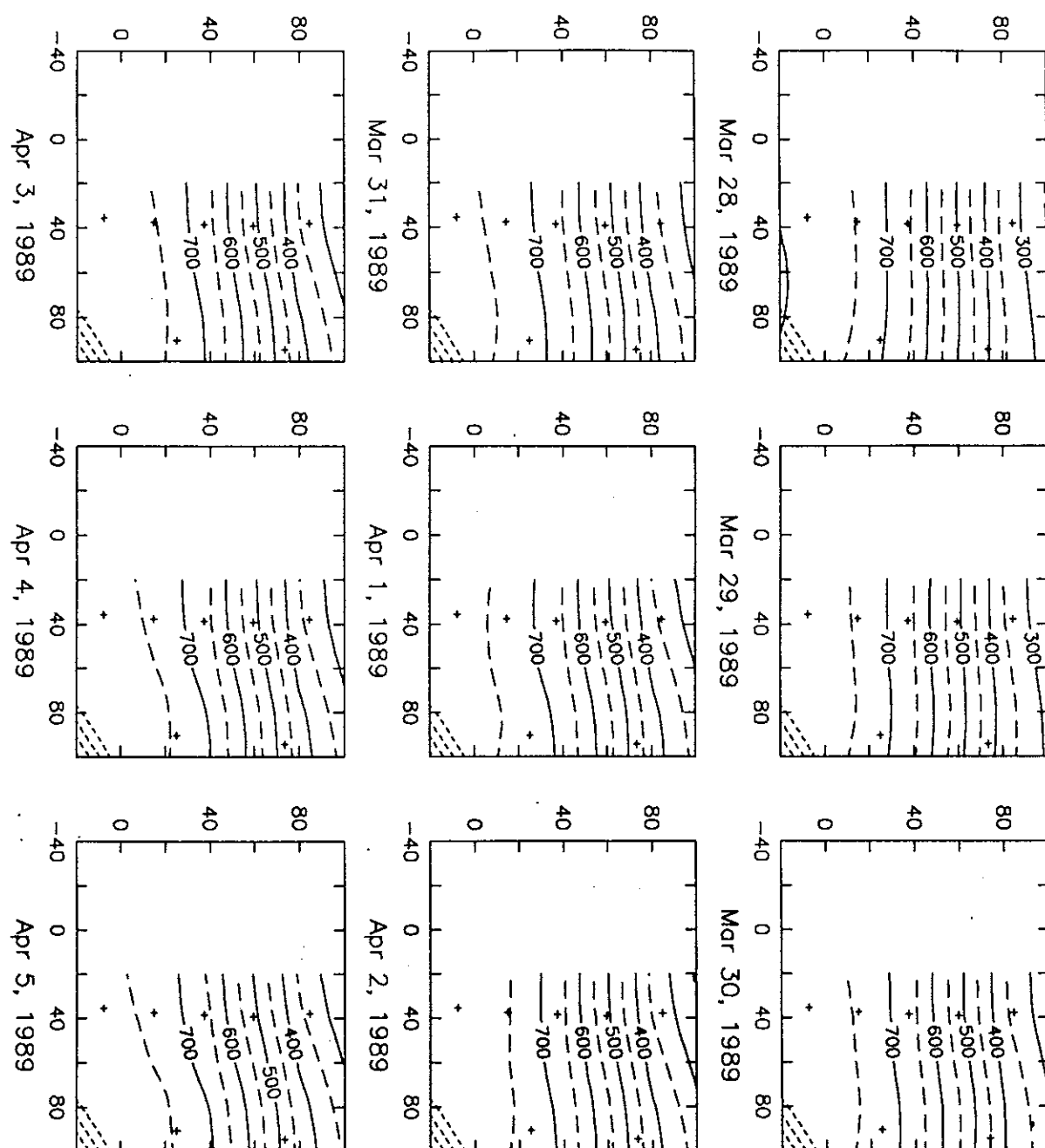


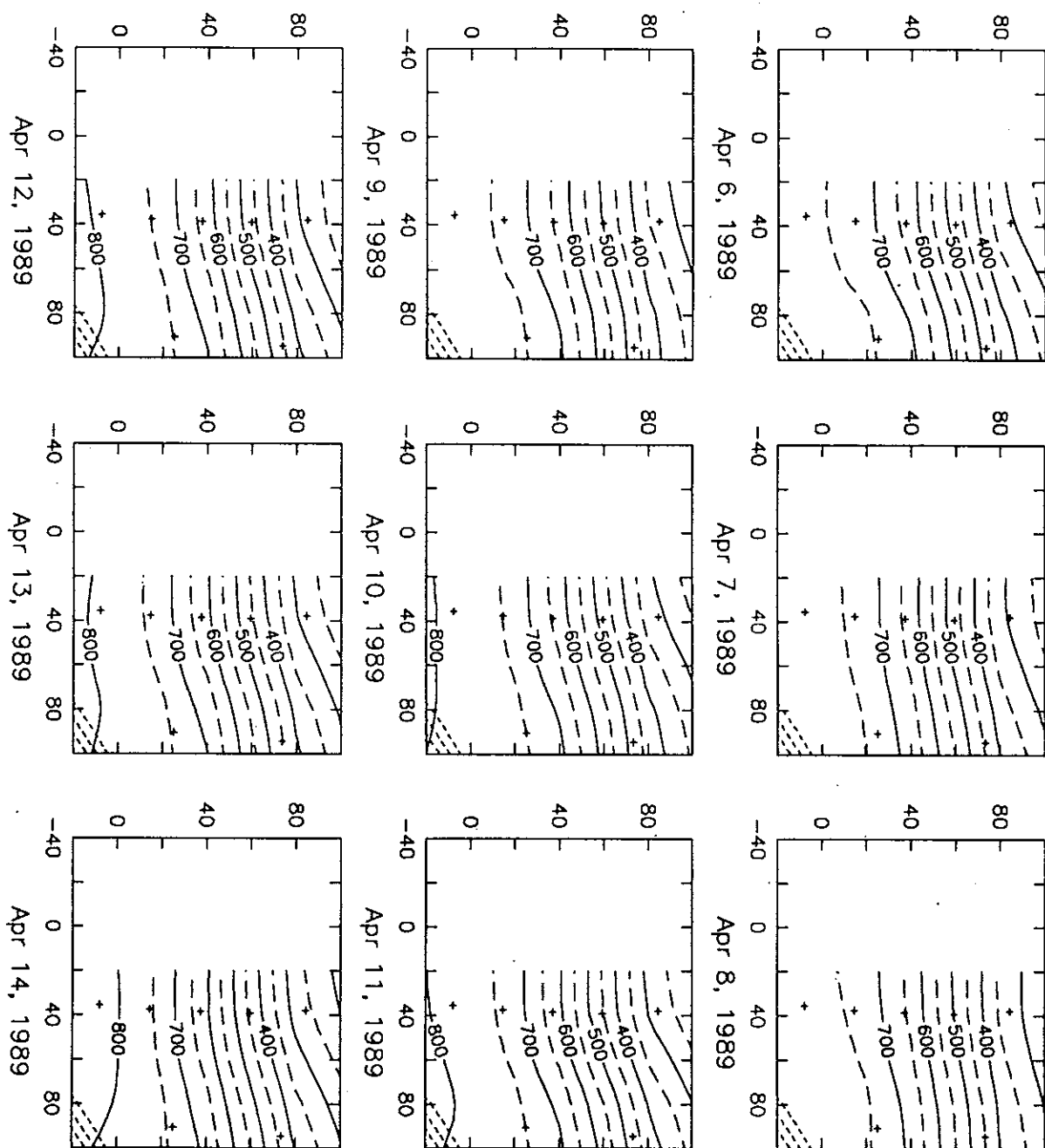


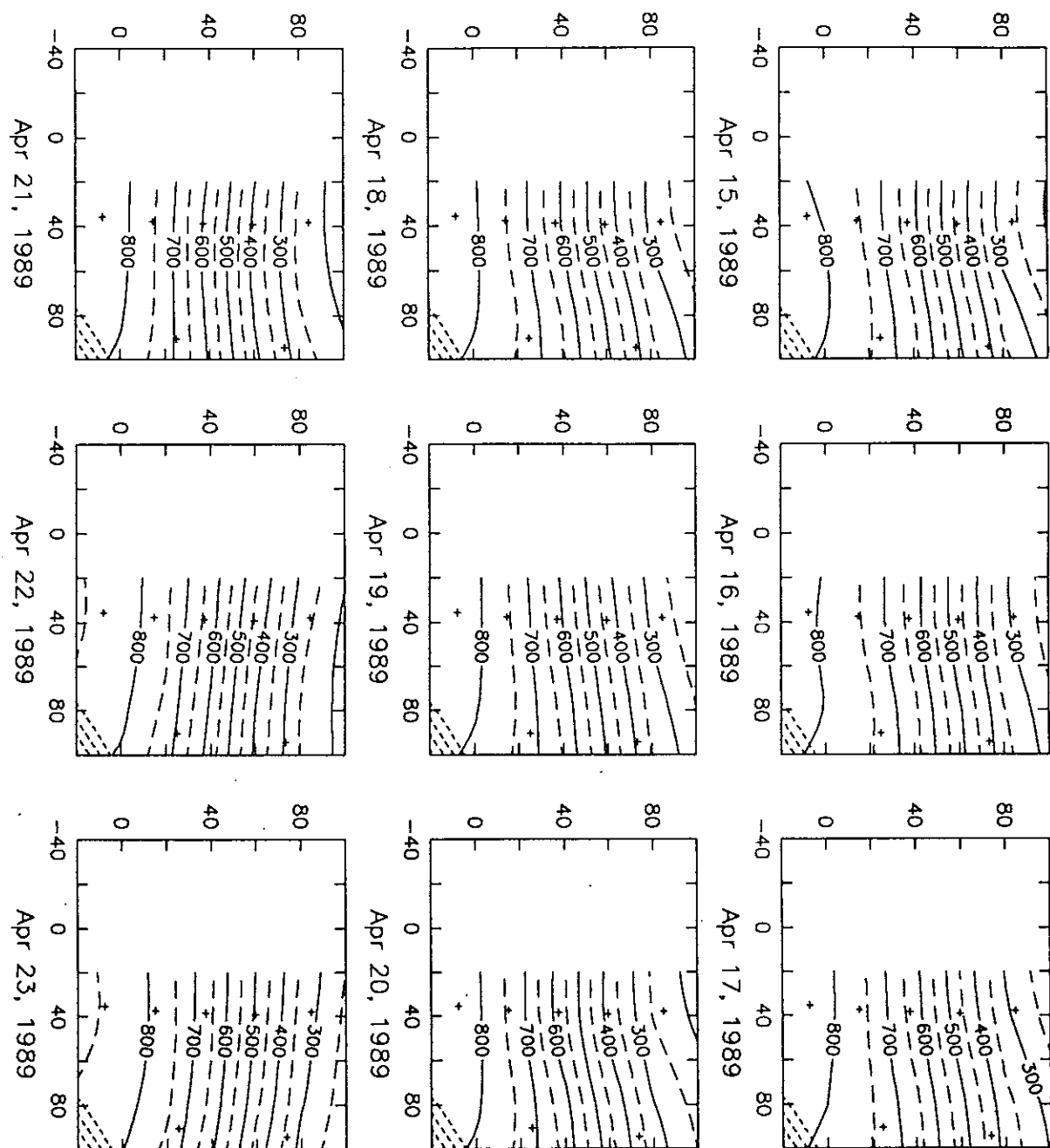


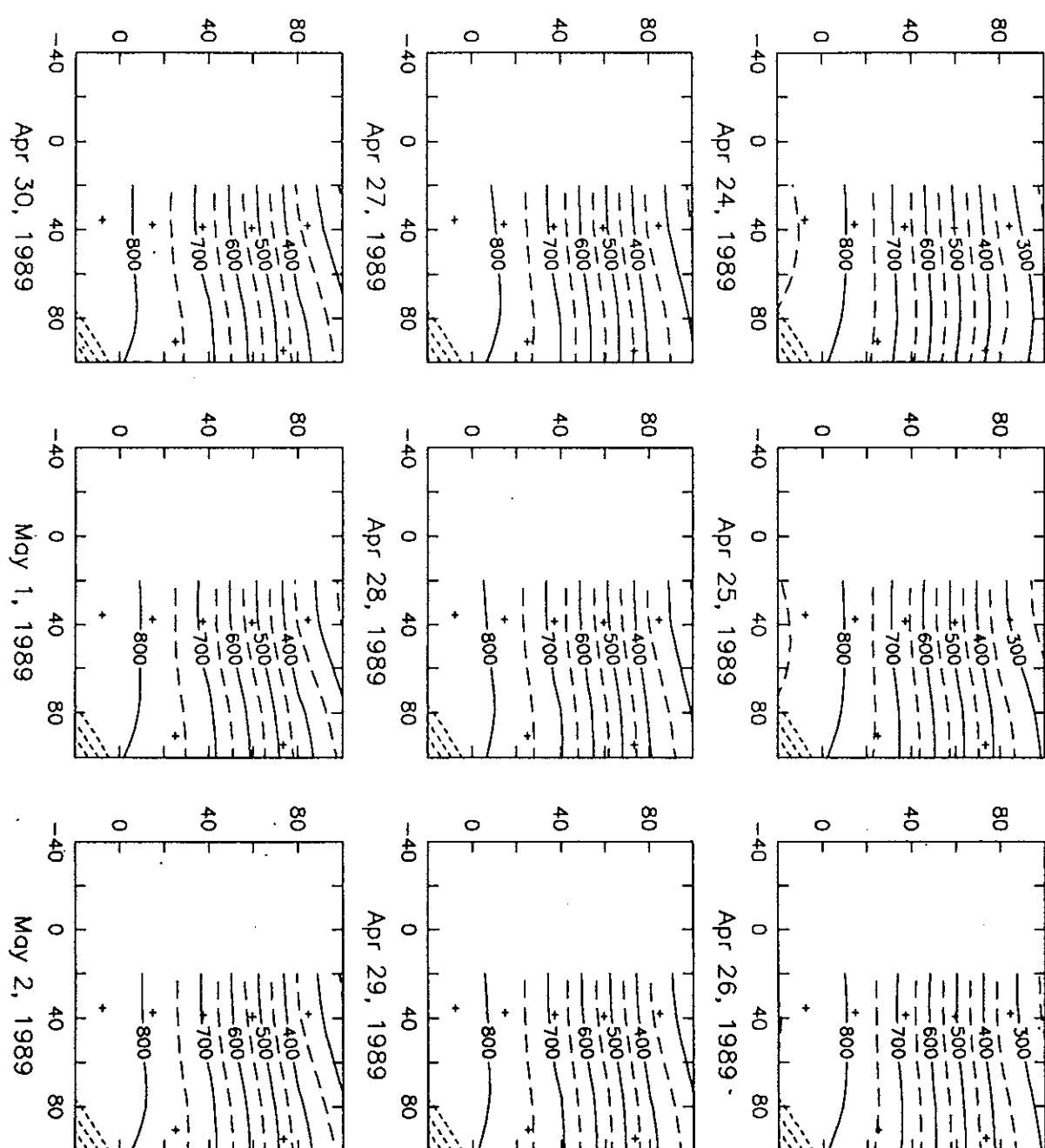


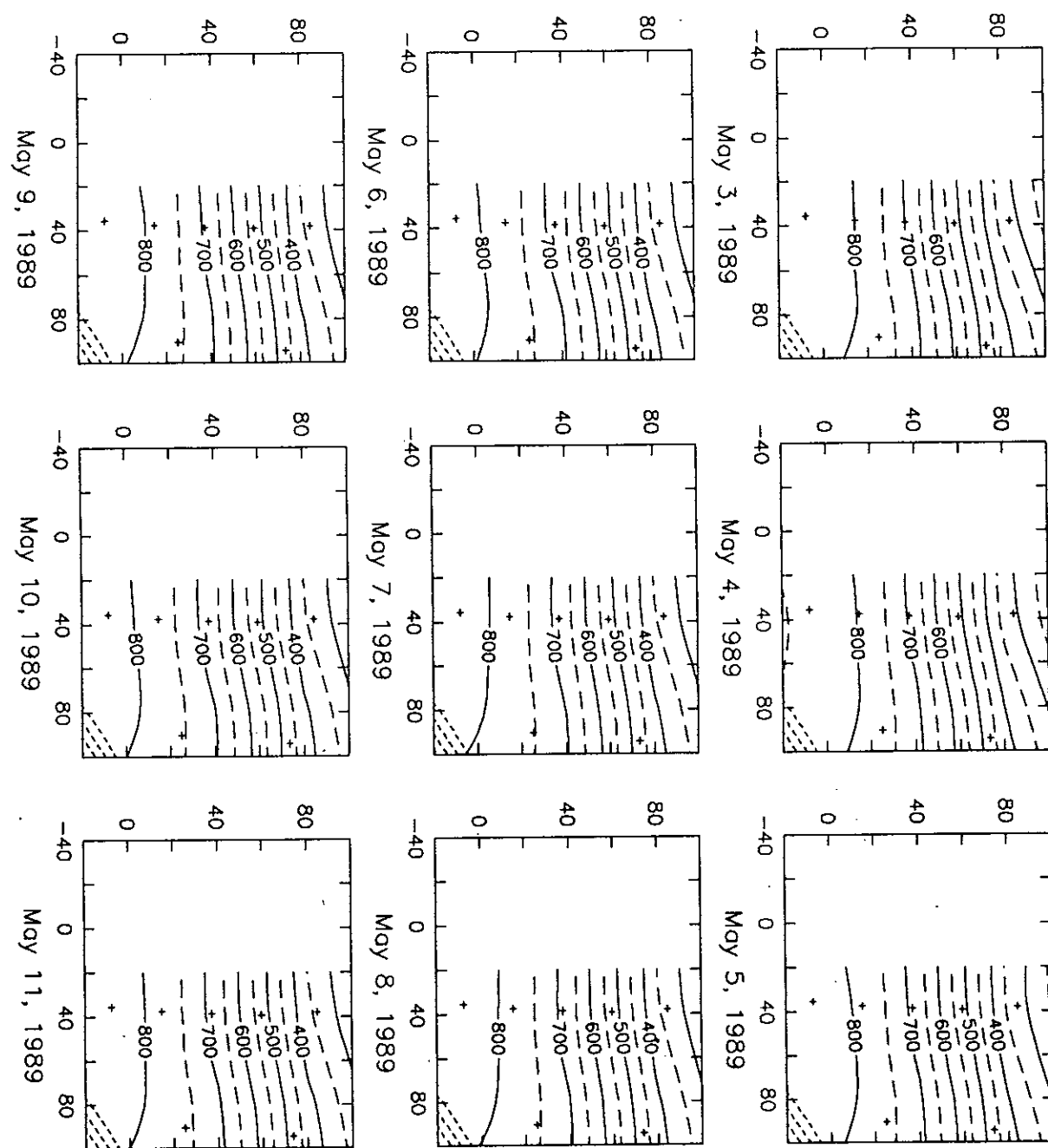


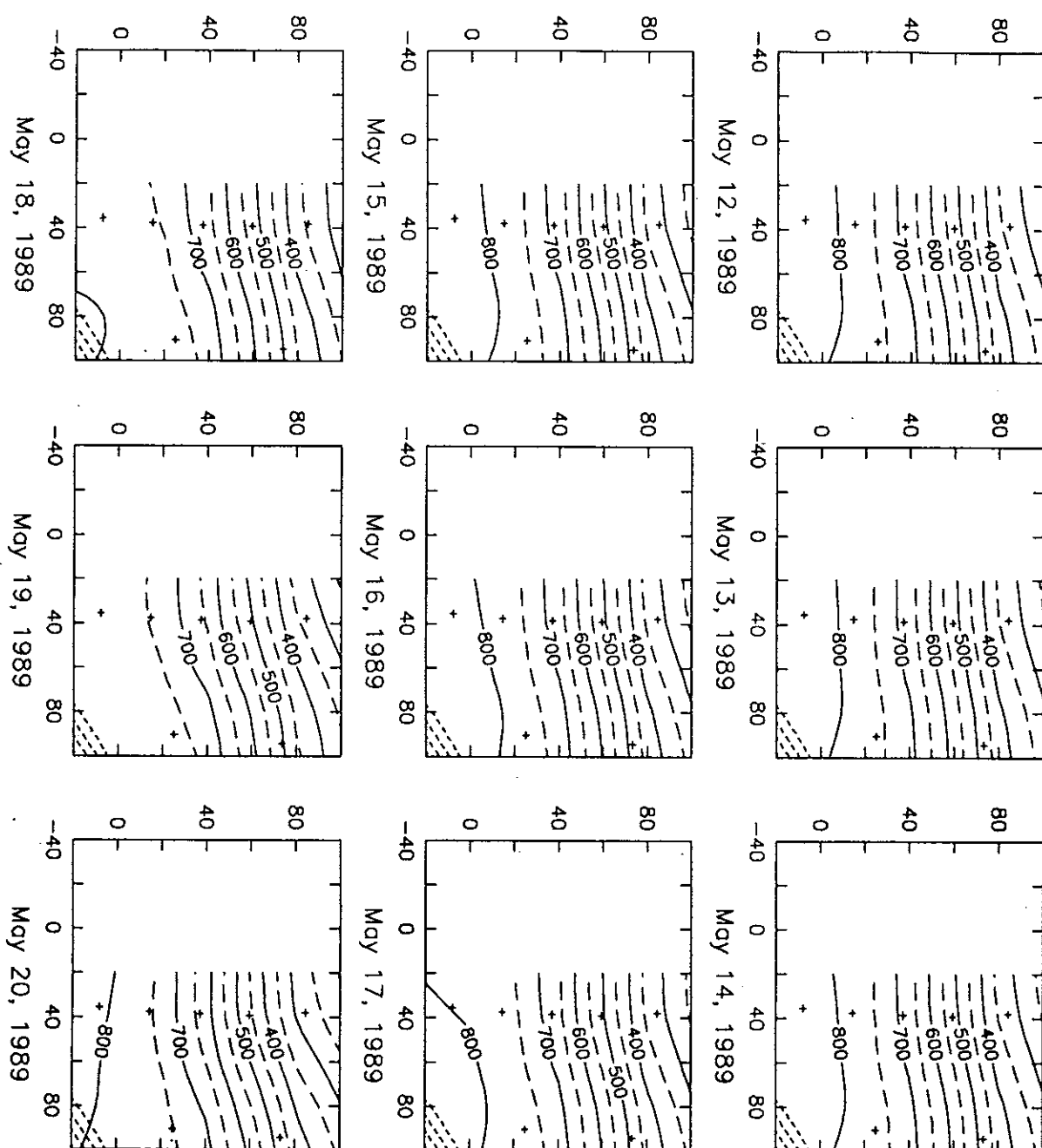


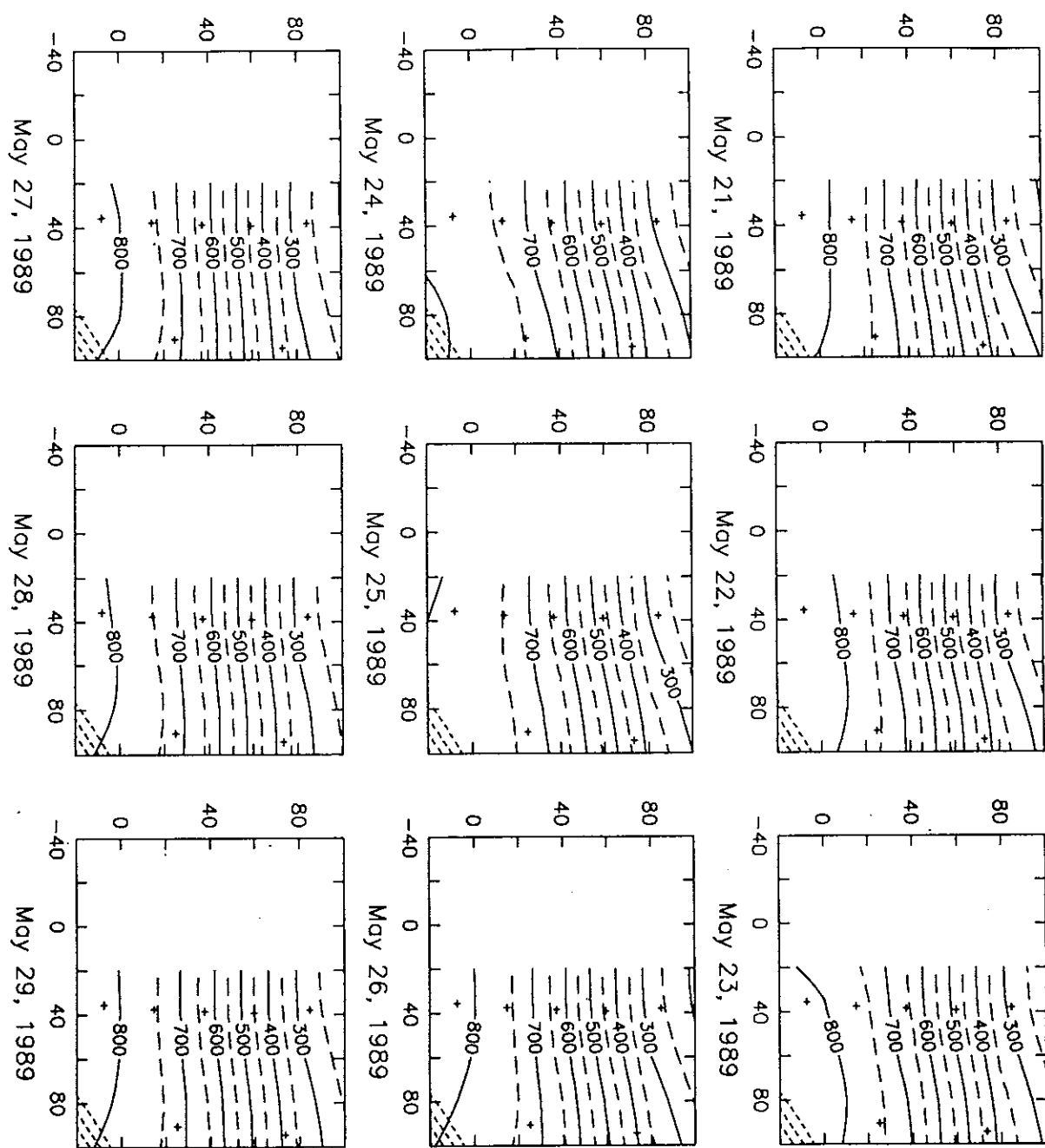


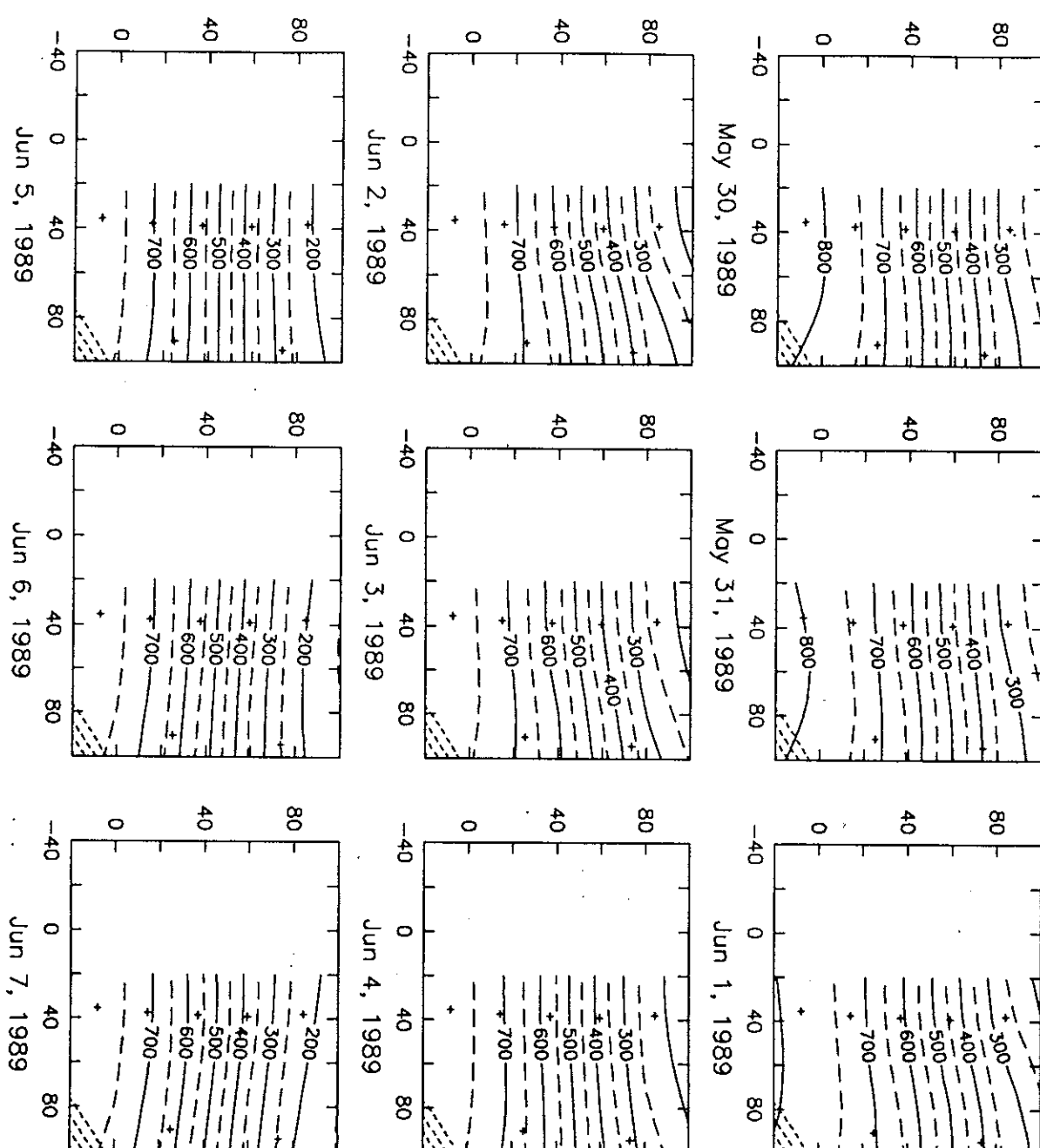


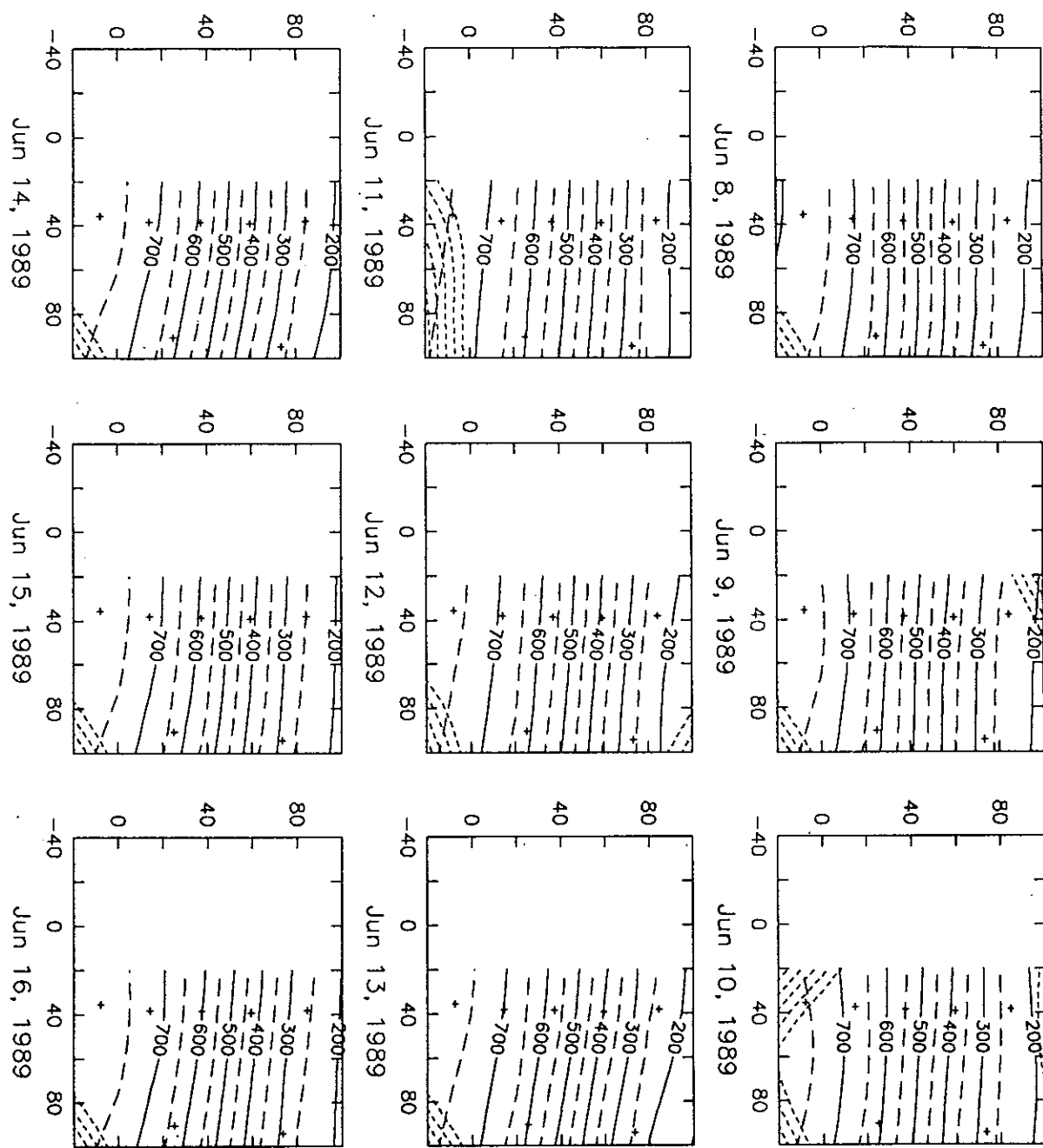


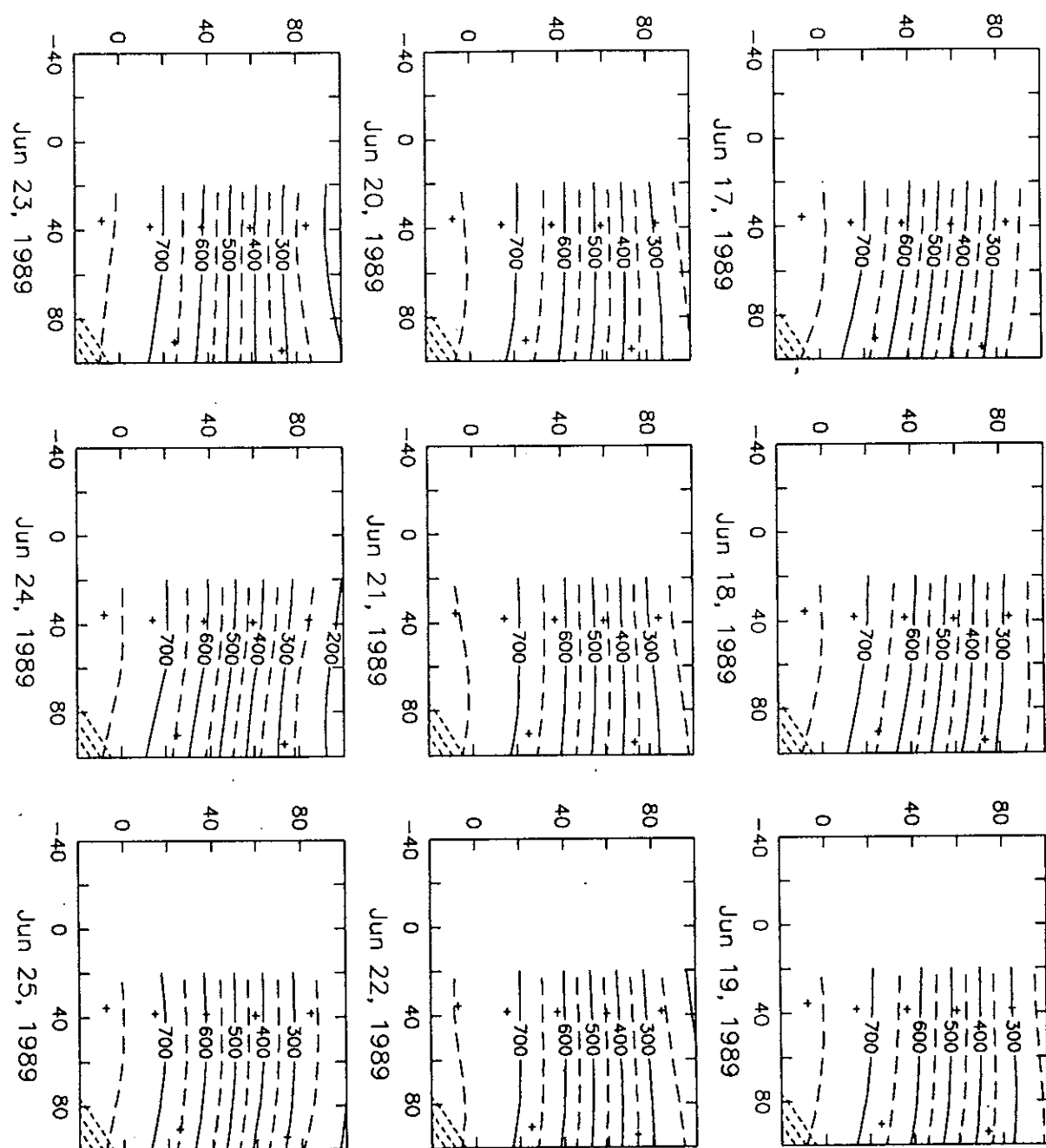


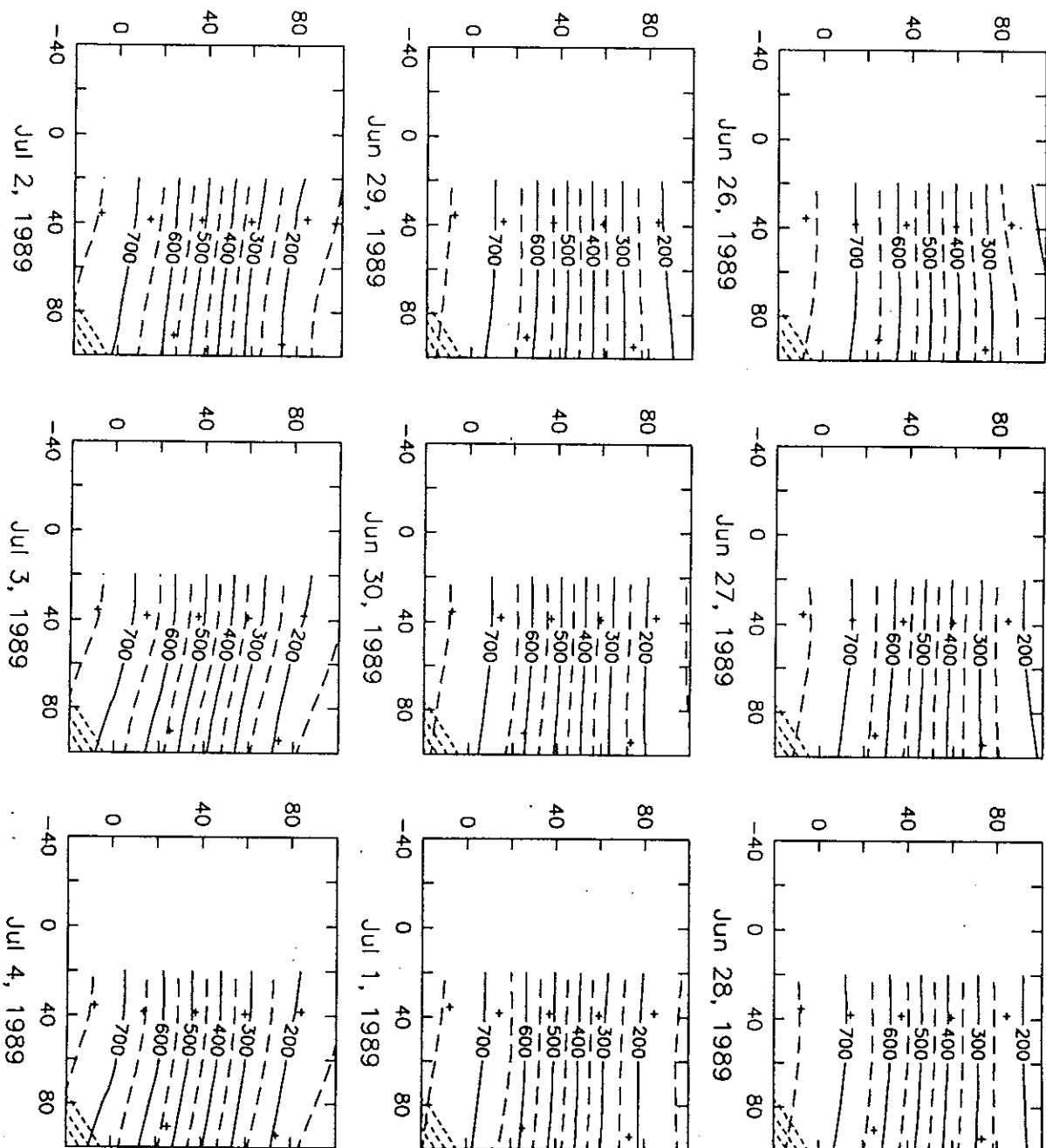


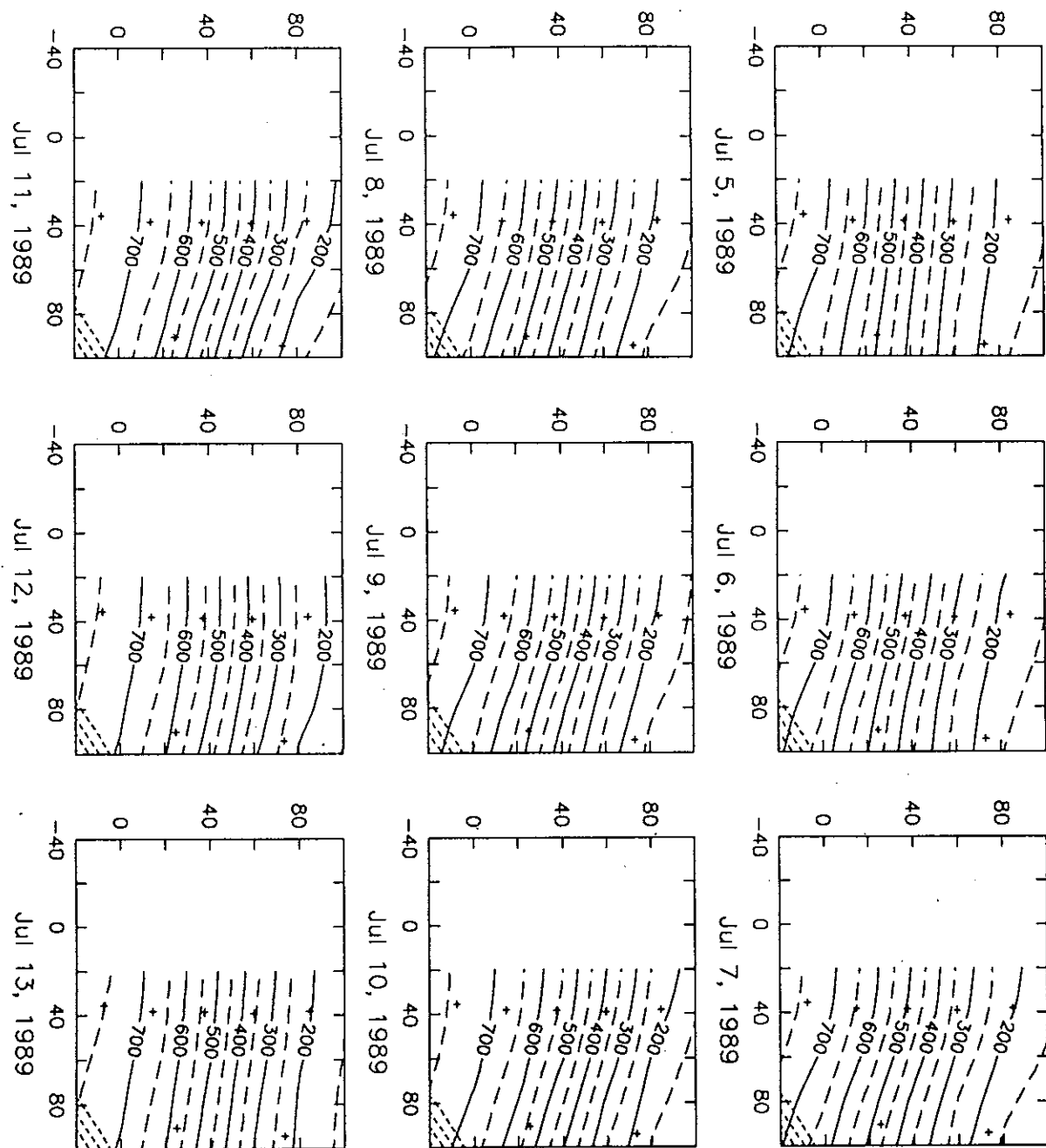


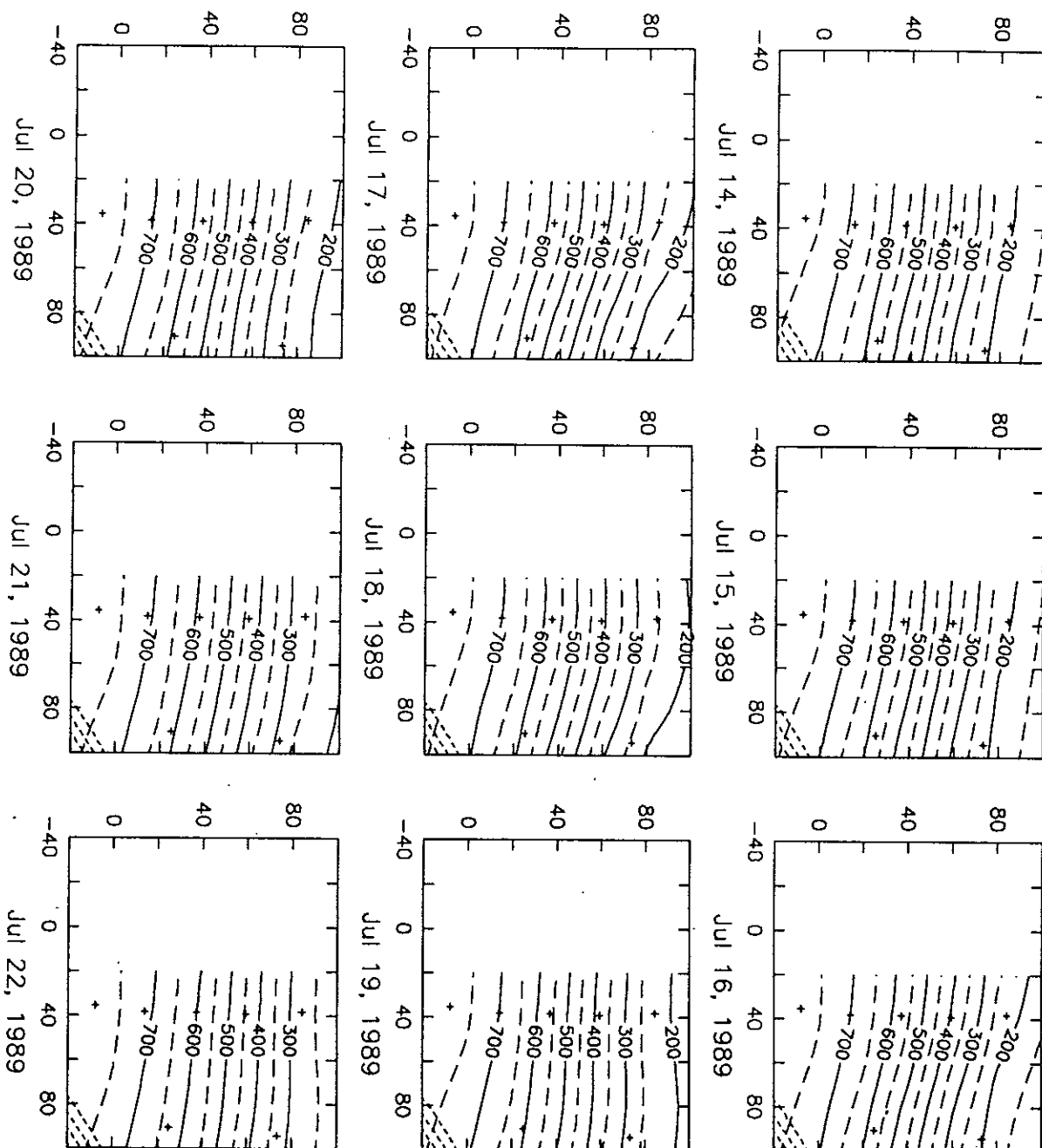


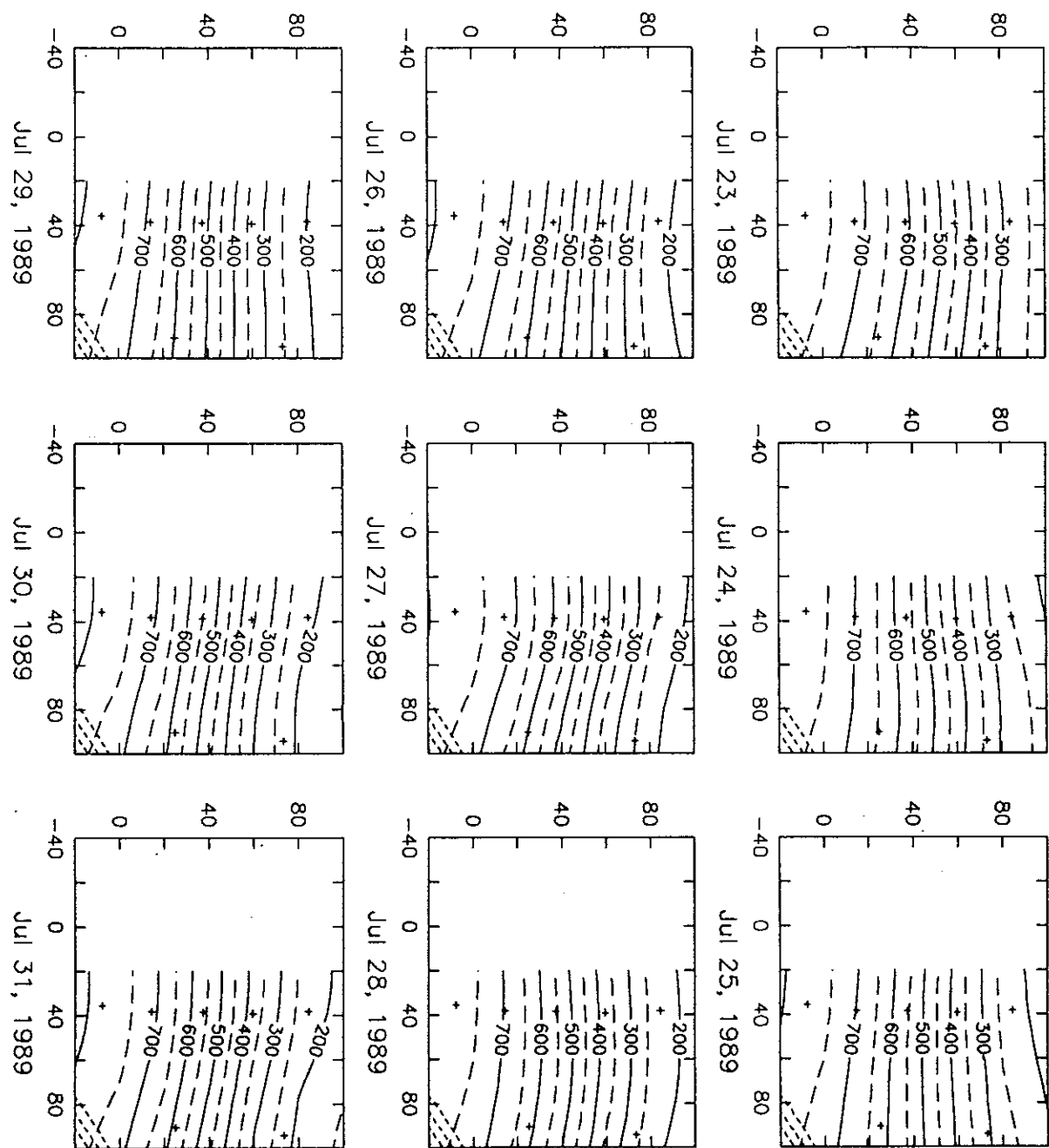


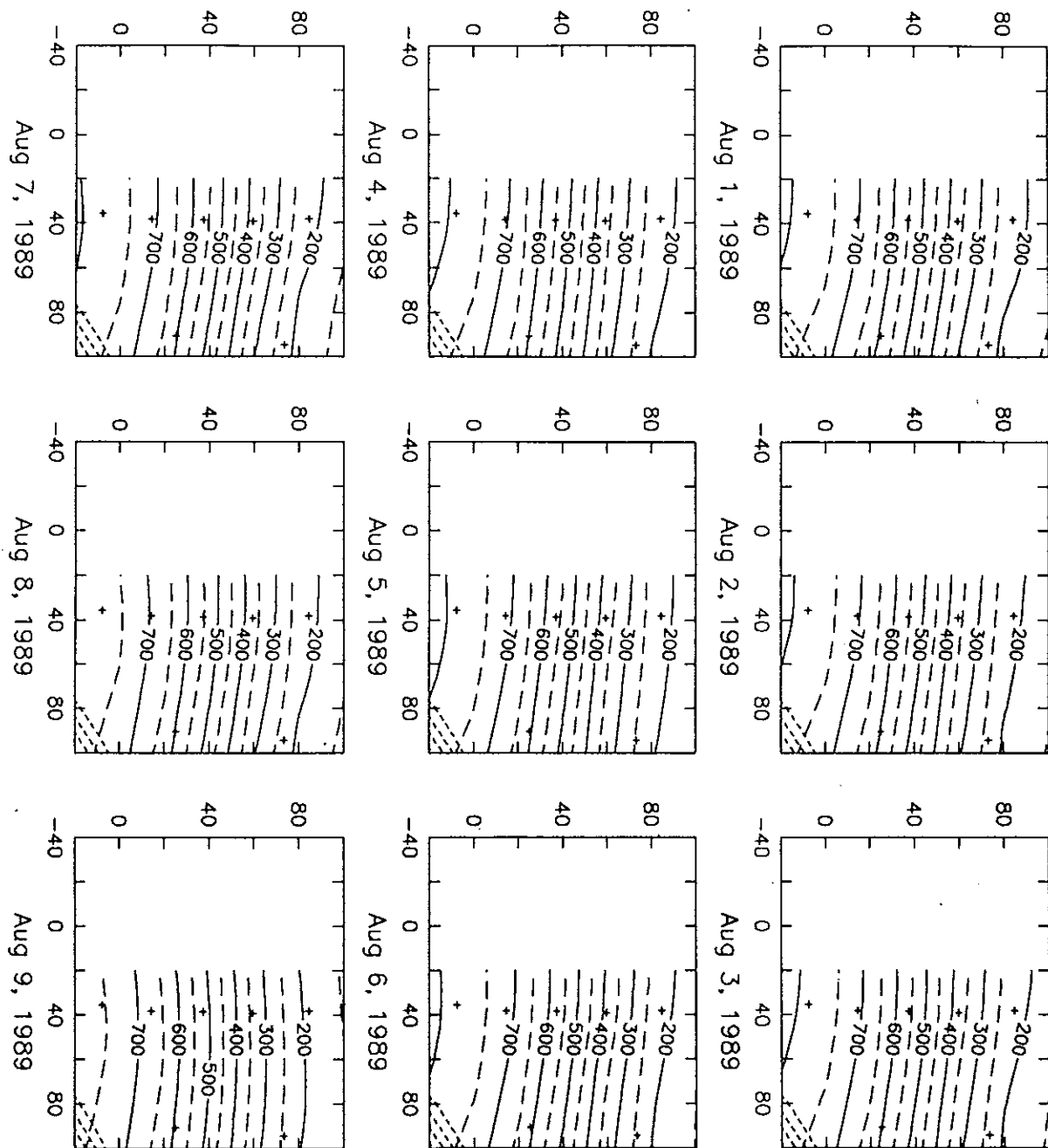


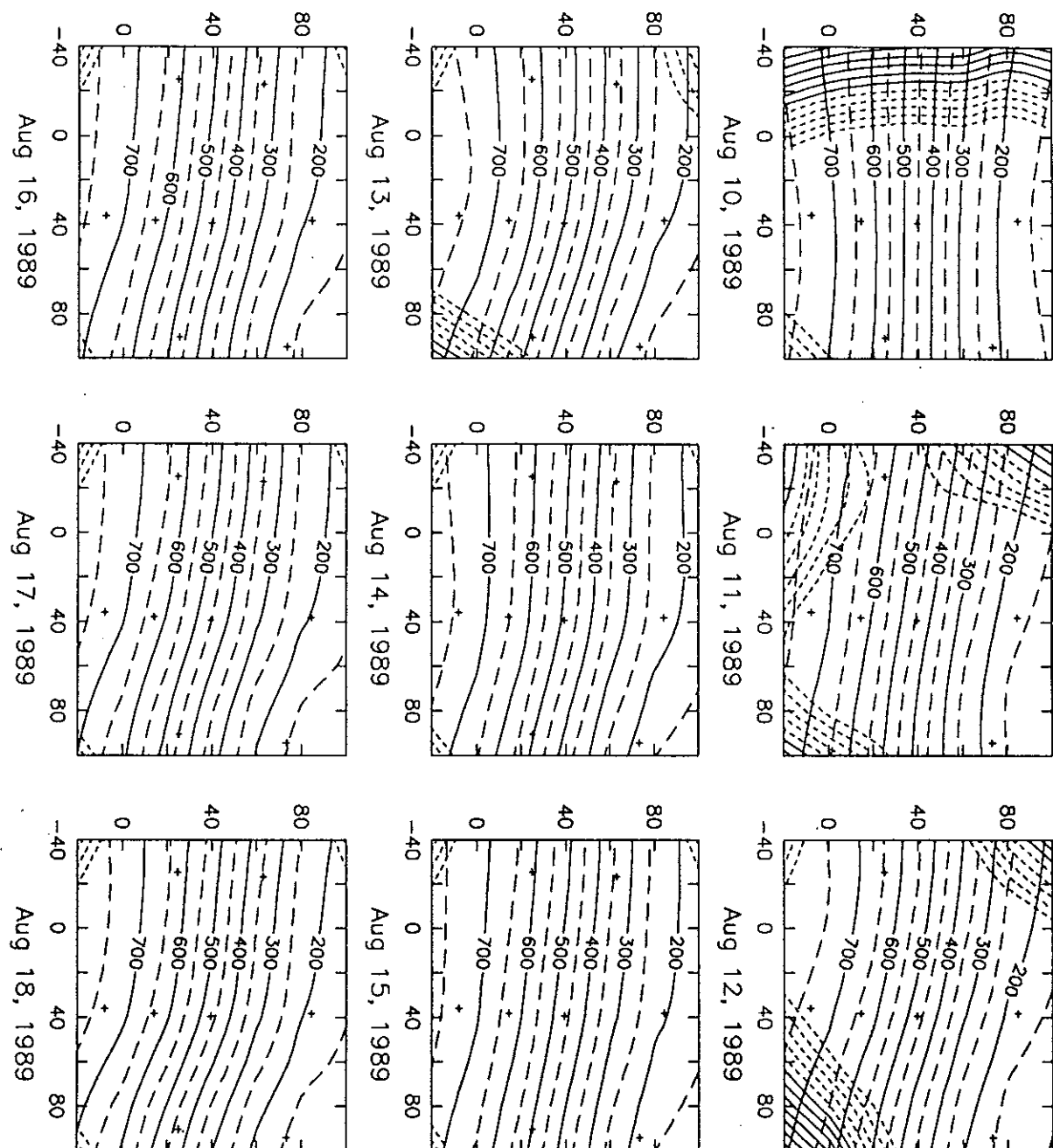


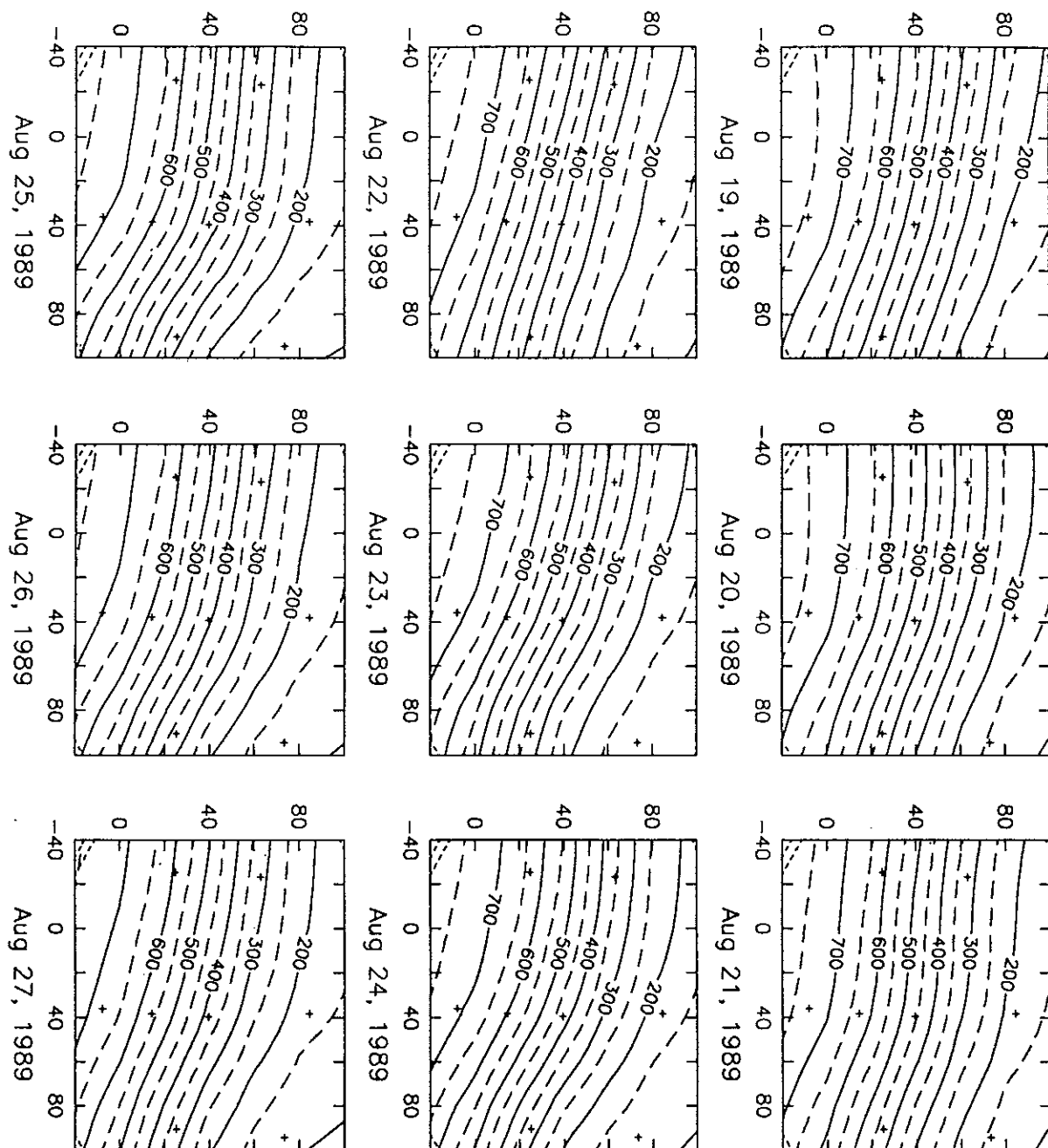


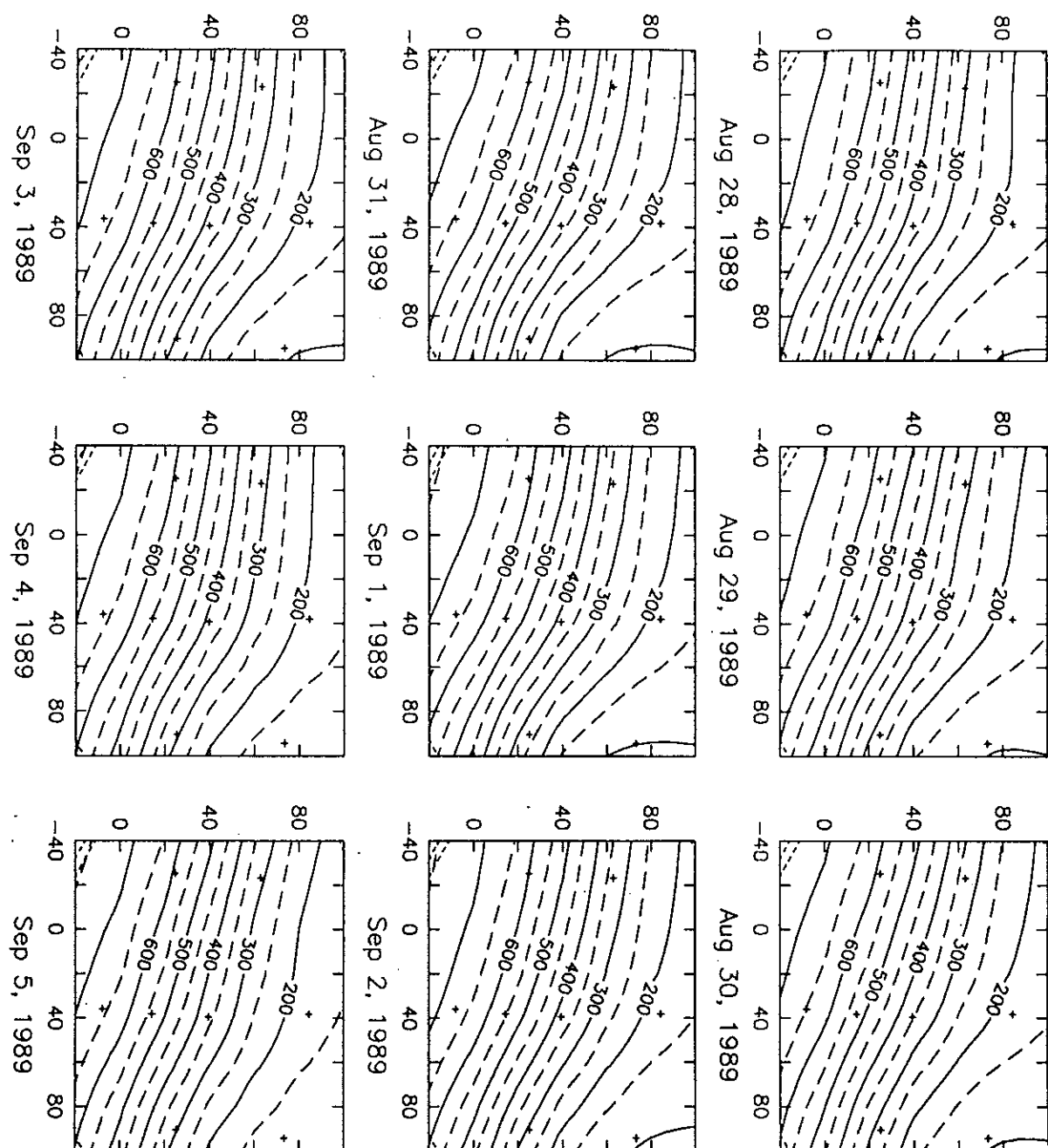


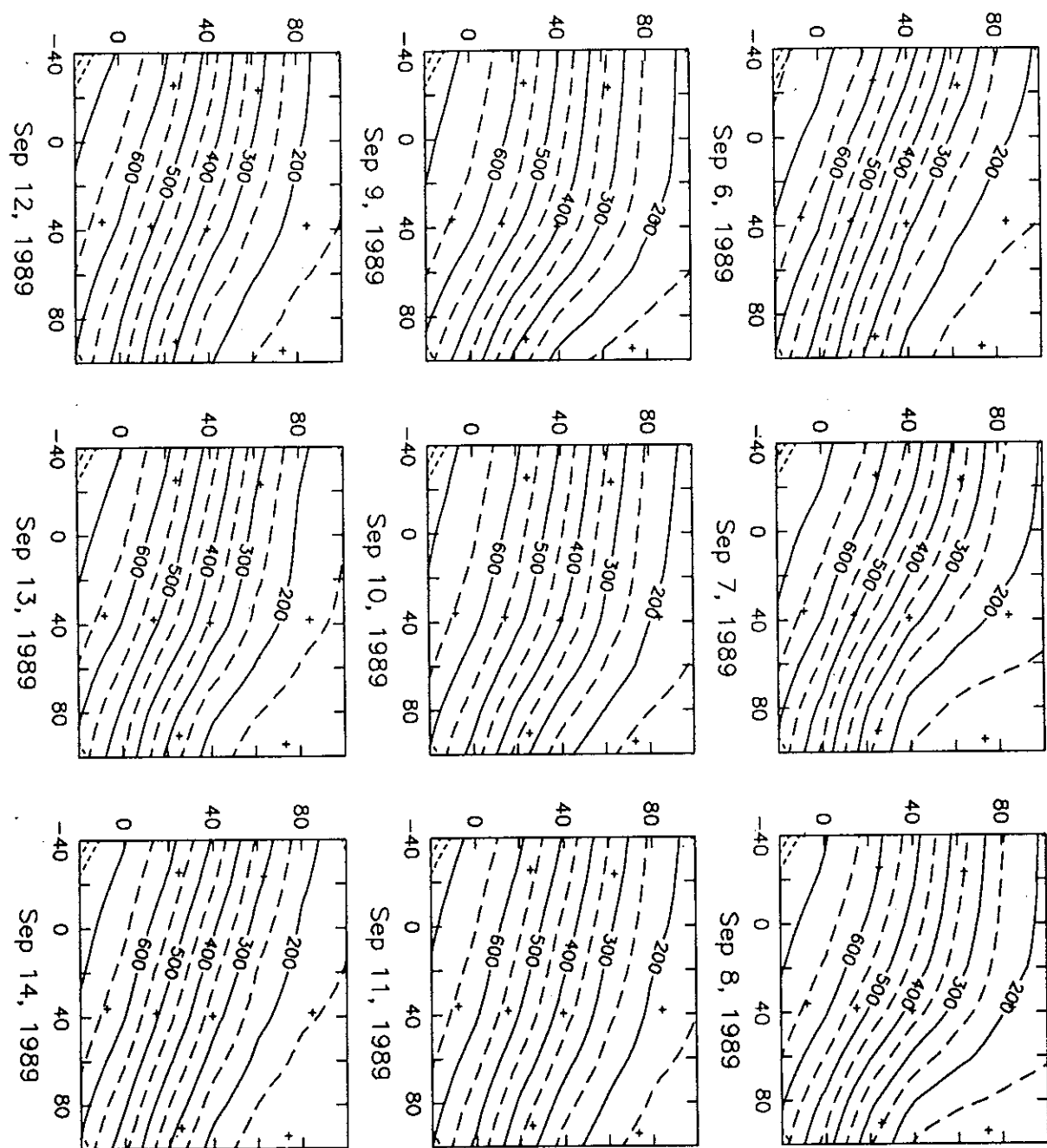


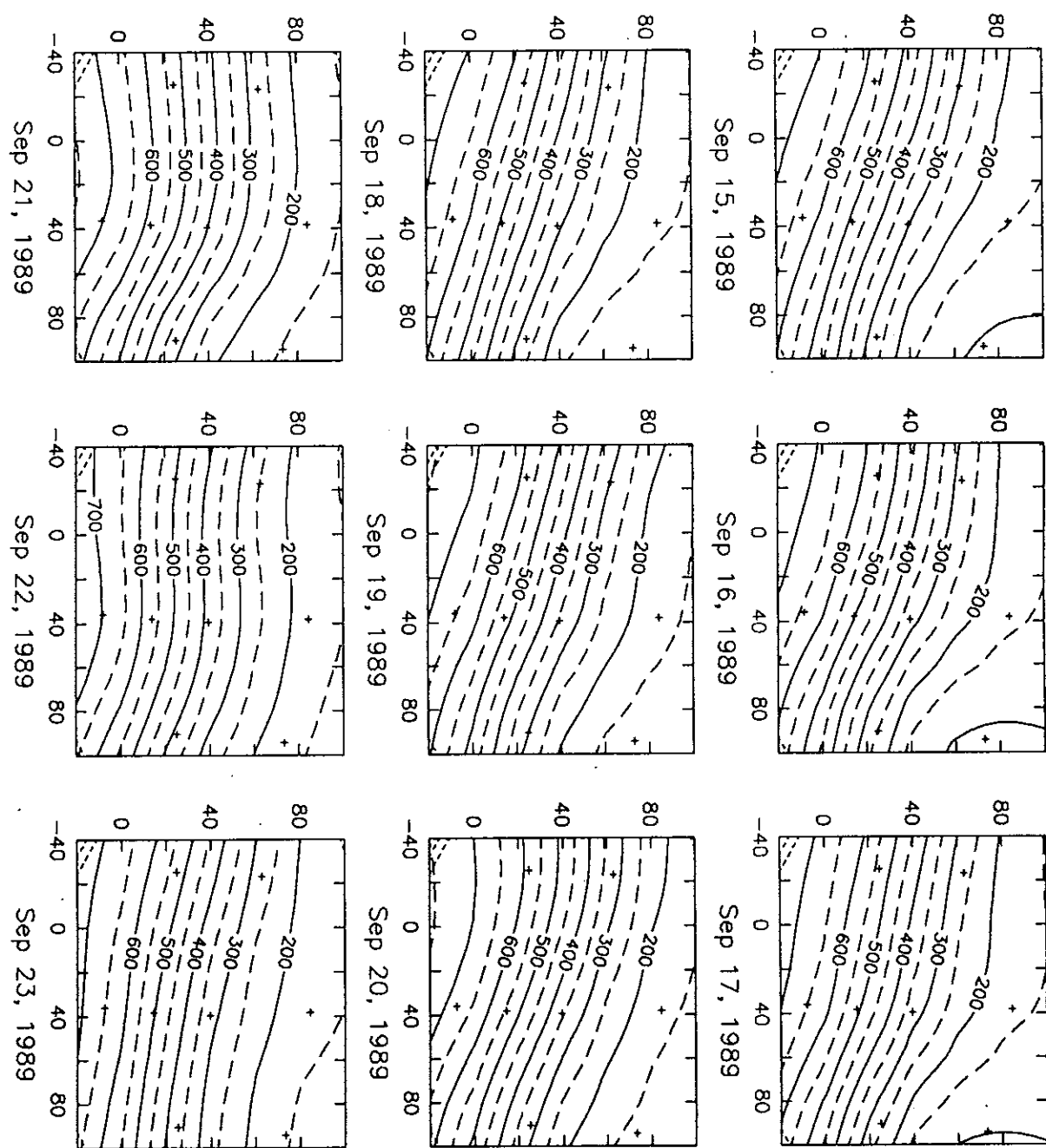


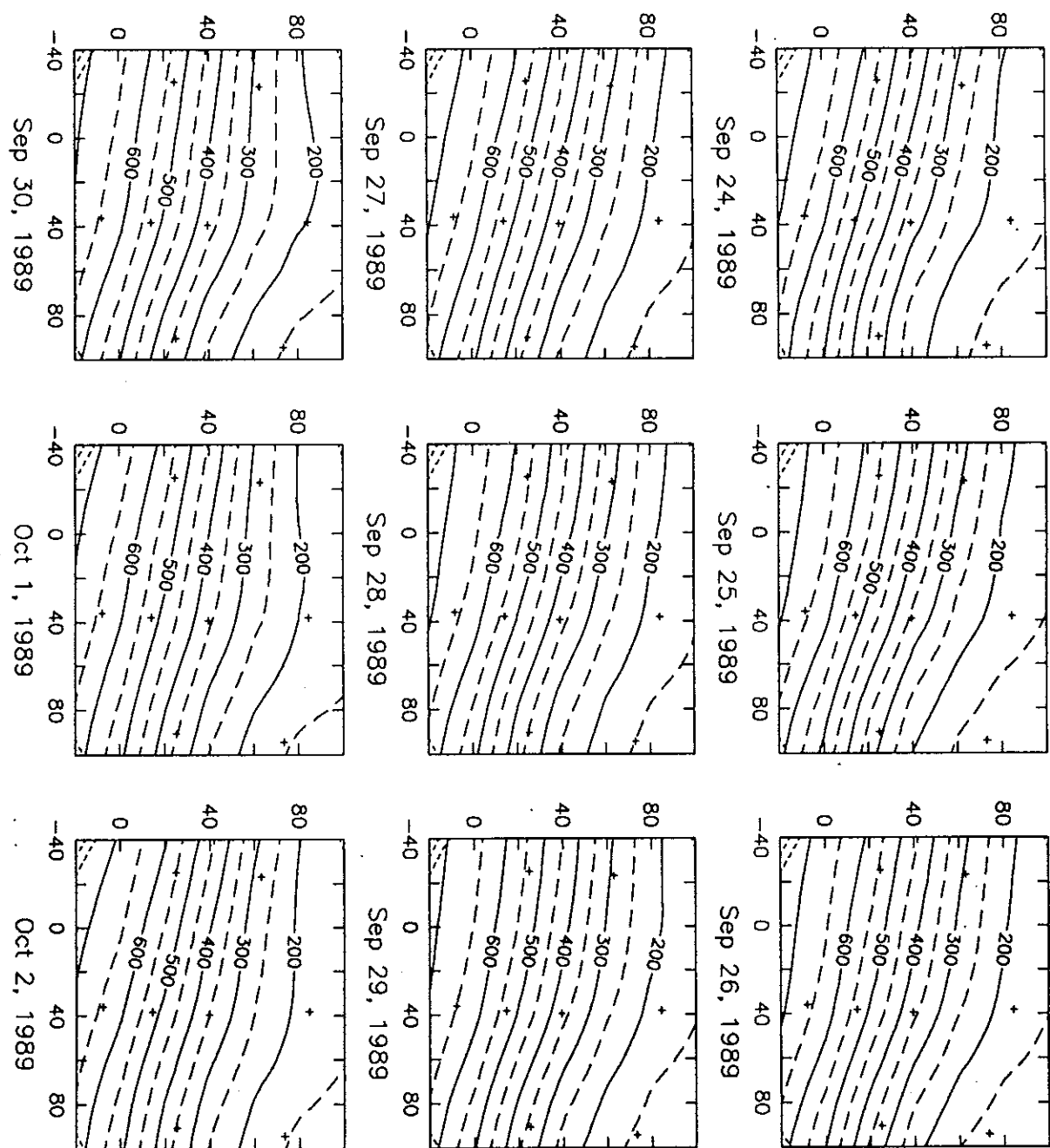


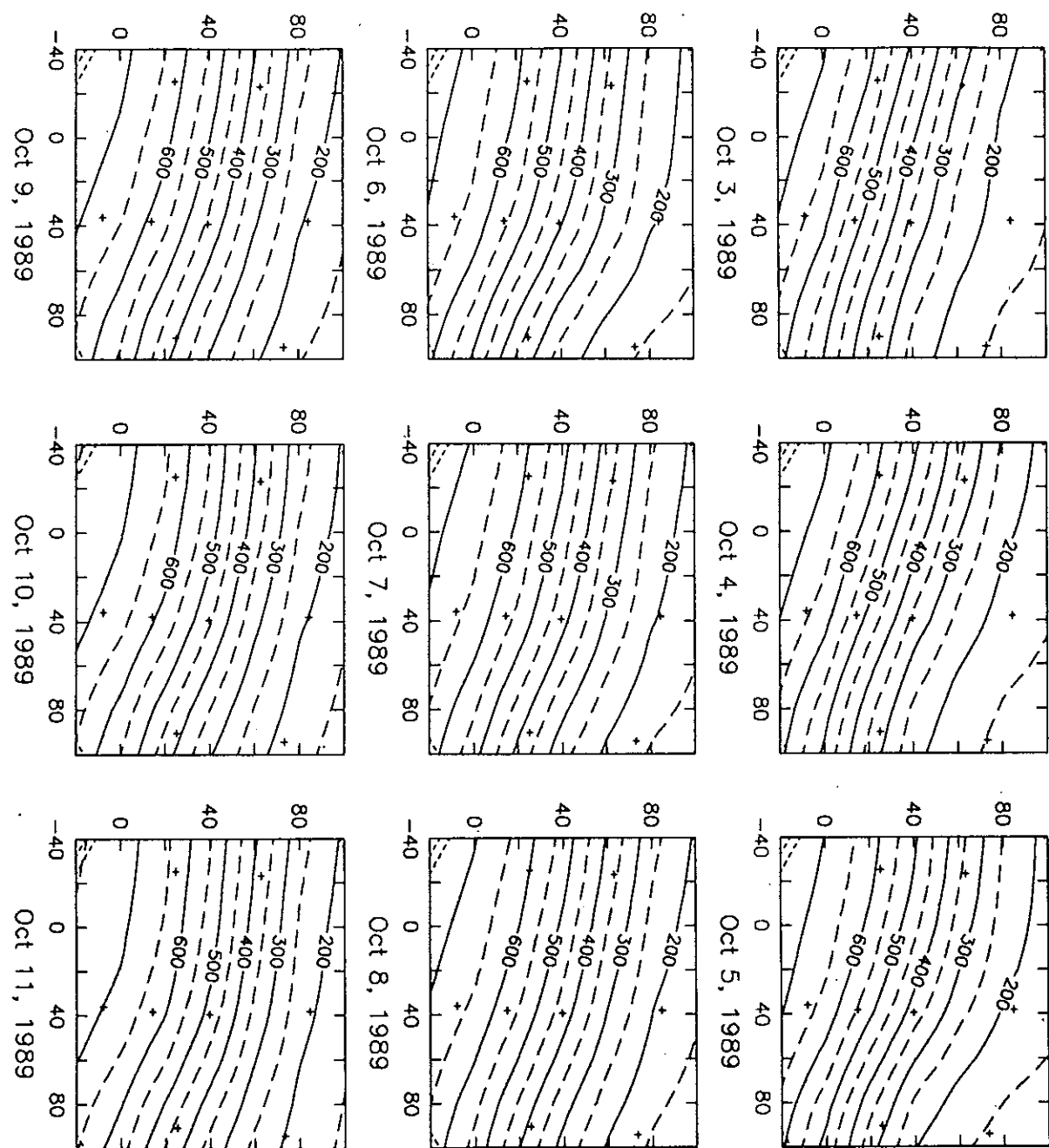


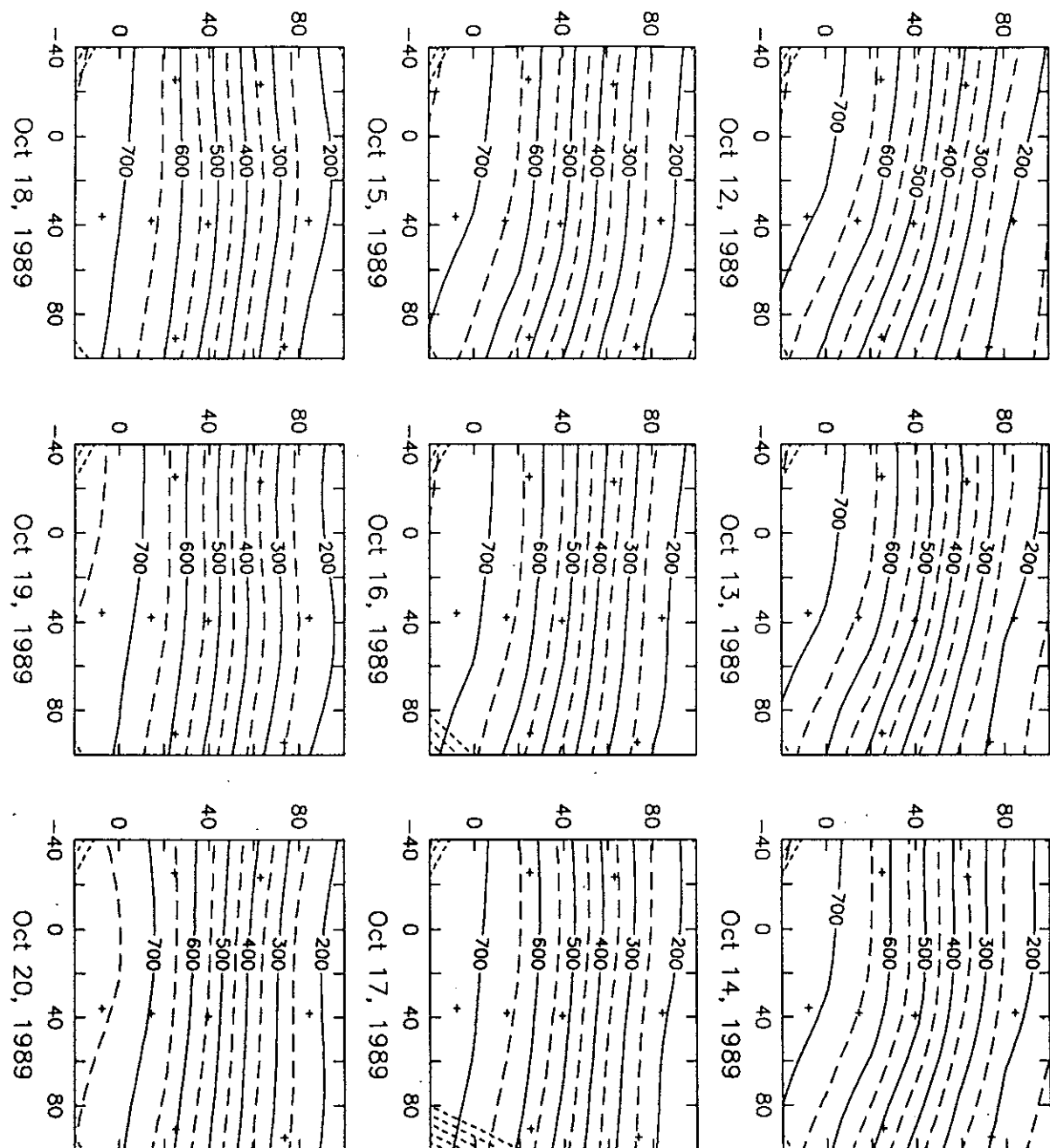


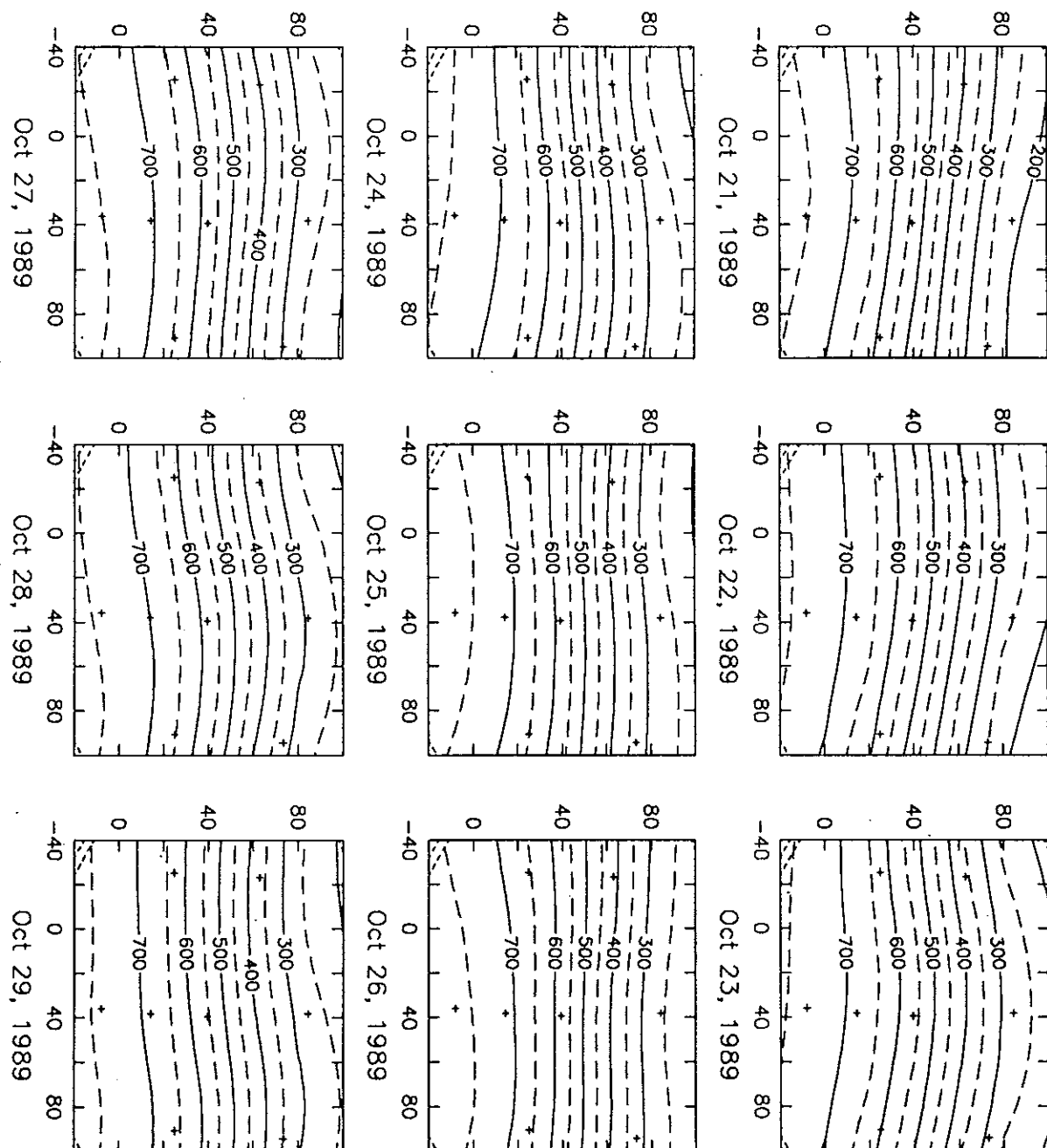


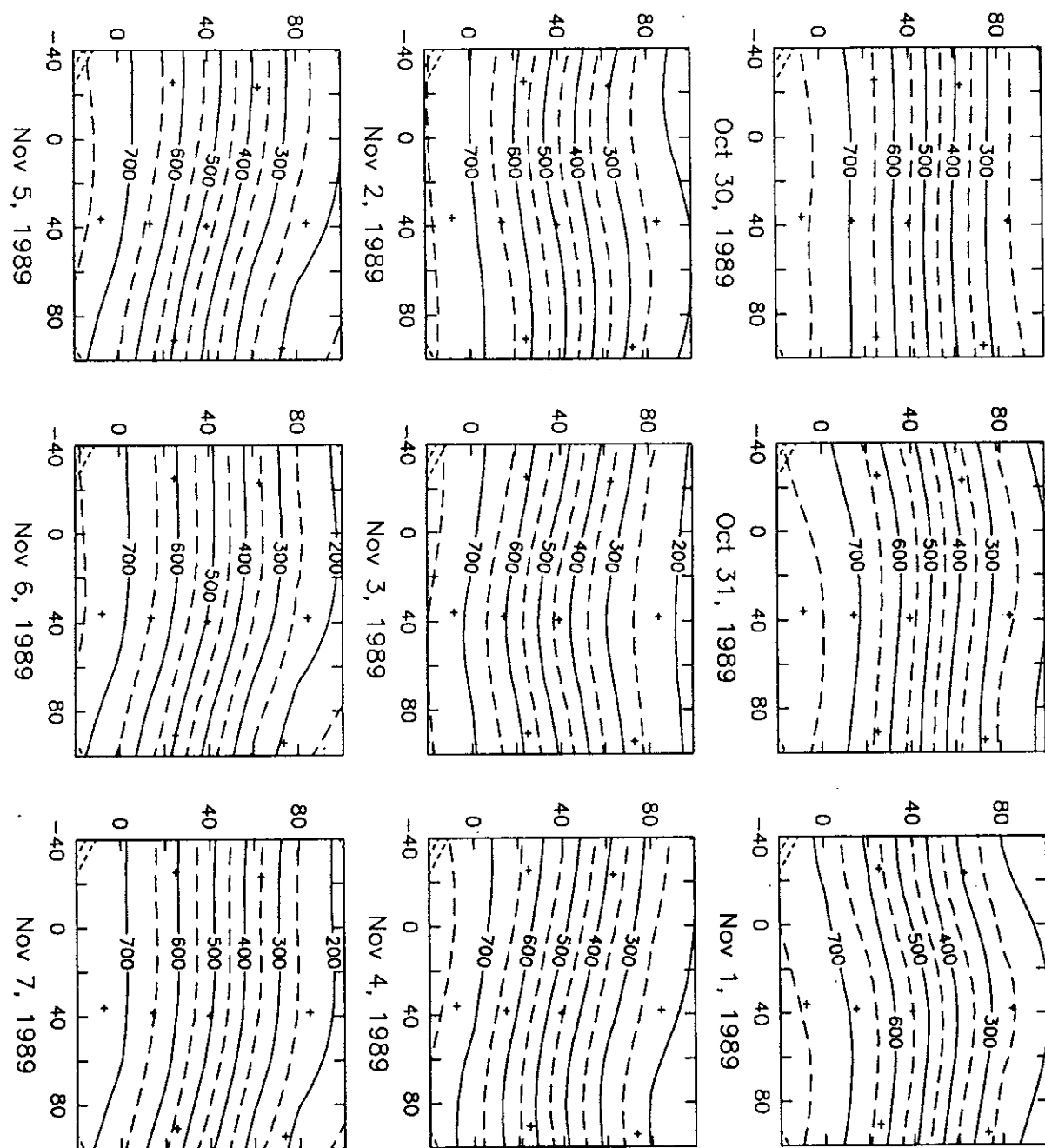


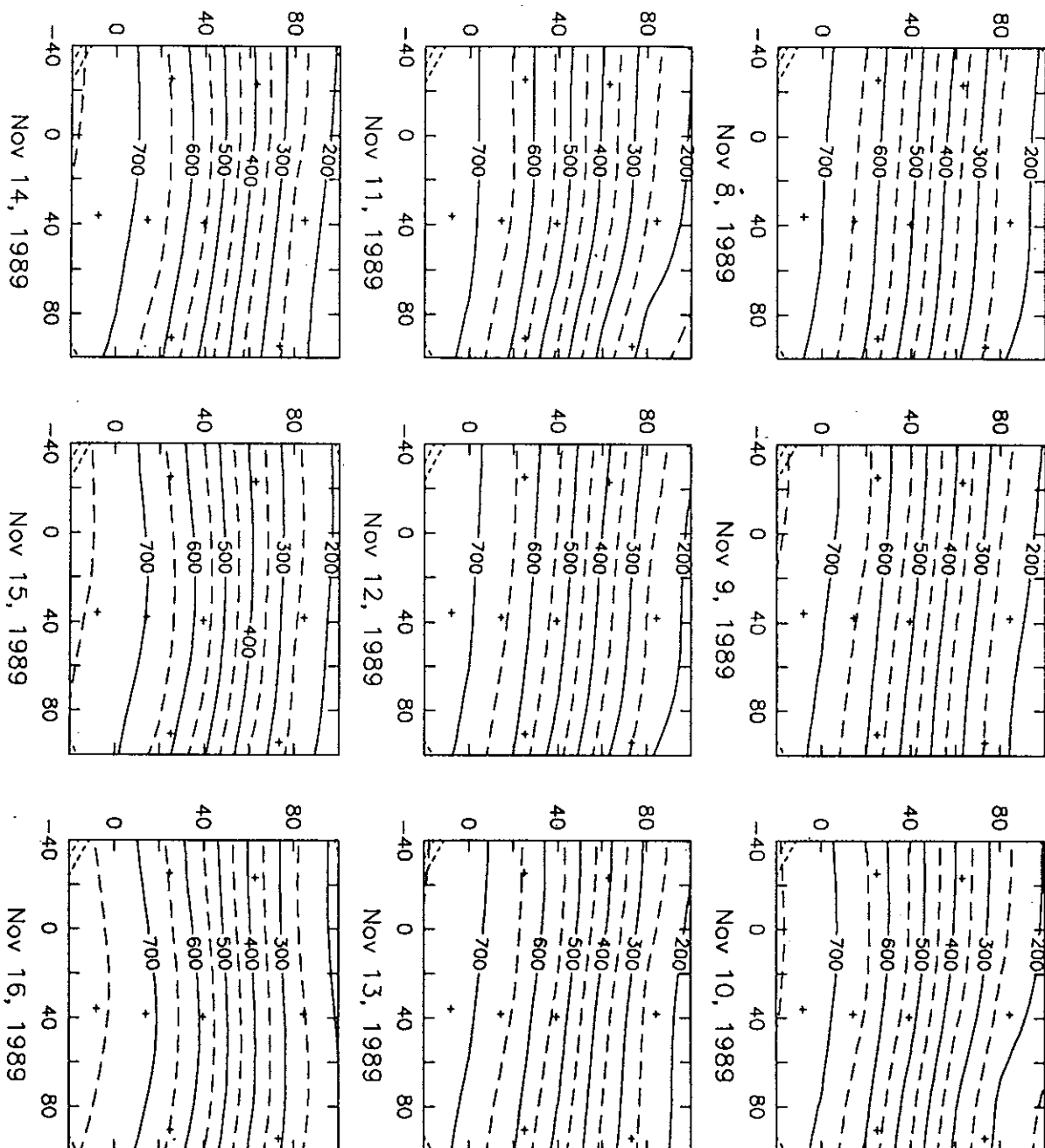


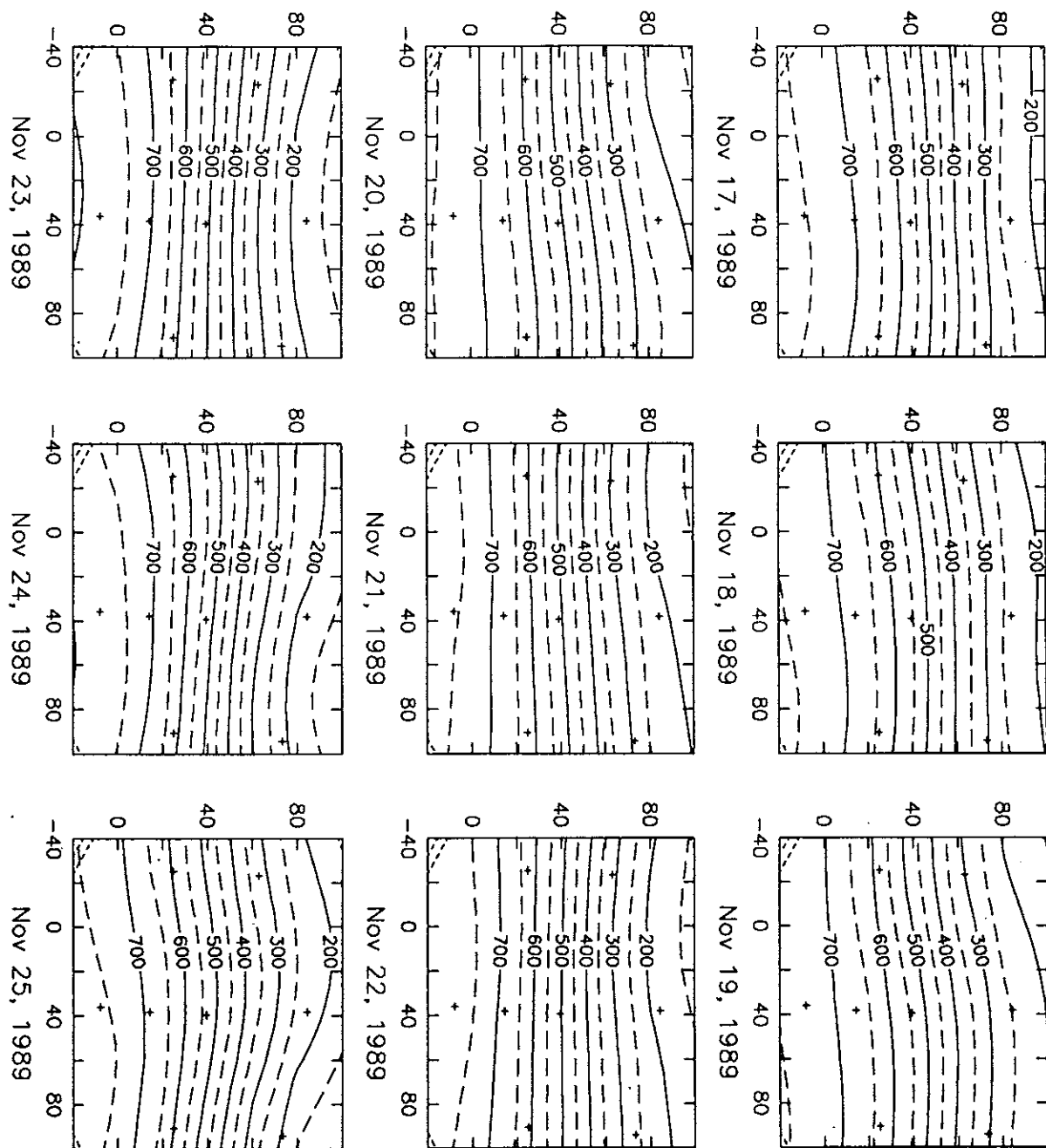


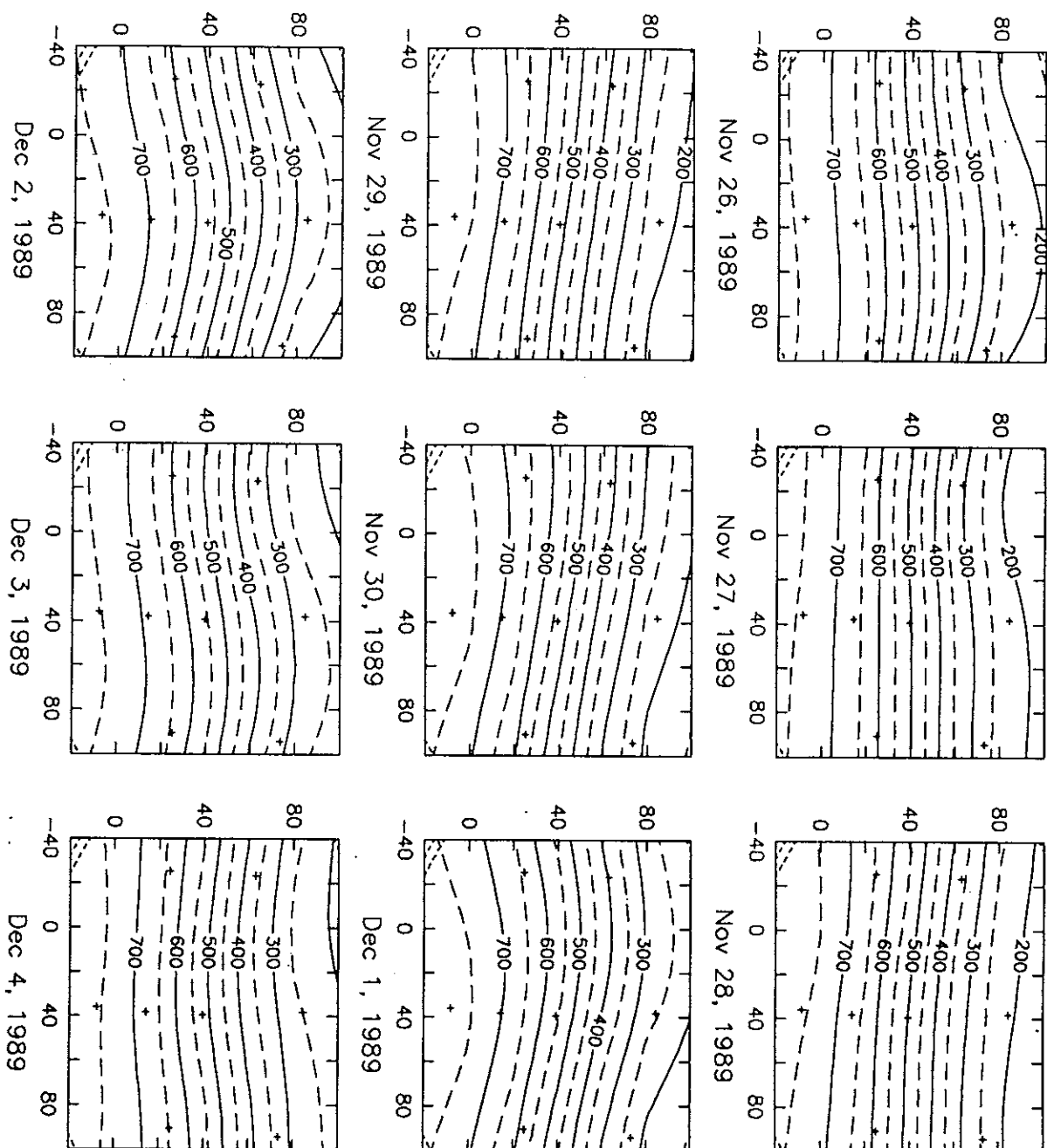


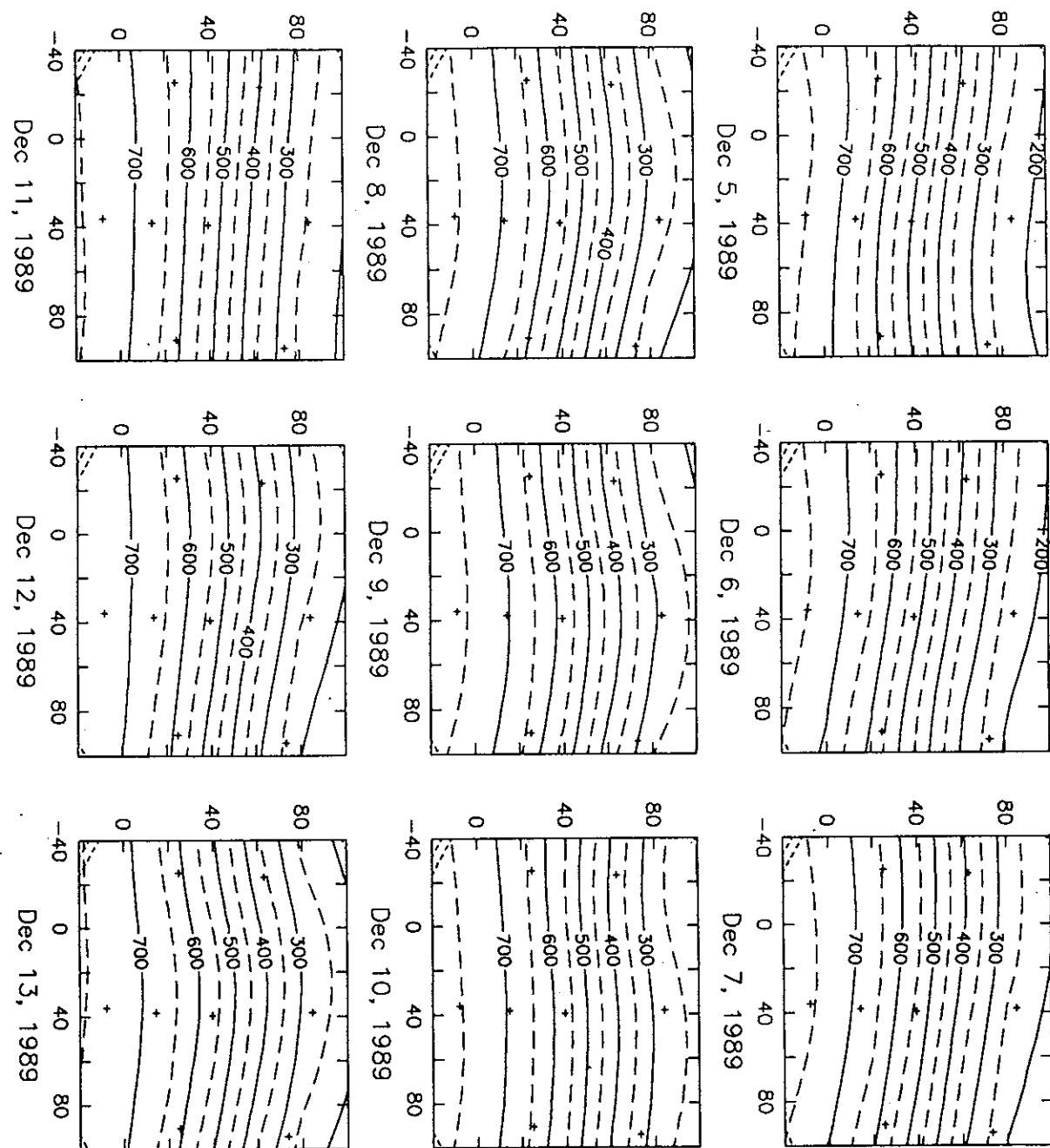


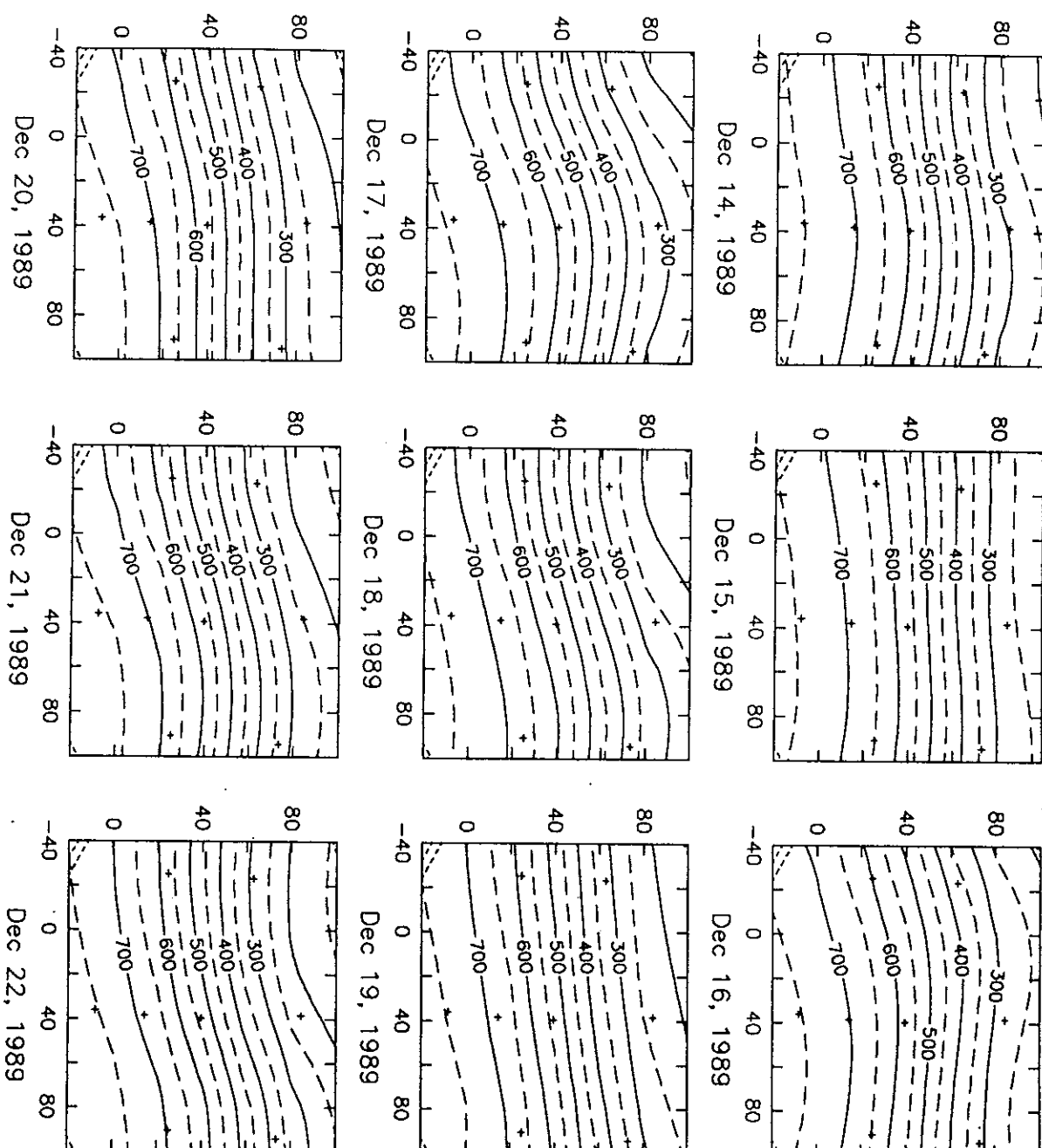


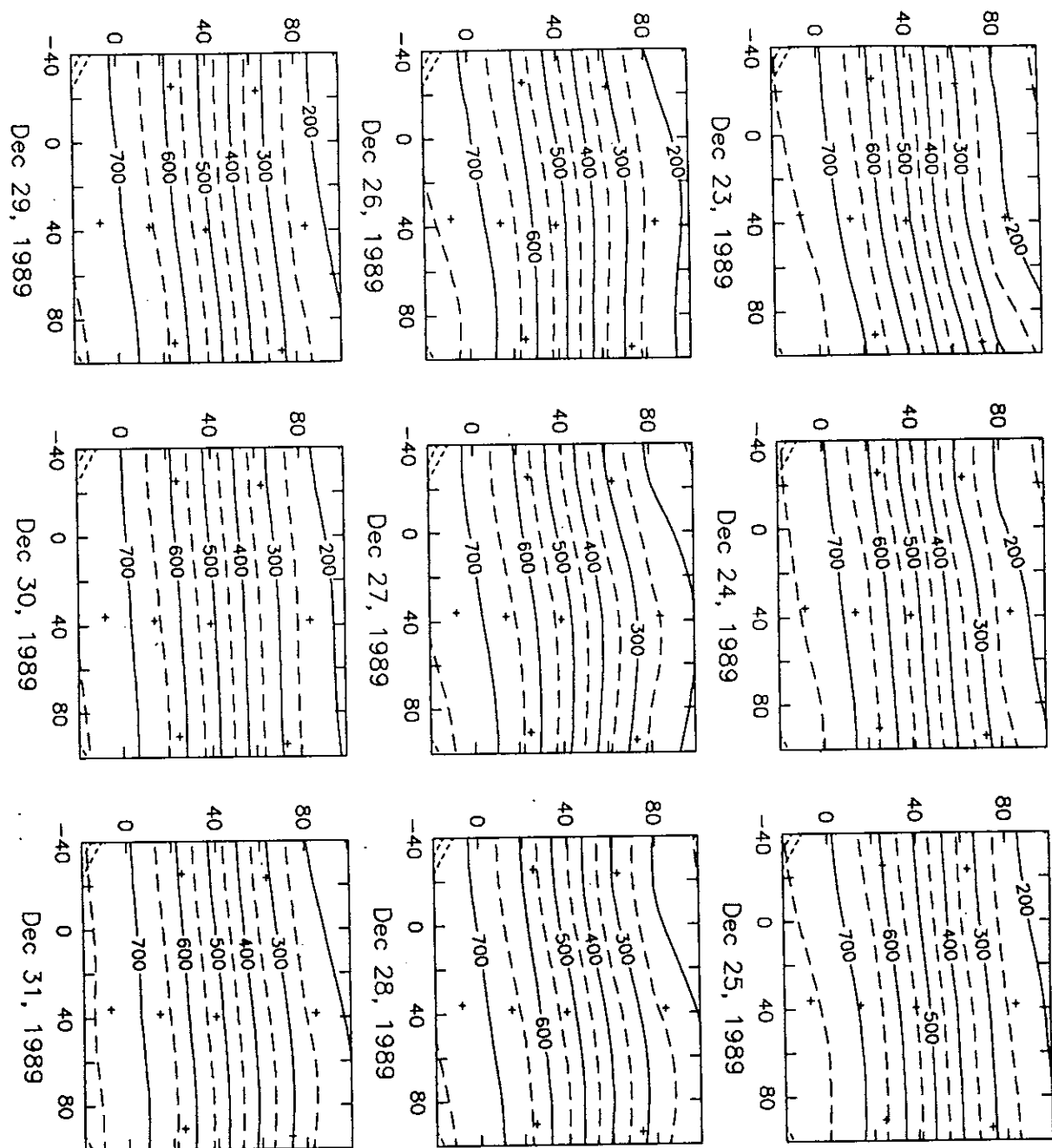


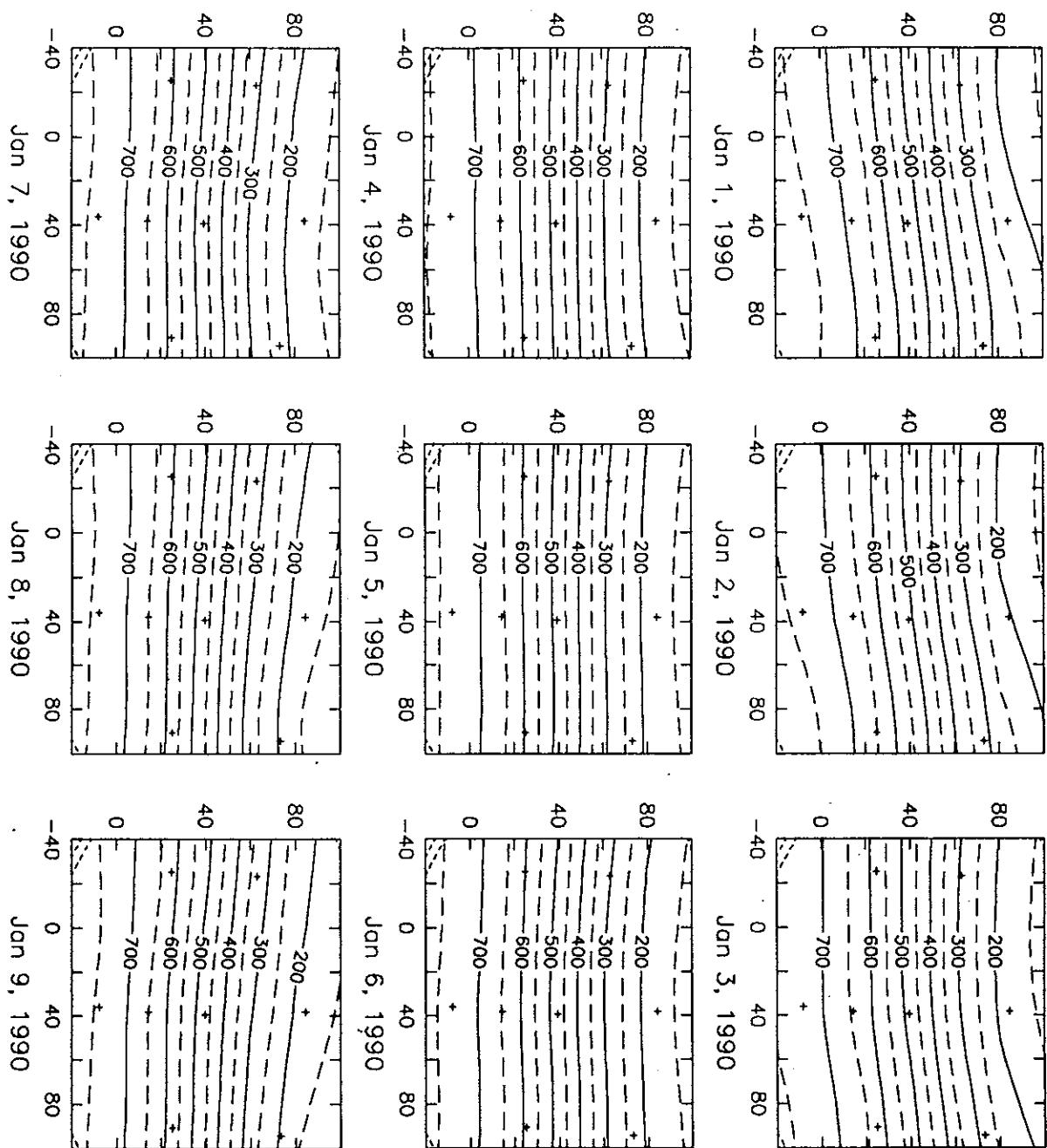


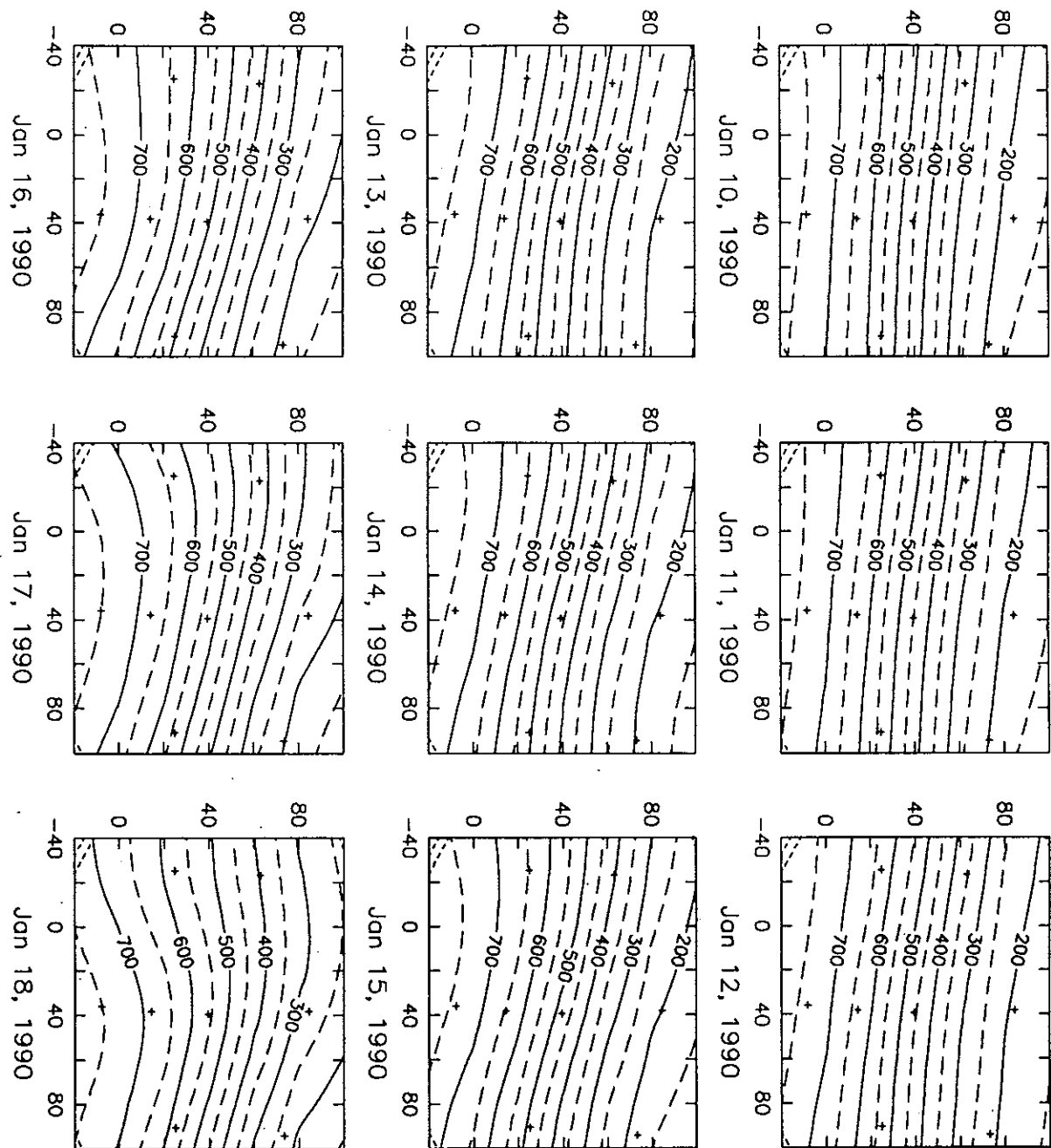


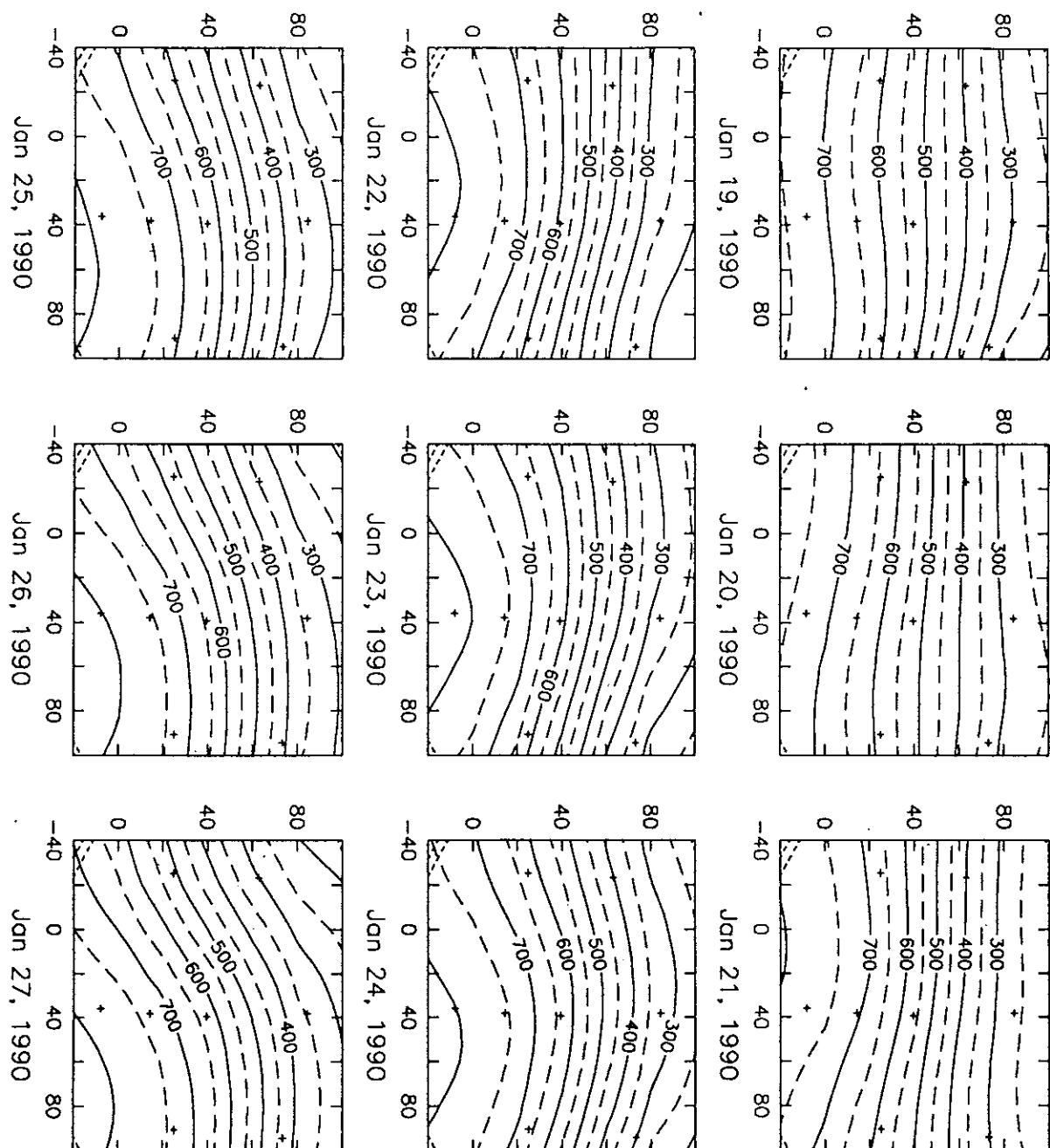


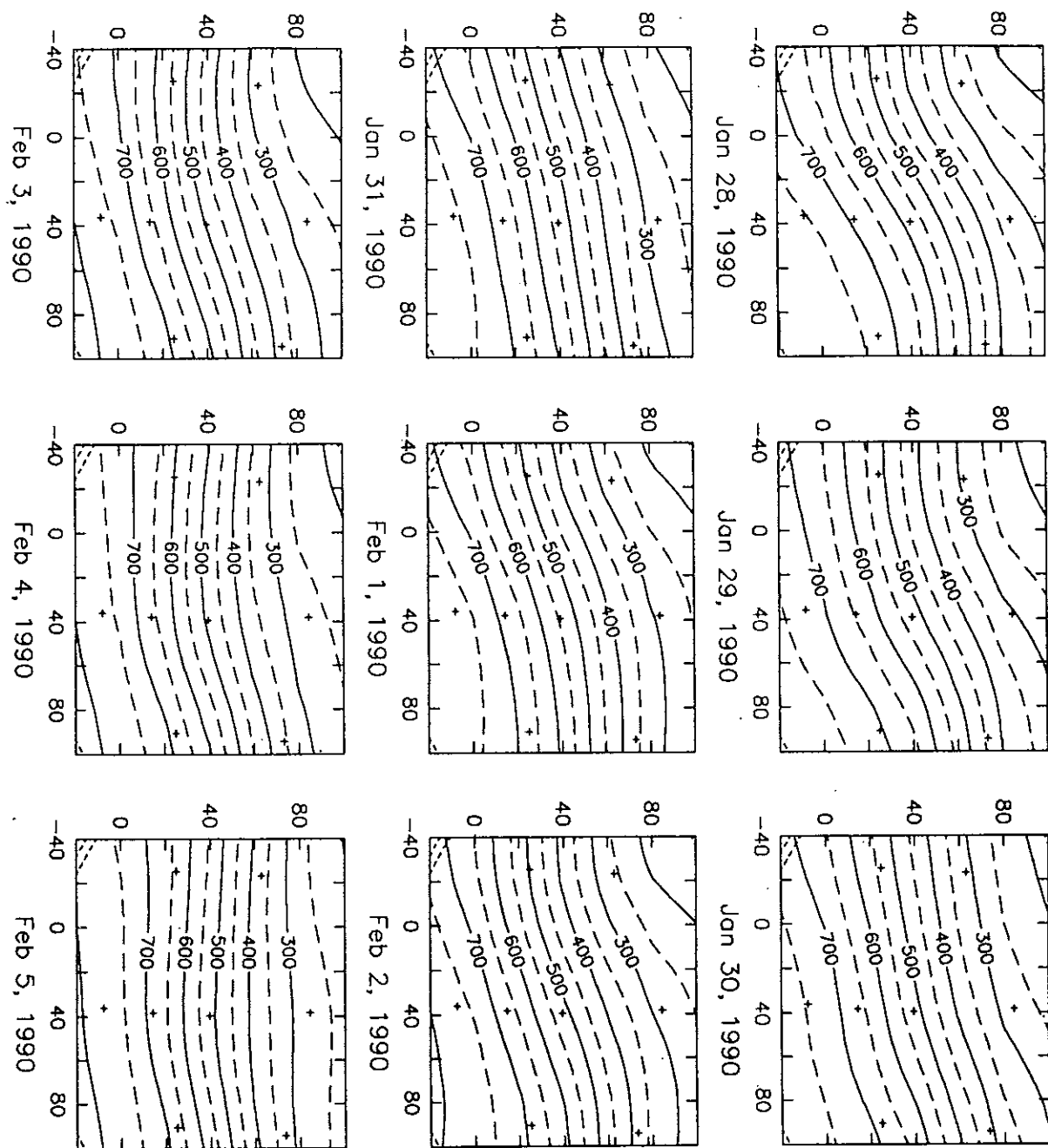


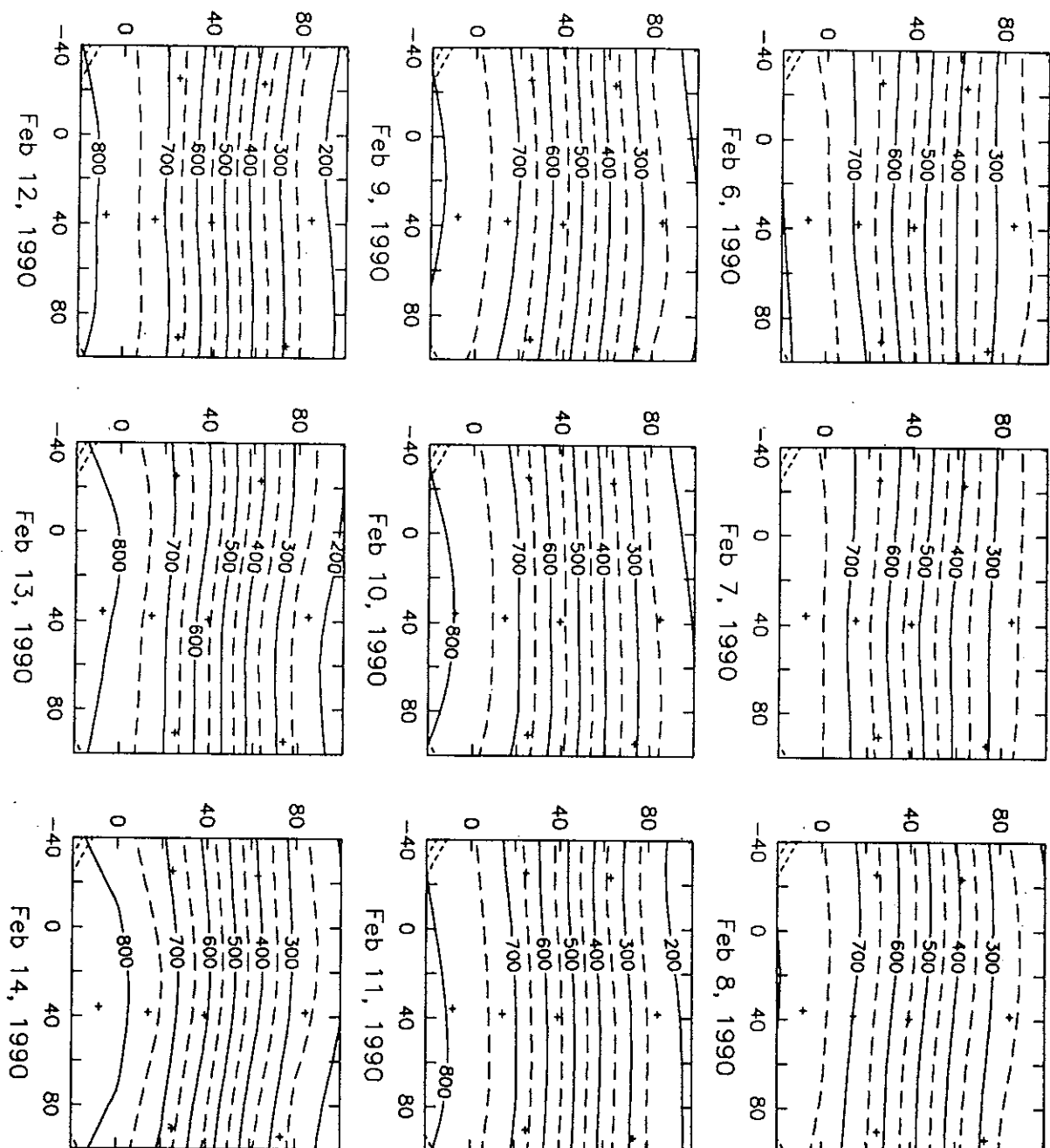


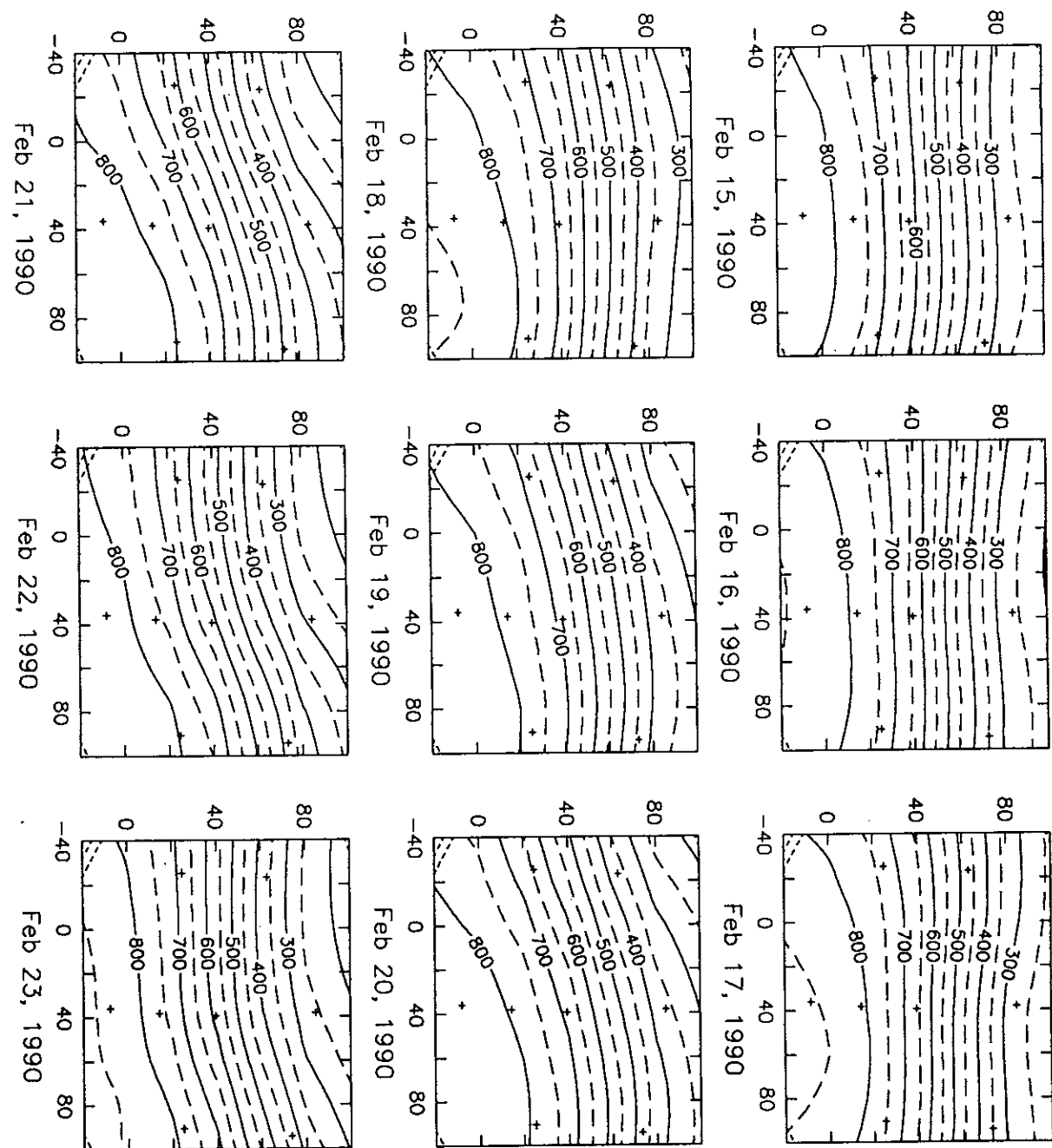


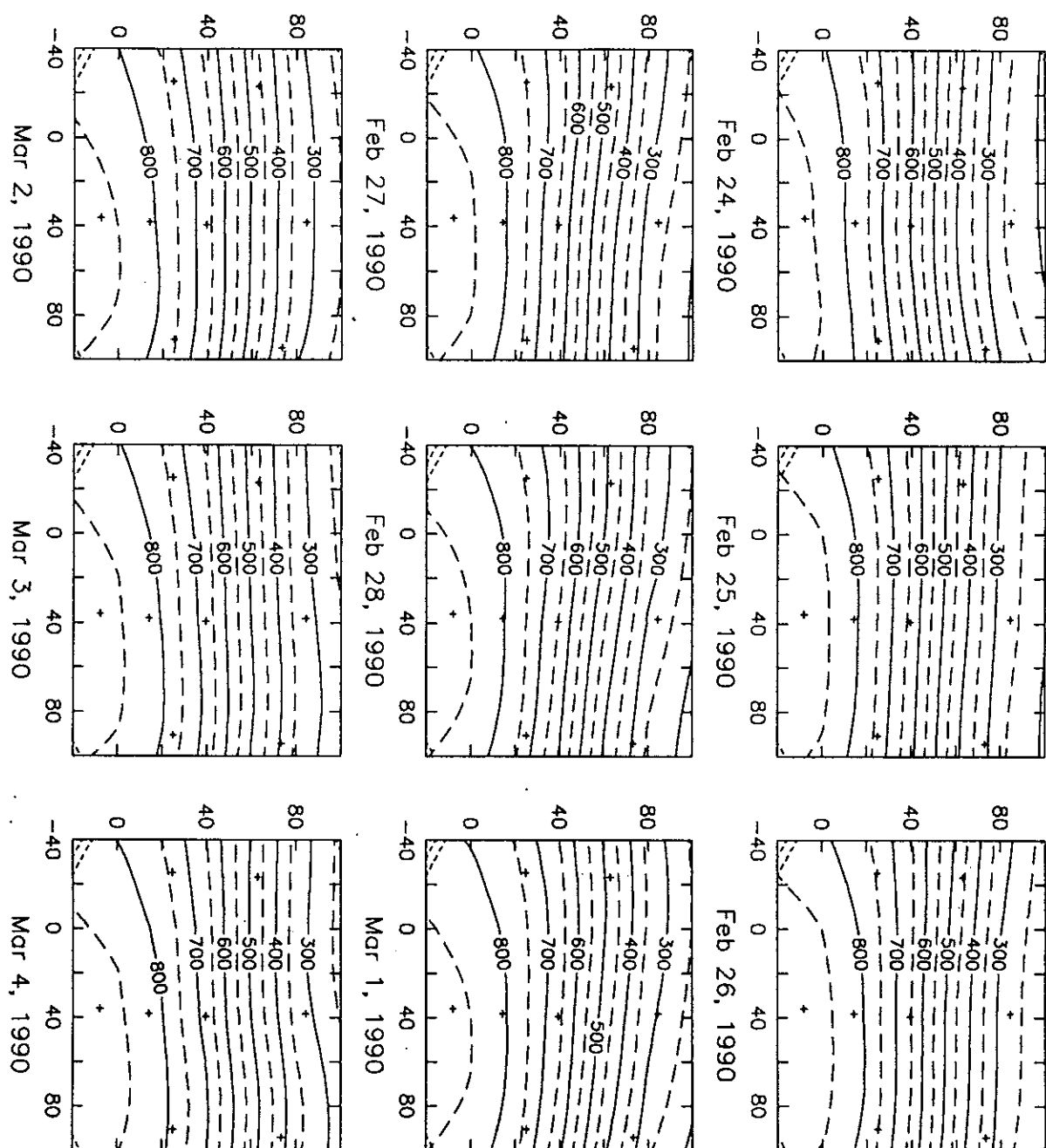


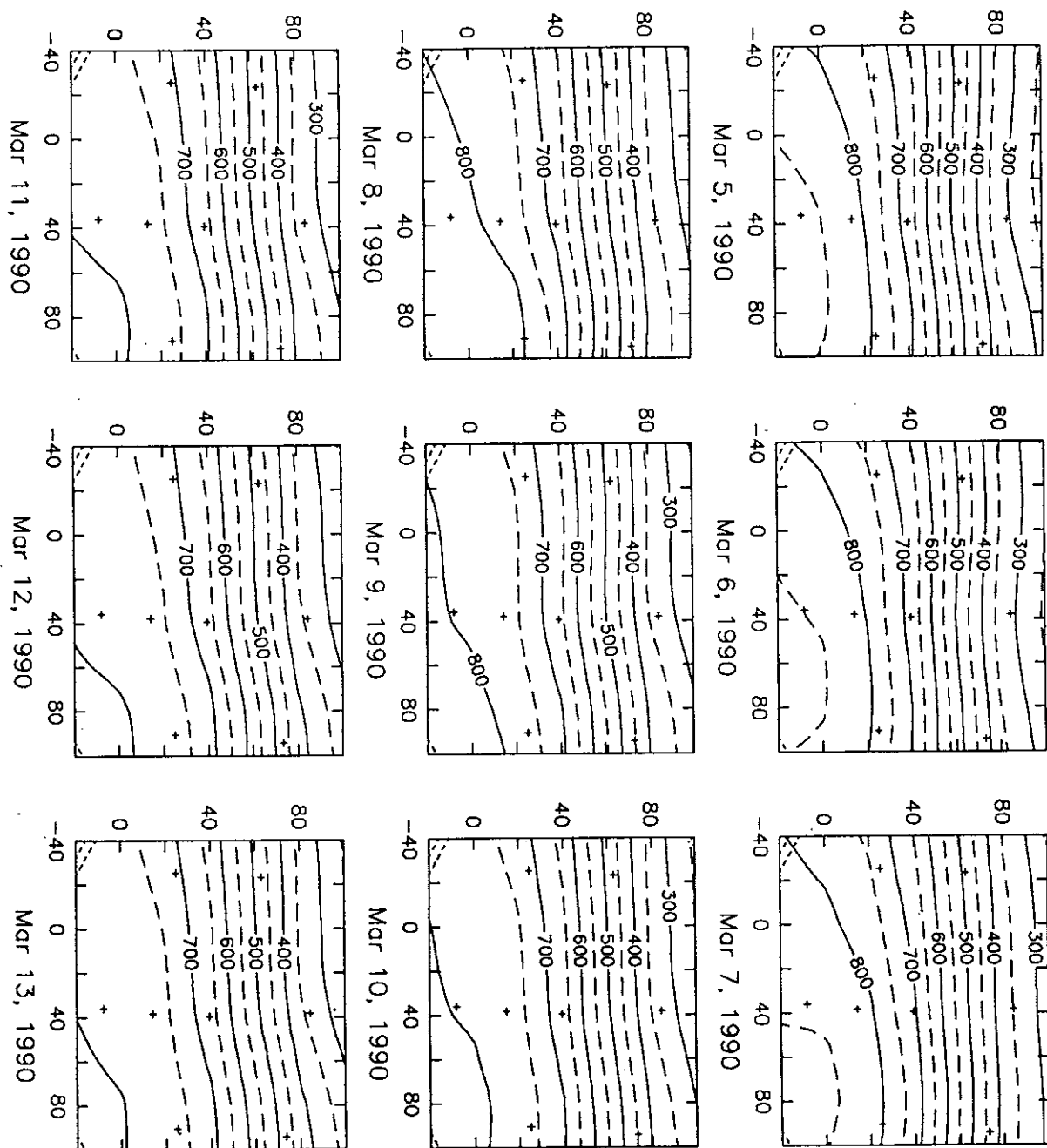


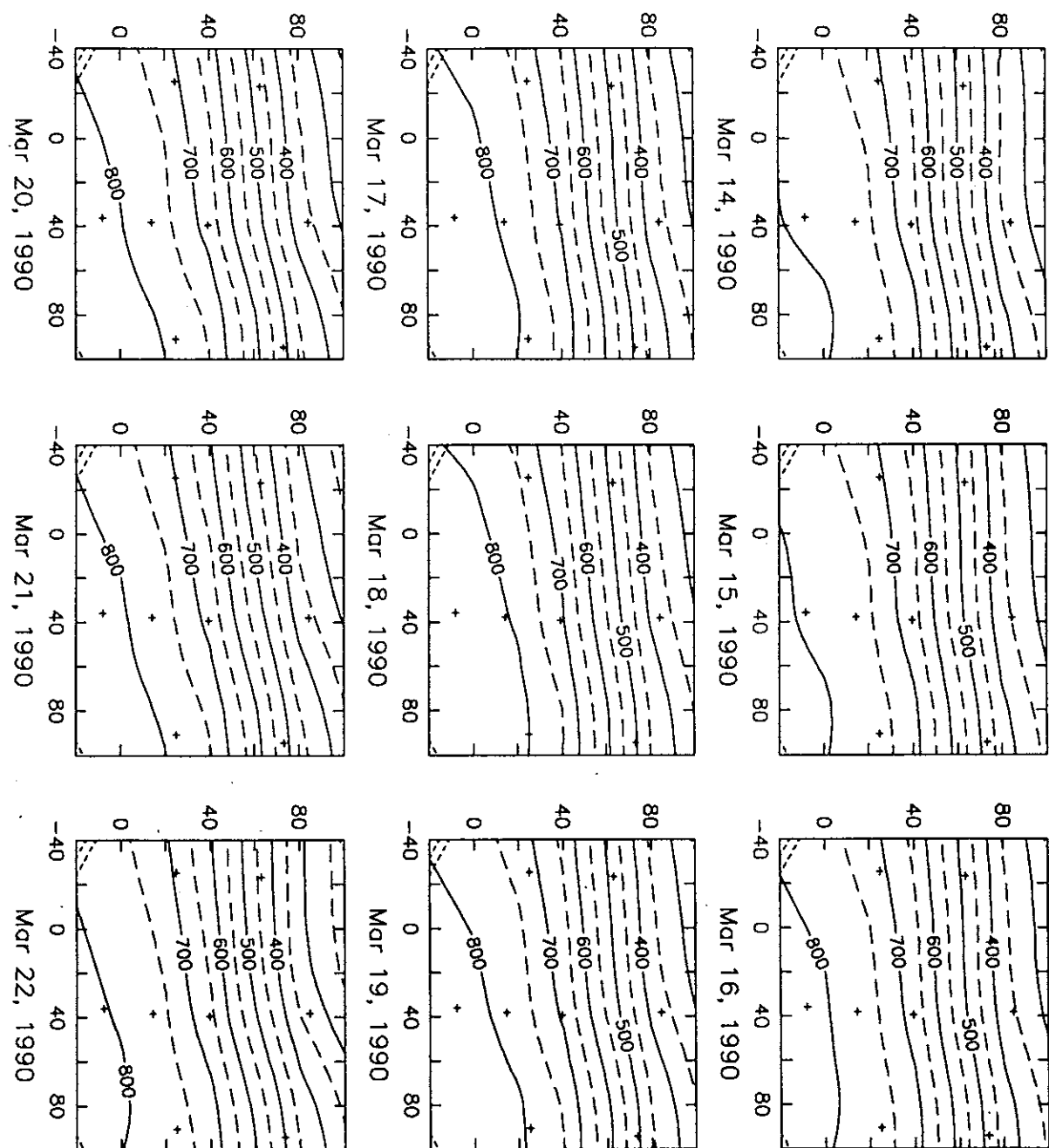


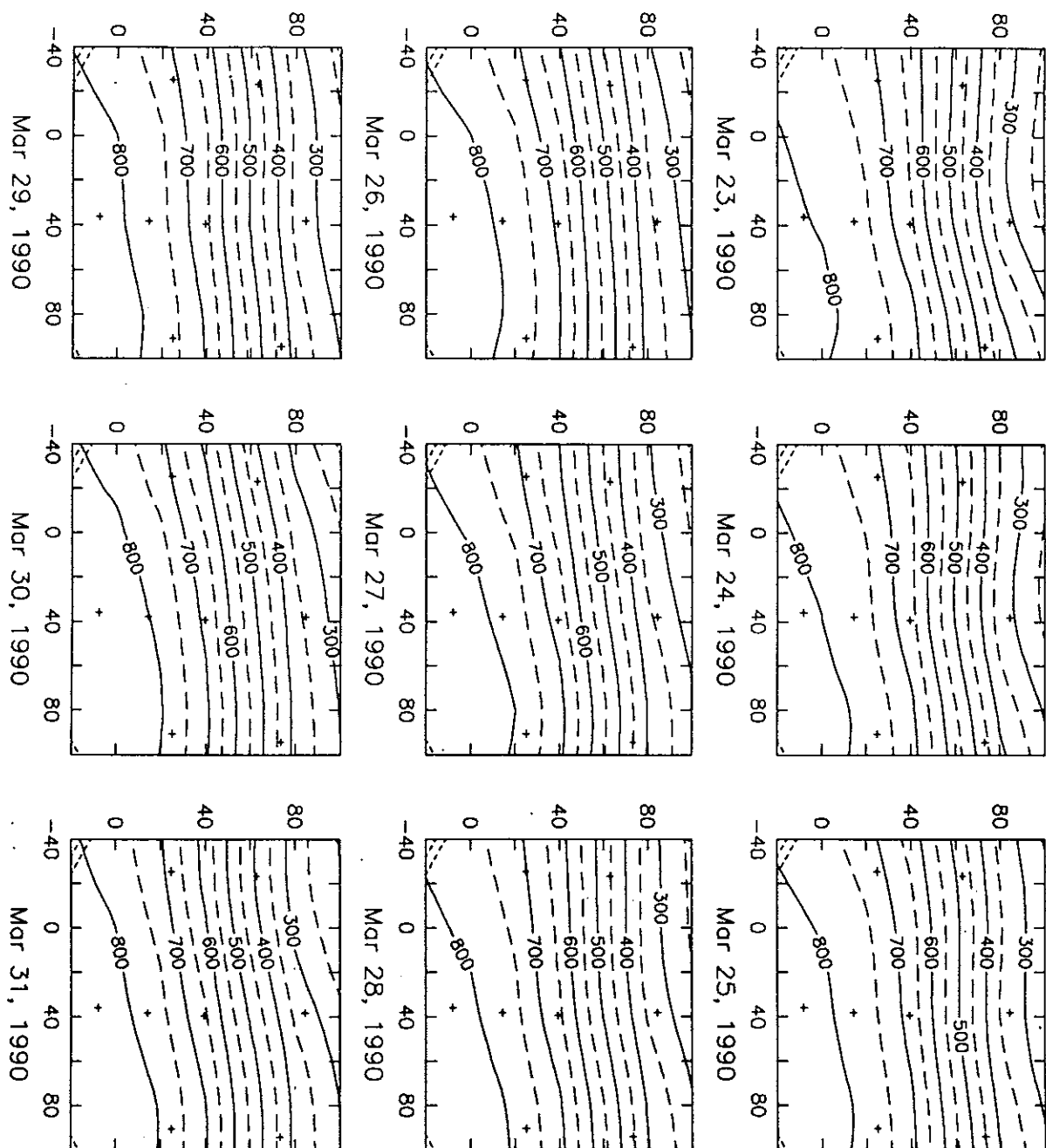


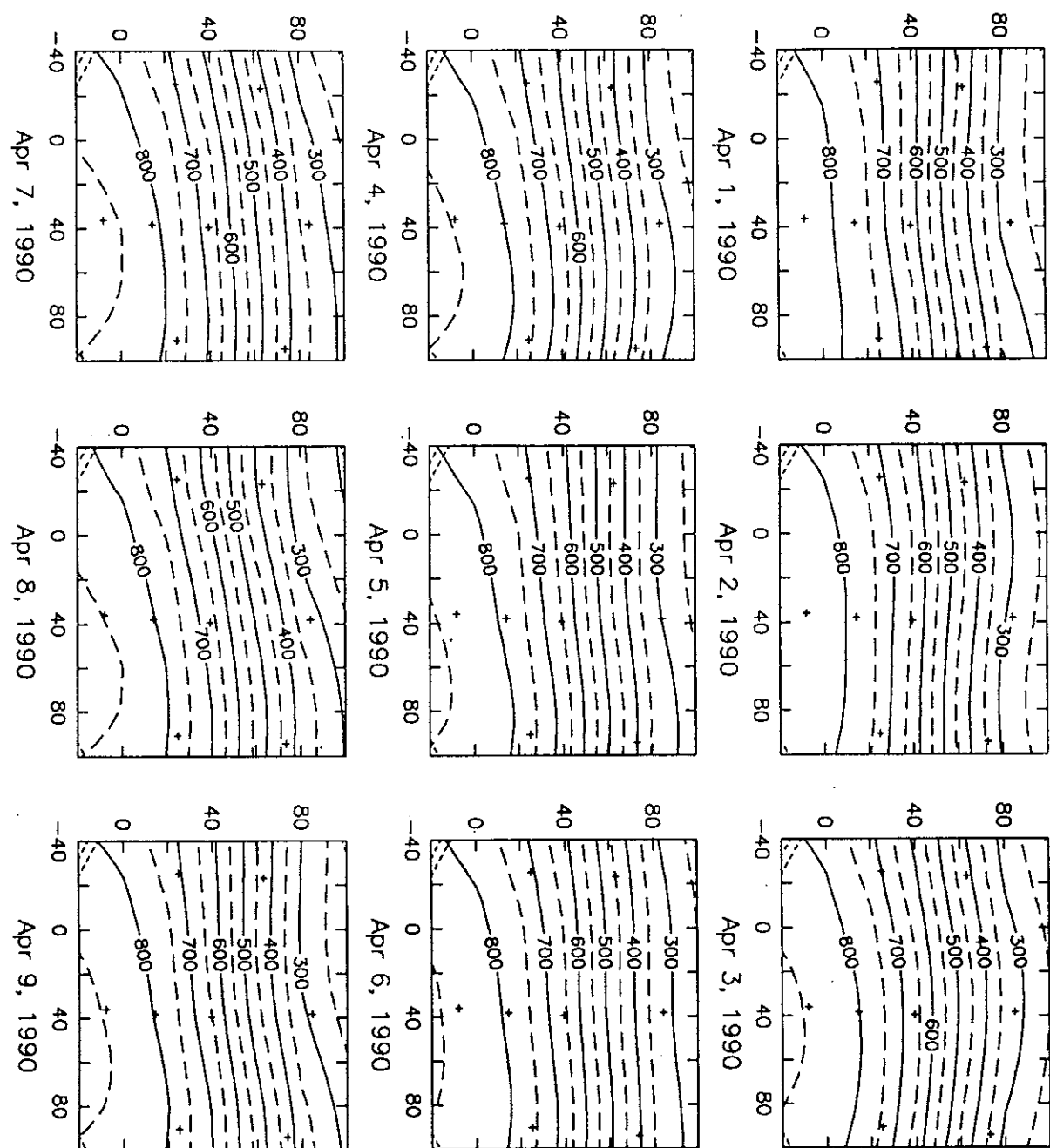


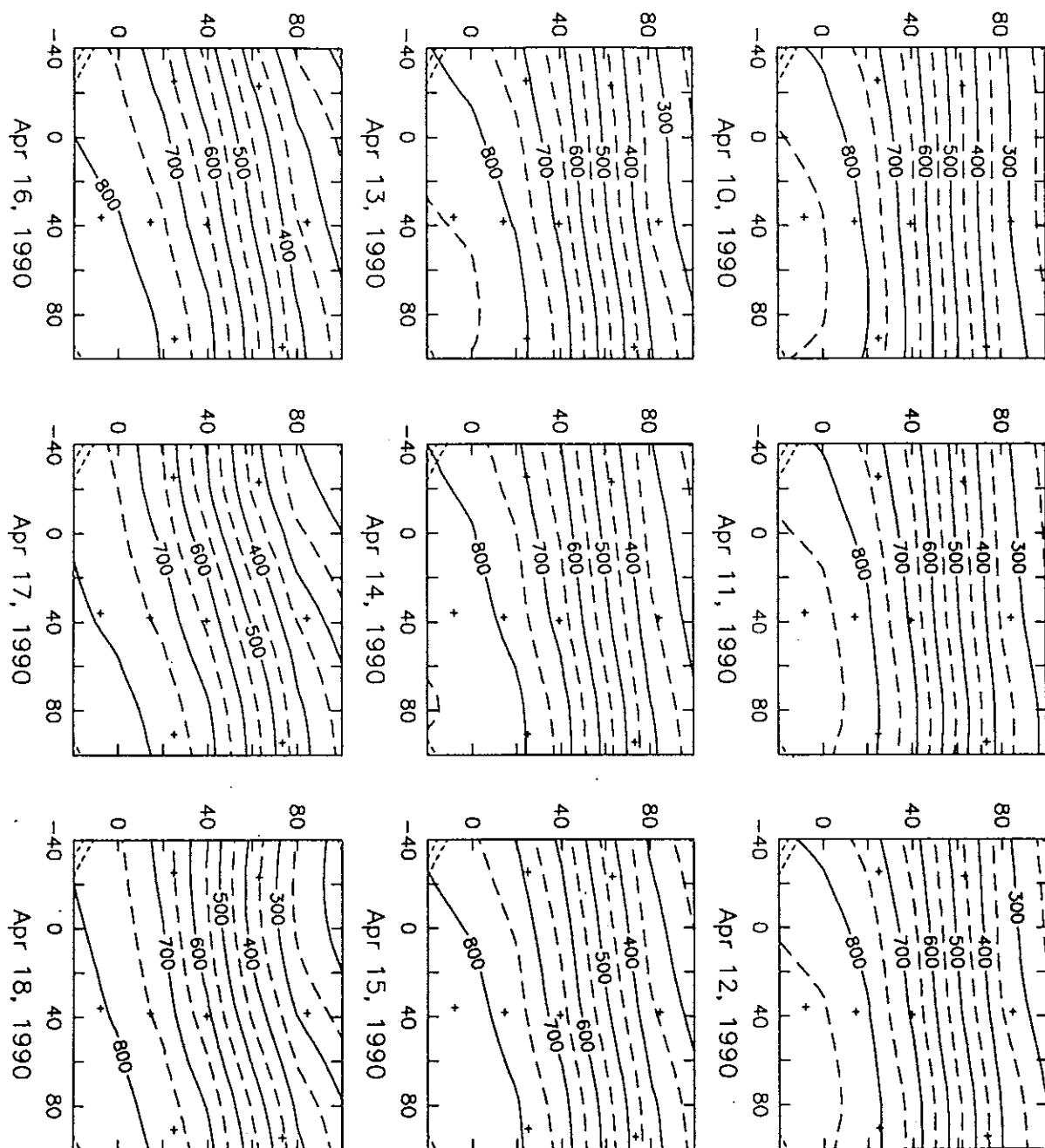


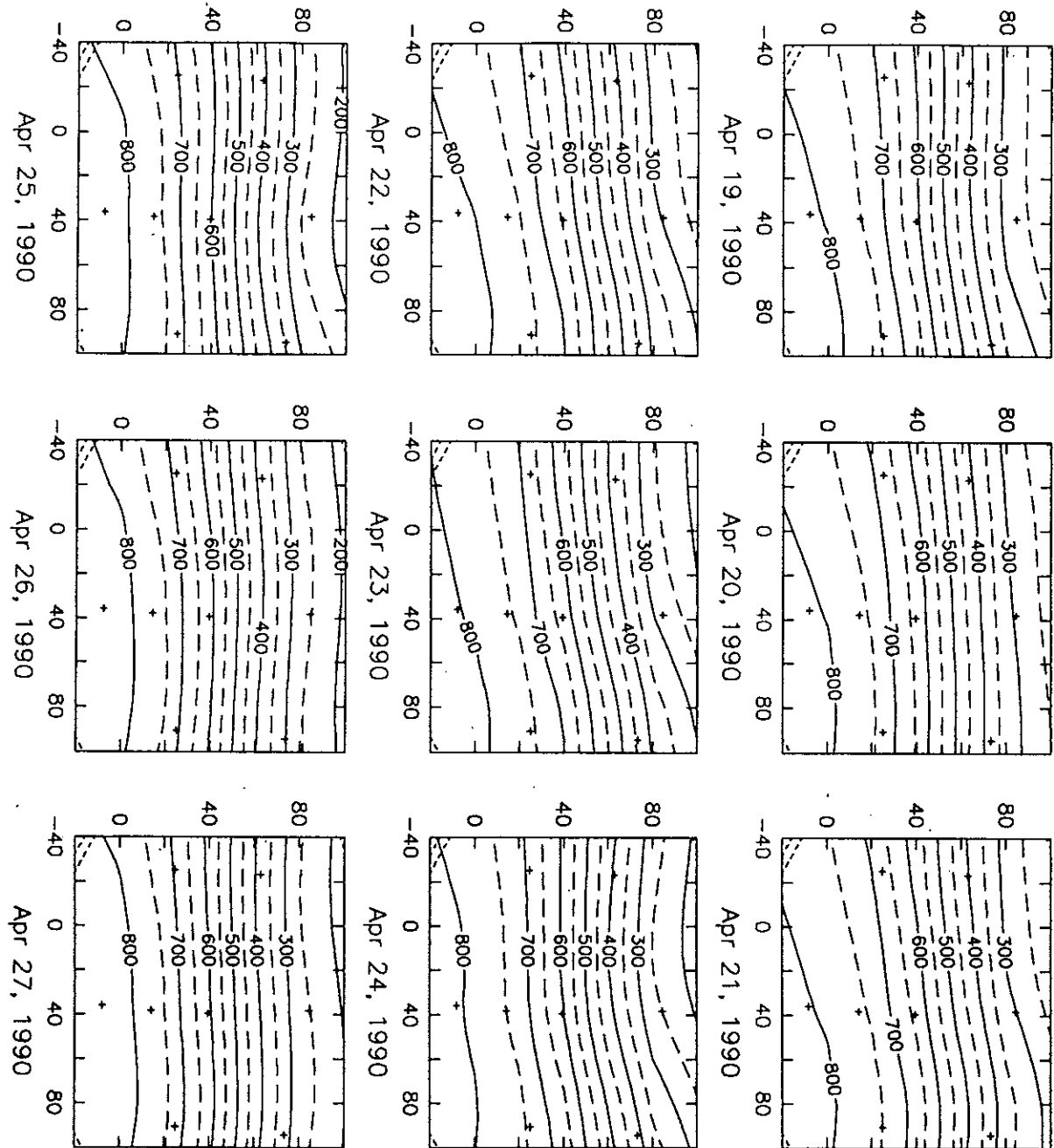


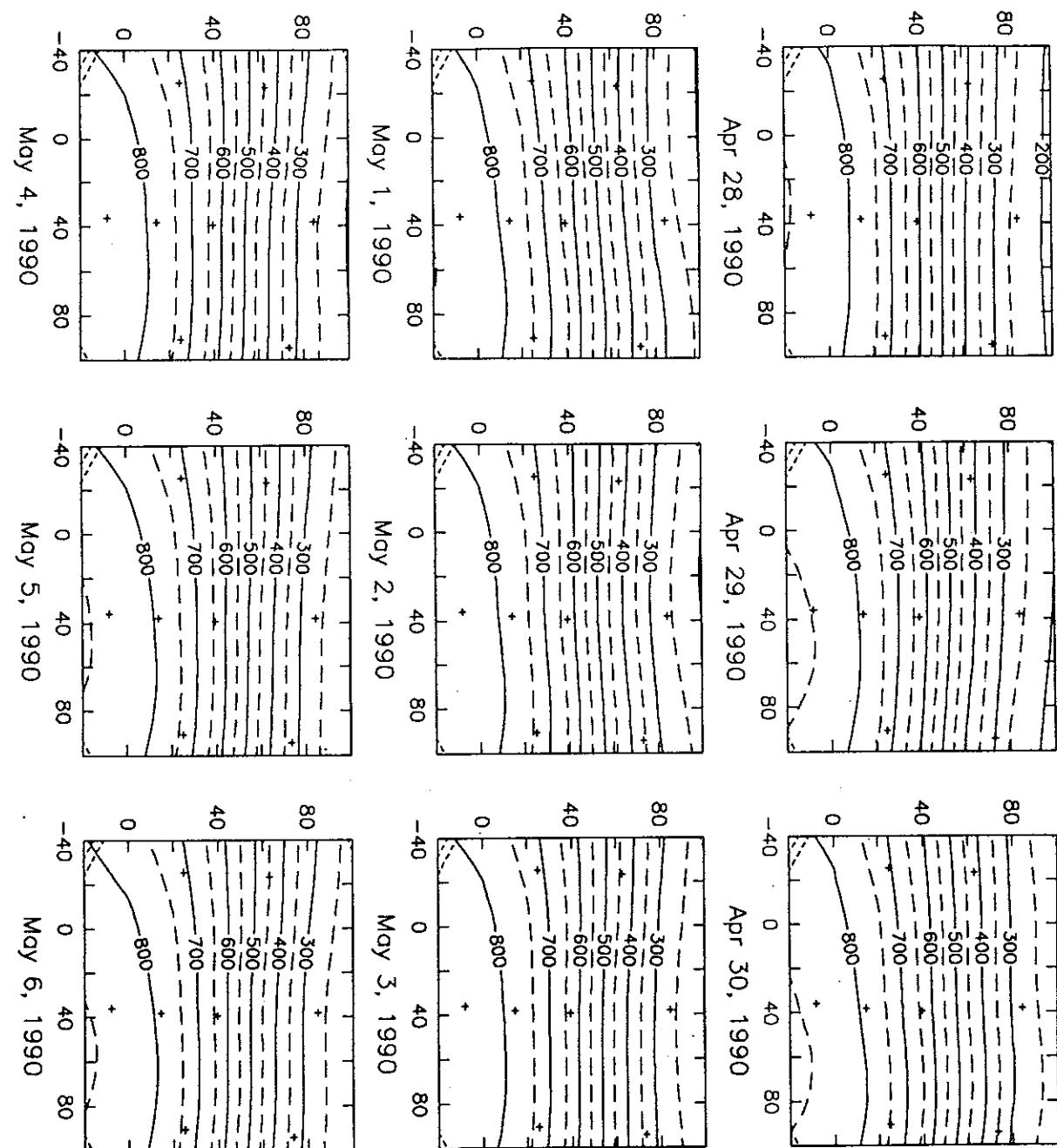


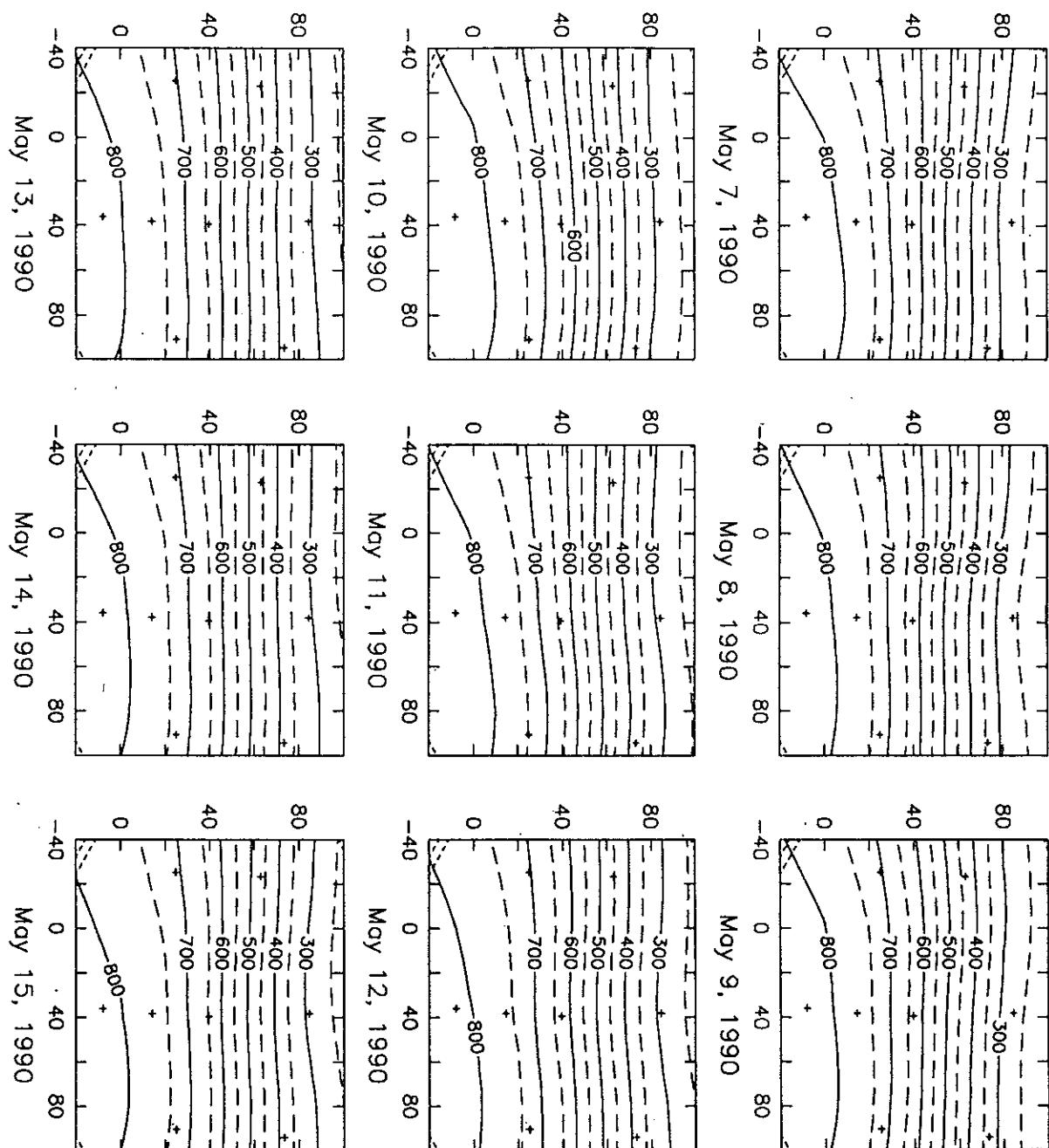


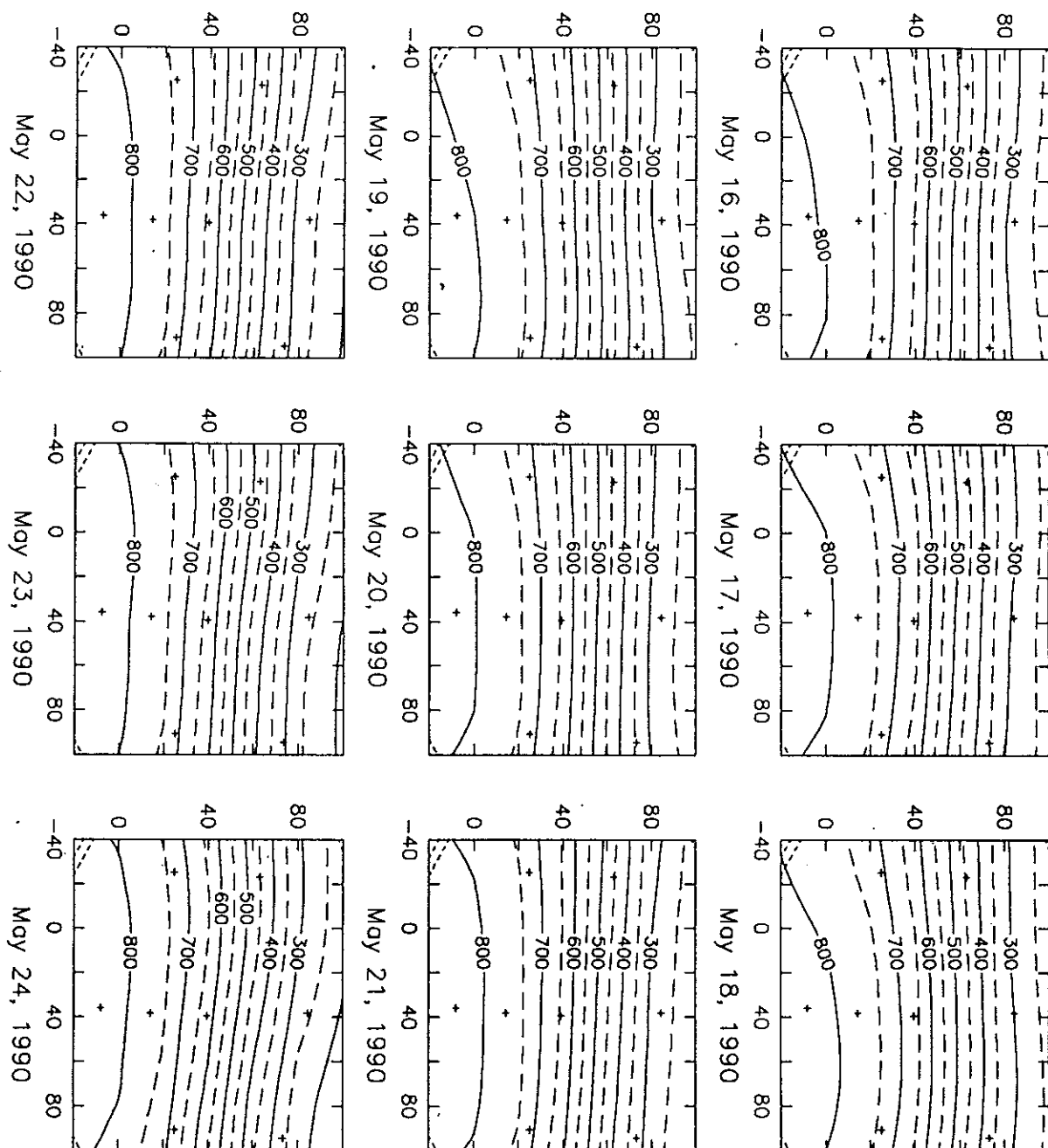


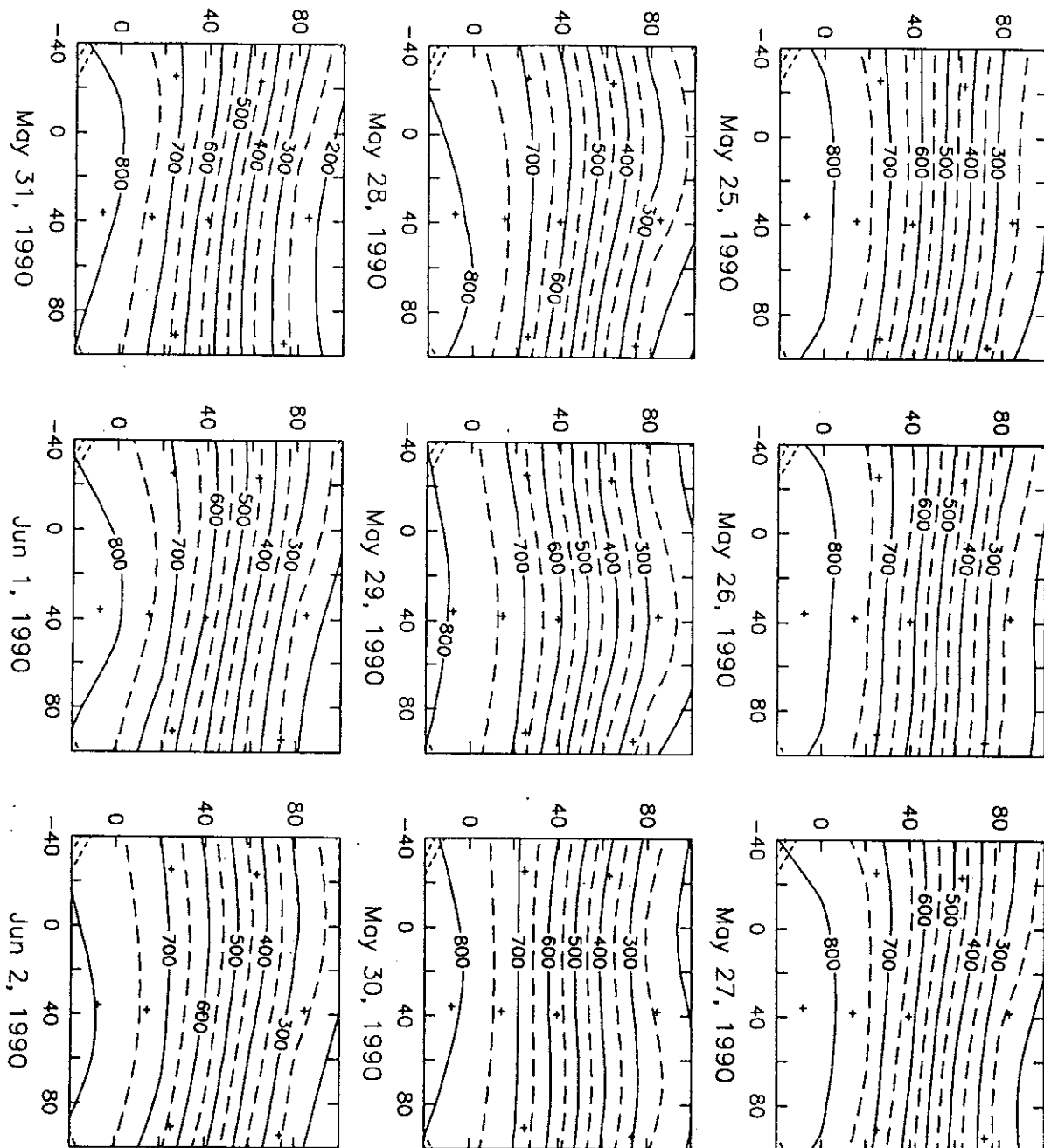


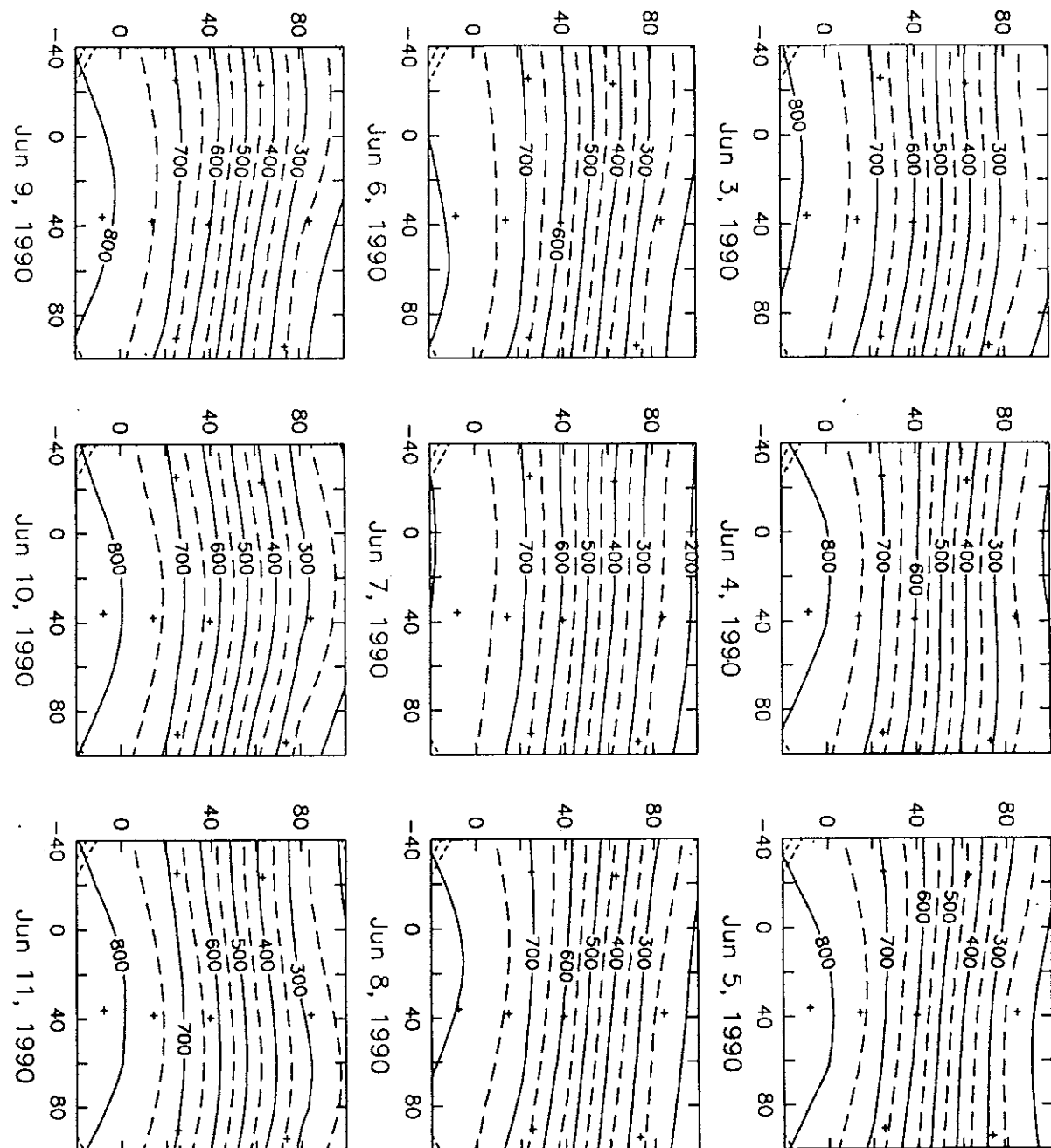


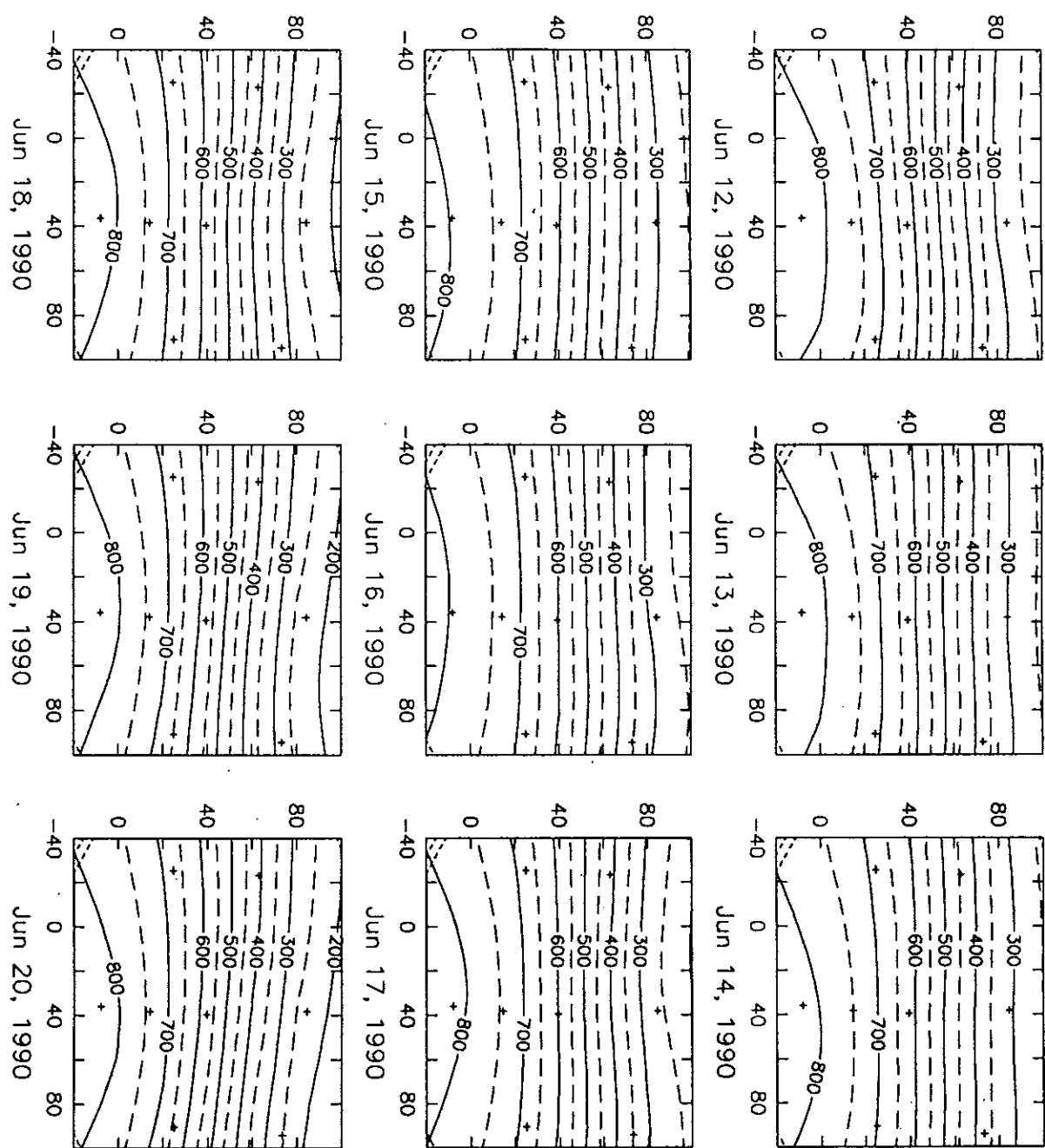


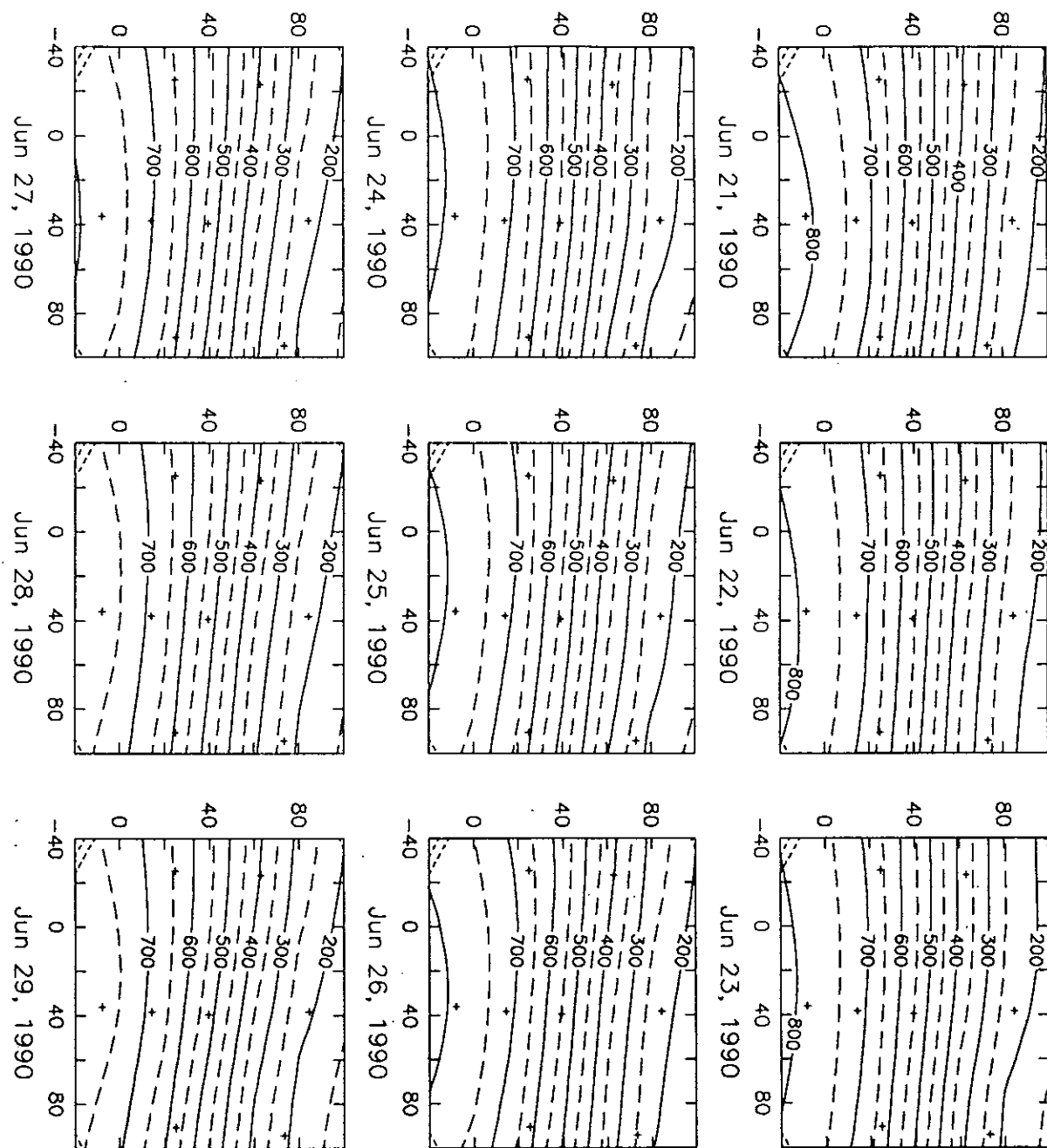


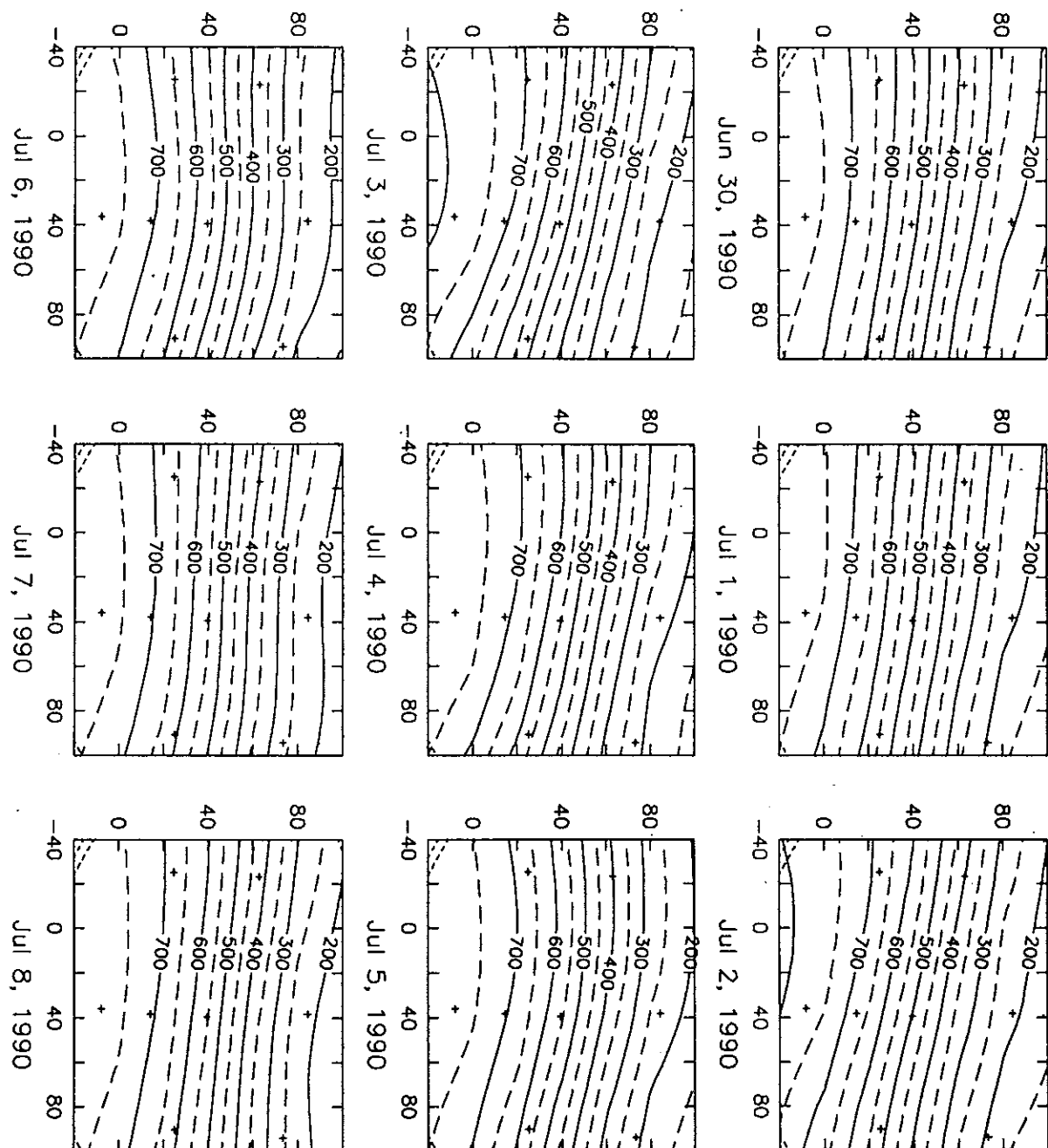


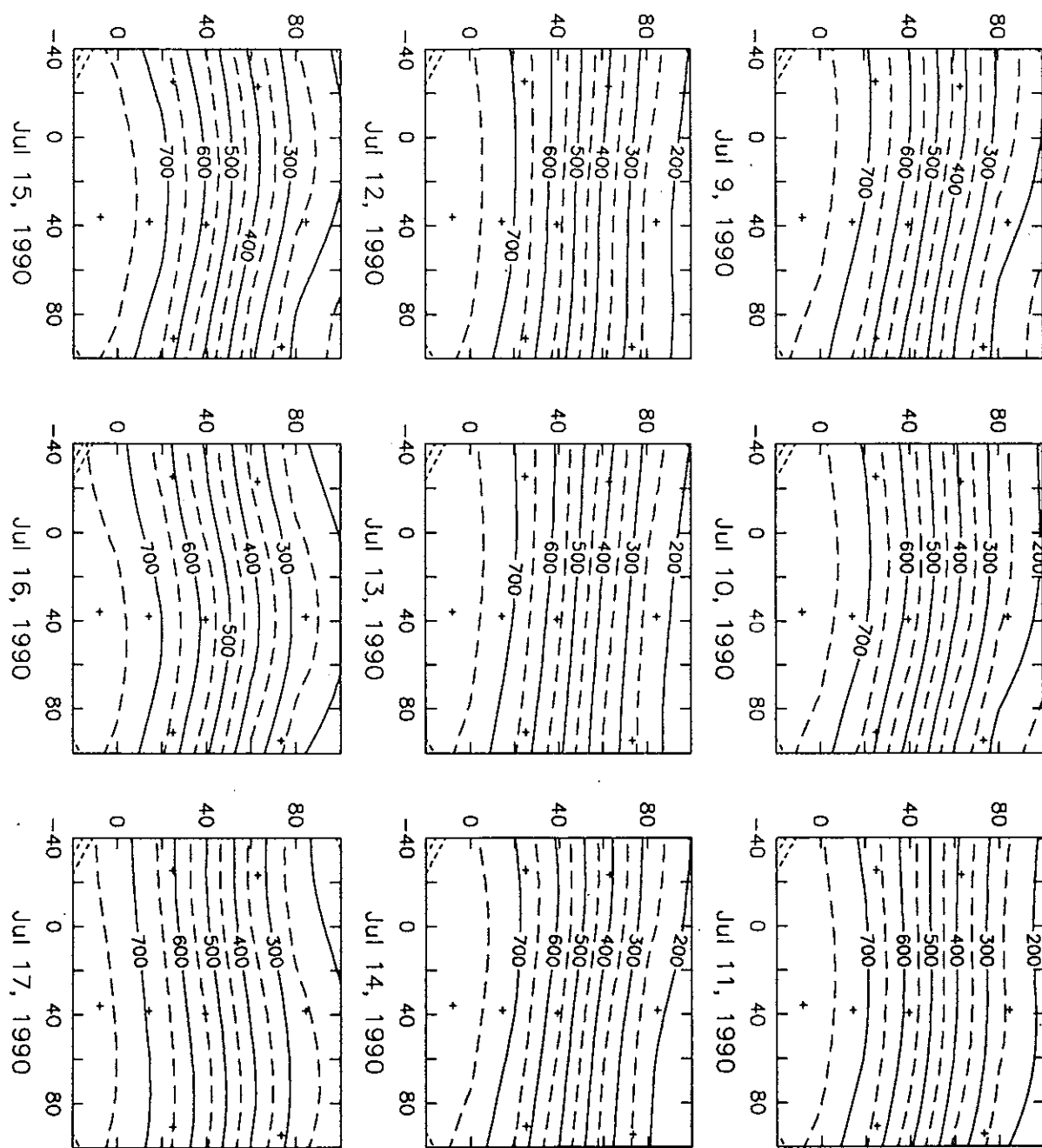


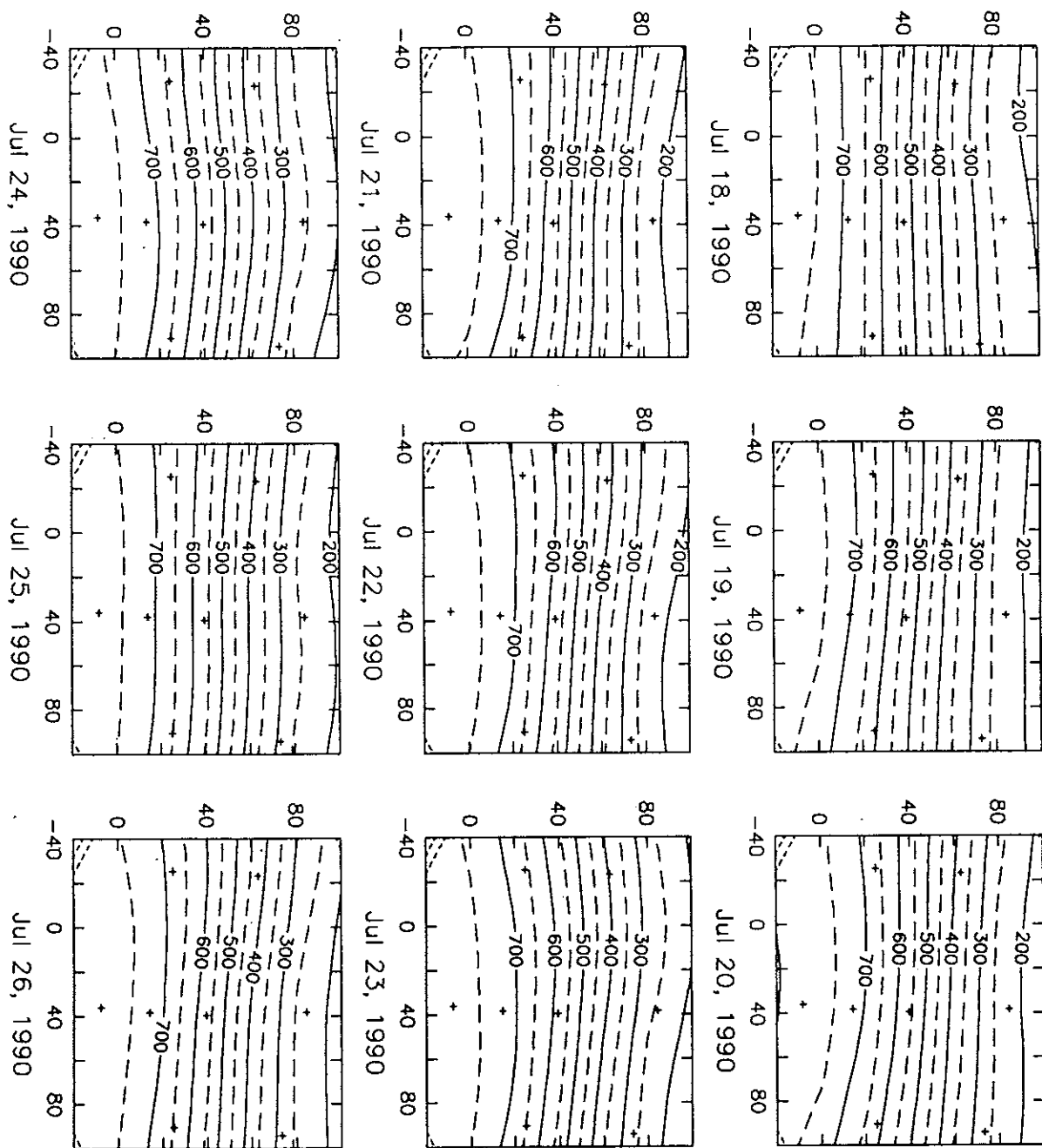


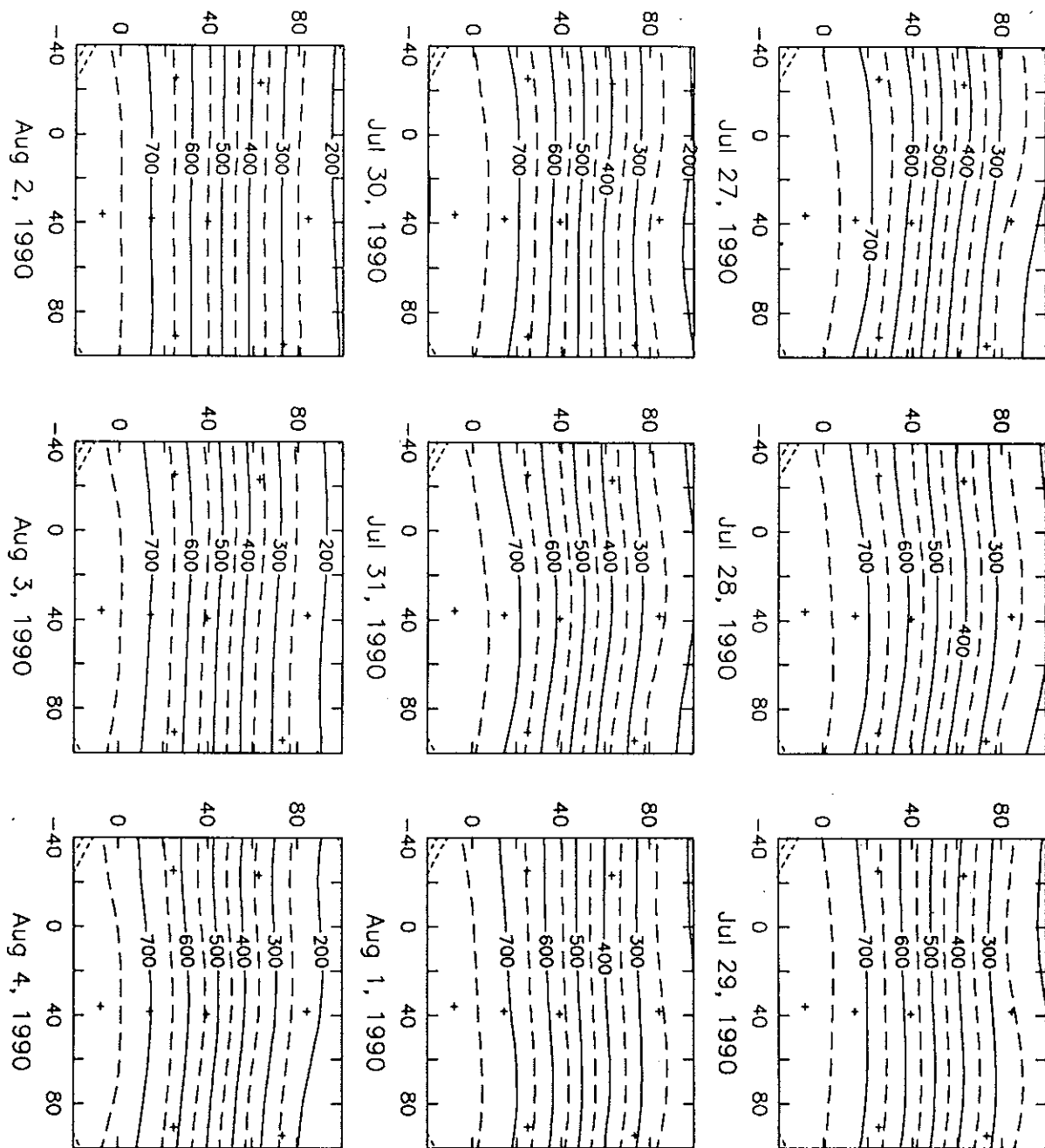


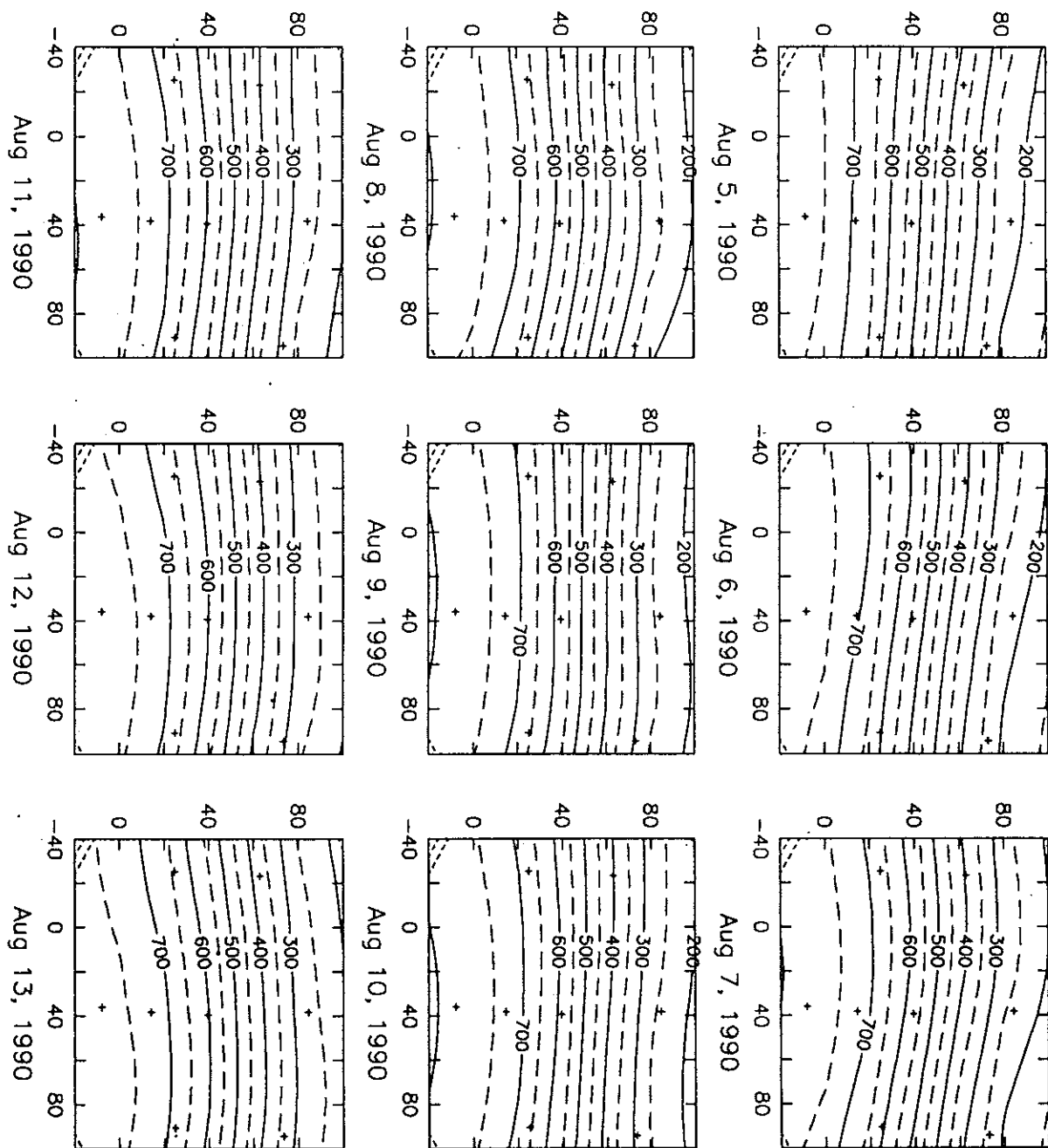


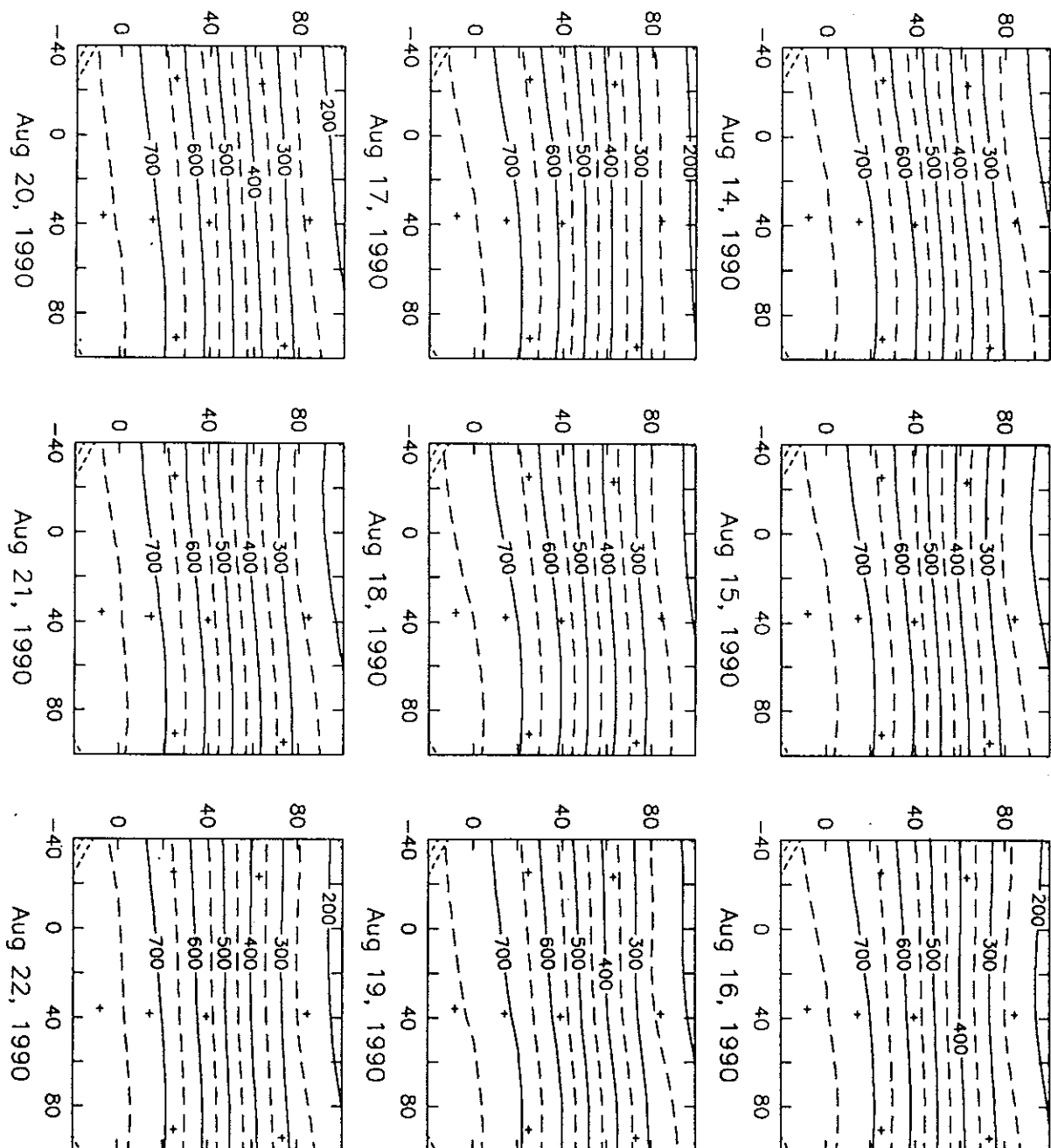


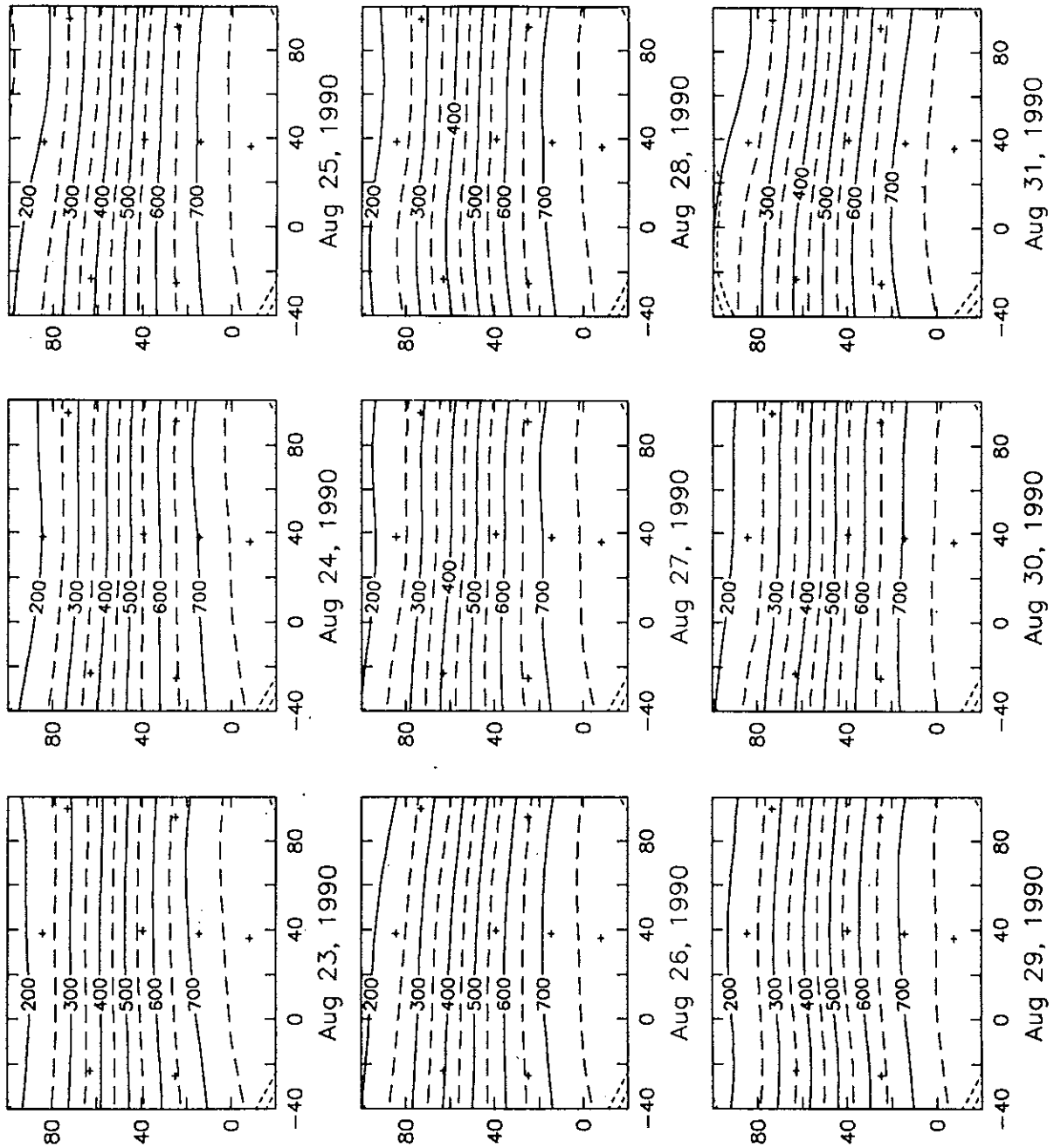












REFERENCES

- Bretherton, F.P., R. E. Davis, and C. B. Fandry. 1976. A technique for objective analysis and design of oceanographic experiments applied to MODE-73. *Deep Sea Res.*, 23, 559-582.
- Carter, E.F. 1983. The statistics and dynamics of ocean eddies. Ph.D. Thesis. Harvard University.
- Carter, E.F. and A. R. Robinson. 1987. Analysis models for the estimation of oceanic fields. *J. Atmos. Oceanic Technol.* 4, 49-74.
- Fields E. and D. R. Watts. 1990. The SYNOP Experiment: Inverted echo sounder data report for May 1988 to Aug 1989. University of Rhode Island. GSO Technical Report 90-2, 232 pp.
- Fields E. and D. R. Watts. 1990. The SYNOP Experiment: Inverted echo sounder data report for Jun 1989 to Sep 1989. University of Rhode Island. GSO Technical Report 91-2, 255 pp.
- Fields E., K.L. Tracey, and D. R. Watts. 1991. Inverted echo sounder data processing report. University of Rhode Island. GSO Technical Report 91-3, 150 pp.
- Gilman, C. and P. Cornillon. 1990. Gulf Stream position time series. *J. Geophys. Res.* (submitted).
- Howden, S. D., E. Fields, X. Qian, K. L. Tracey, D. R. Watts. 1991. IES calibration for main thermocline depth: A method using integrated XBT temperature profiles. University of Rhode Island. GSO Technical Report. (In preparation).
- Pickart, R. S., X. Qian, and D. R. Watts. 1991. The SYNOP Inlet Experiment: Bottom current meter for October 1987 to August 1990 mooring period. University of Rhode Island. GSO Technical Report 91-1.
- Qian, X., K. Tracey, E. Fields and D. R. Watts. 1990. The SYNOP Experiment: Inverted echo sounder data report for October 1987 to May 1988. University of Rhode Island. GSO Technical Report 90-3, 156 pp.
- Shay, T. J., S. Haines, J. M. Bane, and D. R. Watts. 1991. SYNOP Central Array current meter data report: Mooring period May 1988-September 1990. University of North Carolina Technical Report.

- Tracey, K.L. and D. R. Watts. 1986. On Gulf Stream meander characteristics near Cape Hatteras. *J. Geophys. Res.*, 91, 7587-7602.
- Tracey, K.L. and D. R. Watts. 1991. The SYNOP Experiment: Thermocline depth maps for the Central Array October 1987 to August 1990. University of Rhode Island. GSO Technical Report 91-5. 193 pp.
- Watts, D. R. and W. E. Johns. 1982. Gulf Stream meanders: observations on propagation and growth. *J. Geophys. Res.* 87, 9467-9476.
- Watts, D. R. and K. L. Tracey. 1985. Objective analysis of the Gulf Stream thermal front from inverted echo sounders. In *Gulf Stream Workshop Proceedings*, pp. II.525-II.548. University of Rhode Island, Narragansett.
- Watts, D. R., K. L. Tracey and A. I. Friedlander. 1989. Producing accurate maps of the Gulf Stream thermal front using objective analysis. *J. Geophys. Res.* 94, 8040-8052.

REPORT DOCUMENTATION PAGE

1a. REPORT SECURITY CLASSIFICATION Unclassified		1b. RESTRICTIVE MARKINGS	
2a. SECURITY CLASSIFICATION AUTHORITY		3. DISTRIBUTION/AVAILABILITY OF REPORT Distribution for Public release; Distribution is unlimited.	
2b. DECLASSIFICATION/DOWNGRADING SCHEDULE			
4. PERFORMING ORGANIZATION REPORT NUMBER(S) University of Rhode Island Graduate School of Oceanography GSO Technical Report 91-6		5. MONITORING ORGANIZATION REPORT NUMBER(S)	
6a. NAME OF PERFORMING ORGANIZATION Univ. of Rhode Island Grad. School of Oceanography	6b. OFFICE SYMBOL (If applicable) 1122 PO	7a. NAME OF MONITORING ORGANIZATION	
6c ADDRESS (City, State, and ZIP Code) South Ferry Road Narragansett, RI. 02882		7b. ADDRESS (City, State, and ZIP Code)	
8a. NAME OF FUNDING/SPONSORING ORGANIZATION Office of Naval Research National Science Foundation	8b. OFFICE SYMBOL (If applicable)	9. PROCUREMENT INSTRUMENT IDENTIFICATION NUMBER	
8c ADDRESS (City, State, and ZIP Code) 800 N. Quincy St., Arlington, VA 22217 1800 G. St., N.W., Washington, DC 20550		10. SOURCE OF FUNDING NUMBERS	
13a. TYPE OF REPORT Summary	13b. TIME COVERED FROM 10/87 TO 8/90	14. DATE OF REPORT (Year, Month, Day) August 1991	15. PAGE COUNT 137
16. SUPPLEMENTARY NOTATION			
17. COSATI CODES		18. SUBJECT TERMS (Continue on reverse if necessary and identify by block number) Gulf Stream, SYNOP, Inverted Echo Sounders and Thermocline Depth Maps	
19. ABSTRACT (Continue on reverse if necessary and identify by block number) Between October 1987 and August 1990, two arrays of inverted echo sounders were deployed in the Gulf Stream northeast of Cape Hatteras as part of the SYNoptic Ocean Prediction Experiment. The "Inlet Array" consisted of 9 inverted echo sounders (IES). Centered at 74°W, the Inlet Array was designed to measure key parameters that describe the Gulf Stream path variability near Cape Hatteras. The large "Central Array" of 24 IESs was centered on the current near 68°W, about 400 km downstream of the Inlet Array. Spanning nearly 300 km in both the cross-stream and downstream directions, the Central Array was designed to monitor the thermocline structure of the Gulf Stream in the region of large meanders and frequent ring interactions.			
Using objective analysis, we have mapped the Gulf Stream thermal field measured by the IESs in the Inlet Array. In this report, the objective analysis technique is described and the mapping parameters are documented. Daily maps of the thermocline depth field are presented for the period 14 October 1987 through 31 August 1990.			
20. DISTRIBUTION/AVAILABILITY OF ABSTRACT <input checked="" type="checkbox"/> UNCLASSIFIED/UNLIMITED <input type="checkbox"/> SAME AS RPT. <input type="checkbox"/> DTIC USERS		21. ABSTRACT SECURITY CLASSIFICATION	
22a. NAME OF RESPONSIBLE INDIVIDUAL		22b. TELEPHONE (Include Area Code)	22c. OFFICE SYMBOL